Weakly Interacting Bose Gas in Random Environment

im Fachbereich Physik der

Freien Universität Berlin

eingereichte Dissertation

von

Tama Khellil

Januar 2016

Die in vorliegender Dissertation dargestellte Arbeit wurde in der Zeit zwischen Oktober 2011 und Januar 2016 im Fachbereich Physik an der Freien Universität Berlin unter Betreuung von Priv.-Doz. Dr. Axel Pelster durchgeführt.

Erstgutachter: Priv.-Doz. Dr. Axel Pelster

Zweitgutachter: Prof. Dr. Jürgen Bosse

Tag der Disputation: 07.03.2016

Abstract

Weakly interacting Bose gases in a disorder environment have long been a challenging topic in the field of solid-state physics due to the intriguing interplay between superfluidity and localization. In this thesis we investigate theoretically the equilibrium properties of one- and three-dimensional harmonically trapped dirty Bose-Einstein condensates (BECs). In particular we focus on the decomposition of the total particle density into three components, namely, the condensate density, the thermal density, and the density of fragmented local Bose-Einstein condensates within the respective minima of the random potential landscape. In order to determine the different density components we develop a Hartree-Fock mean-field theory for a weakly interacting trapped BEC in a random environment, then specialize it to contact interaction and delta-correlated disorder. This non-perturbative theory is worked out on the basis of the replica method, which represents a well-established tool to deal with disorder problems. With this we calculate the corresponding free energy at finite temperature and derive from it the underlying self-consistency equations for the respective density components.

Then, as a first step, we investigate a quasi one-dimensional Bose-Einstein condensed gas in a harmonic trapping potential with an additional delta-correlated disorder potential at zero temperature. To this end we solve the self-consistency equations within the Thomas-Fermi approximation and find the emergence of a Bose-glass region, where the condensate vanishes. We corroborate this analysis by an elaborate numerical treatment, where the corresponding one-dimensional time-independent Gross-Pitaevskii equation is numerically solved and disorder-ensemble averages of the condensate wave function are performed. The variance of the condensate wave function quantifies the number of bosons which condense in the local minima of the random potential. For weak disorder these mini-condensates turn out to occur preferentially at the border of the condensate, while for intermediate disorder strength this happens in the trap center. Additionally we use a variational ansatz in order to describe analytically the numerically observed redistribution of the fragmented mini-condensates with increasing disorder strength.

In close analogy to the one-dimensional case we then treat the three-dimensional dirty Bose gas in an isotropic harmonic trap and a delta-correlated disorder potential at zero temperature using the corresponding self-consistency equations obtained via the Hartree-Fock mean-field theory within the Thomas-Fermi approximation. Additionally we use a variational ansatz, whose results turn out to coincide qualitatively with those obtained from the Thomas-Fermi approximation. In particular, a first-order quantum phase transition from the superfluid phase, where the condensate density contributes to the total density, to the Bose-glass phase, where all particles are in the mini-condensates, is detected at a critical disorder strength, which agrees with findings in the literature. Furthermore, in a general triaxial harmonic trap, we investigate the geometric effect of different trap aspect ratios on the respective properties of the dirty BEC system.

Finally, we consider the three-dimensional dirty BEC at finite temperature. This allows us to study the impact of both temperature and disorder fluctuations on the respective components of the density as well as their Thomas-Fermi radii. In particular, we find that the superfluid region, the Bose-glass region, and the thermal region coexist. Furthermore, depending on the system parameters, three phase transitions are detected, namely, one from the superfluid to the Bose-glass phase, one from the Bose-glass to the thermal phase, and finally one directly from the superfluid to the thermal phase. All these results could be particularly useful for a quantitative analysis of world-wide on-going experiments with dirty bosons in quasi one-dimensional and three-dimensional harmonic traps.

Kurzzusammenfassung

Schwach wechselwirkende Bose-Gase in einer Unordnungsumgebung sind aufgrund des interessanten Zusammenspiels von Superfluidität und Lokalisierung seit langem ein schwieriges Thema im Gebiet der Festkörperphysik. In dieser Arbeit untersuchen wir theoretisch die Gleichgewichtseigenschaften eines ein- und eines dreidimensionalen harmonisch gefangenen schmutzigen Bose-Einstein-Kondensates (BEKs). Insbesondere konzentrieren wir uns auf die Zerlegung der totalen Teilchendichte in seine drei Komponenten, nämlich die Kondensatdichte, die thermische Dichte und die Dichte der fragmentierten Bose-Einstein-Kondensate innerhalb der jeweiligen Minima der zufälligen Potentiallandschaft. Um die verschiedenen Dichtekomponenten zu bestimmen, entwickeln wir eine Hartree-Fock-Molekularfeldtheorie für ein schwach wechselwirkendes gefangenes BEK in einer Zufallsumgebung, dann spezialisieren wir diese auf eine Kontaktwechselwirkung und eine delta-korrelierter Unordnung. Diese nichtstörungstheoretische Theorie wird auf der Grundlage der Replika-Methode ausgearbeitet, die eine wohletablierte Methode zur Behandlung von Unordnungsproblemen darstellt. Damit berechnen wir die entsprechende freie Energie bei endlicher Temperatur und leiten daraus die zugrunde liegenden Selbstkonsistenzgleichungen für die jeweiligen Dichtekomponenten ab.

Dann untersuchen wir als ersten Schritt ein quasi eindimensionales Bose-Einstein kondensiertes Gas in einem harmonischen Fallenpotential mit einem zusätzlichen delta-korrelierten Unordnungspotential am absoluten Temperaturnullpunkt. Hierzu lösen wir die Selbstkonsistenzgleichungen mit der Thomas-Fermi-Näherung und finden die Emergenz einer Bose-Glas-Region, wo das Kondensat verschwindet. Wir untermauern diese Analyse mit einer aufwändigen numerischen Behandlung, bei der die entsprechende eindimensionale zeitunabhängige Gross-Pitaevskii-Gleichung numerisch gelöst wird und Unordnungsensemble-Mittelwerte für die Kondensatwellenfunktion berechnet werden. Die Varianz der Kondensatwellenfunktion quantifiziert die Zahl der Bosonen, die in den lokalen Minima des Zufallspotentials kondensieren. Für schwache Unordnung stellt sich heraus, dass diese Minikondensate bevorzugt am Rande des Kondensates auftreten, während für mittlere Unordnungsstärke dies nur im Fallenzentrum auftritt. Außerdem verwenden wir einen Variationsansatz, um die numerisch beobachtete Umverteilung der fragmentierten Minikondensate mit zunehmender Unordnungsstärke analytisch beschreiben zu können.

In enger Analogie zum eindimensionalen Fall behandeln wir dann das dreidimensionale schmutzige Bose-Gase in einer isotropen harmonischen Falle und einem delta-korrelierten Unordnungspotential am absoluten Temperaturnullpunkt mit Hilfe der entsprechenden Selbstkonsistenzgleichungen, die im Rahmen der Hartree-Fock-Molekularfeldtheorie in Thomas-Fermi-Näherung gewonnen wurden. Zusätzlich verwenden wir einen Variationsansatz, dessen Resultate qualitativ mit denen der Thomas-Fermi-Näherung übereinstimmen. Insbesondere finden wir einen Quantenphasenübergang erster Ordnung von der superfluiden Phase, wo die Kondensatdichte zur totalen Dichte beiträgt, zu der Bose-Glasphase, wo sich die Teilchen in den Mini-Kondensaten aufhalten, bei einer kritischen Unordnungsstärke, die mit den Ergebnissen der Literatur übereinstimmt. Außerdem untersuchen wir in einer allgemein tri-axialen harmonischen Falle den geometrischen Effekt verschiedener Frequenzverhältnisse auf die entsprechenden Eigenschaften des schmutzigen BEK-Systems.

Abschließend betrachten wir ein dreidimensionales schmutziges BEK bei endlicher Temperatur. Dies erlaubt es uns, den Einfluß sowohl von thermischen als auch von Unordnungs-Fluktuationen auf die jeweiligen Komponenten der Dichte sowie der Thomas-Fermi-Radien zu untersuchen. Insbesondere finden wir, dass die superfluide Region, die Bose-Glas-Region und die thermische Region koexistieren. Ferner werden abhängig von den systemparametern drei Phasenübergänge beobachtet, nämlich einer von der superfluiden zur Bose-Glas-Phase, einer von der Bose-Glas zur thermischen Phase, und schließlich einer direkt von der superfluiden zur thermischen Phase. All diese Resultate könnten besonders nützlich sein, um laufende Experimente mit schutzigen Bosonen in quasi ein- und dreidimensionalen Fallen quantitativ zu analysieren.

Selbstständigkeitserklärung

Hiermit versichere ich, die vorliegende Arbeit ohne unzulässige Hilfe Dritter und ohne Benutzung anderer als der angegebenen Hilfsmittel angefertigt zu haben. Die aus fremden Quellen direkt oder indirekt übernommenen Gedanken sind als solche kenntlich gemacht. Die Arbeit wurde bisher weder im In- noch im Ausland in gleicher oder ähnlicher Form einer anderen Prüfungsbehörde vorgelegt.

Tama Khellil

Contents

1. Introduction **11**
- 1.1. Bose-Einstein Condensates . . . 11
  - 1.1.1. History . . . 11
  - 1.1.2. Experimental Realization . . . 12
- 1.2. Disorder . . . 13
- 1.3. Dirty Bosons . . . 15
- 1.4. Replica Method . . . 17
- 1.5. Outline of Thesis . . . 18

2. Hartree-Fock Mean-Field Theory for Dirty Bosons **21**
- 2.1. Disorder Potential . . . 21
- 2.2. Bose Model . . . 23
- 2.3. Replica Method . . . 24
- 2.4. Hartree-Fock Mean-Field Equations . . . 25
- 2.5. Replica Symmetry . . . 28
- 2.6. Delta-Correlated Disorder and Contact Interaction Potential . . . 31
- 2.7. Schwinger Trick . . . 32
- 2.8. Correlation Functions and Order Parameters . . . 33
- 2.9. Thermodynamic Properties . . . 37
- 2.10. Application of Hartree-Fock Mean-Field Theory in 3D . . . 39
  - 2.10.1. Replica Limit . . . 40
  - 2.10.2. Free Energy . . . 42
  - 2.10.3. Self-Consistency Equations . . . 43
- 2.11. Application of Hartree-Fock Mean-Field Theory in 1D . . . 44

3. 1D Case at Zero Temperature **47**
- 3.1. Homogeneous Case . . . 47
  - 3.1.1. Superfluid Phase . . . 47
  - 3.1.2. Bose-Glass Phase . . . 49
  - 3.1.3. Comparison with Huang-Meng Theory . . . 49
- 3.2. Thomas-Fermi Approximation . . . 50
  - 3.2.1. Superfluid Region . . . 51
  - 3.2.2. Bose-Glass Region . . . 51
  - 3.2.3. Thomas-Fermi Results . . . 52
- 3.3. Numerical Treatment . . . 54
  - 3.3.1. Generating Random Potential . . . 54
  - 3.3.2. Numerical Results . . . 56
- 3.4. Comparison Between Thomas-Fermi Approximation and Numerics . . . 59
- 3.5. Variational Method . . . 62
- 3.6. Comparison of Analytical, Numerical and Variational Results . . . 66

4. 3D at Zero Temperature **71**
- 4.1. Homogeneous Case . . . 71
  - 4.1.1. Superfluid Phase . . . 71
  - 4.1.2. Bose-Glass Phase . . . 72
  - 4.1.3. Comparison with Literature . . . 72
- 4.2. Thomas-Fermi Approximation . . . 73

4.3. Isotropic Trap . . . 74
4.3.1. Superfluid Region . . . 74
4.3.2. Bose-Glass Region . . . 76
4.3.3. Thomas-Fermi Results . . . 76
4.3.4. Variational Method . . . 79
4.3.5. Comparison Between TF Approximation and Variational results . . . 85
4.3.6. Qualitative Comparison Between 1D and 3D Results . . . 86
4.4. Anisotropic Trap . . . 86
4.4.1. Superfluid region . . . 87
4.4.2. Bose-glass region . . . 88
4.4.3. Thomas-Fermi Results . . . 89

5. Dirty Bosons in 3D at Finite Temperature **91**
5.1. Homogeneous Case . . . 91
5.1.1. Superfluid Phase . . . 91
5.1.2. Bose-Glass Phase . . . 93
5.1.3. Thermal phase . . . 93
5.1.4. Phase Diagram . . . 93
5.1.5. Chemical Potential . . . 94
5.2. Thomas-Fermi Approximation . . . 95
5.3. Clean Case . . . 96
5.3.1. Superfluid region . . . 96
5.3.2. Thermal region . . . 98
5.3.3. Thomas-Fermi Results . . . 98
5.4. Disordered Case . . . 100
5.4.1. Thermal Region . . . 101
5.4.2. Bose-Glass Region . . . 101
5.4.3. Superfluid Region . . . 101
5.4.4. Thomas-Fermi Densities . . . 105
5.4.5. Temperature Influence . . . 105
5.4.6. Disorder Influence . . . 107

6. Summary and Outlook **111**
6.1. Summary . . . 111
6.2. Outlook . . . 113

A. Cardan Method **115**

B. Numerical Appendix **117**

Bibliography **119**

List of Publications **128**

1. Introduction

Bose-Einstein condensation has long been an important topic in the field of solid-state physics and has been intensely explored both theoretically and experimentally. The reason of this is that the Bose-Einstein condensation is a promising tool for simulating other quantum many-body systems in the sense of Feynman [1]. Bose-Einstein condensation in a disordered environment, known as the dirty boson problem, represents a quite intriguing theoretical challenge because it involves many parameters and combines the effect of both two-particle interactions and disorder. In order to tackle the dirty boson problem in the present thesis we use a mathematical tool called replica method, which was originally developed for analyzing the spin-glass problem.

In this chapter, we present a brief summary of the history, recent experiments, and the theoretical description of Bose-Einstein condensation and disordered systems. Furthermore, the principle of the replica method will be explained.

1.1. Bose-Einstein Condensates

A Bose-Einstein condensate (BEC) is a state of matter of a dilute gas of weakly interacting bosons confined in an external potential and cooled to temperatures near to absolute zero. As the density increases or the temperature decreases, the number of accessible states per particle becomes smaller, and at some point more particles begin to act collectively and are forced to occupy the lowest quantum state. The latter contains then more particles than maximally allowed according to the thermal occupation. From this point on, any extra particle added goes into the quantum mechanical ground state. So to speak, Bose-Einstein condensation, where the quantum effects become apparent on a macroscopic scale, appears as a saturation in the excited states population resulting from Bose-Einstein statistics. This transition to BEC occurs for a homogeneous system below a critical temperature $T_c = \left(\frac{n}{\varsigma(3/2)}\right)^{2/3} \frac{2\pi\hbar^2}{Mk_B}$, where n denotes the particle density, $\hbar$ the Planck's constant, M the atomic mass, and k_B the Boltzmann constant.

1.1.1. History

In 1924, the Indian physicist and mathematician Bose derived the Planck law for black-body radiation from new statistical counting rules for light quanta (photons), without resorting to the results from classical electrodynamics [2]. Einstein translated his paper into German, reviewed it, extended his work to massive particles, and presented the basic idea of a BEC in 1925 for an ideal gas of identical atoms which are at thermal equilibrium in a box [3]. He predicted that, at sufficiently low temperatures, the particles would accumulate in the lowest quantum state in the box and would merge into a giant superatom. Locked together, moving as one, this condensate of atoms would become a new state of matter, different from solid, liquid or gas. The condition for this to happen is that the de Broglie wavelength, $\lambda_{\mathrm{dB}} = \frac{h}{mv}$, of each atom must be large enough to overlap with its neighbor. Einstein's new theory was criticized at the time, since all real gases were already condensed to liquids or solids. Furthermore, the absence of interactions in the theory made his prediction difficult to test in practice at that time.

After discovering the superfluidity of ^{4}He, which is a boson, in 1938 by Kapitsa, London was the one to suggest an approach for realizing a BEC by using superfluid liquid ^{4}He. After realizing that the predicted T_c was a good estimate of the superfluid transition in ^{4}He and that the specific heat of the ideal gas had a peak at T_c, he came with the idea that BEC is a possible mechanism underlying superfluidity in liquid ^{4}He, although this strongly interacting quantum many-body system is quite different from the ideal gas considered by Einstein. This gave Einstein's theory new life. Einstein's

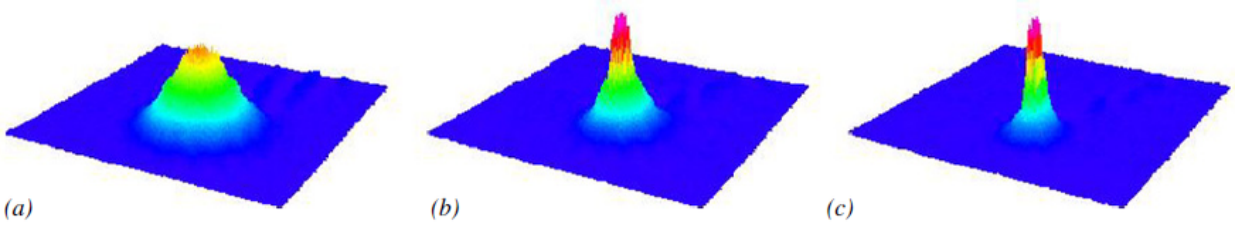

Figure 1.1.: Absorption images of an expanding rubidium cloud. (a) thermal gas, $T = 1.1\,T_c$, (b) double peak structure, with a Bose-Einstein condensate surrounded by a thermal gas, $T = 0.6\,T_c$, and (c) almost pure condensate, $T = 0.3\,T_c$ [4].

theory was extended to describe the interacting Bose gas in 1947 by Bogoliubov, who introduced a mean-field theory to account for atom-atom interactions within a homogeneous gas [5].

In the early 1950s, the interest in finding BEC in a dilute weakly interacting Bose gas started to develop. Yang and his collaborators considered a many-body system with hard-sphere interaction and treated this within Bogoliubov theory at zero temperature [6, 7]. Gross and Pitaevskii derived independently in 1961 a specialization of Bogoliubov's theory [8, 9]. They described in mean-field theory at zero temperature a system of N interacting bosons in an external field where the interaction between two particles is replaced by an effective interaction. The validity of the Gross-Pitaevskii equation is based on the condition that the s-wave scattering length is much smaller than the average distance between the atoms and that the number of particles in the condensate is large.

Due to the developments in magnetic trapping, laser and evaporative cooling of alkali atoms in the 80's, the experimental realization of BEC became finally possible. The laser cooling was first proposed by Wineland and Dehmelt as well as by Hänsch and Schawlow in 1975 and became applicable by Chu, Cohen-Tannoudji, and Phillips, who were awarded the 1997 Nobel Prize in Physics for their work on laser cooling.

Finally, in 1995 Cornell and Wieman from the JILA group created the first BECs in trapped ultracold dilute atomic gas ^{87}Rb [10, 11]. A few months later, one more BEC was created with ^{23}Na at MIT in Ketterle's group [12]. The Nobel Prize in Physics in 2001 was awarded to Cornell, Wieman, and Ketterle for their achievements. One month after the first BEC's realization another one was announced in ^{7}Li, which has attractive interactions, in the Rice University in Hulet's group [13, 14]. In 1998 Kleppner and his co-workers in MIT condensed ^{1}H [15]. ^{4}He was also condensed in 2001 in ENS in Aspect's group [16]. Fig. 1.1. shows the two-component density distribution, which is a signature of Bose-Einstein condensation, as observed in this experiment with time-off-flight absorption pictures. The peaked anisotropic condensate density below T_c is clearly visible in the middle of a spherical thermal cloud.

1.1.2. Experimental Realization

Current research in BEC focuses on the creation of the condensate in dilute gases because at the temperatures needed to produce the BEC, most media condense to liquid or solid and the localization of the atoms/molecules prevents the BEC transition from occurring.

The process starts by trapping atoms moving in all directions. In order to counter each component of motion for particles with either positive or negative velocity one needs six lasers. In the same configuration as the lasers, coils are used to create magnetic fields in order to confine the gas and to keep the atoms from hitting the walls of the apparatus and warming them up.

To cool the dilute trapped gas to a temperature of about 100 μK the laser cooling technique is used. In this technique a laser photon hits the atom in one direction and causes it to emit photons in all directions of a higher average energy than the one it absorbed from the laser. The energy difference comes from thermal excitations within the atoms, and this heat from the thermal excitation is converted into light which then leaves the atom as a photon. This operation is repeated as much as

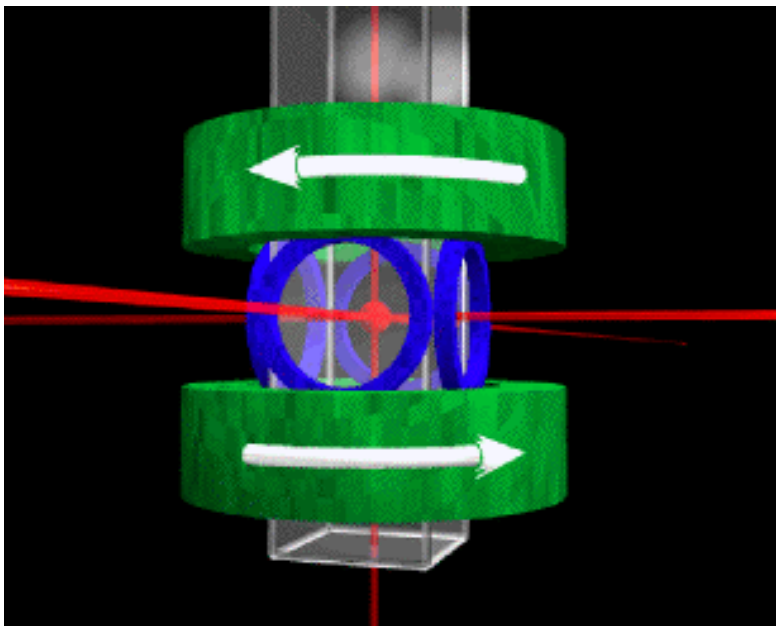

Figure 1.2.: BEC apparatus: the six red lines represent lasers used for laser trapping and cooling, the two green coils are for vertical magnetic field production and the four blue coils are for horizontal magnetic field production. Atoms from the Rb source are trapped in the center of this apparatus [10].

it is needed.

Laser cooling cannot bring the atoms down to the temperature needed for Bose-Einstein condensation. Evaporative cooling allows the most energetic of the trapped atoms to escape, lowering the total energy of the resulting system. A simple BEC apparatus for trapping and cooling atoms is shown in Fig. 1.2.

In order to distinguish between the different components in a BEC cloud, the time-of-flight (TOF) method is used. The idea of TOF is to turn the trap off and to wait a certain amount of time before taking a shadow image of the atoms. During this time, the atoms will drop due to gravity and expand due to their velocity. A normal atom cloud will display a Gaussian distribution after TOF. From the shadow image after a long enough TOF, we should observe a bimodal distribution of atoms right at the BEC transition, see Fig. 1.3. The BEC expansions show a cloud aspect ratio inversion due to Heisenberg principle.

Bose-Einstein condensates have already proven to be a source of inspiration for theoreticians with a background in condensed matter, and reciprocally condensed matter has inspired many beautiful experiments with ultracold gases. A Bose-Einstein condensate of an atomic gas also exhibits superfluidity. Experiments have confirmed the superfluid behavior by demonstrating a critical velocity below which a laser beam could be moved through the gas without causing excitations [17]. The critical velocity is the velocity above which superfluidity is destroyed and the corresponding theory earned Landau the Nobel Prize in physics in 1962 [18]. Another evidence for superfluidity, as it was predicted by Onsager and developed by Feynman, is the observation of quantum vortices in a rotating BEC [19,20]. Recently, a persistent flow of Bose-condensed atoms was observed in a toroidal trap [21], which is a striking demonstration of superfluid behavior. These characteristic properties make the BEC a model system for superfluidity, but although the phenomenon of superfluidity is related to BEC, but it is not identical: not all superfluids are BECs as for instance a two-dimensional weakly interacting Bose gas.

1.2. Disorder

In real systems, disorder is always present to some extent. It is described by a random external potential which is characterized by a strength, which is the average height of its maxima and depth of its minima, as well as a correlation length, which represents the average width of its maxima and

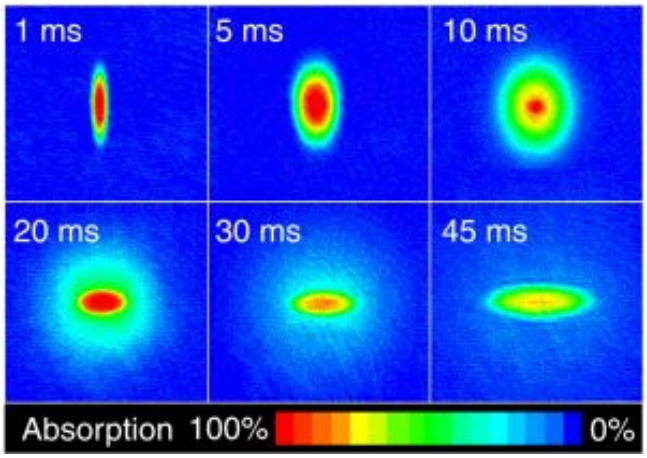

Figure 1.3.: An example of a time of flight expansion of a Bose condensate [22].

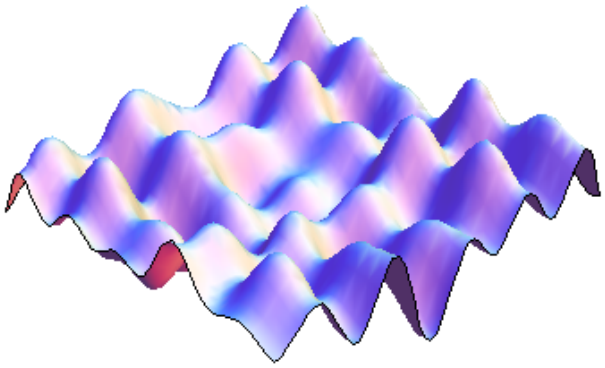

Figure 1.4.: One realization of a disorder potential, which shows a random distribution of maxima and minima.

minima, see Fig. 1.4. Thus, the theory of disordered systems has become increasingly important over the past few decades. It describes unknown properties of a specific model with the help of random functions and has been applied to a wide range of physical, chemical, and biological problems. Taking into account disorder makes theoretical models for these experiments more realistic. Random potentials find areas of application even far from its physical origins. For example, the transport in random media and diffusion-controlled reactions can be modeled by random walks in random trapping environments [23,24]. The dynamics of stock markets have also been modeled as a tracer in a Gaussian random field [25]. Furthermore, the behavior of polymer chains in random media is strongly connected to this field of study [26]. And due to the discovery of new experimental techniques, researchers are currently able to investigate thoroughly this field.

Disorder appears either naturally as, e.g., in magnetic wire traps [27–30], where imperfections of the wire itself can induce local disorder, or it may be created artificially and controllably as, e.g., by the use of laser speckle fields [31–34]. The speckle effect is an interesting disorder problem. It is a result of the interference of many waves of the same frequency, and different phases and amplitudes, which add together to give a resultant wave whose amplitude and intensity is constant over time, but varies randomly in space [35], see Fig. 1.5. The effects of disorder on the phases and phase transitions in many-body quantum systems have been of intense interest for many decades.

In the context of disorder theory, the Sherrington-Kirkpatrick (SK) model describing spin-glasses, i.e., disordered magnets where the magnetic spins of the respective atoms are not aligned in a regular

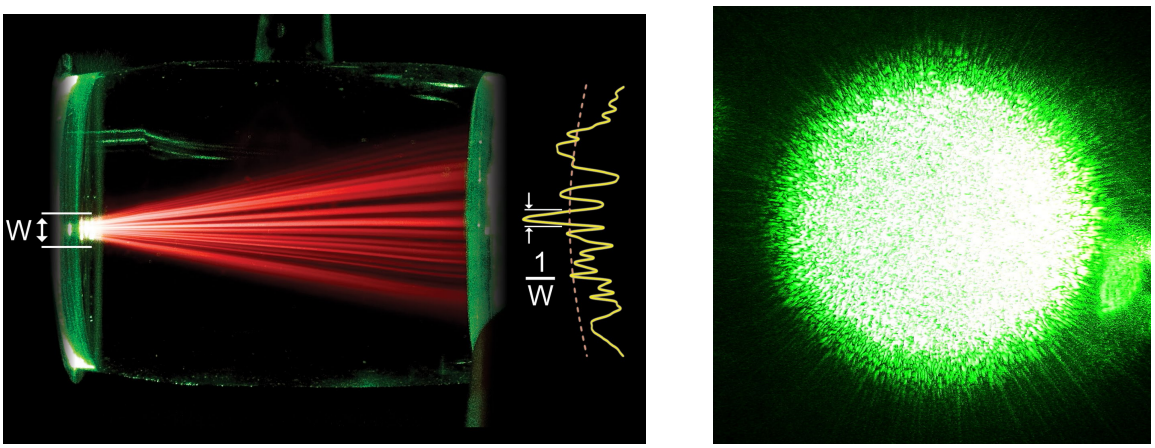

(a) (b)

Figure 1.5.: (a) Schematic representation of speckle formation [36] and (b) typical speckle pattern [37].

pattern, is especially important as it has been studied capaciously [38]. One imagines half of the bonds between two spins randomly chosen as ferromagnetic and the other half as antiferromagnetic. The SK model describes this situation via an Ising model in which the spins are coupled by random infinite-range interactions. These interactions are assumed to be independent and normally distributed [38–40].

1.3. Dirty Bosons

The dirty boson problem is defined as a system of interacting bosons in a random potential [41]. The combined effect of disorder and interactions represents one of the most challenging problems in condensed matter physics due to the delicate interplay between localization and superfluidity. Cold atoms provide a controlled realization in which the question of interacting bosons in a random environment can be addressed in a quantitative way. Furthermore, the presence of disorder in BEC causes the emergence of a new phase, which is called a Bose-glass phase due to the localization of bosons in the random potential landscape. This Bose-glass phase is insulating and is characterized by a finite compressibility, by the absence of a gap, and by an infinite superfluid susceptibility [41].

The earliest relevant experiments, which were central for motivating the research of the dirty boson problem, dealt with superfluidity of thin films of ^{4}He adsorbed in porous Vycor glass in the low density limit [42]. There it was proven that despite disorder superfluidity still persists in Helium in porous media.

An optical lattice is formed by the interference of counter-propagating laser beams, creating a spatially periodic polarization pattern. The resulting periodic potential may trap cooled atoms in the locations of its minima. Imposing a pseudo random potential created by a second additional lattice to an ultra cold Bose gas in an optical lattice is shown to provide an ideal system for controlled analysis of disordered Bose lattice gases [43]. This was, later on, realized experimentally in Hanover [44]. An optical speckle potential was also used to investigate the properties of BEC in the presence of disorder [32], as well as the transport properties of an interacting BEC in a random potential [33].

Non-interacting particles in a random environment can be localized provided that the disorder is sufficiently strong. This phenomenon of Anderson localization occurs as the particles are repeatedly reflected back in the random potential, so interferences yield exponentially localized one-body wave functions [45]. In one dimension Anderson localization was experimentally found in an ultracold Bose gas in Refs. [46,47], where the random or quasi-random disorder potential was either produced by laser speckles or by an incommensurable optical lattice, respectively, where the disorder is created through two interfering laser beams with incommensurable wavelengths producing a quasi periodic potential. One can even speak about Anderson localization of light waves [48, 49], which was experimentally realized in 3D random media [50,51], 2D [52], and 1D [53], where the Anderson localization is observed

in a perturbed periodic potential and is caused by random fluctuations on a photonic lattice.

Within a BEC, which is a many-particle interacting system, the presence of disorder causes the emergence of a new phase besides the superfluid phase (SF), which is called a Bose-glass phase due to the localization of bosons in the respective minima of the random potential landscape. Indications for the existence of the Bose-glass phase were found, for instance, in the experiments of Refs. [32, 54, 55]. There it was shown within the superfluid phase that an increasing disorder strength yields first a fragmentation of the condensate due to the formation of tiny BEC droplets in the minima of the random environment. For sufficiently strong disorder the condensate then turns out to be completely destroyed as all bosons are localized in the minima of the random potential, which represents the Bose-glass phase. Localization inside BEC due to disorder created by atomic impurities of another species trapped in the nodes of an optical lattice was also proposed and studied theoretically by Gavish and Castin [56], and recently observed experimentally in Ref. [57]. In the presence of disorder a phase transition occurring at zero temperature, as a function of some auxiliary control parameter, such as density or magnetic field, is known as a quantum phase transition (QPT) since the particle dynamics are provided purely by the quantum fluctuations of the ground state wave function [58]. One can say that the disorder is so large that it destroys superfluidity. The SF-BG transition attracts a continuous theoretical interest [59–63].

Theoretically, the dirty boson problem was treated via two complementary approaches. The first one applies the Bogoliubov theory [5] and treats disorder, quantum, and thermal fluctuations perturbatively, which is only valid in systems with sufficiently small random potential and interaction strength at low enough temperatures [64]. With this it was found that a weak random disorder potential leads to a depletion of both the condensate and the superfluid density due to the localization of bosons in the respective minima of the random potential. This seminal Huang-Meng theory was later on extended in different research directions. Results for the shift of the velocity of sound as well as for its damping due to collisions with the external field are worked out in Ref. [65]. Furthermore, the original special case of a delta-correlated random potential was generalized to experimentally more realistic disorder correlations with a finite correlation length, which describe, for instance, the pore size dependence of Vycor glass. A Gaussian correlation was discussed in Ref. [66], whereas laser speckles are treated in Refs. [67, 68]. Also the disorder-induced shift of the critical temperature was analyzed in Refs. [69, 70]. Furthermore, it was shown in Refs. [71–75] that dirty dipolar Bose gases yield even at zero temperature characteristic directional dependences for thermodynamic quantities due to the anisotropy of superfluidity. The recent perturbative work [76, 77] studies even in detail the impact of the external random potential upon the quantum fluctuations. Despite all these many theoretical predictions of the Huang-Meng theory, which also affect the collective excitations frequencies of harmonically trapped dirty bosons [78], so far no experiment has tested them quantitatively.

On the other hand the dirty boson problem was also tackled non-perturbatively in different ways. A major result is that, increasing the disorder strength at zero temperature, yields a first-order quantum phase transition from a superfluid to a Bose-glass phase, where in the latter all particles reside in the respective minima of the random potential. This prediction is achieved for three dimensions by solving the underlying Gross-Pitaevskii equation with a random phase approximation [79] as well as by a stochastic self-consistent mean-field approach using two chemical potentials, one for the condensated and one for the excited particles [80, 81]. Dual to that the non-perturbative approach of Refs. [82, 83] investigates energetically shape and size of the local minicondensates in the disorder landscape and deduces from that at which disorder strength the Bose-glass phase becomes unstable and goes over into the superfluid. At finite temperatures the location of superfluid, Bose-glass and normal phase in the phase diagram was qualitatively analyzed in Ref. [84] on the basis of a Hartree-Fock mean-field theory with the replica method. Also Monte-Carlo (MC) simulations have been applied towards the disorder problem. Diffusive MC in Ref. [85] obtained the surprising result that a strong enough disorder yields a superfluid density which is larger than the condensate density. Furthermore, worm MC [86, 87] was able to determine the dynamic critical exponent of the quantum phase transition from the Bose-glass to the superfluid in two dimensions.

Although this intriguing problem has been intensively studied for more than 20 years, many challenges remain. In particular the precise phase diagram is still under debate, and a good control, either

analytical or numerical, on what happens for strong disorder is still lacking.

1.4. Replica Method

A standard method to deal with disorder problems is a mathematical trick called the replica method [40, 88, 89]. It was proposed by Parisi in 1980 and has proven to be successful within the study of the Sherrington-Kirkpatrick (SK) model, which is an Ising model with long range frustrated ferro- and antiferromagnetic couplings, and other disorder problems. This method turned out to give the exact mathematical solution for the SK model. The replica method is used to rewrite a model system in form of a many-particle problem. This has the advantage of stating the problem in terms of its correlation function instead of the random potential. Instead of treating the actual problem, one looks at $\mathcal{N}$ copies of the system. The central idea of the replica trick is to analytically continue the replicated system in the limit $\mathcal{N} \to 0$.

The free energy $\mathcal{F}$ for a fixed realization of the disorder potential of a system can be stated as $-\frac{1}{\beta} \ln \mathcal{Z}$, where $\mathcal{Z}$ is the grand-canonical partition function of the system, $\beta = 1/k_B T$ is the reciprocal temperature, and T is the temperature. Hence, the system's free energy $\mathcal{F}$ is given as the free energy for fixed disorder potential averaged over all its realizations:

$$\mathcal{F} = -\frac{1}{\beta} \overline{\ln \mathcal{Z}}, \tag{1.1}$$

where $\overline{\bullet}$ corresponds to the disorder average over many realizations.

In general it is not possible to explicitly evaluate expression (1.1), as the two operations of averaging with respect to the disorder potential and the nonlinear function of the logarithm do not commute:

$$\overline{\ln \mathcal{Z}} \neq \ln \overline{\mathcal{Z}}\,. \tag{1.2}$$

The replica method, to perform the averaging procedure prescribed by (1.1), is provided by investigating the $\mathcal{N}^{\text{th}}$ power of the grand-canonical partition function $\mathcal{Z}$ in the limit $\mathcal{N} \to 0$:

$$\mathcal{Z}^{\mathcal{N}} = e^{\mathcal{N} \ln \mathcal{Z}} = 1 + \mathcal{N} \ln \mathcal{Z} + \dots \quad , \tag{1.3}$$

where $\mathcal{Z}^{\mathcal{N}}$ is the replicated partition function. Thus, we deduce for the free energy (1.1):

$$\mathcal{F} = -\frac{1}{\beta} \lim_{\mathcal{N} \to 0} \frac{\overline{\mathcal{Z}^{\mathcal{N}}} - 1}{\mathcal{N}}\,. \tag{1.4}$$

The fact that all $\mathcal{N}$ replicas are identical, known as replica symmetry, simplifies the calculation further. Although the replica method has proven to be successful many times, this procedure is still quite ambiguous from a rigorous mathematical point of view because of the $\mathcal{N} \to 0$ limit. After obtaining a solution, it is important to find the area of its stability. Almeida and Thouless [90, 91] developed a mathematical method to determine the Almeida-Thouless line, which separates the stable solutions from the unstable ones, and thus finds the limit of stability for the RS solutions of the SK model. The criterion to test the stability of the system is to evaluate the eigenvalues of the Hessian, which is computed as the second derivative of the free energy with respect to the respective variational parameters. The stability requires the eigenvalues to be positive definite. Thus, at high temperatures or in the case of weak correlation, the replica-symmetric ansatz turns out to be intrinsically correct but it can break down spontaneously under a critical temperature as has been shown in certain models [92], e.g., the SK model. In order to analyze that in more detail, Parisi introduced the scheme of replica-symmetry breaking (RSB) [39, 93–95]. This was shown to give a stable solution for the SK model for all temperatures. His method turned out to be a major breakthrough in disorder theory. The physical origin of RSB is the existence of many local minima of the complicated free energy, which are separated by high barriers. The pattern of RSB depends on the range of correlations of the random potential. For short-range correlations a one-step RSB has been found sufficient, whereas for long-ranged correlations a continuous RSB has turned out to be necessary [95,96]. Practically one can compare the free energies associated with the RS and RSB solutions and verify whether the free energy of the RSB solution is smaller. If this is the case this indicates that RS has to be broken.

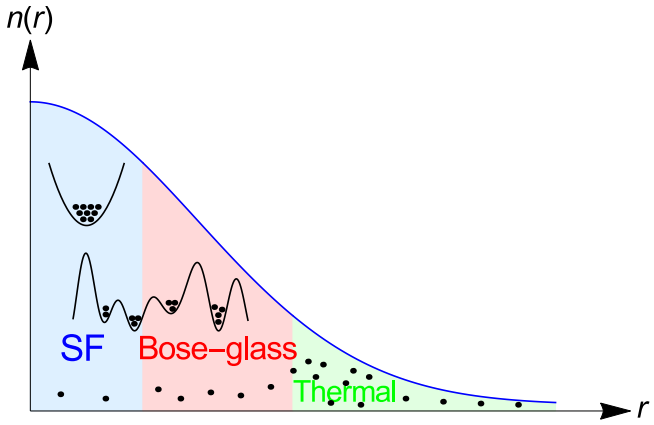

Figure 1.6.: Distribution of bosons in the superfluid (SF) region, where the condensate density $n_0(r)$, the Bose-glass order parameter $q(r)$, and the thermal density $n_{\mathrm{th}}(r)$ contribute to the total density $n(r) = n_0(r) + q(r) + n_{\mathrm{th}}(r)$. In the Bose-glass region the condensate vanishes and in the thermal region all particles are in the excited states.

1.5. Outline of Thesis

In this thesis we investigate the equilibrium properties of one-dimensional and three-dimensional harmonically trapped dirty BEC. In particular, we work out the decomposition of total particle density into three components, namely, the condensate density, the density of fragmented local Bose-Einstein condensates within the respective minima of the random potential landscape, and the thermal density (see Fig. 1.6). We investigate the effect of both disorder and temperature fluctuations on the size of these three regions. To this end, we organize the thesis as follows:

In **Chapter 2**, we extend the non-perturbative mean-field approach of a three-dimensional weakly interacting homogeneous Bose gas in a delta-correlated disorder potential developed in Ref. [84] to the experimentally relevant trapped confinement via a semi-classical approximation and to a general number of spatial dimensions [97]. To accomplish this, we describe a trapped weakly interacting dirty Bose gas at finite temperature, then we develop, for this model, a general Hartree-Fock mean-field theory worked out on the basis of the replica method. At a certain level of this theory we restrict ourselves to a delta-correlated disorder potential and contact interaction potential for the dirty BEC model. Subsequently, we derive the free energy as well as the underlying self-consistency equations for the three components of the particle density, namely, the condensate density, the density of fragmented local Bose-Einstein condensates within the respective minima of the random potential landscape, and the thermal density. In addition, both three and one spatial dimension are treated as special cases.

In **Chapter 3**, we investigate in detail the self-consistency equations and the free energy derived from the Hartree-Fock mean-field theory for the quasi-one-dimensional dirty BEC at zero temperature [98]. We treat first the homogeneous case then the harmonic trap potential in Thomas-Fermi approximation for weak disorder. To this end we determine the particle density, which turns out to be decomposed into the condensate density and the density of fragmented minicondensates in the local minima of the disorder potential. Afterwards, we develop a numerical treatment for solving the underlying one-dimensional time-independent Gross-Pitaevskii equation and performing disorder-ensemble averages of the condensate wave function. In particular, we analyze quantitatively the emergence of mini-condensates in the local minima of the random potential, which occurs for weak disorder preferentially at the border of the condensate, while for intermediate disorder strength this happens in the trap center. In the intermediate disorder regime we additionally use a variational ansatz in order to describe analytically the numerically observed redistribution of the fragmented mini-condensates with increasing disorder strength. Furthermore, we tackle the delicate question whether a quantum phase transition from the superfluid to the Bose-glass phase exists in the one-dimensional dirty BEC.

In **Chapter 4**, we consider the dirty three-dimensional BEC system at zero temperature, so the thermal density vanishes [99]. This allows us, as a first step, to study the impact of the disorder on only the distribution of the condensate density and the Bose-glass order parameter, which is the

density of the bosons in the local minima of the disorder potential, as well as the corresponding Thomas-Fermi radii. We treat first the simpler homogeneous case, then we investigate the isotropic harmonically trapped one. Using the corresponding self-consistency equations obtained via the Hartree-Fock mean-field theory we investigate within the Thomas-Fermi approximation the existence of the Bose-glass phase. We additionally use a variational ansatz, whose results coincide qualitatively with the ones obtained via the Thomas-Fermi approximation. In particular, a first-order quantum phase transition from the superfluid phase to the Bose-glass phase is detected at a critical disorder strength, which agrees qualitatively with the literature. We also compare qualitatively the one-dimensional and the three-dimensional results obtained in Chapters 3 and 4, respectively. Furthermore, in a general triaxial harmonic trap, we investigate the geometric effect of different trap aspect ratios on the different properties of the dirty BEC system.

Then, we consider the three-dimensional BEC system to be at finite temperature in **Chapter 5** [99]. We restrict ourselves first to the dirty homogeneous case, after that to the trapped clean case. Afterwards we treat the disordered trapped case using the Thomas-Fermi approximation. This allows us to study the impact of both temperature and disorder on the respective components of the density as well as the Thomas-Fermi radii. In particular, three regions coexist, namely, the superfluid region, the Bose-glass region, and the thermal region. Furthermore, three phase transitions are detected, one from the superfluid to the Bose-glass phase, one from the Bose-glass to the thermal phase, where all bosons are in the excited states, and finally one directly from the superfluid to the thermal phase.

In **Chapter 6**, finally, we summarize our thesis and present the outlook.

2. Hartree-Fock Mean-Field Theory for Dirty Bosons

After having introduced the problem of dirty bosons in the previous chapter, we proceed now with describing a trapped weakly interacting Bose gas with disorder and working out its thermodynamic properties. In order to study this model, a general Hartree-Fock mean-field theory is developed using the replica method. At a certain level of this theory we restrict ourselves to a δ-correlated disorder potential for our BEC model. Subsequently, the thermodynamic properties are derived from solving the underlying self-consistency equations resulting for both three and one spatial dimension.

2.1. Disorder Potential

Usually, one studies bosons moving in a one-particle potential $U(\mathbf{x})$ which is fixed by an external magneto-optical trap. Here, however, we consider a different physical situation, where the one-particle potential $U(\mathbf{x})$ is fluctuating at each space point $\mathbf{x}$ (see Fig. 2.1). Such a frozen disorder potential serves for modeling superfluid helium in porous media [42, 100–102], where the pores can be modeled by randomly distributed local scatterers. In the following we assume for the disorder potential that it is homogeneous after the disorder ensemble average, i.e., after having performed the average $\overline{\bullet}$ over all possible realizations. Thus, the average value of the disorder potential, without loss of generality, will be assumed to vanish

$$\overline{U(\mathbf{x})} = 0. \tag{2.1}$$

Indeed, due to the homogeneity, the disorder ensemble average $\overline{U(\mathbf{x})}$ represents a constant, which can be absorbed into the chemical potential within a grand-canonical description. Furthermore, a homogeneous disorder potential has a correlation function, which depends on the difference of the space points:

$$\overline{U(\mathbf{x}_1)U(\mathbf{x}_2)} = D(\mathbf{x}_1 - \mathbf{x}_2)\,. \tag{2.2}$$

In case of a Gaussian correlated disorder in n spatial dimensions we have

$$D(\mathbf{x}_1 - \mathbf{x}_2) = D\,\frac{e^{-(\mathbf{x}_1-\mathbf{x}_2)^2/2\sigma^2}}{(2\pi\sigma^2)^{n/2}}\,, \tag{2.3}$$

where its correlation length σ can be identified with the average extension of the pores [103]. If one is not interested in a quantitative model for interpreting experimental measurements, one can neglect this spatial extension of the pores. In the limit of a vanishing correlation length σ we obtain a qualitative model for disordered bosons with a delta correlation:

$$D(\mathbf{x}_1 - \mathbf{x}_2) = D\,\delta(\mathbf{x}_1 - \mathbf{x}_2)\,. \tag{2.4}$$

Here the parameter D is proportional to the density of pores and represents a measure for the disorder strength.

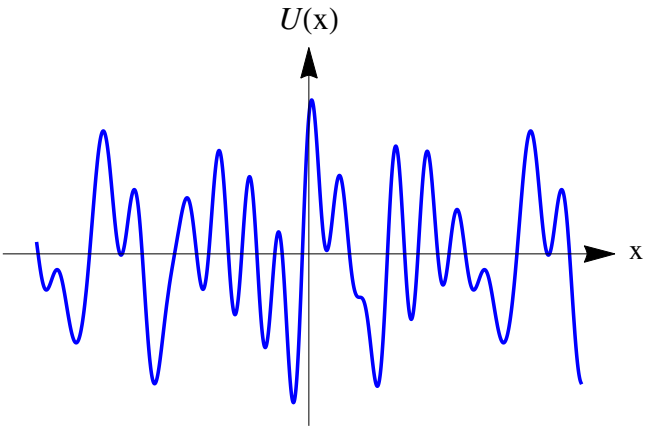

Figure 2.1.: Example for a realization of a frozen disorder potential $U(\mathbf{x})$ with vanishing expectation value (2.1).

As a next step we consider the probability distribution $P[U]$, which is a functional of the disorder potential $U(\mathbf{x})$. To this end we define expectation values such as (2.1) and (2.2) by the functional integral:

$$\overline{\bullet} = \int \mathcal{D}U \; \bullet \; P[U] \, . \tag{2.5}$$

Here the functional integral stands for an infinite product of ordinary integrals with respect to all possible values of the disorder potential $U(\mathbf{x})$ at all space points $\mathbf{x}$ [104, Chap.1]:

$$\int \mathcal{D}U = \prod_{\mathbf{x}} \int_{-\infty}^{\infty} dU(\mathbf{x}) \, . \tag{2.6}$$

The functional integral measure has to be chosen according to

$$\int \mathcal{D}U \, P[U] = 1 \, , \tag{2.7}$$

so that the probability distribution is normalized: $\overline{1} = 1$. Provided that $P[U]$ is Gaussian distributed, it is uniquely fixed by both expectation values (2.1) and (2.2) according to

$$P[U] = \exp\left\{ -\frac{1}{2} \int d^n x \int d^n x' \, D^{-1}(\mathbf{x} - \mathbf{x}') U(\mathbf{x}) U(\mathbf{x}') \right\} \, , \tag{2.8}$$

where the integral kernel $D^{-1}(\mathbf{x} - \mathbf{x}')$ represents the functional inverse of the correlation function (2.3):

$$\int d^n x \, D^{-1}(\mathbf{x}_1 - \mathbf{x}) D(\mathbf{x} - \mathbf{x}_2) = \delta(\mathbf{x}_1 - \mathbf{x}_2) \, . \tag{2.9}$$

For instance, we obtain for the δ-correlation (2.4) from (2.9) the integral kernel:

$$D^{-1}(\mathbf{x}_1 - \mathbf{x}_2) = \frac{1}{D} \, \delta(\mathbf{x}_1 - \mathbf{x}_2) \, . \tag{2.10}$$

We are interested in calculating higher moments of the probability distribution (2.8). To this end we consider the following generating functional

$$I[j] = \overline{\exp\left\{ \int d^n x \, j(\mathbf{x}) U(\mathbf{x}) \right\}}, \tag{2.11}$$

with the auxiliary current field $j(\mathbf{x})$ which leads according to (2.5) and (2.8) to the Gaussian functional integral

$$I[j] = \int \mathcal{D}U \, \exp\left\{ -\frac{1}{2} \int d^n x \int d^n x' \, D^{-1}(\mathbf{x} - \mathbf{x}') U(\mathbf{x}) U(\mathbf{x}') + \int d^n x \, j(\mathbf{x}) U(\mathbf{x}) \right\} \tag{2.12}$$

with the result [104, Chap.1]

$$I[j] = \exp\left\{\frac{1}{2}\int d^n x \int d^n x'\, D(\mathbf{x}-\mathbf{x}')j(\mathbf{x})j(\mathbf{x}')\right\} \quad . \tag{2.13}$$

The respective moments of the probability distribution (2.8) follow from successive functional derivatives of the generating functional (2.11) with respect to the auxiliary current field $j(\mathbf{x})$. Thus, we obtain for the first two moments

$$\overline{U(\mathbf{x}_1)} = \int \mathcal{D}U\, U(\mathbf{x}_1)\, \exp\left\{-\frac{1}{2}\int d^n x \int d^n x'\, D^{-1}(\mathbf{x}-\mathbf{x}')U(\mathbf{x})U(\mathbf{x}')\right\}, \tag{2.14}$$

$$\overline{U(\mathbf{x}_1)U(\mathbf{x}_2)} = \int \mathcal{D}U\, U(\mathbf{x}_1)U(\mathbf{x}_2)\, \exp\left\{-\frac{1}{2}\int d^n x \int d^n x'\, D^{-1}(\mathbf{x}-\mathbf{x}')U(\mathbf{x})U(\mathbf{x}')\right\} \tag{2.15}$$

by taking into account (2.12):

$$\overline{U(\mathbf{x}_1)} = \left.\frac{\delta I[j]}{\delta j(\mathbf{x}_1)}\right|_{j(\mathbf{x})=0}, \tag{2.16}$$

$$\overline{U(\mathbf{x}_1)U(\mathbf{x}_2)} = \left.\frac{\delta^2 I[j]}{\delta j(\mathbf{x}_1)\delta j(\mathbf{x}_2)}\right|_{j(\mathbf{x})=0}. \tag{2.17}$$

Inserting (2.13) into (2.16) and (2.17) leads then, indeed, to (2.1) and (2.2). In a similar way also higher correlation functions are evaluated. Whereas the expectation values of all odd products of disorder potentials vanish, those with an even product are evaluated according to the Wick rule. So we obtain, for instance:

$$\begin{aligned}\overline{U(\mathbf{x}_1)U(\mathbf{x}_2)U(\mathbf{x}_3)U(\mathbf{x}_4)} = {} & D(\mathbf{x}_1-\mathbf{x}_2)D(\mathbf{x}_3-\mathbf{x}_4) + D(\mathbf{x}_1-\mathbf{x}_3)D(\mathbf{x}_2-\mathbf{x}_4) \\ & + D(\mathbf{x}_1-\mathbf{x}_4)D(\mathbf{x}_2-\mathbf{x}_3)\,.\end{aligned} \tag{2.18}$$

In the case that the probability distribution $P[U]$ is not Gaussian, its generating functional (2.11) contains more than the second cumulant [105], so we have as a straight-forward generalization of (2.13):

$$I[j] = \exp\left\{\sum_{i=2}^{\infty}\frac{(-1)^{i-1}}{i!}\int d^n x_1 \cdots \int d^n x_i\, D^{(i)}(\mathbf{x}_1,\ldots,\mathbf{x}_i)j(\mathbf{x}_1)\cdots j(\mathbf{x}_i)\right\}, \tag{2.19}$$

where $D^{(i)}(\mathbf{x}_1,\ldots,\mathbf{x}_i)$ denotes the i^{th} cumulant. Indeed, Eq. (2.19) reduces with $D^{(2)}(\mathbf{x}_1,\mathbf{x}_2) = D(\mathbf{x}_1,\mathbf{x}_2)$ and $D^{(i)}(\mathbf{x}_1,\ldots,\mathbf{x}_i) = 0$ for $i \geq 3$ to Eq. (2.13).

2.2. Bose Model

A model of a three-dimensional weakly interacting homogeneous Bose gas in a δ-correlated disorder potential was studied within a Hartree-Fock mean-field theory in Ref. [84]. Motivated by this we extend this theory in the present thesis for a n-dimensional Bose gas in an arbitrary trap $V(\mathbf{x})$, a generally correlated disorder landscape $U(\mathbf{x})$ and a general interaction potential $V^{(\text{int})}(\mathbf{x}-\mathbf{x}')$ at finite temperature T. The starting point is the functional integral for the grand-canonical partition function

$$\mathcal{Z} = \oint\mathcal{D}\psi^* \oint\mathcal{D}\psi e^{-\mathcal{A}[\psi^*,\psi]/\hbar}, \tag{2.20}$$

where the integration is performed over all Bose fields $\psi^*(\mathbf{x},\tau), \psi(\mathbf{x},\tau)$ which are periodic in imaginary time τ, i.e., $\psi(\mathbf{x},\tau) = \psi(\mathbf{x},\tau+\hbar\beta)$. The Euclidean action is given in standard notation by

$$\begin{aligned}\mathcal{A}[\psi^*,\psi] = \int_0^{\hbar\beta} d\tau \int d^n x \Bigg\{ & \psi^*(\mathbf{x},\tau)\left[\hbar\frac{\partial}{\partial\tau} - \frac{\hbar^2}{2M}\boldsymbol{\Delta} + V(\mathbf{x}) + U(\mathbf{x}) - \mu\right]\psi(\mathbf{x},\tau) \\ & + \frac{1}{2}\int d^n x' \psi^*(\mathbf{x},\tau)\,\psi(\mathbf{x},\tau)\,V^{(\text{int})}(\mathbf{x}-\mathbf{x}')\psi^*(\mathbf{x}',\tau)\,\psi(\mathbf{x}',\tau)\Bigg\},\end{aligned} \tag{2.21}$$

where M denotes the particle mass and μ the chemical potential.

Note that, in order to guarantee the normal ordering within the functional integral, we should work with adjoint fields $\psi^*(\mathbf{x},\tau^+)$ with a shifted imaginary time $\tau^+ = \tau+\eta$ with $\eta \downarrow 0$ which is infinitesimally later than the imaginary time τ of the fields $\psi(\mathbf{x},\tau)$. However, for the sake of simplicity, we mainly use in the following the notation $\psi^*(\mathbf{x},\tau)$ and emphasize the normal ordering only when it is indispensable.

2.3. Replica Method

Now we apply the replica method which was already explained in Section 1.4. The $\mathcal{N}$-fold replication of the disordered Bose gas (2.20), (2.21) and a subsequent averaging with respect to the disorder potential $U(\mathbf{x})$ results in:

$$\begin{aligned}\overline{\mathcal{Z}^{\mathcal{N}}} &= \left\{\prod_{\alpha=1}^{\mathcal{N}} \oint \mathcal{D}\psi_\alpha^* \oint \mathcal{D}\psi_\alpha\right\} \exp\left\{\frac{-1}{\hbar}\int_0^{\hbar\beta} d\tau \int d^n x \sum_{\alpha=1}^{\mathcal{N}} \left\{\psi_\alpha^*(\mathbf{x},\tau)\left[\hbar\frac{\partial}{\partial\tau} - \frac{\hbar^2}{2M}\mathbf{\Delta} + \mathbf{V}(\mathbf{x}) - \mu\right]\right.\right. \\ &\quad \left.\left. \times\, \psi_\alpha(\mathbf{x},\tau) + \frac{1}{2}\int d^n x' \psi_\alpha^*(\mathbf{x},\tau)\,\psi_\alpha(\mathbf{x},\tau)\,V^{(\mathrm{int})}(\mathbf{x}-\mathbf{x}')\psi_\alpha^*(\mathbf{x}',\tau)\,\psi_\alpha(\mathbf{x}',\tau)\right\}\right\} \\ &\quad \times \overline{\exp\left\{\int d^n x \frac{-1}{\hbar}\int_0^{\hbar\beta} d\tau \sum_{\alpha=1}^{\mathcal{N}} \psi_\alpha^*(\mathbf{x},\tau)\psi_\alpha(\mathbf{x},\tau)U(\mathbf{x})\right\}}, \end{aligned} \tag{2.22}$$

where $\psi_\alpha^*(\mathbf{x},\tau)$, $\psi_\alpha(\mathbf{x},\tau)$ are the replica fields with the replica index α. Comparing (2.22) with (2.11) shows that the averaging with respect to the disorder potential $U(\mathbf{x})$ corresponds to the generating functional (2.19) with the auxiliary current field:

$$j(\mathbf{x}) = \frac{-1}{\hbar}\int_0^{\hbar\beta} d\tau \sum_{\alpha=1}^{\mathcal{N}} \psi_\alpha^*(\mathbf{x},\tau)\psi_\alpha(\mathbf{x},\tau)\,. \tag{2.23}$$

Therefore, the disordered Bose gas is described by the disorder averaged, replicated grand-canonical partition function

$$\overline{\mathcal{Z}^{\mathcal{N}}} = \left\{\prod_{\alpha=1}^{\mathcal{N}} \oint \mathcal{D}\psi_\alpha^* \oint \mathcal{D}\psi_\alpha\right\} e^{-\mathcal{A}^{(\mathcal{N})}[\psi^*,\psi]/\hbar}, \tag{2.24}$$

with the following replica action

$$\begin{aligned}\mathcal{A}^{(\mathcal{N})}[\psi^*,\psi] &= \int_0^{\hbar\beta} d\tau \int d^n x \sum_{\alpha=1}^{\mathcal{N}} \left\{\psi_\alpha^*(\mathbf{x},\tau)\left[\hbar\frac{\partial}{\partial\tau} - \frac{\hbar^2}{2M}\mathbf{\Delta} + V(\mathbf{x}) - \mu\right]\psi_\alpha(\mathbf{x},\tau)\right. \\ &\quad \left. + \frac{1}{2}\int d^n x' \psi_\alpha^*(\mathbf{x},\tau)\,\psi_\alpha(\mathbf{x},\tau)\,V^{(\mathrm{int})}(\mathbf{x}-\mathbf{x}')\psi_\alpha^*(\mathbf{x}',\tau)\,\psi_\alpha(\mathbf{x}',\tau)\right\} \\ &\quad + \sum_{i=2}^{\infty}\frac{1}{i!}\left(\frac{-1}{\hbar}\right)^{i-1}\int_0^{\hbar\beta} d\tau_1 \cdots \int_0^{\hbar\beta} d\tau_i \int d^n x_1 \cdots \int d^n x_i \\ &\quad \times \sum_{\alpha_1=1}^{\mathcal{N}} \cdots \sum_{\alpha_i=1}^{\mathcal{N}} D^{(i)}(\mathbf{x}_1,\ldots,\mathbf{x}_i)\,|\psi_{\alpha_1}(\mathbf{x}_1,\tau_1)|^2 \cdots |\psi_{\alpha_i}(\mathbf{x}_i,\tau_i)|^2\,. \end{aligned} \tag{2.25}$$

For any experimental realistic disorder potential the dominant cumulant is of second order. Therefore, it is physically justified to restrict ourselves in the following to the second cumulant, i.e., only $D^{(2)}(\mathbf{x}_1-\mathbf{x}_2) = D(\mathbf{x}_1-\mathbf{x}_2)$ is assumed to contribute to the replicated action (2.25). Thus, we conclude that, in this case, disorder leads to a residual attractive interaction between the replica fields $\psi_\alpha^*(\mathbf{x},\tau)$, $\psi_\alpha(\mathbf{x},\tau)$ which is, in general, bilocal in both space and imaginary time. With this simplification the

replicated action (2.25) reduces to:

$$\begin{aligned}\mathcal{A}^{(\mathcal{N})}[\psi^*,\psi] &= \int_0^{\hbar\beta} d\tau \int d^n x \sum_{\alpha=1}^{\mathcal{N}} \left\{ \psi_\alpha^*(\mathbf{x},\tau) \left[\hbar\frac{\partial}{\partial\tau} - \frac{\hbar^2}{2M}\mathbf{\Delta} + V(\mathbf{x}) - \mu \right] \psi_\alpha(\mathbf{x},\tau) \right. \\ &\left. + \frac{1}{2}\int d^n x' \psi_\alpha^*(\mathbf{x},\tau)\, \psi_\alpha(\mathbf{x},\tau)\, V^{(\mathrm{int})}(\mathbf{x}-\mathbf{x}') \psi_\alpha^*(\mathbf{x}',\tau)\, \psi_\alpha(\mathbf{x}',\tau) \right\} \\ &- \frac{1}{2\hbar}\int_0^{\hbar\beta} d\tau \int_0^{\hbar\beta} d\tau' \int d^n x \int d^n x' \sum_{\alpha=1}^{\mathcal{N}} \sum_{\alpha'=1}^{\mathcal{N}} D(\mathbf{x}-\mathbf{x}') \\ &\times \psi_\alpha^*(\mathbf{x},\tau)\psi_\alpha(\mathbf{x},\tau)\psi_{\alpha'}^*(\mathbf{x}',\tau')\psi_{\alpha'}(\mathbf{x}',\tau')\,. \end{aligned} \tag{2.26}$$

2.4. Hartree-Fock Mean-Field Equations

Now we apply standard methods for developing a self-consistent mean-field approximation [106, 107] in order to derive Hartree-Fock mean-field equations for the Bose gas in a random potential. To this end we use the Bogoliubov approximation, i.e., we split the Bose fields $\psi_\alpha^*(\mathbf{x},\tau)$, $\psi_\alpha(\mathbf{x},\tau)$ into their background $\Psi_\alpha^*(\mathbf{x},\tau)$, $\Psi_\alpha(\mathbf{x},\tau)$ describing the condensate wave function and the fluctuations $\delta\psi_\alpha^*(\mathbf{x},\tau)$, $\delta\psi_\alpha(\mathbf{x},\tau)$ describing the non-condensed fractions:

$$\psi_\alpha^*(\mathbf{x},\tau) = \Psi_\alpha^*(\mathbf{x},\tau) + \delta\psi_\alpha^*(\mathbf{x},\tau)\,, \qquad \psi_\alpha(\mathbf{x},\tau) = \Psi_\alpha(\mathbf{x},\tau) + \delta\psi_\alpha(\mathbf{x},\tau)\,. \tag{2.27}$$

Thus, the replica action (2.26) decomposes according to:

$$\mathcal{A}^{(\mathcal{N})}[\psi^*,\psi] = \sum_{k=0}^{4} \mathcal{A}^{(\mathcal{N},k)}[\delta\psi^*,\delta\psi]\,, \tag{2.28}$$

where $\mathcal{A}^{(\mathcal{N},k)}[\delta\psi^*,\delta\psi]$ denotes all terms that contain fluctuations $\delta\psi_\alpha^*(\mathbf{x},\tau)$, $\delta\psi_\alpha(\mathbf{x},\tau)$ of the k^{th} power. Then, we approximate the higher nonlinear terms $k=3$ and $k=4$ within a Gaussian factorization, where the expectation value $\langle\,\bullet\,\rangle$ is determined self-consistently below. As we restrict ourselves to a Hartree-Fock mean-field theory, we only keep normal correlations $\langle\delta\psi_\alpha(\mathbf{x},\tau)\,\delta\psi_{\alpha'}^*(\mathbf{x}',\tau')\rangle$ and neglect all anomalous correlations of the form $\langle\delta\psi_\alpha(\mathbf{x},\tau)\,\delta\psi_{\alpha'}(\mathbf{x}',\tau')\rangle$ or $\langle\delta\psi_\alpha^*(\mathbf{x},\tau)\,\delta\psi_{\alpha'}^*(\mathbf{x}',\tau')\rangle$. With this we obtain for the cubic terms in the fluctuations:

$$\delta\psi_\alpha^*(\mathbf{x},\tau)\,\delta\psi_\alpha(\mathbf{x},\tau)\,\delta\psi_{\alpha'}(\mathbf{x}',\tau') \approx \langle\delta\psi_\alpha^*(\mathbf{x},\tau^+)\,\delta\psi_\alpha(\mathbf{x},\tau)\rangle\,\delta\psi_{\alpha'}(\mathbf{x}',\tau') + \langle\delta\psi_\alpha^*(\mathbf{x},\tau)\,\delta\psi_{\alpha'}(\mathbf{x}',\tau')\rangle\,\delta\psi_\alpha(\mathbf{x},\tau) \tag{2.29}$$

together with its complex conjugate

$$\delta\psi_\alpha(\mathbf{x},\tau)\,\delta\psi_\alpha^*(\mathbf{x},\tau)\,\delta\psi_{\alpha'}^*(\mathbf{x}',\tau') \approx \langle\delta\psi_\alpha(\mathbf{x},\tau^+)\,\delta\psi_\alpha^*(\mathbf{x},\tau)\rangle\,\delta\psi_{\alpha'}^*(\mathbf{x}',\tau') + \langle\delta\psi_\alpha(\mathbf{x},\tau)\,\delta\psi_{\alpha'}^*(\mathbf{x}',\tau')\rangle\,\delta\psi_\alpha^*(\mathbf{x},\tau) \tag{2.30}$$

and, correspondingly, the fourth order terms in the fluctuations reduce to:

$$\begin{aligned}&\delta\psi_\alpha^*(\mathbf{x},\tau)\,\delta\psi_\alpha(\mathbf{x},\tau)\,\delta\psi_{\alpha'}^*(\mathbf{x}',\tau')\,\delta\psi_{\alpha'}(\mathbf{x}',\tau') \\ &\approx \langle\delta\psi_\alpha^*(\mathbf{x},\tau^+)\,\delta\psi_\alpha(\mathbf{x},\tau)\rangle\,\delta\psi_{\alpha'}^*(\mathbf{x}',\tau')\,\delta\psi_{\alpha'}(\mathbf{x}',\tau') + \langle\delta\psi_{\alpha'}^*(\mathbf{x}',\tau'^+)\,\delta\psi_{\alpha'}(\mathbf{x}',\tau')\rangle\,\delta\psi_\alpha^*(\mathbf{x},\tau)\,\delta\psi_\alpha(\mathbf{x},\tau) \\ &+\langle\delta\psi_\alpha^*(\mathbf{x},\tau)\,\delta\psi_{\alpha'}(\mathbf{x}',\tau')\rangle\,\delta\psi_\alpha(\mathbf{x},\tau)\,\delta\psi_{\alpha'}^*(\mathbf{x}',\tau') + \langle\delta\psi_\alpha(\mathbf{x},\tau)\,\delta\psi_{\alpha'}^*(\mathbf{x}',\tau')\rangle\rangle\,\delta\psi_\alpha^*(\mathbf{x},\tau)\,\delta\psi_{\alpha'}(\mathbf{x}',\tau') \\ &-\langle\delta\psi_\alpha^*(\mathbf{x},\tau^+)\,\delta\psi_\alpha(\mathbf{x},\tau)\rangle\,\langle\delta\psi_{\alpha'}^*(\mathbf{x}',\tau'^+)\,\delta\psi_{\alpha'}(\mathbf{x}',\tau')\rangle - \langle\delta\psi_\alpha^*(\mathbf{x},\tau)\,\delta\psi_{\alpha'}(\mathbf{x}',\tau')\rangle\,\langle\delta\psi_\alpha(\mathbf{x},\tau)\,\delta\psi_{\alpha'}^*(\mathbf{x}',\tau')\rangle\,. \end{aligned} \tag{2.31}$$

Here we have used τ^+ as an imaginary time which is infinitesimally later than τ in order to guarantee the normal ordering of the fluctuations within the respective expectation values. Therefore, the Gaussian factorization procedure for a Hartree-Fock mean-field theory leads to an approximation of the replica action (2.26):

$$\mathcal{A}^{(\mathcal{N})}[\psi^*,\psi] \approx \tilde{\mathcal{A}}^{(\mathcal{N},0)}[\delta\psi^*,\delta\psi] + \tilde{\mathcal{A}}^{(\mathcal{N},1)}[\delta\psi^*,\delta\psi] + \tilde{\mathcal{A}}^{(\mathcal{N},2)}[\delta\psi^*,\delta\psi]\,, \tag{2.32}$$

where $\tilde{\mathcal{A}}^{(\mathcal{N},k)}[\delta\psi^*,\delta\psi]$ denotes the k^{th}-order terms of the replica action (2.26). The fluctuations in (2.29)–(2.31) can be expressed in terms of the following mean-fields:

$$
\begin{aligned}
Q_{\alpha\alpha'}(\mathbf{x},\tau;\mathbf{x}',\tau') &= \Psi_\alpha(\mathbf{x},\tau)\,\Psi^*_{\alpha'}(\mathbf{x}',\tau') + \langle \delta\psi_\alpha(\mathbf{x},\tau)\,\delta\psi^*_{\alpha'}(\mathbf{x}',\tau')\rangle\,, && (2.33)\\
Q^*_{\alpha\alpha'}(\mathbf{x},\tau;\mathbf{x}',\tau') &= Q_{\alpha'\alpha}(\mathbf{x}',\tau';\mathbf{x},\tau)\,, && (2.34)\\
\Sigma_\alpha(\mathbf{x},\tau) &= Q_{\alpha\alpha}(\mathbf{x},\tau;\mathbf{x},\tau^+)\,. && (2.35)
\end{aligned}
$$

The first term of the replica action (2.32) is independent of the fluctuations $\delta\psi^*_\alpha(\mathbf{x},\tau)$, $\delta\psi_\alpha(\mathbf{x},\tau)$ and reads:

$$
\begin{aligned}
\tilde{\mathcal{A}}^{(\mathcal{N},0)}[\delta\psi^*,\delta\psi] = \int_0^{\hbar\beta} d\tau \int d^n x \sum_{\alpha=1}^{\mathcal{N}} \Bigg\{ & \Psi^*_\alpha(\mathbf{x},\tau)\left[\hbar\frac{\partial}{\partial\tau} - \frac{\hbar^2}{2M}\boldsymbol{\Delta} + V(\mathbf{x}) - \mu\right]\Psi_\alpha(\mathbf{x},\tau)\\
& - \frac{1}{2}\int d^n x' V^{(\text{int})}(\mathbf{x}-\mathbf{x}')\Big[\Psi^*_\alpha(\mathbf{x},\tau)\Psi_\alpha(\mathbf{x},\tau)\Psi^*_\alpha(\mathbf{x}',\tau)\Psi_\alpha(\mathbf{x}',\tau) + \Sigma_\alpha(\mathbf{x},\tau)\,\Sigma_\alpha(\mathbf{x}',\tau)\\
& - 2\Sigma_\alpha(\mathbf{x},\tau)\,\Psi^*_\alpha(\mathbf{x}',\tau)\Psi_\alpha(\mathbf{x}',\tau) + Q_{\alpha\alpha}(\mathbf{x},\tau;\mathbf{x}',\tau)Q^*_{\alpha\alpha}(\mathbf{x},\tau;\mathbf{x}',\tau)\\
& - Q_{\alpha\alpha}(\mathbf{x},\tau;\mathbf{x}',\tau)\Psi_\alpha(\mathbf{x}',\tau)\Psi^*_\alpha(\mathbf{x},\tau) - Q^*_{\alpha\alpha}(\mathbf{x},\tau;\mathbf{x}',\tau)\Psi_\alpha(\mathbf{x},\tau)\Psi^*_\alpha(\mathbf{x}',\tau)\Big]\Bigg\}\\
& + \frac{1}{2\hbar}\int_0^{\hbar\beta} d\tau \int_0^{\hbar\beta} d\tau' \int d^n x \int d^n x' \sum_{\alpha=1}^{\mathcal{N}}\sum_{\alpha'=1}^{\mathcal{N}} D(\mathbf{x}-\mathbf{x}')\\
& \times \Big\{\Psi^*_\alpha(\mathbf{x},\tau)\Psi_\alpha(\mathbf{x},\tau)\Psi^*_{\alpha'}(\mathbf{x}',\tau')\Psi_{\alpha'}(\mathbf{x}',\tau') + \Sigma_\alpha(\mathbf{x},\tau)\,\Sigma_{\alpha'}(\mathbf{x}',\tau')\\
& - 2\Sigma_\alpha(\mathbf{x},\tau)\,\Psi^*_{\alpha'}(\mathbf{x}',\tau')\Psi_{\alpha'}(\mathbf{x}',\tau') + Q_{\alpha\alpha'}(\mathbf{x},\tau;\mathbf{x}',\tau')Q^*_{\alpha\alpha'}(\mathbf{x},\tau;\mathbf{x}',\tau')\\
& - Q_{\alpha\alpha'}(\mathbf{x},\tau;\mathbf{x}',\tau')\Psi_{\alpha'}(\mathbf{x}',\tau')\Psi^*_\alpha(\mathbf{x},\tau) - Q^*_{\alpha\alpha'}(\mathbf{x},\tau;\mathbf{x}',\tau')\Psi_\alpha(\mathbf{x},\tau)\Psi^*_{\alpha'}(\mathbf{x}',\tau')\Big\}\,,
\end{aligned}
\tag{2.36}
$$

whereas the second term of (2.32) is linear in the fluctuations $\delta\psi^*_\alpha(\mathbf{x},\tau)$, $\delta\psi_\alpha(\mathbf{x},\tau)$:

$$
\begin{aligned}
\tilde{\mathcal{A}}^{(\mathcal{N},1)}[\delta\psi^*,\delta\psi] = \int_0^{\hbar\beta} d\tau \int d^n x \sum_{\alpha=1}^{\mathcal{N}} \Bigg\{ & \delta\psi^*_\alpha(\mathbf{x},\tau)\left[\hbar\frac{\partial}{\partial\tau} - \frac{\hbar^2}{2M}\boldsymbol{\Delta} + V(\mathbf{x}) - \mu\right]\Psi_\alpha(\mathbf{x},\tau)\\
& + \Psi^*_\alpha(\mathbf{x},\tau)\left[\hbar\frac{\partial}{\partial\tau} - \frac{\hbar^2}{2M}\boldsymbol{\Delta} + V(\mathbf{x}) - \mu\right]\delta\psi_\alpha(\mathbf{x},\tau) + \int d^n x' V^{(\text{int})}(\mathbf{x}-\mathbf{x}')\\
& \times \Big[\Sigma_\alpha(\mathbf{x}',\tau)\Psi_\alpha(\mathbf{x},\tau)\delta\psi^*_\alpha(\mathbf{x},\tau) + Q_{\alpha\alpha}(\mathbf{x},\tau;\mathbf{x}',\tau)\Psi_\alpha(\mathbf{x}',\tau)\delta\psi^*_\alpha(\mathbf{x},\tau)\\
& - \Psi_\alpha(\mathbf{x},\tau)\Psi_\alpha(\mathbf{x}',\tau)\Psi^*_\alpha(\mathbf{x}',\tau)\delta\psi^*_\alpha(\mathbf{x},\tau) - \Psi_\alpha(\mathbf{x}',\tau)\Psi^*_\alpha(\mathbf{x},\tau)\Psi^*_\alpha(\mathbf{x}',\tau)\delta\psi_\alpha(\mathbf{x},\tau)\\
& + Q^*_{\alpha\alpha}(\mathbf{x},\tau;\mathbf{x}',\tau)\Psi^*_\alpha(\mathbf{x}',\tau)\delta\psi_\alpha(\mathbf{x},\tau) + \Sigma_\alpha(\mathbf{x}',\tau)\Psi^*_\alpha(\mathbf{x},\tau)\delta\psi_\alpha(\mathbf{x},\tau)\Big]\Bigg\}\\
& - \frac{1}{\hbar}\int_0^{\hbar\beta} d\tau \int_0^{\hbar\beta} d\tau' \int d^n x \int d^n x' \sum_{\alpha=1}^{\mathcal{N}}\sum_{\alpha'=1}^{\mathcal{N}} D(\mathbf{x}-\mathbf{x}')\\
& \times \Big\{\Sigma_{\alpha'}(\mathbf{x}',\tau')\Psi_\alpha(\mathbf{x},\tau)\delta\psi^*_\alpha(\mathbf{x},\tau) + Q_{\alpha\alpha'}(\mathbf{x},\tau;\mathbf{x}',\tau')\Psi_{\alpha'}(\mathbf{x}',\tau')\delta\psi^*_\alpha(\mathbf{x},\tau)\\
& - \Psi_\alpha(\mathbf{x},\tau)\Psi_{\alpha'}(\mathbf{x}',\tau')\Psi^*_{\alpha'}(\mathbf{x}',\tau')\delta\psi^*_\alpha(\mathbf{x},\tau) - \Psi_{\alpha'}(\mathbf{x}',\tau')\Psi^*_\alpha(\mathbf{x},\tau)\Psi^*_{\alpha'}(\mathbf{x}',\tau')\delta\psi_\alpha(\mathbf{x},\tau)\\
& + Q^*_{\alpha\alpha'}(\mathbf{x},\tau;\mathbf{x}',\tau')\Psi^*_{\alpha'}(\mathbf{x}',\tau')\delta\psi_\alpha(\mathbf{x},\tau) + \Sigma_{\alpha'}(\mathbf{x}',\tau')\Psi^*_\alpha(\mathbf{x},\tau)\delta\psi_\alpha(\mathbf{x},\tau)\Big\}\,,
\end{aligned}
\tag{2.37}
$$

and the third term of (2.32) is quadratic in the fluctuations:

$$\begin{aligned}\tilde{\mathcal{A}}^{(\mathcal{N},2)}[\delta\psi^*,\delta\psi] &= \int_0^{\hbar\beta} d\tau \int d^n x \sum_{\alpha=1}^{\mathcal{N}} \Bigg\{ \delta\psi_\alpha^*(\mathbf{x},\tau)\left[\hbar\frac{\partial}{\partial\tau} - \frac{\hbar^2}{2M}\mathbf{\Delta} + V(\mathbf{x}) - \mu\right]\delta\psi_\alpha(\mathbf{x},\tau) \\ &+\frac{1}{2}\int d^n x' V^{(\mathrm{int})}(\mathbf{x}-\mathbf{x}')\Bigg[2\Sigma_\alpha(\mathbf{x},\tau)\,\delta\psi_\alpha^*(\mathbf{x}',\tau)\,\delta\psi_\alpha(\mathbf{x}',\tau) \\ &+Q_{\alpha\alpha}(\mathbf{x},\tau;\mathbf{x}',\tau)\,\delta\psi_\alpha(\mathbf{x}',\tau)\,\delta\psi_\alpha^*(\mathbf{x},\tau) + Q_{\alpha\alpha}^*(\mathbf{x},\tau;\mathbf{x}',\tau)\,\delta\psi_\alpha(\mathbf{x},\tau)\,\delta\psi_\alpha^*(\mathbf{x}',\tau)\Bigg]\Bigg\} \\ &-\frac{1}{2\hbar}\int_0^{\hbar\beta} d\tau \int_0^{\hbar\beta} d\tau' \int d^n x \int d^n x' \sum_{\alpha=1}^{\mathcal{N}}\sum_{\alpha'=1}^{\mathcal{N}} D(\mathbf{x}-\mathbf{x}') \\ &\times\Bigg\{2\,\Sigma_\alpha(\mathbf{x},\tau)\,\delta\psi_{\alpha'}^*(\mathbf{x}',\tau')\,\delta\psi_{\alpha'}(\mathbf{x}',\tau') + Q_{\alpha\alpha'}(\mathbf{x},\tau;\mathbf{x}',\tau')\,\delta\psi_{\alpha'}(\mathbf{x}',\tau')\,\delta\psi_\alpha^*(\mathbf{x},\tau) \\ &+Q_{\alpha\alpha'}^*(\mathbf{x},\tau;\mathbf{x}',\tau')\,\delta\psi_\alpha(\mathbf{x},\tau)\,\delta\psi_{\alpha'}^*(\mathbf{x}',\tau')\Bigg\}. \end{aligned} \tag{2.38}$$

Following the field-theoretic background field method [108,109] the first-order terms $\tilde{\mathcal{A}}^{(\mathcal{N},1)}[\delta\psi^*,\delta\psi]$ can be neglected as the background fields $\Psi_\alpha^*(\mathbf{x},\tau)$, $\Psi_\alpha(\mathbf{x},\tau)$ are later on determined from extremising $\tilde{\mathcal{A}}^{(\mathcal{N},0)}[\delta\psi^*,\delta\psi]$.

Inserting (2.32) together with (2.36) and (2.38) into (2.24) leads to the replicated effective potential:

$$V_{\mathrm{eff}}^{(\mathcal{N})} = -\frac{1}{\beta}\ln\overline{\mathcal{Z}^{\mathcal{N}}}, \tag{2.39}$$

which is given by:

$$V_{\mathrm{eff}}^{(\mathcal{N})} = \frac{\tilde{\mathcal{A}}^{(\mathcal{N},0)}[\delta\psi^*,\delta\psi]}{\hbar\beta} - \frac{1}{\beta}\ln\left\{\left[\prod_{\alpha=1}^{\mathcal{N}}\oint\mathcal{D}\delta\psi_\alpha^*\oint\mathcal{D}\delta\psi_\alpha\right]e^{-\tilde{\mathcal{A}}^{(\mathcal{N},2)}[\delta\psi^*,\delta\psi]/\hbar}\right\}. \tag{2.40}$$

It represents a functional of all mean-fields: $V_{\mathrm{eff}}^{(\mathcal{N})} = V_{\mathrm{eff}}^{(\mathcal{N})}[\Psi^*,\,\Psi,\,Q^*,\,Q,\,\Sigma]$. Extremising (2.40) with respect to the mean-fields $Q_{\alpha\alpha'}^*(\mathbf{x},\tau;\mathbf{x}',\tau')$, $Q_{\alpha\alpha'}(\mathbf{x},\tau;\mathbf{x}',\tau')$, and $\Sigma_\alpha(\mathbf{x},\tau)$ reproduces their definitions (2.33)–(2.35), where the expectation values turn out to be calculated with respect to the fluctuation action (2.38):

$$\langle\ \bullet\ \rangle = \frac{\left\{\prod_{\alpha=1}^{\mathcal{N}}\oint\mathcal{D}\delta\psi_\alpha^*\oint\mathcal{D}\delta\psi_\alpha\right\}\ \bullet\ e^{-\tilde{\mathcal{A}}^{(\mathcal{N},2)}[\delta\psi^*,\delta\psi]/\hbar}}{\left\{\prod_{\alpha=1}^{\mathcal{N}}\oint\mathcal{D}\delta\psi_\alpha^*\oint\mathcal{D}\delta\psi_\alpha\right\}e^{-\tilde{\mathcal{A}}^{(\mathcal{N},2)}[\delta\psi^*,\delta\psi]/\hbar}}. \tag{2.41}$$

Furthermore, an extremisation of the replicated effective potential (2.40) with respect to the background fields $\Psi_\alpha^*(\mathbf{x},\tau)$, $\Psi_\alpha(\mathbf{x},\tau)$ leads to the Gross-Pitaevskii equation:

$$\begin{aligned}&\left\{\hbar\frac{\partial}{\partial\tau} - \frac{\hbar^2}{2M}\mathbf{\Delta} + V(\mathbf{x}) - \mu\right\}\Psi_\alpha(\mathbf{x},\tau) - \int d^n x' V^{(\mathrm{int})}(\mathbf{x}-\mathbf{x}') \\ &\times\Bigg[\Psi_\alpha(\mathbf{x},\tau)\Psi_\alpha^*(\mathbf{x}',\tau)\Psi_\alpha(\mathbf{x}',\tau) - \Sigma_\alpha(\mathbf{x},\tau)\,\Psi_\alpha(\mathbf{x}',\tau) - Q_{\alpha\alpha}(\mathbf{x},\tau;\mathbf{x}',\tau)\Psi_\alpha(\mathbf{x}',\tau)\Bigg] \\ &= \frac{1}{\hbar}\int_0^{\hbar\beta} d\tau' \int d^n x' \sum_{\alpha'=1}^{N} D(\mathbf{x}-\mathbf{x}')\Bigg\{\Bigg[\Sigma_{\alpha'}(\mathbf{x}',\tau') - \Psi_{\alpha'}(\mathbf{x}',\tau')\Psi_{\alpha'}^*(\mathbf{x}',\tau')\Bigg]\Psi_\alpha(\mathbf{x},\tau) \\ &+Q_{\alpha\alpha'}(\mathbf{x},\tau;\mathbf{x}',\tau')\Psi_{\alpha'}(\mathbf{x}',\tau')\Bigg\} \end{aligned} \tag{2.42}$$

and its complex conjugate. Indeed, we observe that $\tilde{\mathcal{A}}^{(\mathcal{N},1)}[\delta\psi^*, \delta\psi]$ in (2.37) vanishes due to the Gross-Pitaevskii equation (2.42) and its complex conjugate which determine the background fields $\Psi_\alpha(\mathbf{x},\tau)$, $\Psi^*_\alpha(\mathbf{x},\tau)$.

2.5. Replica Symmetry

Now we apply the replica symmetry, where we assume that all the respective replica indices α contribute in the same way. Furthermore, the dirty boson problem is translationally invariant in imaginary time. With this we get for the background:

$$\Psi_\alpha(\mathbf{x},\tau) = \Psi(\mathbf{x}), \quad \Psi^*_\alpha(\mathbf{x},\tau) = \Psi^*(\mathbf{x}), \quad \Sigma_\alpha(\mathbf{x},\tau) = \Sigma(\mathbf{x}) \tag{2.43}$$

and for the mean fields:

$$Q_{\alpha\alpha'}(\mathbf{x},\tau;\mathbf{x}',\tau') = Q\left(\mathbf{x}-\mathbf{x}', \frac{\mathbf{x}+\mathbf{x}'}{2}; \tau-\tau'\right)\delta_{\alpha\alpha'} + q\left(\mathbf{x}-\mathbf{x}', \frac{\mathbf{x}+\mathbf{x}'}{2}; \tau-\tau'\right) + \Psi^*(\mathbf{x})\Psi(\mathbf{x}), \tag{2.44}$$

$$Q^*_{\alpha\alpha'}(\mathbf{x},\tau;\mathbf{x}',\tau') = Q^*\left(\mathbf{x}-\mathbf{x}', \frac{\mathbf{x}+\mathbf{x}'}{2}; \tau-\tau'\right)\delta_{\alpha\alpha'} + q^*\left(\mathbf{x}-\mathbf{x}', \frac{\mathbf{x}+\mathbf{x}'}{2}; \tau-\tau'\right) + \Psi^*(\mathbf{x})\Psi(\mathbf{x}). \tag{2.45}$$

In (2.44) and (2.45) we perform a Fourier-Matsubara decomposition with respect to the differences in space and time, i.e., $\mathbf{x}-\mathbf{x}'$ and $\tau-\tau'$. Furthermore, we assume within a semi-classical approximation that the dependence on the center of mass coordinate $(\mathbf{x}+\mathbf{x}')/2$ is smooth, so we get

$$Q(\mathbf{x}-\mathbf{x}', \frac{\mathbf{x}+\mathbf{x}'}{2}; \tau-\tau') = \int \frac{d^nk}{(2\pi)^n} e^{i\mathbf{k}(\mathbf{x}-\mathbf{x}')} \frac{1}{\hbar\beta} \sum_{m=-\infty}^{\infty} e^{-i\omega_m(\tau-\tau')} Q_m(\mathbf{k}, \frac{\mathbf{x}+\mathbf{x}'}{2}), \tag{2.46}$$

$$q(\mathbf{x}-\mathbf{x}', \frac{\mathbf{x}+\mathbf{x}'}{2}; \tau-\tau') = \int \frac{d^nk}{(2\pi)^n} e^{i\mathbf{k}(\mathbf{x}-\mathbf{x}')} \frac{1}{\hbar\beta} \sum_{m=-\infty}^{\infty} e^{-i\omega_m(\tau-\tau')} q_m(\mathbf{k}, \frac{\mathbf{x}+\mathbf{x}'}{2}), \tag{2.47}$$

and their complex conjugate, where $\omega_m = 2\pi m/(\hbar\beta)$ denote the bosonic Matsubara frequencies and $\mathbf{k}$ the wave vector.

Using this ansatz, we have to evaluate the expectation values in the mean-field equations (2.33)–(2.35) and (2.42). To this end we note that the fluctuation action (2.38) is of the general form

$$\begin{aligned}\tilde{\mathcal{A}}^{(\mathcal{N},2)}[\delta\psi^*, \delta\psi] = \int_0^{\hbar\beta} d\tau \int_0^{\hbar\beta} d\tau' \int d^nx \int d^nx' \sum_{\alpha=1}^{\mathcal{N}} \sum_{\alpha'=1}^{\mathcal{N}} \\ \frac{1}{2}\Big(\delta\psi^*_\alpha(\mathbf{x},\tau),\, \delta\psi_\alpha(\mathbf{x},\tau)\Big) G^{-1}_{\alpha\alpha'}\left(\mathbf{x}-\mathbf{x}', \frac{\mathbf{x}+\mathbf{x}'}{2}; \tau-\tau'\right) \begin{pmatrix} \delta\psi_{\alpha'}(\mathbf{x}',\tau') \\ \delta\psi^*_{\alpha'}(\mathbf{x}',\tau') \end{pmatrix},\end{aligned} \tag{2.48}$$

where the integral kernel decomposes according to

$$\begin{aligned}G^{-1}_{\alpha\alpha'}\left(\mathbf{x}-\mathbf{x}', \frac{\mathbf{x}+\mathbf{x}'}{2}; \tau-\tau'\right) = \begin{pmatrix} a(\mathbf{x}-\mathbf{x}', \frac{\mathbf{x}+\mathbf{x}'}{2}; \tau-\tau') & 0 \\ 0 & a^*(\mathbf{x}-\mathbf{x}', \frac{\mathbf{x}+\mathbf{x}'}{2}; \tau-\tau') \end{pmatrix} \delta_{\alpha\alpha'} \\ + \begin{pmatrix} b(\mathbf{x}-\mathbf{x}', \frac{\mathbf{x}+\mathbf{x}'}{2}; \tau-\tau') & 0 \\ 0 & b^*(\mathbf{x}-\mathbf{x}', \frac{\mathbf{x}+\mathbf{x}'}{2}; \tau-\tau') \end{pmatrix},\end{aligned} \tag{2.49}$$

with the abbreviations

$$\begin{aligned}a\left(\mathbf{x}-\mathbf{x}', \frac{\mathbf{x}+\mathbf{x}'}{2}; \tau-\tau'\right) = \left[\hbar\frac{\partial}{\partial\tau'} - \frac{\hbar^2}{2M}\boldsymbol{\Delta}' + V(\mathbf{x}') - \mu + \Sigma(\mathbf{x}') \int d^Dx'' V^{(\mathrm{int})}(\mathbf{x}'')\right] \delta(\mathbf{x}-\mathbf{x}') \\ \times \delta(\tau-\tau') - \frac{1}{\hbar} D(\mathbf{x}-\mathbf{x}') \left[Q\left(\mathbf{x}-\mathbf{x}', \frac{\mathbf{x}+\mathbf{x}'}{2}, \tau-\tau'\right) + \mathcal{N}\Sigma(\mathbf{x}')\right] + V^{(\mathrm{int})}(\mathbf{x}-\mathbf{x}')\delta(\tau-\tau') \\ \times \left[\Psi^*(\mathbf{x})\Psi(\mathbf{x}) + q\left(\mathbf{x}-\mathbf{x}', \frac{\mathbf{x}+\mathbf{x}'}{2}, \tau-\tau'\right) + Q\left(\mathbf{x}-\mathbf{x}', \frac{\mathbf{x}+\mathbf{x}'}{2}, \tau-\tau'\right)\right]\end{aligned} \tag{2.50}$$

and

$$b\left(\mathbf{x}-\mathbf{x}',\frac{\mathbf{x}+\mathbf{x}'}{2};\tau-\tau'\right)=-\frac{1}{\hbar}D(\mathbf{x}-\mathbf{x}')\left[\Psi^*(\mathbf{x})\Psi(\mathbf{x})+q\left(\mathbf{x}-\mathbf{x}',\frac{\mathbf{x}+\mathbf{x}'}{2},\tau-\tau'\right)\right]. \tag{2.51}$$

The corresponding Green function is determined by performing the semi-classical Fourier-Matsubara transformation

$$G^{-1}_{\alpha\alpha'}\left(\mathbf{x}-\mathbf{x}',\frac{\mathbf{x}+\mathbf{x}'}{2};\tau-\tau'\right)=\int\frac{d^nk}{(2\pi)^n}\,e^{i\mathbf{k}(\mathbf{x}-\mathbf{x}')}\frac{1}{\hbar\beta}\sum_{m=-\infty}^{\infty}e^{-i\omega_m(\tau-\tau')}\,G^{-1}_{\alpha\alpha'}\left(\mathbf{k},\omega_m,\frac{\mathbf{x}+\mathbf{x}'}{2}\right), \tag{2.52}$$

so that the decomposition (2.49) is converted to

$$G^{-1}_{\alpha\alpha'}\left(\mathbf{k},\omega_m,\frac{\mathbf{x}+\mathbf{x}'}{2}\right)=\begin{pmatrix}a(\mathbf{k},\omega_m,\frac{\mathbf{x}+\mathbf{x}'}{2}) & 0\\ 0 & a^*(\mathbf{k},\omega_m,\frac{\mathbf{x}+\mathbf{x}'}{2})\end{pmatrix}\delta_{\alpha\alpha'}+\begin{pmatrix}b(\mathbf{k},\omega_m,\frac{\mathbf{x}+\mathbf{x}'}{2}) & 0\\ 0 & b^*(\mathbf{k},\omega_m,\frac{\mathbf{x}+\mathbf{x}'}{2})\end{pmatrix}, \tag{2.53}$$

where we have used the abbreviations

$$\begin{aligned}a\left(\mathbf{k},\omega_m,\frac{\mathbf{x}+\mathbf{x}'}{2}\right)=&-i\hbar\omega_m+\epsilon(\mathbf{k})+V\left(\frac{\mathbf{x}+\mathbf{x}'}{2}\right)-\mu+V^{(\mathrm{int})}(\mathbf{k})\Psi^*\left(\frac{\mathbf{x}+\mathbf{x}'}{2}\right)\Psi\left(\frac{\mathbf{x}+\mathbf{x}'}{2}\right)\\&-\frac{1}{\hbar}\int\frac{d^nk'}{(2\pi)^n}D\left(\mathbf{k}'\right)Q_m\left(\mathbf{k}-\mathbf{k}',\frac{\mathbf{x}+\mathbf{x}'}{2}\right)-\mathcal{N}\beta D\left(\mathbf{k}\right)\Sigma\left(\frac{\mathbf{x}+\mathbf{x}'}{2}\right)\delta_{m,0}+\Sigma\left(\frac{\mathbf{x}+\mathbf{x}'}{2}\right)\\&\times\int d^nx''V^{(\mathrm{int})}(\mathbf{x}'')+\int\frac{d^nk'}{(2\pi)^n}V^{(\mathrm{int})}(\mathbf{k}')\left[q_m\left(\mathbf{k}-\mathbf{k}',\frac{\mathbf{x}+\mathbf{x}'}{2}\right)+Q_m\left(\mathbf{k}-\mathbf{k}',\frac{\mathbf{x}+\mathbf{x}'}{2}\right)\right],\end{aligned} \tag{2.54}$$

$$\begin{aligned}b\left(\mathbf{k},\omega_m,\frac{\mathbf{x}+\mathbf{x}'}{2}\right)=-\frac{1}{\hbar}\Bigg[&\int\frac{d^nk'}{(2\pi)^n}D\left(\mathbf{k}'\right)q_m\left(\mathbf{k}-\mathbf{k}',\frac{\mathbf{x}+\mathbf{x}'}{2}\right)\\&+\hbar\beta D\left(\mathbf{k}\right)\Psi^*\left(\frac{\mathbf{x}+\mathbf{x}'}{2}\right)\Psi\left(\frac{\mathbf{x}+\mathbf{x}'}{2}\right)\delta_{m,0}\Bigg],\end{aligned} \tag{2.55}$$

and the free dispersion:

$$\epsilon(\mathbf{k})=\frac{\hbar^2\mathbf{k}^2}{2M}. \tag{2.56}$$

Furthermore, $D\left(\mathbf{k}\right)$ and $V^{(\mathrm{int})}(\mathbf{k})$ are the Fourier transformed of the disorder correlation function $D(\mathbf{x})$ and the two-particle interaction potential $V^{(\mathrm{int})}(\mathbf{x})$, respectively:

$$D(\mathbf{x})=\int\frac{d^nk}{(2\pi)^n}\,D(\mathbf{k})e^{i\mathbf{k}\mathbf{x}}, \tag{2.57}$$

$$V^{(\mathrm{int})}(\mathbf{x})=\int\frac{d^nk}{(2\pi)^n}\,V^{(\mathrm{int})}(\mathbf{k})e^{i\mathbf{k}\mathbf{x}}. \tag{2.58}$$

Note that $a(\mathbf{k},\omega_m,\frac{\mathbf{x}+\mathbf{x}'}{2})$ and $b(\mathbf{k},\omega_m,\frac{\mathbf{x}+\mathbf{x}'}{2})$ are the semi-classical Fourier-Matsubara transformations of the quantities $a(\mathbf{x}-\mathbf{x}',\frac{\mathbf{x}+\mathbf{x}'}{2};\tau-\tau')$ and $b(\mathbf{x}-\mathbf{x}',\frac{\mathbf{x}+\mathbf{x}'}{2};\tau-\tau')$:

$$a\left(\mathbf{x}-\mathbf{x}',\frac{\mathbf{x}+\mathbf{x}'}{2};\tau-\tau'\right)=\int\frac{d^nk}{(2\pi)^n}\,e^{i\mathbf{k}(\mathbf{x}-\mathbf{x}')}\frac{1}{\hbar\beta}\sum_{m=-\infty}^{\infty}e^{-i\omega_m(\tau-\tau')}a\left(\mathbf{k},\omega_m,\frac{\mathbf{x}+\mathbf{x}'}{2}\right), \tag{2.59}$$

$$b\left(\mathbf{x}-\mathbf{x}',\frac{\mathbf{x}+\mathbf{x}'}{2};\tau-\tau'\right)=\int\frac{d^nk}{(2\pi)^n}\,e^{i\mathbf{k}(\mathbf{x}-\mathbf{x}')}\frac{1}{\hbar\beta}\sum_{m=-\infty}^{\infty}e^{-i\omega_m(\tau-\tau')}b\left(\mathbf{k},\omega_m,\frac{\mathbf{x}+\mathbf{x}'}{2}\right), \tag{2.60}$$

Indeed, the defining equation for the Green function

$$\int_0^{\hbar\beta} d\tau \int d^n x \sum_{\alpha=1}^{\mathcal{N}} G^{-1}_{\alpha_1\alpha}\left(\mathbf{x}-\mathbf{x}_1, \frac{\mathbf{x}+\mathbf{x}_1}{2}; \tau-\tau_1\right) G_{\alpha\alpha_2}\left(\mathbf{x}_2-\mathbf{x}, \frac{\mathbf{x}+\mathbf{x}_2}{2}; \tau_2-\tau\right)$$
$$= \hbar\delta(\mathbf{x}_1-\mathbf{x}_2)\delta(\tau_1-\tau_2)\delta_{\alpha_1\alpha_2} \tag{2.61}$$

reduces with a semi-classical Fourier-Matsubara transformation to the algebraic identity:

$$\sum_{\alpha=1}^{\mathcal{N}} G^{-1}_{\alpha_1\alpha}\left(\mathbf{k}, \omega_m, \frac{\mathbf{x}+\mathbf{x}'}{2}\right) G_{\alpha\alpha_2}\left(\mathbf{k}, \omega_m, \frac{\mathbf{x}+\mathbf{x}'}{2}\right) = \hbar\,\delta_{\alpha_1\alpha_2}\,. \tag{2.62}$$

The latter is solved with a decomposition similar to (2.53):

$$G_{\alpha\alpha'}\left(\mathbf{k}, \omega_m, \frac{\mathbf{x}+\mathbf{x}'}{2}\right) = \hbar \begin{pmatrix} \dfrac{1}{a(\mathbf{k},\omega_m,\frac{\mathbf{x}+\mathbf{x}'}{2})} & 0 \\ 0 & \dfrac{1}{a^*(\mathbf{k},\omega_m,\frac{\mathbf{x}+\mathbf{x}'}{2})} \end{pmatrix} \delta_{\alpha\alpha'} \tag{2.63}$$
$$- \hbar \begin{pmatrix} \dfrac{b(\mathbf{k},\omega_m,\frac{\mathbf{x}+\mathbf{x}'}{2})}{a(\mathbf{k},\omega_m,\frac{\mathbf{x}+\mathbf{x}'}{2})\left[\mathcal{N}b(\mathbf{k},\omega_m,\frac{\mathbf{x}+\mathbf{x}'}{2})+a(\mathbf{k},\omega_m,\frac{\mathbf{x}+\mathbf{x}'}{2})\right]} & 0 \\ 0 & \dfrac{b^*(\mathbf{k},\omega_m,\frac{\mathbf{x}+\mathbf{x}'}{2})}{a^*(\mathbf{k},\omega_m,\frac{\mathbf{x}+\mathbf{x}'}{2})\left[\mathcal{N}b^*(\mathbf{k},\omega_m,\frac{\mathbf{x}+\mathbf{x}'}{2})+a^*(\mathbf{k},\omega_m,\frac{\mathbf{x}+\mathbf{x}'}{2})\right]} \end{pmatrix}.$$

Thus, the corresponding Green function

$$G_{\alpha\alpha'}\left(\mathbf{x}-\mathbf{x}', \frac{\mathbf{x}+\mathbf{x}'}{2}; \tau-\tau'\right) = g_1\left(\mathbf{x}-\mathbf{x}', \frac{\mathbf{x}+\mathbf{x}'}{2}; \tau-\tau'\right)\delta_{\alpha\alpha'} + g_2\left(\mathbf{x}-\mathbf{x}', \frac{\mathbf{x}+\mathbf{x}'}{2}; \tau-\tau'\right) \tag{2.64}$$

follows from evaluating the semi-classical Fourier-Matsubara transformation:

$$G_{\alpha\alpha'}\left(\mathbf{x}-\mathbf{x}', \frac{\mathbf{x}+\mathbf{x}'}{2}; \tau-\tau'\right) = \int \frac{d^n k}{(2\pi)^n}\, e^{i\mathbf{k}(\mathbf{x}-\mathbf{x}')} \frac{1}{\hbar\beta} \sum_{m=-\infty}^{\infty} e^{-i\omega_m(\tau-\tau')}\, G_{\alpha\alpha'}\left(\mathbf{k}, \omega_m, \frac{\mathbf{x}+\mathbf{x}'}{2}\right). \tag{2.65}$$

As the Green function contains expectation values according to

$$G_{\alpha\alpha'}\left(\mathbf{x}-\mathbf{x}', \frac{\mathbf{x}+\mathbf{x}'}{2}; \tau-\tau'\right) = \begin{pmatrix} \langle\delta\psi_\alpha(\mathbf{x},\tau)\delta\psi^*_{\alpha'}(\mathbf{x}',\tau')\rangle & 0 \\ 0 & \langle\delta\psi^*_\alpha(\mathbf{x},\tau)\delta\psi_{\alpha'}(\mathbf{x}',\tau')\rangle \end{pmatrix}, \tag{2.66}$$

we arrive at the expression:

$$\langle\delta\psi_\alpha(\mathbf{x},\tau)\delta\psi^*_{\alpha'}(\mathbf{x}',\tau')\rangle = g_1\left(\mathbf{x}-\mathbf{x}', \frac{\mathbf{x}+\mathbf{x}'}{2}; \tau-\tau'\right)\delta_{\alpha\alpha'} + g_2\left(\mathbf{x}-\mathbf{x}', \frac{\mathbf{x}+\mathbf{x}'}{2}; \tau-\tau'\right) \tag{2.67}$$

with the contributions:

$$g_1\left(\mathbf{x}-\mathbf{x}', \frac{\mathbf{x}+\mathbf{x}'}{2}; \tau-\tau'\right) = \int \frac{d^n k}{(2\pi)^n}\, e^{i\mathbf{k}(\mathbf{x}-\mathbf{x}')} \sum_{m=-\infty}^{\infty} \frac{e^{-i\omega_m(\tau-\tau')}}{\beta a(\mathbf{k},\omega_m,\frac{\mathbf{x}+\mathbf{x}'}{2})}, \tag{2.68}$$

$$g_2\left(\mathbf{x}-\mathbf{x}', \frac{\mathbf{x}+\mathbf{x}'}{2}; \tau-\tau'\right) = \int \frac{d^n k}{(2\pi)^n}\, e^{i\mathbf{k}(\mathbf{x}-\mathbf{x}')} \sum_{m=-\infty}^{\infty} \frac{e^{-i\omega_m(\tau-\tau')}}{\beta\mathcal{N}}$$
$$\times\left[\frac{1}{\mathcal{N}b(\mathbf{k},\omega_m,\frac{\mathbf{x}+\mathbf{x}'}{2})+a(\mathbf{k},\omega_m,\frac{\mathbf{x}+\mathbf{x}'}{2})} - \frac{1}{a(\mathbf{k},\omega_m,\frac{\mathbf{x}+\mathbf{x}'}{2})}\right]. \tag{2.69}$$

Comparing (2.33)–(2.35), (2.44), (2.46), and (2.47) with (2.67)–(2.69) yields:

$$Q_m\left(\mathbf{k}, \frac{\mathbf{x}+\mathbf{x}'}{2}\right) = \frac{\hbar}{a(\mathbf{k},\omega_m,\frac{\mathbf{x}+\mathbf{x}'}{2})}, \tag{2.70}$$

$$q_m\left(\mathbf{k}, \frac{\mathbf{x}+\mathbf{x}'}{2}\right) = \frac{\hbar}{\mathcal{N}}\left[\frac{1}{\mathcal{N}b(\mathbf{k},\omega_m,\frac{\mathbf{x}+\mathbf{x}'}{2}) + a(\mathbf{k},\omega_m,\frac{\mathbf{x}+\mathbf{x}'}{2})} - \frac{1}{a(\mathbf{k},\omega_m,\frac{\mathbf{x}+\mathbf{x}'}{2})}\right] \tag{2.71}$$

and their complex conjugate. Eqs. (2.70), (2.71) represent due to (2.54) and (2.55) two coupled integral mean-field equations of the quantities $Q_m(\mathbf{k}, \frac{\mathbf{x}+\mathbf{x}'}{2})$ and $q_m(\mathbf{k}, \frac{\mathbf{x}+\mathbf{x}'}{2})$. As it is not possible to solve them analytically for a general disorder potential and a general interaction potential, we specialize now to a δ-correlated disorder potential and a contact interaction potential.

2.6. Delta-Correlated Disorder and Contact Interaction Potential

Now we elaborate a solution of our mean-field equations for the special case of a δ-correlated disorder potential (2.4), i.e., we assume:

$$D(\mathbf{x}-\mathbf{x}') = D\delta(\mathbf{x}-\mathbf{x}'), \tag{2.72}$$

which yields

$$D(\mathbf{k}) = D, \tag{2.73}$$

where D denotes the disorder strength. In this case formulas (2.54) and (2.55) reduce to:

$$\begin{aligned} a\left(\mathbf{k},\omega_m,\frac{\mathbf{x}+\mathbf{x}'}{2}\right) =& -i\hbar\omega_m + \epsilon(\mathbf{k}) + V\left(\frac{\mathbf{x}+\mathbf{x}'}{2}\right) - \mu + \Sigma\left(\frac{\mathbf{x}+\mathbf{x}'}{2}\right)\int d^n x'' V^{(\mathrm{int})}(\mathbf{x}'') \\ &- \frac{D}{\hbar}Q_m\left(\frac{\mathbf{x}+\mathbf{x}'}{2}\right) - \mathcal{N}\beta D\Sigma\left(\frac{\mathbf{x}+\mathbf{x}'}{2}\right)\delta_{m,0} + V^{(\mathrm{int})}(\mathbf{k})\Psi^*\left(\frac{\mathbf{x}+\mathbf{x}'}{2}\right)\Psi\left(\frac{\mathbf{x}+\mathbf{x}'}{2}\right) \\ &+ \int \frac{d^n k'}{(2\pi)^n} V^{(\mathrm{int})}(\mathbf{k}')\left[q_m\left(\mathbf{k}-\mathbf{k}', \frac{\mathbf{x}+\mathbf{x}'}{2}\right) + Q_m\left(\mathbf{k}-\mathbf{k}', \frac{\mathbf{x}+\mathbf{x}'}{2}\right)\right] \end{aligned} \tag{2.74}$$

and

$$b\left(\mathbf{k},\omega_m,\frac{\mathbf{x}+\mathbf{x}'}{2}\right) = -\frac{D}{\hbar}\left[q_m\left(\frac{\mathbf{x}+\mathbf{x}'}{2}\right) + \hbar\beta\Psi^*\left(\frac{\mathbf{x}+\mathbf{x}'}{2}\right)\Psi\left(\frac{\mathbf{x}+\mathbf{x}'}{2}\right)\delta_{m,0}\right], \tag{2.75}$$

where we have introduced the abbreviations

$$Q_m\left(\frac{\mathbf{x}+\mathbf{x}'}{2}\right) = \int \frac{d^n k'}{(2\pi)^n} Q_m\left(\mathbf{k}-\mathbf{k}', \frac{\mathbf{x}+\mathbf{x}'}{2}\right), \tag{2.76}$$

$$q_m\left(\frac{\mathbf{x}+\mathbf{x}'}{2}\right) = \int \frac{d^n k'}{(2\pi)^n} q_m\left(\mathbf{k}-\mathbf{k}', \frac{\mathbf{x}+\mathbf{x}'}{2}\right). \tag{2.77}$$

Furthermore, we choose a contact interaction potential

$$V^{(\mathrm{int})}(\mathbf{x}-\mathbf{x}') = g\delta(\mathbf{x}-\mathbf{x}'), \tag{2.78}$$

where g denotes the interaction coupling strength. Using the definitions (2.33), (2.35), and (2.44), formula (2.74) reduces in this case further to

$$\begin{aligned} a\left(\mathbf{k},\omega_m,\frac{\mathbf{x}+\mathbf{x}'}{2}\right) =& -i\hbar\omega_m + \epsilon(\mathbf{k}) - \mu + 2g\Sigma\left(\frac{\mathbf{x}+\mathbf{x}'}{2}\right) + V\left(\frac{\mathbf{x}+\mathbf{x}'}{2}\right) \\ &- \frac{D}{\hbar}Q_m\left(\frac{\mathbf{x}+\mathbf{x}'}{2}\right) - \mathcal{N}\beta D\Sigma\left(\frac{\mathbf{x}+\mathbf{x}'}{2}\right)\delta_{m,0}, \end{aligned} \tag{2.79}$$

while (2.75) does not change. Thus, (2.70) and (2.71) yield then together with (2.76) and (2.77) algebraic mean-field equations, which we can solve.

2.7. Schwinger Trick

Inserting (2.75) and (2.79) into (2.70) and (2.71), then inserting the resulting expressions into (2.76) and (2.77) and taking $\mathbf{x} = \mathbf{x}'$ yield the following self-consistency equations:

$$Q_m(\mathbf{x}) = \int \frac{d^n k}{(2\pi)^n} \frac{\hbar}{-i\hbar\omega_m + \epsilon(\mathbf{k}) - \mu + 2g\Sigma(\mathbf{x}) + V(\mathbf{x}) - \frac{D}{\hbar} Q_m(\mathbf{x}) - \mathcal{N}\beta D\Sigma(\mathbf{x})\,\delta_{m,0}}\,, \tag{2.80}$$

$$q_m(\mathbf{x}) = D \int \frac{d^n k}{(2\pi)^n} \frac{q_m(\mathbf{x}) + \hbar\beta\Psi^*(\mathbf{x})\Psi(\mathbf{x})\,\delta_{m,0}}{-i\hbar\omega_m + \epsilon(\mathbf{k}) - \mu + 2g\Sigma(\mathbf{x}) + V(\mathbf{x}) - \frac{D}{\hbar} Q_m(\mathbf{x}) - \mathcal{N}\beta D\Sigma(\mathbf{x})\,\delta_{m,0}} \tag{2.81}$$

$$\times \frac{1}{-i\hbar\omega_m + \epsilon(\mathbf{k}) - \mu + 2g\Sigma(\mathbf{x}) + V(\mathbf{x}) - \frac{D}{\hbar} Q_m(\mathbf{x}) - \mathcal{N}\beta D\Sigma(\mathbf{x})\,\delta_{m,0} - \mathcal{N}\left[q_m(\mathbf{x}) + \hbar\beta\Psi^*(\mathbf{x})\Psi(\mathbf{x})\,\delta_{m,0}\right]}.$$

The Fourier integral (2.81) converges for $n \leqslant 3$, whereas the Fourier integral (2.80) converges only in one dimension and has an ultraviolet divergency in the case of two and three dimensions. Therefore, in order to deal with this ultraviolet divergency, we use the dimensional regularization method, which consists of performing an analytic continuation of the Γ-function [110]. To this end we use Schwinger integral:

$$\frac{1}{a^\nu} = \frac{1}{\Gamma(\nu)} \int_0^\infty ds\, s^{\nu-1}\, e^{-as}, \tag{2.82}$$

so that the wave vector integrals become Gaussian, which can be solved explicitly. Thus, we obtain from (2.80) and (2.81) the remaining integrals over the Schwinger parameter s:

$$\begin{aligned} Q_m(\mathbf{x}) = \hbar \left(\frac{M}{2\pi\hbar^2}\right)^{n/2} \int_0^\infty ds\, s^{-n/2} \exp\left[-\frac{M(\mathbf{x}-\mathbf{x}')^2}{2\hbar^2 s}\right] \\ \times \exp\left\{-s\left[-i\hbar\omega_m - \mu + 2g\Sigma(\mathbf{x}) + V(\mathbf{x}) - \frac{D}{\hbar} Q_m(\mathbf{x}) - \mathcal{N}\beta D\Sigma(\mathbf{x})\,\delta_{m,0}\right]\right\}, \end{aligned} \tag{2.83}$$

$$\begin{aligned} q_m(\mathbf{x}) = &-\frac{\hbar}{\mathcal{N}} \left(\frac{M}{2\pi\hbar^2}\right)^{n/2} \int_0^\infty ds\, s^{-n/2} \exp\left[-\frac{M(\mathbf{x}-\mathbf{x}')^2}{2\hbar^2 s}\right] \\ &\times \exp\left\{-s\left[-i\hbar\omega_m - \mu + 2g\Sigma(\mathbf{x}) + V(\mathbf{x}) - \frac{D}{\hbar} Q_m(\mathbf{x}) - \mathcal{N}\beta D\Sigma(\mathbf{x})\,\delta_{m,0}\right]\right\} \\ &+ \frac{\hbar}{\mathcal{N}} \left(\frac{M}{2\pi\hbar^2}\right)^{n/2} \int_0^\infty ds\, s^{-n/2} \exp\left[-\frac{M(\mathbf{x}-\mathbf{x}')^2}{2\hbar^2 s}\right] \\ &\times \exp\left\{-s\left[-i\hbar\omega_m - \mu + 2g\Sigma(\mathbf{x}) + V(\mathbf{x}) - \frac{D}{\hbar} Q_m(\mathbf{x}) - \mathcal{N}\beta D\Sigma(\mathbf{x})\,\delta_{m,0}\right]\right\} \\ &\times \exp\left\{s\mathcal{N}\frac{D}{\hbar}\left[q_m(\mathbf{x}) + \hbar\beta\Psi^*(\mathbf{x})\Psi(\mathbf{x})\,\delta_{m,0}\right]\right\}. \end{aligned} \tag{2.84}$$

Using [111, (8.310.1)], Eqs. (2.83) and (2.84) reduce to the following mean-field equations:

$$Q_m(\mathbf{x}) = \Gamma\left(1 - \frac{n}{2}\right) \hbar \left(\frac{M}{2\pi\hbar^2}\right)^{n/2} \left[-i\hbar\omega_m - \mu + 2g\Sigma(\mathbf{x}) + V(\mathbf{x}) - \frac{D}{\hbar} Q_m(\mathbf{x}) - \mathcal{N}\beta D\Sigma(\mathbf{x})\,\delta_{m,0}\right]^{\frac{n}{2}-1}, \tag{2.85}$$

$$\begin{aligned} q_m(\mathbf{x}) = &-\Gamma\left(1 - \frac{n}{2}\right) \frac{\hbar}{\mathcal{N}} \left(\frac{M}{2\pi\hbar^2}\right)^{n/2} \left[-i\hbar\omega_m - \mu + 2g\Sigma(\mathbf{x}) + V(\mathbf{x}) - \frac{D}{\hbar} Q_m(\mathbf{x}) - \mathcal{N}\beta D\Sigma(\mathbf{x})\,\delta_{m,0}\right]^{\frac{n}{2}-1} \\ &+ \Gamma\left(1 - \frac{n}{2}\right) \frac{\hbar}{\mathcal{N}} \left(\frac{M}{2\pi\hbar^2}\right)^{n/2} \left\{-i\hbar\omega_m - \mu + 2g\Sigma(\mathbf{x}) + V(\mathbf{x}) - \frac{D}{\hbar} Q_m(\mathbf{x}) - \mathcal{N}\beta D\Sigma(\mathbf{x})\,\delta_{m,0}\right. \\ &\left. - \mathcal{N}\frac{D}{\hbar}\left[q_m(\mathbf{x}) + \hbar\beta\Psi^*(\mathbf{x})\Psi(\mathbf{x})\,\delta_{m,0}\right]\right\}^{\frac{n}{2}-1}, \end{aligned} \tag{2.86}$$

from which we conclude the symmetries

$$Q_m^*(\mathbf{x}) = Q_{-m}(\mathbf{x}), \tag{2.87}$$

$$q_m^*(\mathbf{x}) = \quad q_{-m}(\mathbf{x})\,. \tag{2.88}$$

We read off from (2.46), (2.47), (2.87), and (2.88) that $Q^*(\mathbf{x};\tau'-\tau) = Q(\mathbf{x};\tau-\tau')$ and $q^*(\mathbf{x};\tau'-\tau) = q(\mathbf{x};\tau-\tau')$, respectively.

We note in equations (2.85) and (2.86) that the terms containing the parameter β are always multiplied by the number of replicas $\mathcal{N}$. This is important because it means that in the zero temperature case, i.e., $\beta \to \infty$, those terms will be eliminated in the replica limit, i.e., $\mathcal{N} \to 0$, otherwise they would diverge.

The expressions of $Q_m(\mathbf{x})$ and $q_m(\mathbf{x})$ in (2.85) and (2.86) turn out to diverge in two dimensions because of the prefactor $\Gamma\left(1-\frac{n}{2}\right)$, meaning that our theory in its actual form is not valid in the two-dimensional case. In order to get valid self-consistency equations also in two dimensions, one way would be to choose a disorder potential with a finite correlation length, e.g., a Lorentzian potential. Then this finite correlation length would provide a regularization which yields finite self-consistency equations. As the treatment of a Lorentzian disorder potential lies out at the scope of the present thesis, we will restrict ourselves later on to the study of the one- and the three-dimensional cases.

Note that in the replica limit $\mathcal{N} \to 0$, Eqs. (2.85) and (2.86) yield

$$Q_m(\mathbf{x}) = \Gamma\left(1-\frac{n}{2}\right)\hbar\left(\frac{M}{2\pi\hbar^2}\right)^{n/2}\left[-i\hbar\omega_m - \mu + 2g\Sigma(\mathbf{x}) + V(\mathbf{x}) - \frac{D}{\hbar}Q_m(\mathbf{x})\right]^{\frac{n}{2}-1} \tag{2.89}$$

and

$$q(\mathbf{x}) = D\Gamma\left(2-\frac{n}{2}\right)\left(\frac{M}{2\pi\hbar^2}\right)^{n/2}\frac{q(\mathbf{x}) + \Psi^*(\mathbf{x})\Psi(\mathbf{x})}{\left[-\mu + 2g\Sigma(\mathbf{x}) + V(\mathbf{x}) - \frac{D}{\hbar}Q_0(\mathbf{x})\right]^{2-\frac{n}{2}}}, \tag{2.90}$$

where $q(\mathbf{x}) = q_0(\mathbf{x})/\hbar\beta$ and $q_m(\mathbf{x}) = 0$ for $m \neq 0$. Note that this last simplification occurs only in the replica limit $\mathcal{N} \to 0$.

Now we insert the replica-symmetric solution ansatz (2.44), (2.46) also in the other mean-field equations (2.35) and (2.42). In this way we obtain in the replica limit $\mathcal{N} \to 0$ the Gross-Pitaevskii equation

$$\left[-\mu + 2g\Sigma(\mathbf{x}) + V(\mathbf{x}) - gn_0(\mathbf{x}) - \frac{D}{\hbar}Q_0(\mathbf{x}) - \frac{\hbar^2}{2M}\boldsymbol{\Delta}\right]\sqrt{n_0(\mathbf{x})} = 0 \tag{2.91}$$

and the mean-field:

$$\Sigma(\mathbf{x}) = q(\mathbf{x}) + n_0(\mathbf{x}) + \lim_{\eta\downarrow 0}\sum_{m=-\infty}^{\infty} e^{i\omega_m\eta}\,\frac{Q_m(\mathbf{x})}{\hbar\beta}\,, \tag{2.92}$$

where we have set $n_0(\mathbf{x}) = \Psi^*(\mathbf{x})\Psi(\mathbf{x})$.

2.8. Correlation Functions and Order Parameters

In the following we fix the physical interpretation of the two order parameters $n_0(\mathbf{x})$ and $q(\mathbf{x})$ of our mean-field theory. To this end we follow the notion of classical and quantum spin-glass theory [58, 94, 112] and investigate how these quantities are related to correlation functions.

We start with considering the grand-canonical average of the Bose field:

$$\langle\psi(\mathbf{x},\tau)\rangle = \frac{1}{\mathcal{Z}}\oint\mathcal{D}\psi^*\oint\mathcal{D}\psi\,\psi(\mathbf{x},\tau)\,e^{-\mathcal{A}[\psi^*,\psi]/\hbar}\,, \tag{2.93}$$

which represents a functional of the disorder potential $U(\mathbf{x})$ due to the action (2.21). In order to evaluate its disorder expectation value we apply again the replica method. To this end we identify $\psi(\mathbf{x},\tau)$ with $\psi_\alpha(\mathbf{x},\tau)$ and add further $\mathcal{N}-1$ Bose fields according to:

$$\langle\psi(\mathbf{x},\tau)\rangle = \frac{1}{\mathcal{Z}^{\mathcal{N}}}\left\{\prod_{\alpha'=1}^{N}\oint\mathcal{D}\psi^*_{\alpha'}\oint\mathcal{D}\psi_{\alpha'}\right\}\psi_\alpha(\mathbf{x},\tau)\,\exp\left\{-\frac{1}{\hbar}\sum_{\alpha'=1}^{\mathcal{N}}\mathcal{A}[\psi^*_{\alpha'},\psi_{\alpha'}]\right\}. \tag{2.94}$$

As the right-hand side is independent of the replica index α, we obtain in the replica limit $N\to 0$:

$$\langle\psi(\mathbf{x},\tau)\rangle = \lim_{\mathcal{N}\to 0}\frac{1}{\mathcal{N}}\sum_{\alpha=1}^{\mathcal{N}}\left\{\prod_{\alpha'=1}^{\mathcal{N}}\oint\mathcal{D}\psi^*_{\alpha'}\oint\mathcal{D}\psi_{\alpha'}\right\}\psi_\alpha(\mathbf{x},\tau)\,\exp\left\{-\frac{1}{\hbar}\sum_{\alpha'=1}^{\mathcal{N}}\mathcal{A}[\psi^*_{\alpha'},\psi_{\alpha'}]\right\}. \tag{2.95}$$

Now we are in a position to perform the averaging with respect to the disorder potential $U(\mathbf{x})$ by applying again the generating functional (2.19) with the auxiliary current field (2.23). Thus, we obtain the following replica representation of the grand-canonical average of the Bose field:

$$\overline{\langle\psi(\mathbf{x},\tau)\rangle} = \lim_{\mathcal{N}\to 0}\frac{1}{\mathcal{N}}\sum_{\alpha=1}^{\mathcal{N}}\left\{\prod_{\alpha'=1}^{\mathcal{N}}\oint\mathcal{D}\psi^*_{\alpha'}\oint\mathcal{D}\psi_{\alpha'}\right\}\psi_\alpha(\mathbf{x},\tau)\,e^{-\mathcal{A}^{(\mathcal{N})}[\psi^*,\psi]/\hbar} \tag{2.96}$$

with the replica action (2.26). In a similar way we yield for the 2-point function:

$$\overline{\langle\psi(\mathbf{x},\tau)\psi^*(\mathbf{x}',\tau')\rangle} = \lim_{\mathcal{N}\to 0}\frac{1}{\mathcal{N}}\sum_{\alpha=1}^{\mathcal{N}}\left\{\prod_{\alpha'=1}^{\mathcal{N}}\oint\mathcal{D}\psi^*_{\alpha'}\oint\mathcal{D}\psi_{\alpha'}\right\}\psi_\alpha(\mathbf{x},\tau)\psi^*_\alpha(\mathbf{x}',\tau')\,e^{-\mathcal{A}^{(\mathcal{N})}[\psi^*,\psi]/\hbar}. \tag{2.97}$$

In order to further evaluate n-point functions of the form (2.96) and (2.97), we introduce the generating functional:

$$\overline{\mathcal{Z}[j^*,j]} = \left\{\prod_{\alpha=1}^{\mathcal{N}}\oint\mathcal{D}\psi^*_\alpha\oint\mathcal{D}\psi_\alpha\right\}e^{-\mathcal{A}^{(\mathcal{N})}[\psi^*,\psi;j^*,j]/\hbar}, \tag{2.98}$$

where each Bose field $\psi^*_\alpha(\mathbf{x},\tau),\psi_\alpha(\mathbf{x},\tau)$ is coupled to its own current field $j_\alpha(\mathbf{x},\tau),j^*_\alpha(\mathbf{x},\tau)$ via the action:

$$\mathcal{A}^{(\mathcal{N})}[\psi^*,\psi;j^*,j] = \mathcal{A}^{(\mathcal{N})}[\psi^*,\psi] - \int_0^{\hbar\beta}d\tau\int d^nx\sum_{\alpha=1}^{\mathcal{N}}\Big\{j^*_\alpha(\mathbf{x},\tau)\psi_\alpha(\mathbf{x},\tau)+\psi^*_\alpha(\mathbf{x},\tau)j_\alpha(\mathbf{x},\tau)\Big\}. \tag{2.99}$$

Indeed, performing successive functional derivatives with respect to the current fields $j_\alpha(\mathbf{x},\tau),j^*_\alpha(\mathbf{x},\tau)$, we obtain the 1- and 2-point function (2.96) and (2.97) from the generating functional (2.98) and (2.99) according to:

$$\overline{\langle\psi(\mathbf{x},\tau)\rangle} = \lim_{\mathcal{N}\to 0}\frac{\hbar}{\mathcal{N}}\sum_{\alpha=1}^{\mathcal{N}}\frac{\delta\overline{\mathcal{Z}[j^*,j]}}{\delta j^*_\alpha(\mathbf{x},\tau)}\bigg|_{j(\mathbf{x},\tau)=0}^{j^*(\mathbf{x},\tau)=0}, \tag{2.100}$$

$$\overline{\langle\psi(\mathbf{x},\tau)\psi^*(\mathbf{x}',\tau')\rangle} = \lim_{\mathcal{N}\to 0}\frac{\hbar^2}{\mathcal{N}}\sum_{\alpha=1}^{\mathcal{N}}\frac{\delta^2\overline{\mathcal{Z}[j^*,j]}}{\delta j^*_\alpha(\mathbf{x},\tau)\delta j_\alpha(\mathbf{x}',\tau')}\bigg|_{j(\mathbf{x},\tau)=0}^{j^*(\mathbf{x},\tau)=0}. \tag{2.101}$$

Thus, it remains to calculate the generating functional $\overline{\mathcal{Z}[j^*,j]}$ within our mean-field theory. To this end we perform the background expansions (2.27). Assuming again that the background fields have the replica symmetry form (2.43), we have:

$$\begin{aligned}\overline{\mathcal{Z}[j^*,j]} = \exp\Bigg\{&-\beta V^{(N)}_{\text{eff}}+\frac{1}{\hbar}\int_0^{\hbar\beta}d\tau\int d^nx\sum_{\alpha=1}^{N}\Big[j^*_\alpha(\mathbf{x},\tau)\,\Psi(\mathbf{x})+\Psi^*(\mathbf{x})\,j_\alpha(\mathbf{x},\tau)\Big] \\ &+\frac{1}{\hbar^2}\int_0^{\hbar\beta}d\tau\int_0^{\hbar\beta}d\tau'\int d^nx\int d^nx'\sum_{\alpha=1}^{N}\sum_{\alpha'=1}^{N}j^*_\alpha(\mathbf{x},\tau)\,\langle\delta\psi_\alpha(\mathbf{x},\tau)\delta\psi^*_{\alpha'}(\mathbf{x}',\tau')\rangle j_{\alpha'}(\mathbf{x}',\tau')\Bigg\}.\end{aligned} \tag{2.102}$$

Thus, inserting (2.102) into (2.100) and (2.101), yields

$$\overline{\langle\psi(\mathbf{x},\tau)\rangle} = \sqrt{n_0(\mathbf{x})} \tag{2.103}$$

and, by taking into account (2.67):

$$\begin{aligned}\overline{\langle\psi(\mathbf{x},\tau)\psi^*(\mathbf{x}',\tau')\rangle} &= \sqrt{n_0(\mathbf{x})n_0(\mathbf{x}')} + g_1\left(\mathbf{x}-\mathbf{x}', \frac{\mathbf{x}+\mathbf{x}'}{2}; \tau-\tau'\right) \\ &\quad + g_2\left(\mathbf{x}-\mathbf{x}', \frac{\mathbf{x}+\mathbf{x}'}{2}; \tau-\tau'\right) . \end{aligned} \tag{2.104}$$

Now we need just to evaluate the functions $g_1(\mathbf{x}-\mathbf{x}', \frac{\mathbf{x}+\mathbf{x}'}{2}; \tau-\tau')$ and $g_2(\mathbf{x}-\mathbf{x}', \frac{\mathbf{x}+\mathbf{x}'}{2}; \tau-\tau')$, respectively.

Inserting (2.75), (2.79) into (2.68), (2.69) yield:

$$\begin{aligned} g_1(\mathbf{x}-\mathbf{x}', \frac{\mathbf{x}+\mathbf{x}'}{2}; \tau-\tau') &= \int \frac{d^n k}{\beta(2\pi)^n}\, e^{i\mathbf{k}(\mathbf{x}-\mathbf{x}')} \sum_{m=-\infty}^{\infty} e^{-i\omega_m(\tau-\tau')} \\ &\times \left[-i\hbar\omega_m + \epsilon(\mathbf{k}) - \mu + 2g\Sigma\left(\frac{\mathbf{x}+\mathbf{x}'}{2}\right) + V\left(\frac{\mathbf{x}+\mathbf{x}'}{2}\right) - \frac{D}{\hbar}Q_m\left(\frac{\mathbf{x}+\mathbf{x}'}{2}\right) - \mathcal{N}\beta D\Sigma\left(\frac{\mathbf{x}+\mathbf{x}'}{2}\right)\delta_{m,0}\right]^{-1}, \end{aligned} \tag{2.105}$$

$$\begin{aligned} g_2\left(\mathbf{x}-\mathbf{x}', \frac{\mathbf{x}+\mathbf{x}'}{2}; \tau-\tau'\right) &= \int \frac{d^n k}{(2\pi)^n}\, e^{i\mathbf{k}(\mathbf{x}-\mathbf{x}')} \sum_{m=-\infty}^{\infty} e^{-i\omega_m(\tau-\tau')} \\ &\times \frac{D\left[q_m\left(\frac{\mathbf{x}+\mathbf{x}'}{2}\right) + \hbar\beta\Psi^*\left(\frac{\mathbf{x}+\mathbf{x}'}{2}\right)\Psi\left(\frac{\mathbf{x}+\mathbf{x}'}{2}\right)\delta_{m,0}\right]}{\hbar\beta\left[-i\hbar\omega_m + \epsilon(\mathbf{k}) - \mu + 2g\Sigma\left(\frac{\mathbf{x}+\mathbf{x}'}{2}\right) + V\left(\frac{\mathbf{x}+\mathbf{x}'}{2}\right) - \frac{D}{\hbar}Q_m\left(\frac{\mathbf{x}+\mathbf{x}'}{2}\right) - \mathcal{N}\beta D\Sigma\left(\frac{\mathbf{x}+\mathbf{x}'}{2}\right)\delta_{m,0}\right]} \\ &\times \left\{-i\hbar\omega_m + \epsilon(\mathbf{k}) - \mu + 2g\Sigma\left(\frac{\mathbf{x}+\mathbf{x}'}{2}\right) + V\left(\frac{\mathbf{x}+\mathbf{x}'}{2}\right) - \frac{D}{\hbar}Q_m\left(\frac{\mathbf{x}+\mathbf{x}'}{2}\right) - \mathcal{N}\beta D\Sigma\left(\frac{\mathbf{x}+\mathbf{x}'}{2}\right)\delta_{m,0}\right. \\ &\left. -\mathcal{N}\frac{D}{\hbar}\left[q_m\left(\frac{\mathbf{x}+\mathbf{x}'}{2}\right) + \hbar\beta\Psi^*\left(\frac{\mathbf{x}+\mathbf{x}'}{2}\right)\Psi\left(\frac{\mathbf{x}+\mathbf{x}'}{2}\right)\delta_{m,0}\right]\right\}^{-1}. \end{aligned} \tag{2.106}$$

Note that the Fourier integral (2.106) converges in all dimensions, whereas the Fourier integral (2.105) converges only in three dimensions but has an ultraviolet divergency in the case of one and two dimensions. Therefore, we use again the Schwinger integral (2.82) and obtain from (2.105) and (2.106):

$$\begin{aligned} g_1\left(\mathbf{x}-\mathbf{x}', \frac{\mathbf{x}+\mathbf{x}'}{2}; \tau-\tau'\right) &= \frac{1}{\beta}\left(\frac{M}{2\pi\hbar^2}\right)^{n/2} \sum_{m=-\infty}^{\infty} e^{-i\omega_m(\tau-\tau')} \int_0^\infty ds\, s^{-n/2} \exp\left\{-\frac{M(\mathbf{x}-\mathbf{x}')^2}{2\hbar^2 s}\right\} \\ &\times \exp\left\{-s\left[-i\hbar\omega_m - \mu + 2g\Sigma\left(\frac{\mathbf{x}+\mathbf{x}'}{2}\right) + V\left(\frac{\mathbf{x}+\mathbf{x}'}{2}\right) - \frac{D}{\hbar}Q_m\left(\frac{\mathbf{x}+\mathbf{x}'}{2}\right) - \mathcal{N}\beta D\Sigma\left(\frac{\mathbf{x}+\mathbf{x}'}{2}\right)\delta_{m,0}\right]\right\}, \end{aligned} \tag{2.107}$$

$$\begin{aligned} g_2\left(\mathbf{x}-\mathbf{x}', \frac{\mathbf{x}+\mathbf{x}'}{2}; \tau-\tau'\right) &= -\frac{1}{\mathcal{N}\beta}\left(\frac{M}{2\pi\hbar^2}\right)^{n/2} \sum_{m=-\infty}^{\infty} e^{-i\omega_m(\tau-\tau')} \int_0^\infty ds\, s^{-n/2} \exp\left[-\frac{M(\mathbf{x}-\mathbf{x}')^2}{2\hbar^2 s}\right] \\ &\times \exp\left\{-s\left[-i\hbar\omega_m + V\left(\frac{\mathbf{x}+\mathbf{x}'}{2}\right) - \mu + 2g\Sigma\left(\frac{\mathbf{x}+\mathbf{x}'}{2}\right) - \frac{D}{\hbar}Q_m\left(\frac{\mathbf{x}+\mathbf{x}'}{2}\right) - \mathcal{N}\beta D\Sigma\left(\frac{\mathbf{x}+\mathbf{x}'}{2}\right)\delta_{m,0}\right]\right\} \\ &+ \frac{1}{\mathcal{N}\beta}\left(\frac{M}{2\pi\hbar^2}\right)^{n/2} \sum_{m=-\infty}^{\infty} e^{-i\omega_m(\tau-\tau')} \int_0^\infty ds\, s^{-n/2} \exp\left[-\frac{M(\mathbf{x}-\mathbf{x}')^2}{2\hbar^2 s}\right] \\ &\times \exp\left\{-s\left[-i\hbar\omega_m + V\left(\frac{\mathbf{x}+\mathbf{x}'}{2}\right) - \mu + 2g\Sigma\left(\frac{\mathbf{x}+\mathbf{x}'}{2}\right) - \frac{D}{\hbar}Q_m\left(\frac{\mathbf{x}+\mathbf{x}'}{2}\right) - \mathcal{N}\beta D\Sigma\left(\frac{\mathbf{x}+\mathbf{x}'}{2}\right)\delta_{m,0}\right]\right\} \\ &\times \exp\left\{s\mathcal{N}\frac{D}{\hbar}\left[q_m\left(\frac{\mathbf{x}+\mathbf{x}'}{2}\right) + \hbar\beta\Psi^*\left(\frac{\mathbf{x}+\mathbf{x}'}{2}\right)\Psi\left(\frac{\mathbf{x}+\mathbf{x}'}{2}\right)\delta_{m,0}\right]\right\}. \end{aligned} \tag{2.108}$$

Using [111, (3.471.9)] and [111, (8.469.3)], Eqs. (2.107) and (2.108) reduce, after performing the replica limit $\mathcal{N} \to 0$, to:

$$g_1\left(\mathbf{x}-\mathbf{x}', \frac{\mathbf{x}+\mathbf{x}'}{2}; \tau-\tau'\right) = \frac{\sqrt{\pi}}{\beta}\left(\frac{M}{2\pi\hbar^2}\right)^{n/2}\left[\frac{2\hbar^2}{M(\mathbf{x}-\mathbf{x}')^2}\right]^{\frac{n-1}{4}} \sum_{m=-\infty}^{\infty} e^{-i\omega_m(\tau-\tau')} \tag{2.109}$$
$$\times\left[-i\hbar\omega_m + V\left(\frac{\mathbf{x}+\mathbf{x}'}{2}\right) - \mu + 2g\Sigma\left(\frac{\mathbf{x}+\mathbf{x}'}{2}\right) - \frac{D}{\hbar}Q_m\left(\frac{\mathbf{x}+\mathbf{x}'}{2}\right)\right]^{\frac{n-3}{4}}$$
$$\times\exp\left\{-\sqrt{\frac{2M}{\hbar^2}\left[-i\hbar\omega_m + V\left(\frac{\mathbf{x}+\mathbf{x}'}{2}\right) - \mu + 2g\Sigma\left(\frac{\mathbf{x}+\mathbf{x}'}{2}\right) - \frac{D}{\hbar}Q_m\left(\frac{\mathbf{x}+\mathbf{x}'}{2}\right)\right]}\,|\mathbf{x}-\mathbf{x}'|\right\}$$

and

$$g_2\left(\mathbf{x}-\mathbf{x}', \frac{\mathbf{x}+\mathbf{x}'}{2}; \tau-\tau'\right) = \sqrt{\pi}D\left(\frac{M}{2\pi\hbar^2}\right)^{n/2}\left[\frac{2\hbar^2}{M(\mathbf{x}-\mathbf{x}')^2}\right]^{\frac{n-1}{4}} \tag{2.110}$$
$$\times\frac{q\left(\frac{\mathbf{x}+\mathbf{x}'}{2}\right) + \Psi^*\left(\frac{\mathbf{x}+\mathbf{x}'}{2}\right)\Psi\left(\frac{\mathbf{x}+\mathbf{x}'}{2}\right)}{\left[V\left(\frac{\mathbf{x}+\mathbf{x}'}{2}\right) - \mu + 2g\Sigma\left(\frac{\mathbf{x}+\mathbf{x}'}{2}\right) - \frac{D}{\hbar}Q_0\left(\frac{\mathbf{x}+\mathbf{x}'}{2}\right)\right]^{\frac{7-n}{4}}}$$
$$\times\left\{\sqrt{\frac{M}{2\hbar^2}\left[V\left(\frac{\mathbf{x}+\mathbf{x}'}{2}\right) - \mu + 2g\Sigma\left(\frac{\mathbf{x}+\mathbf{x}'}{2}\right) - \frac{D}{\hbar}Q_0\left(\frac{\mathbf{x}+\mathbf{x}'}{2}\right)\right]}\,|\mathbf{x}-\mathbf{x}'| + \frac{3-n}{4}\right\}$$
$$\times\exp\left\{-\sqrt{\frac{2M}{\hbar^2}\left[V\left(\frac{\mathbf{x}+\mathbf{x}'}{2}\right) - \mu + 2g\Sigma\left(\frac{\mathbf{x}+\mathbf{x}'}{2}\right) - \frac{D}{\hbar}Q_0\left(\frac{\mathbf{x}+\mathbf{x}'}{2}\right)\right]}\,|\mathbf{x}-\mathbf{x}'|\right\}$$

respectively. Note that the function $g_2\left(\mathbf{x}-\mathbf{x}', \frac{\mathbf{x}+\mathbf{x}'}{2}; \tau-\tau'\right)$ turns out not to depend on $\tau-\tau'$ at all.

Since we developed the expressions of $g_1\left(\mathbf{x}-\mathbf{x}', \frac{\mathbf{x}+\mathbf{x}'}{2}; \tau-\tau'\right)$ and $g_2\left(\mathbf{x}-\mathbf{x}', \frac{\mathbf{x}+\mathbf{x}'}{2}; \tau-\tau'\right)$, let us now determine the disorder average of the 4-point function:

$$\left|\langle\psi(\mathbf{x},\tau)\psi^*(\mathbf{x}',\tau')\rangle\right|^2 = \langle\psi(\mathbf{x},\tau)\psi^*(\mathbf{x}',\tau')\rangle\,\langle\psi^*(\mathbf{x},\tau)\psi(\mathbf{x}',\tau')\rangle\,, \tag{2.111}$$

which turns out to have the replica representation:

$$\overline{\left|\langle\psi(\mathbf{x},\tau)\psi^*(\mathbf{x}',\tau')\rangle\right|^2} = \lim_{N\to 0}\frac{\hbar^4}{\mathcal{N}(\mathcal{N}-1)}\sum_{\alpha\neq\alpha'}\frac{\delta^4\overline{\mathcal{Z}[j^*,j]}}{\delta j^*_\alpha(\mathbf{x},\tau)j_\alpha(\mathbf{x}',\tau')\delta j^*_{\alpha'}(\mathbf{x}',\tau')j_{\alpha'}(\mathbf{x},\tau)}\Bigg|_{j(\mathbf{x},\tau)=0}^{j^*(\mathbf{x},\tau)=0}. \tag{2.112}$$

Inserting the generating functional (2.102) into (2.112) leads to:

$$\overline{\left|\langle\psi(\mathbf{x},\tau)\psi^*(\mathbf{x}',\tau')\rangle\right|^2} = \left|\overline{\langle\psi(\mathbf{x},\tau)\psi^*(\mathbf{x}',\tau')\rangle}\right|^2 + n_0(\mathbf{x})\,g_2(\mathbf{0},\mathbf{x}';0) + n_0(\mathbf{x}')\,g_2(\mathbf{0},\mathbf{x};0)$$
$$+ g_2(\mathbf{0},\mathbf{x};0)g_2(\mathbf{0},\mathbf{x}';0)\,. \tag{2.113}$$

Now we are in the position to investigate the 2- and the 4-point function (2.104) and (2.113) for special values of their spatio-temporal arguments. At first, we set $\tau=\tau'$ and study their behavior in the long-range limit $|\mathbf{x}-\mathbf{x}'|\to\infty$. From (2.104) with (2.109) and (2.110) we obtain for the 2-point function:

$$\lim_{|\mathbf{x}-\mathbf{x}'|\to\infty}\overline{\langle\psi(\mathbf{x},\tau)\psi^*(\mathbf{x}',\tau)\rangle} = \sqrt{n_0(\mathbf{x})n_0(\mathbf{x}')}\,. \tag{2.114}$$

Correspondingly, the 4-point function (2.113) leads together with (2.90) and (2.110) to:

$$\lim_{|\mathbf{x}-\mathbf{x}'|\to\infty}\overline{\left|\langle\psi(\mathbf{x},\tau)\psi^*(\mathbf{x}',\tau)\rangle\right|^2} = \left[n_0(\mathbf{x})+q(\mathbf{x})\right]\left[n_0(\mathbf{x}')+q(\mathbf{x}')\right]\,. \tag{2.115}$$

Following the notion of classical spin-glass theory [94,112], this result justifies to consider the quantities $n_0(\mathbf{x})$ and $q(\mathbf{x})$ as the order parameters of the condensate and the Bose-glass phase, respectively.

However, in analogy to quantum spin-glass theory [58], the Bose-glass order parameter $q(\mathbf{x})$, which has been introduced in Ref. [84] in close analogy to the Edward-Anderson order parameter of spin-glasses [113], should also be related to the long-time limit $|\tau-\tau'|\to\infty$ of the 2-point function (2.104) at $T=0$. At $T=0$ the term (2.109) vanishes, whereas (2.110) remains valid as it is temperature independent. By setting $\mathbf{x}=\mathbf{x}'$, we consider the behavior of the 2-point function (2.104) in the long-time limit $|\tau-\tau'|\to\infty$. From (2.90), (2.104), (2.109), and (2.110), we read off:

$$\lim_{|\tau-\tau'|\to\infty}\overline{\langle\psi(\mathbf{x},\tau)\psi^*(\mathbf{x},\tau')\rangle}=n_0(\mathbf{x})+q(\mathbf{x})\,. \tag{2.116}$$

Note, furthermore, that the localization of the Bose-glass states can be inferred from the spatial exponential fall-off of the correlation function $g_2(\mathbf{x}-\mathbf{x}',\frac{\mathbf{x}+\mathbf{x}'}{2};\tau-\tau')$ describing correlations of the locally condensed component. In the Bose-glass phase Eq. (2.90) yields $-\mu+2g\Sigma(\mathbf{x})+V(\mathbf{x})-\frac{D}{\hbar}Q_0(\mathbf{x})=\left[D\Gamma\left(2-\frac{n}{2}\right)\left(\frac{M}{2\pi\hbar^2}\right)^{n/2}\right]^{\frac{2}{4-n}}$. Inserting this result into the exponential part of function (2.110) allows us to extract the temperature-independent Larkin length $\mathcal{L}=\frac{\hbar}{\sqrt{2M}}\left[D\Gamma\left(2-\frac{n}{2}\right)\left(\frac{M}{2\pi\hbar^2}\right)^{n/2}\right]^{\frac{1}{n-4}}$, which is the length where this exponential fall-off, which is also found in Refs. [82, 83, 114]. Note that this Larkin length is independent of both the densities and the interaction strength g, since the Hartree-Fock approximation is an effective free-particle theory.

2.9. Thermodynamic Properties

Now we return to the replicated effective potential (2.40) and evaluate it for the special case of a δ-correlated disorder potential (2.72) and contact interaction potential (2.78) at the replica-symmetric background fields (2.43) and (2.44) by taking into account (2.46). Thus, the replicated effective potential decomposes according to $V_{\rm eff}^{(\mathcal{N})}=V_{\rm eff}^{(\mathcal{N},1)}+V_{\rm eff}^{(\mathcal{N},2)}$. The first term reads

$$\begin{aligned}V_{\rm eff}^{(\mathcal{N},1)} &= \mathcal{N}\int d^nx\Bigg\{-g\Sigma^2(\mathbf{x})-\frac{g}{2}\Psi^{*2}(\mathbf{x})\Psi^2(\mathbf{x})+\Psi^*(\mathbf{x})\left[-\mu-\frac{\hbar^2}{2M}\boldsymbol{\Delta}+2g\Sigma(\mathbf{x})+V(\mathbf{x})-\frac{D}{2\hbar}Q_0^*(\mathbf{x})\right.\\ &\quad\left.-\frac{D}{2\hbar}Q_0(\mathbf{x})\right]\Psi(\mathbf{x})+\frac{D}{2\beta\hbar^2}\lim_{\eta\downarrow0}\sum_{m=-\infty}^{\infty}e^{i\omega_m\eta}\left[Q_m^*(\mathbf{x})+Q_m(\mathbf{x})\right]q_m(\mathbf{x})+\frac{D}{2\hbar}\left[Q_0^*(\mathbf{x})+Q_0(\mathbf{x})\right]\\ &\quad\times\Psi^*(\mathbf{x})\Psi(\mathbf{x})+\frac{D}{2\hbar^2\beta}\lim_{\eta\downarrow0}\sum_{m=-\infty}^{\infty}e^{i\omega_m\eta}\,Q_m(\mathbf{x})Q_{-m}^*(\mathbf{x})\Bigg\}+\frac{\mathcal{N}^2\beta D}{2}\int d^nx\\ &\quad\left\{\left[\Sigma(\mathbf{x})-\Psi^*(\mathbf{x})\Psi(\mathbf{x})\right]^2+\frac{1}{(\beta\hbar)^2}\lim_{\eta\downarrow0}\sum_{m=-\infty}^{\infty}e^{i\omega_m\eta}\,q_m(\mathbf{x})q_{-m}^*(\mathbf{x})-\Psi^{*2}(\mathbf{x})\Psi^2(\mathbf{x})\right\},\end{aligned} \tag{2.117}$$

where, again, the normal ordering is explicitly emphasized and the second term is given by the tracelog of the integral kernel (2.49):

$$V_{\rm eff}^{(\mathcal{N},2)}=\frac{1}{2\beta}\,{\rm Tr}\,\ln G^{-1}\,. \tag{2.118}$$

With the help of the Fourier-Matsubara transformation (2.52) the latter reduces to

$$V_{\rm eff}^{(\mathcal{N},2)}=\frac{1}{2\beta}\int d^nx\int\frac{d^nk}{(2\pi)^n}\lim_{\eta\downarrow0}\sum_{m=-\infty}^{\infty}e^{i\omega_m\eta}\ln\left[{\rm Det}\,G^{-1}_{\alpha\alpha'}(\mathbf{k},\omega_m,\mathbf{x})\right]\,, \tag{2.119}$$

where the determinant of the matrix (2.53) yields

$$\begin{aligned}{\rm Det}\,G^{-1}_{\alpha\alpha'}(\mathbf{k},\omega_m,\mathbf{x}) &= \left[a(\mathbf{k},\omega_m,\mathbf{x})a^*(\mathbf{k},\omega_m,\mathbf{x})\right]^{\mathcal{N}-1}\left[a(\mathbf{k},\omega_m,\mathbf{x})+\mathcal{N}b(\mathbf{k},\omega_m,\mathbf{x})\right]\\ &\quad\left[a^*(\mathbf{k},\omega_m,\mathbf{x})+\mathcal{N}b^*(\mathbf{k},\omega_m,\mathbf{x})\right]\,.\end{aligned} \tag{2.120}$$

Inserting (2.75) and (2.79) with (2.120) into (2.119), we obtain:

$$
\begin{aligned}
V_{\text{eff}}^{(\mathcal{N},2)} &= \frac{1}{2\beta}\int d^n x \int \frac{d^n k}{(2\pi)^n}\left\{\mathcal{N}\lim_{\eta\downarrow 0}\sum_{m=-\infty}^{\infty} e^{i\omega_m\eta}\ln\left[-i\hbar\omega_m+\epsilon(\mathbf{k})-\mu+2g\Sigma\left(\mathbf{x}\right)+V\left(\mathbf{x}\right)\right.\right. \\
&\left.-\frac{D}{\hbar}Q_m\left(\mathbf{x}\right)\right]+\mathcal{N}\lim_{\eta\downarrow 0}\sum_{m=-\infty}^{\infty} e^{i\omega_m\eta}\ln\left[i\hbar\omega_m+\epsilon(\mathbf{k})-\mu+2g\Sigma\left(\mathbf{x}\right)+V\left(\mathbf{x}\right)-\frac{D}{\hbar}Q_m^*\left(\mathbf{x}\right)\right] \\
&+\ln\left[1-\mathcal{N}\frac{\beta D\left[\Sigma\left(\mathbf{x}\right)+q\left(\mathbf{x}\right)+\Psi^*\left(\mathbf{x}\right)\Psi\left(\mathbf{x}\right)\right]}{\epsilon(\mathbf{k})-\mu+2g\Sigma\left(\mathbf{x}\right)+V\left(\mathbf{x}\right)-\frac{D}{\hbar}Q_0^*\left(\mathbf{x}\right)}\right] \\
&+\ln\left[1-\mathcal{N}\frac{\beta D\left[\Sigma\left(\mathbf{x}\right)+q\left(\mathbf{x}\right)+\Psi^*\left(\mathbf{x}\right)\Psi\left(\mathbf{x}\right)\right]}{\epsilon(\mathbf{k})-\mu+2g\Sigma\left(\mathbf{x}\right)+V\left(\mathbf{x}\right)-\frac{D}{\hbar}Q_0\left(\mathbf{x}\right)}\right] \\
&+(\mathcal{N}-1)\ln\left[1-\mathcal{N}\frac{\beta D\Sigma\left(\mathbf{x}\right)}{\epsilon(\mathbf{k})-\mu+2g\Sigma\left(\mathbf{x}\right)+V\left(\mathbf{x}\right)-\frac{D}{\hbar}Q_0^*\left(\mathbf{x}\right)}\right] \\
&\left.+(\mathcal{N}-1)\ln\left[1-\mathcal{N}\frac{\beta D\Sigma\left(\mathbf{x}\right)}{\epsilon(\mathbf{k})-\mu+2g\Sigma\left(\mathbf{x}\right)+V\left(\mathbf{x}\right)-\frac{D}{\hbar}Q_0\left(\mathbf{x}\right)}\right]\right\}. \qquad (2.121)
\end{aligned}
$$

In Ref. [84] the replica limit is taken as soon as the replica number $\mathcal{N}$ appears at different steps of the calculation. In our work, and contrary to Ref. [84], until this level of the calculation no replica limit was performed yet for the free energy. We are taking this limit as late as possible in order to avoid any possible loss of terms due to the performance of the replica limit in an earlier step of the calculation. Performing the replica limit $\mathcal{N}\to 0$ the respective contributions to the replicated effective potential reduce to

$$
\begin{aligned}
V_{\text{eff}}^{(1)} &= \lim_{\mathcal{N}\to 0}\frac{V_{\text{eff}}^{(\mathcal{N},1)}}{\mathcal{N}}=\int d^n x\left\{-g\Sigma^2(\mathbf{x})-\frac{g}{2}\Psi^{*2}(\mathbf{x})\Psi^2(\mathbf{x})\right. \qquad (2.122)\\
&+\Psi^*(\mathbf{x})\left[-\mu-\frac{\hbar^2}{2M}\mathbf{\Delta}+2g\Sigma(\mathbf{x})+V\left(\mathbf{x}\right)-\frac{D}{2\hbar}Q_0^*(\mathbf{x})-\frac{D}{2\hbar}Q_0(\mathbf{x})\right]\Psi(\mathbf{x}) \\
&\left.+\frac{D}{2\hbar^2\beta}\lim_{\eta\downarrow 0}\sum_{m=-\infty}^{\infty} e^{i\omega_m\eta}\,Q_m(\mathbf{x})Q_{-m}^*(\mathbf{x})+\frac{D}{2\hbar}\left[Q_0^*(\mathbf{x})+Q_0(\mathbf{x})\right]\left[q(\mathbf{x})+\Psi^*(\mathbf{x})\Psi(\mathbf{x})\right]\right\}
\end{aligned}
$$

and

$$
\begin{aligned}
V_{\text{eff}}^{(2)} &= \lim_{\mathcal{N}\to 0}\frac{V_{\text{eff}}^{(\mathcal{N},2)}}{\mathcal{N}}=\frac{1}{2\beta}\int d^n x\int\frac{d^n k}{(2\pi)^n} \qquad (2.123)\\
&\left\{\lim_{\eta\downarrow 0}\sum_{m=-\infty}^{\infty} e^{i\omega_m\eta}\ln\left[-i\hbar\omega_m+\epsilon(\mathbf{k})-\mu+2g\Sigma(\mathbf{x})+V(\mathbf{x})-\frac{D}{\hbar}Q_m(\mathbf{x})\right]\right. \\
&+\lim_{\eta\downarrow 0}\sum_{m=-\infty}^{\infty} e^{i\omega_m\eta}\ln\left[i\hbar\omega_m+\epsilon(\mathbf{k})-\mu+2g\Sigma(\mathbf{x})+V(\mathbf{x})-\frac{D}{\hbar}Q_m^*(\mathbf{x})\right] \\
&\left.-\frac{\beta D\left[q(\mathbf{x})+\Psi^*(\mathbf{x})\Psi(\mathbf{x})\right]}{\epsilon(\mathbf{k})-\mu+2g\Sigma(\mathbf{x})+V(\mathbf{x})-\frac{D}{\hbar}Q_0(\mathbf{x})}-\frac{\beta D\left[q(\mathbf{x})+\Psi^*(\mathbf{x})\Psi(\mathbf{x})\right]}{\epsilon(\mathbf{k})-\mu+2g\Sigma(\mathbf{x})+V(\mathbf{x})-\frac{D}{\hbar}Q_0^*(\mathbf{x})}\right\}.
\end{aligned}
$$

The remaining $\mathbf{k}$-integrals of the logarithmic functions in (2.123) are UV-divergent in all dimensions, while the $\mathbf{k}$-integrals of the third and the fourth terms in (2.123) diverges in two and three dimensions and converges only in one dimension. Thus, we evaluate (2.123) by using, again, the dimensional regularization method. With the Schwinger integral (2.82) and the corresponding Schwinger representation of the logarithm:

$$
\ln a=-\frac{\partial}{\partial x}\left[\frac{1}{\Gamma(x)}\int_0^\infty ds\, s^{x-1}\,e^{-as}\right]\Big|_{x=0}, \qquad (2.124)
$$

we obtain from (2.123):

$$
\begin{aligned}
V_{\text{eff}}^{(2)} &= -\frac{1}{2\beta}\left(\frac{M}{2\pi\hbar^2}\right)^{n/2}\lim_{\eta\downarrow 0}\sum_{m=-\infty}^{\infty}e^{i\omega_m\eta}\int d^nx\,\Gamma\left(-\frac{n}{2}\right)\\
&\times\left\{\left[-i\hbar\omega_m-\mu+2g\Sigma(\mathbf{x})+V(\mathbf{x})-\frac{D}{\hbar}Q_m(\mathbf{x})\right]^{n/2}+\left[i\hbar\omega_m-\mu+2g\Sigma(\mathbf{x})+V(\mathbf{x})-\frac{D}{\hbar}Q_m^*(\mathbf{x})\right]^{n/2}\right\}\\
&-\frac{D}{2}\int d^nx\left[q(\mathbf{x})+\Psi^*(\mathbf{x})\Psi(\mathbf{x})\right]\Gamma\left(-\frac{n}{2}+1\right)\left(\frac{M}{2\pi\hbar^2}\right)^{n/2}\\
&\times\left\{\left[-\mu+2g\Sigma(\mathbf{x})+V(\mathbf{x})-\frac{D}{\hbar}Q_0(\mathbf{x})\right]^{\frac{n}{2}-1}+\left[-\mu+2g\Sigma(\mathbf{x})+V(\mathbf{x})-\frac{D}{\hbar}Q_0^*(\mathbf{x})\right]^{\frac{n}{2}-1}\right\}. \qquad (2.125)
\end{aligned}
$$

The effective potential $V_{\text{eff}}=V_{\text{eff}}^{(1)}+V_{\text{eff}}^{(2)}$ resulting from (2.122) and (2.125) represents a function of all degrees of freedom of the replica-symmetric background fields (2.44). It is extremal with respect to all these variables $\Psi^*(\mathbf{x})$, $\Psi(\mathbf{x})$, $\Sigma(\mathbf{x})$, $Q_m^*(\mathbf{x})$, $Q_m(\mathbf{x})$, $q(\mathbf{x})$, if the mean-field Eqs. (2.89)–(2.92) are fulfilled.
As the extremum of the effective potential yields the thermodynamic potential, we obtain from (2.122) and (2.125) at first:

$$
\begin{aligned}
\mathcal{F} &= \int d^nx\left\{-g\Sigma^2(\mathbf{x})-\frac{g}{2}n_0^2(\mathbf{x})-\sqrt{n_0(\mathbf{x})}\left[\mu+\frac{\hbar^2}{2M}\mathbf{\Delta}-2g\Sigma(\mathbf{x})-V(\mathbf{x})+\frac{D}{\hbar}Q_0(\mathbf{x})\right]\sqrt{n_0(\mathbf{x})}\right.\\
&+\frac{D}{\hbar}Q_0(\mathbf{x})\left[q(\mathbf{x})+n_0(\mathbf{x})\right]+\frac{D}{2\hbar^2\beta}\lim_{\eta\downarrow 0}\sum_{m=-\infty}^{\infty}e^{i\omega_m\eta}\,Q_m^2(\mathbf{x}) \qquad (2.126)\\
&-D\Gamma\left(-\frac{n}{2}+1\right)\left(\frac{M}{2\pi\hbar^2}\right)^{n/2}\left[q(\mathbf{x})+n_0(\mathbf{x})\right]\left[-\mu+2g\Sigma(\mathbf{x})+V(\mathbf{x})-\frac{D}{\hbar}Q_0(\mathbf{x})\right]^{\frac{n}{2}-1}\\
&\left.-\frac{1}{\beta}\Gamma\left(-\frac{n}{2}\right)\left(\frac{M}{2\pi\hbar^2}\right)^{n/2}\lim_{\eta\downarrow 0}\sum_{m=-\infty}^{\infty}e^{i\omega_m\eta}\left[-i\hbar\omega_m-\mu+2g\Sigma(\mathbf{x})+V(\mathbf{x})-\frac{D}{\hbar}Q_m(\mathbf{x})\right]^{n/2}\right\}.
\end{aligned}
$$

Thus, the particle density $n(\mathbf{x})$ defined according to

$$N=-\frac{\partial\mathcal{F}}{\partial\mu}=\int d^nx\,n(\mathbf{x}), \qquad (2.127)$$

where N denotes the particle number, turns out to coincide with the mean-field $\Sigma(\mathbf{x})$ due to (2.89), (2.90), and (2.92):

$$\Sigma(\mathbf{x})=n(\mathbf{x}). \qquad (2.128)$$

Furthermore, all self-consistency equations (2.89)–(2.91) can be directly obtained by extremising the thermodynamic potential (2.126) with respect to its variables $Q_{m\neq 0}(\mathbf{x})$, $Q_0(\mathbf{x})$, $q(\mathbf{x})$, and $\sqrt{n_0(\mathbf{x})}$. Indeed, the combination of the two extremisations $\frac{\delta\mathcal{F}}{\delta Q_{m\neq 0}(\mathbf{x}')}=0$ and $\frac{\delta\mathcal{F}}{\delta q(\mathbf{x}')}=0$ gives us equation (2.89), while the extremisations $\frac{\delta\mathcal{F}}{\delta Q_0(\mathbf{x}')}=0$ and $\frac{\delta\mathcal{F}}{\delta\sqrt{n_0(\mathbf{x}')}}=0$ yield equations (2.90) and (2.91), respectively.

Now we apply our theory, which is formulated for a general n-dimensional homogeneous system, to first the three-dimensional dirty bosons, since it is less complicated, and then to the one-dimensional dirty bosons. The two-dimensional case can not be treated using the actual form of the theory as has already been discussed in detail below Eq. (2.86).

2.10. Application of Hartree-Fock Mean-Field Theory in 3D

We treat first the three-dimensional case since it is less complicated than the one-dimensional case. In three dimensions, i.e., $n=3$, Eqs. (2.85) and (2.86) reduce to:

$$Q_m(\mathbf{x}) = -2\sqrt{\pi}\hbar \left(\frac{M}{2\pi\hbar^2}\right)^{3/2} \sqrt{-i\hbar\omega_m - \mu + 2gn(\mathbf{x}) + V(\mathbf{x}) - \frac{D}{\hbar}Q_m(\mathbf{x}) - \mathcal{N}\beta D n(\mathbf{x})\,\delta_{m,0}}\,, \quad (2.129)$$

$$\begin{aligned} q_m(\mathbf{x}) =& \frac{2\sqrt{\pi}\hbar}{\mathcal{N}} \left(\frac{M}{2\pi\hbar^2}\right)^{3/2} \left\{ \sqrt{-i\hbar\omega_m - \mu + 2gn(\mathbf{x}) + V(\mathbf{x}) - \frac{D}{\hbar}Q_m(\mathbf{x}) - \mathcal{N}\beta D n(\mathbf{x})\,\delta_{m,0}} \right. \\ & \left. - \sqrt{-i\hbar\omega_m - \mu + 2gn(\mathbf{x}) + V(\mathbf{x}) - \frac{D}{\hbar}Q_m(\mathbf{x}) - \mathcal{N}\beta D n(\mathbf{x})\,\delta_{m,0} - \mathcal{N}\frac{D}{\hbar}\left[q_m(\mathbf{x}) + \hbar\beta\Psi^*(\mathbf{x})\Psi(\mathbf{x})\,\delta_{m,0}\right]} \right\}. \end{aligned} \quad (2.130)$$

Squaring (2.129) yields a quadratic equation for the corresponding Matsubara coefficients $Q_m(\mathbf{x})$ which is solved by:

$$\begin{aligned} Q_m(\mathbf{x}) =& -2\pi\hbar D \left(\frac{M}{2\pi\hbar^2}\right)^3 \pm 2\sqrt{\pi}\hbar \left(\frac{M}{2\pi\hbar^2}\right)^{3/2} \\ & \times \sqrt{-i\hbar\omega_m - \mu + 2gn(\mathbf{x}) + V(\mathbf{x}) + \pi D^2 \left(\frac{M}{2\pi\hbar^2}\right)^3 + \mathcal{N}\beta D n(\mathbf{x})\,\delta_{m,0}}\,. \end{aligned} \quad (2.131)$$

Now we have to check whether both solutions (2.131) really solve the original algebraic equation (2.129). To this end we reinsert (2.131) into (2.129), yielding:

$$\begin{aligned} Q_m(\mathbf{x}) =& -2\sqrt{\pi}\hbar \left(\frac{M}{2\pi\hbar^2}\right)^{3/2} \\ & \times \sqrt{\left[\sqrt{-i\hbar\omega_m - \mu + 2gn(\mathbf{x}) + V(\mathbf{x}) + \pi D^2 \left(\frac{M}{2\pi\hbar^2}\right)^3 + \mathcal{N}\beta D n(\mathbf{x})\,\delta_{m,0}} \mp \sqrt{\pi} D \left(\frac{M}{2\pi\hbar^2}\right)^{3/2}\right]^2}\,. \end{aligned} \quad (2.132)$$

Squaring (2.129) and inserting it into (2.130) yields also a quadratic equation for the corresponding Matsubara coefficients $q_m(\mathbf{x})$ which is solved by:

$$\begin{aligned} q_m(\mathbf{x}) =& -\frac{1}{\mathcal{N}}\left[2\pi\hbar D \left(\frac{M}{2\pi\hbar^2}\right)^3 + Q_m(\mathbf{x})\right] \\ & \pm \frac{1}{\mathcal{N}}\sqrt{\left[2\pi\hbar D \left(\frac{M}{2\pi\hbar^2}\right)^3 + Q_m(\mathbf{x})\right]^2 - 4\mathcal{N}\pi\hbar^2\beta D \left(\frac{M}{2\pi\hbar^2}\right)^3 \Psi^*(\mathbf{x})\Psi(\mathbf{x})\,\delta_{m,0}}\,. \end{aligned} \quad (2.133)$$

2.10.1. Replica Limit

Now we perform the replica limit $\mathcal{N} \to 0$ and, in parallel, we treat both cases $m = 0$ and $m \neq 0$ separately.

At first, we consider the case $m = 0$ and note that $Q_0(\mathbf{x})$ has to be real according to (2.87). Furthermore, we find that the compatibility of (2.131) and (2.132) for $m = 0$ fixes $Q_0(\mathbf{x})$ to be:

$$Q_0(\mathbf{x}) = \begin{cases} -2\sqrt{\pi}\hbar\left(\frac{M}{2\pi\hbar^2}\right)^{3/2}\left[\sqrt{\pi}D\left(\frac{M}{2\pi\hbar^2}\right)^{3/2} + \sqrt{-\mu_r(\mathbf{x})}\right]\,; & \mu_r(\mathbf{x}) \leq 0 \\ -2\sqrt{\pi}\hbar\left(\frac{M}{2\pi\hbar^2}\right)^{3/2}\left[\sqrt{\pi}D\left(\frac{M}{2\pi\hbar^2}\right)^{3/2} - \sqrt{-\mu_r(\mathbf{x})}\right]\,; & \mu_r^{(\mathrm{crit})} \leq \mu_r(\mathbf{x}) \leq 0\,, \end{cases} \quad (2.134)$$

where we have introduced the renormalized chemical potential:

$$\mu_r(\mathbf{x}) = \mu - V(\mathbf{x}) - 2gn(\mathbf{x}) - \pi D^2 \left(\frac{M}{2\pi\hbar^2}\right)^3 \tag{2.135}$$

and the critical chemical potential is defined by:

$$\mu_r^{(\mathrm{crit})} = -\pi D^2 \left(\frac{M}{2\pi\hbar^2}\right)^3 . \tag{2.136}$$

Thus, we obtain from (2.132) that the condition $\mu_r(\mathbf{x}) \leq 0$ has to be fulfilled.

Now, we consider the case $m \neq 0$, where (2.131) and (2.132) are only compatible for the lower sign, i.e., we conclude:

$$Q_m(\mathbf{x}) = -2\pi\hbar D \left(\frac{M}{2\pi\hbar^2}\right)^3 - 2\sqrt{\pi}\hbar \left(\frac{M}{2\pi\hbar^2}\right)^{3/2} \sqrt{-i\hbar\omega_m - \mu_r(\mathbf{x})}\,, \qquad m \neq 0\,. \tag{2.137}$$

According to (2.133) $q_0(\mathbf{x})$ has also to be real and in the replica limit

$$q_m(\mathbf{x}) = \begin{cases} q_{m\neq 0}(\mathbf{x}) & m \neq 0 \\ \hbar\beta q(\mathbf{x}) & m = 0, \end{cases} \tag{2.138}$$

where $q(\mathbf{x})$ satisfies the algebraic equation:

$$q(\mathbf{x}) = \begin{cases} \sqrt{\pi} D \left(\frac{M}{2\pi\hbar^2}\right)^{3/2} \frac{n_0(\mathbf{x})}{\sqrt{-\mu_r(\mathbf{x})}}\,; & \mu_r(\mathbf{x}) \leq 0 \\ -\sqrt{\pi} D \left(\frac{M}{2\pi\hbar^2}\right)^{3/2} \frac{n_0(\mathbf{x})}{\sqrt{-\mu_r(\mathbf{x})}}\,; & \mu_r^{(\mathrm{crit})} \leq \mu_r(\mathbf{x}) \leq 0 \end{cases} \tag{2.139}$$

and

$$q_{m\neq 0}(\mathbf{x}) = \begin{cases} 0\,; & \mu_r(\mathbf{x}) \leq 0, \\ \lim\limits_{N\to 0} -\frac{2}{N} \left[2\pi\hbar D \left(\frac{M}{2\pi\hbar^2}\right)^3 + Q_m(\mathbf{x})\right]\,; & \mu_r^{(\mathrm{crit})} \leq \mu_r(\mathbf{x}) \leq 0\,. \end{cases} \tag{2.140}$$

Since, as it is already shown in the end of Section 2.8, $q(\mathbf{x})$ is a density, i. e., it has to be positive, so the negative solution in equation (2.139) is rejected. Furthermore, the second solution of (2.140) has to be rejected since it diverges in the replica limit. Thus,

$$q_m(\mathbf{x}) = \begin{cases} 0 & m \neq 0 \\ \hbar\beta\sqrt{\pi} D \left(\frac{M}{2\pi\hbar^2}\right)^{3/2} \frac{n_0(\mathbf{x})}{\sqrt{-\mu_r(\mathbf{x})}} & m = 0, \end{cases} \tag{2.141}$$

Due to the assumed homogeneity in time we had to put $q(\mathbf{x}-\mathbf{x}', \frac{\mathbf{x}+\mathbf{x}'}{2}, \tau - \tau')$ in equation (2.44) to be time dependent, but according to equation (2.141) this quantity turns out to be time independent. We note also that the replica limit eliminates the disorder contribution with $\mathcal{N}\beta D n(\mathbf{x})\,\delta_{m,0}$ in (2.131) and (2.133).

Taking into account (2.134) and (2.137), we get at first:

$$\begin{aligned} n(\mathbf{x}) \;=\; & q(\mathbf{x}) + n_0(\mathbf{x}) + \frac{\Delta Q_0(\mathbf{x})}{\hbar\beta} \\ & -\frac{2\sqrt{\pi}}{\beta} \left(\frac{M}{2\pi\hbar^2}\right)^{3/2} \lim_{\eta\downarrow 0} \sum_{m=-\infty}^{\infty} e^{i\omega_m\eta} \left[\sqrt{\pi} D \left(\frac{M}{2\pi\hbar^2}\right)^{3/2} + \sqrt{-i\hbar\omega_m - \mu_r(\mathbf{x})}\right], \end{aligned} \tag{2.142}$$

where the following abbreviation has been introduced:

$$\Delta Q_0(\mathbf{x}) = Q_0(\mathbf{x}) - \lim_{m\to 0} Q_m(\mathbf{x}) = \begin{cases} 0\,; & \mu_r(\mathbf{x}) \leq 0 \\ 4\sqrt{\pi}\hbar \left(\frac{M}{2\pi\hbar^2}\right)^{3/2} \sqrt{-\mu_r(\mathbf{x})}\,; & \mu_r^{(\mathrm{crit})} \leq \mu_r(\mathbf{x}) \leq 0 \end{cases} \tag{2.143}$$

Then the remaining Matsubara sums (2.142) are evaluated by using the zeta function regularization method [115]. The first sum in (2.142) vanishes immediately due to the Poisson formula:

$$\sum_{m=-\infty}^{\infty} \delta(x-m) = \sum_{n=-\infty}^{\infty} e^{-2\pi i n x}\,. \tag{2.144}$$

In order to calculate the second sum in (2.142), we apply both the Schwinger integral (2.82) and the Poisson formula (2.144) to obtain:

$$\lim_{\eta\downarrow 0} \sum_{m=-\infty}^{\infty} e^{i\omega_m \eta} \left(-i\hbar\omega_m + a\right)^{\nu} = \frac{\zeta_{\nu+1}\left(e^{-a\beta}\right)}{\beta^{\nu}\,\Gamma(-\nu)}, \tag{2.145}$$

with the polylogarithmic function:

$$\zeta_{\nu}(z) = \sum_{\mathtt{n}=1}^{\infty} \frac{z^{\mathtt{n}}}{\mathtt{n}^{\nu}}\,. \tag{2.146}$$

Thus, we result in mean-field:

$$n(\mathbf{x}) = q(\mathbf{x}) + n_0(\mathbf{x}) + \frac{\Delta Q_0(\mathbf{x})}{\hbar\beta} + \left(\frac{M}{2\pi\hbar^2\beta}\right)^{3/2} \zeta_{3/2}\left(e^{\beta\mu_r(\mathbf{x})}\right)\,. \tag{2.147}$$

2.10.2. Free Energy

The remaining Matsubara sums in the expression of the thermodynamic potential (2.126) are evaluated in three dimensions by using, again, the zeta function regularization method. Taking into account (2.134), (2.137), and (2.145) yields

$$\frac{D}{2\hbar^2\beta} \lim_{\eta\downarrow 0} \sum_{m=-\infty}^{\infty} e^{i\omega_m\eta}\, Q_m^2(\mathbf{x}) = -2\pi D^2 \left(\frac{M}{2\pi\hbar^2}\right)^3 \left(\frac{M}{2\pi\hbar^2\beta}\right)^{3/2} \zeta_{3/2}\left(e^{\beta\mu_r(\mathbf{x})}\right) - \frac{2\pi D^2 \Delta Q_0(\mathbf{x})}{\hbar\beta} \left(\frac{M}{2\pi\hbar^2}\right)^3 \tag{2.148}$$

and, correspondingly,

$$\begin{aligned}
&-\frac{4\sqrt{\pi}}{3\beta} \left(\frac{M}{2\pi\hbar^2}\right)^{3/2} \lim_{\eta\downarrow 0} \sum_{m=-\infty}^{\infty} e^{i\omega_m\eta} \left[-i\hbar\omega_m - \mu + 2gn(\mathbf{x}) + V(\mathbf{x}) - \frac{D}{\hbar} Q_m(\mathbf{x})\right]^{3/2} \\
&= 2\pi D^2 \left(\frac{M}{2\pi\hbar^2}\right)^3 \left(\frac{M}{2\pi\hbar^2\beta}\right)^{3/2} \zeta_{3/2}\left(e^{\beta\mu_r(\mathbf{x})}\right) - \frac{1}{\beta} \left(\frac{M}{2\pi\hbar^2\beta}\right)^{3/2} \zeta_{5/2}\left(e^{\beta\mu_r(\mathbf{x})}\right) \\
&+ \frac{2\pi D^2 \Delta Q_0(\mathbf{x})}{\hbar\beta} \left(\frac{M}{2\pi\hbar^2}\right)^3 + \frac{\Delta Q_0^3(\mathbf{x})}{24\pi\hbar^3\beta} \left(\frac{M}{2\pi\hbar^2}\right)^{-3}\,.
\end{aligned} \tag{2.149}$$

Using the mean-field equation (2.91), the thermodynamic potential (2.126) is now given in three dimensions by:

$$\begin{aligned}
\mathcal{F} \;=\; & \int d\mathbf{x} \Bigg\{ -g\, n^2(\mathbf{x}) - \frac{g}{2} n_0^2(\mathbf{x}) - \sqrt{n_0(\mathbf{x})} \Bigg\{ \mu + \frac{\hbar^2}{2M}\boldsymbol{\Delta} - 2gn(\mathbf{x}) - V(\mathbf{x}) \\
& -2\sqrt{\pi} D \left(\frac{M}{2\pi\hbar^2}\right)^{3/2} \left[\sqrt{\pi} D \left(\frac{M}{2\pi\hbar^2}\right)^{3/2} + \sqrt{-\mu + 2gn(\mathbf{x}) + V(\mathbf{x}) + \pi D^2 \left(\frac{M}{2\pi\hbar^2}\right)^3}\right] \Bigg\} \sqrt{n_0(\mathbf{x})} \\
& -\frac{1}{\beta} \left(\frac{M}{2\pi\hbar^2\beta}\right)^{3/2} \zeta_{5/2}\left(e^{\beta\mu_r(\mathbf{x})}\right) + \frac{\Delta Q_0^3(\mathbf{x})}{24\pi\hbar^3\beta} \left(\frac{M}{2\pi\hbar^2}\right)^{-3} \Bigg\}\,.
\end{aligned} \tag{2.150}$$

Note that we have according to (2.143) two solution branches of our mean-field equations for $\mu_r^{(\mathrm{crit})} \leq \mu_r(\mathbf{x}) \leq 0$, one with $\Delta Q_0(\mathbf{x}) = 0$ and another one with $\Delta Q_0(\mathbf{x}) > 0$. As the latter solution branch yields via (2.150) a higher thermodynamic potential, we do no longer consider it in the following and restrict ourselves to the minimum $\Delta Q_0(\mathbf{x}) = 0$. With this equation (2.150) reduces to:

$$\begin{aligned}\mathcal{F} &= \int d\mathbf{x} \Bigg\{ -g\, n^2(\mathbf{x}) + \frac{g}{2} n_0^2(\mathbf{x}) - \frac{1}{\beta} \left(\frac{M}{2\pi\hbar^2\beta} \right)^{3/2} \zeta_{5/2} \left(e^{\beta\mu_r(\mathbf{x})} \right) + \sqrt{n_0(\mathbf{x})} \Bigg\{ -g n_0(\mathbf{x}) \qquad (2.151) \\ &\quad + \left[\sqrt{\pi} D \left(\frac{M}{2\pi\hbar^2} \right)^{3/2} + \sqrt{-\mu + 2gn(\mathbf{x}) + V(\mathbf{x}) + \pi D^2 \left(\frac{M}{2\pi\hbar^2} \right)^3} \right]^2 - \frac{\hbar^2}{2M} \boldsymbol{\Delta} \Bigg\} \sqrt{n_0(\mathbf{x})} \Bigg\}.\end{aligned}$$

Note that the order parameter $q(\mathbf{x})$ does not explicitly contribute to the thermodynamic potential (2.151). During the derivation of (2.151) from (2.126) the explicit dependence on $q(\mathbf{x})$ drops out due to the mean-field equation (2.129).

2.10.3. Self-Consistency Equations

Inserting (2.128) into (2.91), (2.139), and (2.147) we obtain for the particle density $n(\mathbf{x})$:

$$n(\mathbf{x}) = n_0(\mathbf{x}) + q(\mathbf{x}) + n_{\mathrm{th}}(\mathbf{x}), \qquad (2.152)$$

as well as self-consistency equations for its three components: the order parameter of the superfluid $n_0(\mathbf{x})$, which represents the density of the particles in the condensate, the order parameter of the Bose-glass phase $q(\mathbf{x})$, which stands for the density of the particles in the respective minima of the disorder potential and which vanishes in absence of disorder, and the thermal component $n_{\mathrm{th}}(\mathbf{x})$ which vanishes in case of zero temperature. Thus, a boson can be in one of the following three components: in the condensate, in the local condensate or in the thermal phase. The resulting self-consistency equations for $n_0(\mathbf{x})$, $q(\mathbf{x})$, and $n_{\mathrm{th}}(\mathbf{x})$ read:

$$\left\{ -g n_0(\mathbf{x}) + \left[\sqrt{-\mu + d^2 + 2gn(\mathbf{x}) + V(\mathbf{x})} + d \right]^2 - \frac{\hbar^2}{2M} \boldsymbol{\Delta} \right\} \sqrt{n_0(\mathbf{x})} = 0, \qquad (2.153)$$

$$q(\mathbf{x}) = \frac{d n_0(\mathbf{x})}{\sqrt{-\mu + d^2 + 2gn(\mathbf{x}) + V(\mathbf{x})}}, \qquad (2.154)$$

$$n_{\mathrm{th}}(\mathbf{x}) = \left(\frac{M}{2\pi\beta\hbar^2} \right)^{3/2} \varsigma_{3/2} \left(e^{\beta\,[\mu - d^2 - 2gn(\mathbf{x}) - V(\mathbf{x})]} \right). \qquad (2.155)$$

For physical reasons it is plausible to assume that particles accumulate in the center of the trap. Thus, the differential self-consistency equation (2.153) has to be solved with the boundary conditions:

$$\left. \frac{\partial n(\mathbf{x})}{\partial \mathbf{x}} \right|_{\mathbf{x}=\mathbf{0}} = 0, \qquad \left. \frac{\partial n_0(\mathbf{x})}{\partial \mathbf{x}} \right|_{\mathbf{x}=\mathbf{0}} = 0 \qquad (2.156)$$

and the normalization condition

$$N = \int n(\mathbf{x}) d^3x, \qquad (2.157)$$

where $d = \sqrt{\pi} D \left(M/2\pi\hbar^2 \right)^{3/2}$characterizes the disorder strength. In total we have four coupled equations, among them three algebraic equations (2.152), (2.154), (2.155) and one partial differential equation (2.153). In the absence of the disorder, i.e., $d = 0$, the Bose-glass order parameter vanishes and equation (2.153) reduces to the Hartree-Fock Gross-Pitaevskii equation in the clean case.

The self-consistency equations (2.152) and (2.153)–(2.155) are also obtained by first rewriting the thermodynamic potential (2.151) as a function of the chemical potential μ, the condensate density $n_0(\mathbf{x})$, the Bose-glass order parameter $q(\mathbf{x})$ and the thermal contribution $n_{\rm th}(\mathbf{x})$:

$$\begin{aligned}\mathcal{F} &= \int d\mathbf{x}\Bigg\{-g\left[n_0(\mathbf{x})+q(\mathbf{x})+n_{\rm th}(\mathbf{x})\right]^2+\frac{g}{2}n_0^2(\mathbf{x})\\ &-\frac{1}{\beta}\left(\frac{M}{2\pi\hbar^2\beta}\right)^{3/2}\zeta_{5/2}\left(e^{\beta\left\{\mu-2g[n_0(\mathbf{x})+q(\mathbf{x})+n_{\rm th}(\mathbf{x})]-V(\mathbf{x})+d^2\right\}}\right)+\sqrt{n_0(\mathbf{x})}\Bigg\{-gn_0(\mathbf{x})\\ &+\left[d+\sqrt{-\mu+2g\left[n_0(\mathbf{x})+q(\mathbf{x})+n_{\rm th}(\mathbf{x})\right]+V(\mathbf{x})-d^2}\right]^2-\frac{\hbar^2}{2M}\mathbf{\Delta}\Bigg\}\sqrt{n_0(\mathbf{x})}\Bigg\}. \quad (2.158)\end{aligned}$$

and then by performing a partial derivative with respect to μ and extremising with respect to the condensate density, the Bose-glass order parameter, and the thermal contribution:

$$-\frac{\partial\mathcal{F}}{\partial\mu}=N, \qquad \frac{\delta\mathcal{F}}{\delta n_0(\mathbf{x}')}=0, \qquad \frac{\delta\mathcal{F}}{\delta q(\mathbf{x}')}=0, \qquad \frac{\delta\mathcal{F}}{\delta n_{\rm th}(\mathbf{x}')}=0. \quad (2.159)$$

Thus, we recognize that in our mean-field theory the order parameters can be considered as variational parameters. This allows, in principle, to use a variational solution method which is a based on the principle that, among all possible configurations of a physical system, the system realizes the one that extremises the free energy. This method is used in physics both for theory construction and for calculational purposes, see, for instance, the successful variational perturbation theory worked out in Refs. [110, 115–117].

2.11. Application of Hartree-Fock Mean-Field Theory in 1D

Now we come to the one-dimensional case, i.e., $n=1$, where the equations (2.89)–(2.92) reduce to

$$Q_m(x)=\sqrt{\frac{M}{2}}\frac{1}{\sqrt{-i\hbar\omega_m-\mu+2gn(x)+V(x)-\frac{D}{\hbar}Q_m(x)}}, \quad (2.160)$$

$$q(x)=\frac{D}{\hbar M}Q_0^3(x)\,\frac{n_0(x)}{1-\frac{D}{\hbar M}Q_0^3(x)}, \quad (2.161)$$

the Gross-Pitaevskii equation

$$\left[-\mu+2gn(x)+V(x)-gn_0(x)-\frac{D}{\hbar}Q_0(x)-\frac{\hbar^2}{2M}\frac{\partial^2}{\partial x^2}\right]\sqrt{n_0(x)}=0 \quad (2.162)$$

and the particle density

$$n(x)=q(x)+n_0(x)+\lim_{\eta\downarrow 0}\sum_{m=-\infty}^{\infty}e^{i\omega_m\eta}\,\frac{Q_m(x)}{\hbar\beta}\,. \quad (2.163)$$

Equation (2.160) represents a cubic equation with respect to $Q_m(x)$:

$$-\frac{D}{\hbar}Q_m^3(x)+\left[-i\hbar\omega_m-\mu+2gn(x)+V(x)\right]Q_m^2(x)-\frac{M}{2}=0, \quad (2.164)$$

whose result should be inserted into equations (2.161)–(2.164). To this end we have to use the Cardan method which is a mathematical tool to solve an algebraic cubic equation exactly [118]. It is characterized by a discriminant δ according to Appendix A, which has for equation (2.164) the following form:

$$\delta_m = \frac{\hbar^2 M}{108 D^4}\left\{27D^2M + 8\hbar^2\left[i\hbar\omega_m + \mu - 2gn(x) - V(x)\right]^3\right\}. \tag{2.165}$$

As the finite temperature case is too complicated to deal with, we restrict ourselves to zero temperature, where only the $m = 0$ term contributes. In this case the discriminant δ has a real value and the Cardan method can be applied. According to the sign of the discriminant δ_0 we get the following real solutions for $Q_0(x)$:

$$Q_0(x) = \begin{cases} \sqrt[3]{\frac{-\mathfrak{q}+\sqrt{\delta_0}}{2}} + \sqrt[3]{\frac{-\mathfrak{q}-\sqrt{\delta_0}}{2}} + \frac{\hbar}{3D}\left[-\mu + 2gn(x) + V(x)\right]; & \delta_0 > 0 \\ \sqrt[3]{\frac{-\mathfrak{q}+i\sqrt{-\delta_0}}{2}} + \sqrt[3]{\frac{-\mathfrak{q}-i\sqrt{-\delta_0}}{2}} + \frac{\hbar}{3D}\left[-\mu + 2gn(x) + V(x)\right]; & \delta_0 \leq 0 \\ e^{\pm\frac{2i\pi}{3}}\sqrt[3]{\frac{-\mathfrak{q}+i\sqrt{-\delta_0}}{2}} + e^{\mp\frac{2i\pi}{3}}\sqrt[3]{\frac{-\mathfrak{q}-i\sqrt{-\delta_0}}{2}} + \frac{\hbar}{3D}\left[-\mu + 2gn(x) + V(x)\right]; & \delta_0 \leq 0 \end{cases} \tag{2.166}$$

with the abbreviation:

$$\mathfrak{q} = -\frac{2\hbar^3}{27D^3}\left[-\mu + 2gn(x) + V(x)\right]^3 + \frac{\hbar M}{2D}. \tag{2.167}$$

The correct solution of $Q_0(x)$ has, according to (2.161), to be positive and can only be selected after choosing the form of the trap to be positive and to ensure a minimal free energy.

At zero temperature equations (2.161) and (2.162) remain the same but equation (2.163) reduces to:

$$n(x) \;=\; q(x) + n_0(x) \tag{2.168}$$

and the free energy (2.126) reduces using (2.160) to:

$$\begin{aligned} \mathcal{F} \;=\; & \int dx \Bigg\{ -g\left[n_0(x) + q(x)\right]^2 - \frac{g}{2}n_0^2(x) \\ & -\sqrt{n_0(x)}\left\{\mu + \frac{\hbar^2}{2M}\frac{\partial^2}{\partial x^2} - 2g\left[n_0(x) + q(x)\right] - V(x) + \frac{D}{\hbar}Q_0(x)\right\}\sqrt{n_0(x)}\Bigg\}. \end{aligned} \tag{2.169}$$

After inserting (2.168) into (2.166) and then inserting the result into the free energy expression (2.169), the three self-consistency equations (2.161), (2.162), and (2.168) can be directly obtained by extremising the free energy with respect to its variables $q(x)$, $n_0(x)$ and μ, i.e., $-\frac{\partial \mathcal{F}}{\partial \mu} = N$, $\frac{\delta \mathcal{F}}{\delta n_0(x')} = 0$ and $\frac{\delta \mathcal{F}}{\delta q(x')} = 0$, respectively. So also in one dimension our mean-field theory is based on identifying the order parameters as variational parameters.

3. 1D Case at Zero Temperature

In this chapter we investigate in detail the self-consistency equations and the free energy derived from the Hartree-Fock mean-field theory for the one-dimensional BEC developed in Section 2.11 at zero temperature. We restrict ourselves to the homogeneous case and treat then a harmonic trap potential in Thomas-Fermi approximation, where we work out the different densities as well as the respective Thomas-Fermi radii. Furthermore, we develop a numerical treatment for solving the corresponding one-dimensional Gross-Pitaevskii equation. The respective analytical and numerical results are qualitatively and quantitatively compared.

3.1. Homogeneous Case

The simplest case to discuss is the homogeneous one, which is even a prerequisite to study the trapped one in Thomas-Fermi approximation. In the homogeneous case we have $V(x) = 0$, furthermore, we distinguish two different phases, the superfluid phase and the Bose-glass phase, and both are treated separately.

3.1.1. Superfluid Phase

In the superfluid phase both the condensate density and the Bose-glass order parameter contribute to the total density. In this phase Eqs. (2.160)–(2.163) reduce at zero temperature to:

$$Q_0 = \sqrt{\frac{M}{2}} \frac{1}{\sqrt{-\mu + 2gn - \frac{D}{\hbar} Q_0}}, \tag{3.1}$$

$$q = \frac{D}{\hbar M} Q_0^3 \frac{n_0}{1 - \frac{D}{\hbar M} Q_0^3}, \tag{3.2}$$

$$-\mu + 2gn - gn_0 - \frac{D}{\hbar} Q_0 = 0, \tag{3.3}$$

$$n = q + n_0 \,. \tag{3.4}$$

Since all densities are spatially constant in the homogeneous case, we denote them in this section by n, n_0, q, and Q_0, respectively.

Inserting (3.3) into (3.1) yields $Q_0 = \sqrt{\frac{M}{2gn_0}}$, this allows us to get rid of the auxiliary quantity Q_0 in all equations, and reduces Eqs. (3.2) and (3.3) to

$$q = \frac{D}{\hbar M} \frac{n_0}{\left(\frac{2gn_0}{M}\right)^{\frac{3}{2}} - \frac{D}{\hbar M}}, \tag{3.5}$$

$$gn_0 = -\mu + 2gn - \frac{D}{\hbar} \sqrt{\frac{M}{2gn_0}}, \tag{3.6}$$

which represent together with (3.4) three coupled algebraic equations for the three respective densities.

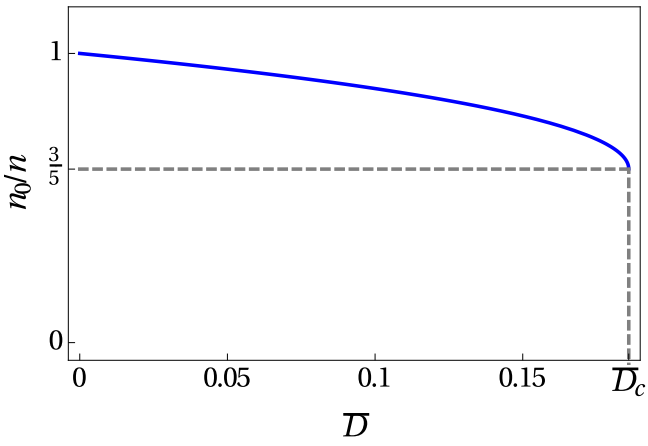

Figure 3.1.: Condensate fraction n_0/n as function of dimensionless disorder strength $\overline{D}$.

Inserting (3.4) into (3.5) gives us $q = \frac{D}{\hbar M}\left(\frac{M}{2gn_0}\right)^{\frac{3}{2}} n$. Inserting this result again into (3.4), then dividing by $n^{5/2}$ yields the following algebraic fifth order equation for the condensate fraction n_0/n:

$$\left(\frac{n_0}{n}\right)^{5/2} - \left(\frac{n_0}{n}\right)^{3/2} + \overline{D} = 0, \tag{3.7}$$

where $\overline{D} = \frac{\xi^3}{\mathcal{L}^3}$ denotes the dimensionless disorder strength, $\xi = \frac{\hbar}{\sqrt{2Mgn}}$ the coherence length, which is the distance over which the coherence significantly decays, and $\mathcal{L} = \left(\frac{\hbar^4}{M^2 D}\right)^{1/3}$ the Larkin length [82,119]. Figure 3.1 shows that the resulting condensate fraction decreases with increasing the disorder strength. As more and more particles are localized in the minima of the random potential, our mean-field theory predicts that the condensate density stops to exist at the critical value $\overline{D}_{\mathrm{c}} = \frac{6}{25}\sqrt{\frac{3}{5}} \simeq 0.185$. This corresponds to the value $\overline{D}_{\mathrm{c_{FNP}}} = 1$, that was found in the non-perturbative approach of Refs. [82,83], which investigate at which disorder strength the Bose-glass phase becomes energetically unstable and goes over into the superfluid phase. We interpret this as a sign of the occurrence of a first-order quantum phase transition in the homogeneous BEC from the superfluid phase, where the particles are either condensed or in the local minima of the disorder, to the Bose-glass phase, where there is no condensate at all and all bosons are localized in the minima of the disorder potential. Thus, we expect that a quantum phase transition will also appear in the trapped case studied in the next section.

Now we look for the equation of state in the superfluid phase. To this end we divide equation (3.6) by gn, which yields:

$$\overline{D} = -\frac{1}{2}\left[\left(\frac{n_0}{n}\right)^{3/2} + \left(\frac{\mu}{gn} - 2\right)\sqrt{\frac{n_0}{n}}\right]. \tag{3.8}$$

Inserting this result into equation (3.7) yield the following quadratic equation with respect to $\frac{n_0}{n}$

$$\left(\frac{n_0}{n}\right)^2 - \frac{3}{2}\left(\frac{n_0}{n}\right) - \frac{\mu}{2gn} + 1 = 0, \tag{3.9}$$

which has two real solutions $\frac{n_0}{n} = \frac{1}{4}\left(3 \pm \sqrt{-7 + 8\frac{\mu}{gn}}\right)$. Inserting those two solutions again into the the condensate fraction equation (3.7) yields the algebraic fifth order equation of state:

$$\left[\frac{1}{4}\left(3 \pm \sqrt{-7 + 8\frac{\mu}{gn}}\right)\right]^{5/2} - \left[\frac{1}{4}\left(3 \pm \sqrt{-7 + 8\frac{\mu}{gn}}\right)\right]^{3/2} + \overline{D} = 0. \tag{3.10}$$

Equation (3.10) can be solved only numerically and has five solutions, three real ones and two complex, and each one has the degeneracy two. Among them we chose the one which satisfies the boundary conditions: $\left(\overline{D} = 0,\ \mu = gn\right)$ and $\left(\overline{D} = \overline{D}_{\mathrm{c}},\ \frac{n_0}{n} = \frac{3}{5}\right)$.

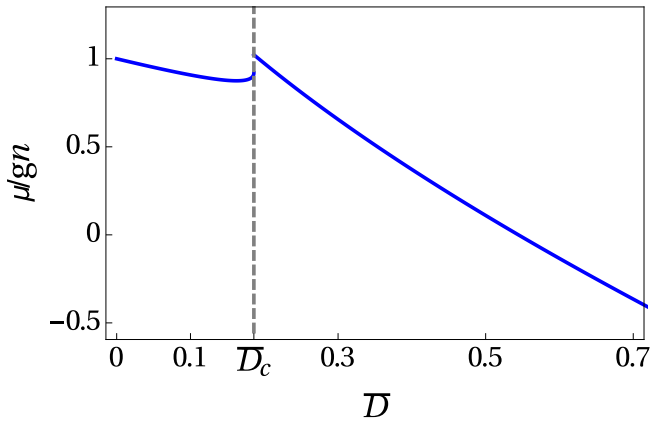

Figure 3.2.: Chemical potential μ in units of gn as function of dimensionless disorder strength $\overline{D}$.

3.1.2. Bose-Glass Phase

In the Bose-glass phase we have $n_0 = 0$ and $n = q$, in this case Eqs. (2.160), (2.161) reduce to:

$$Q_0 = \left(\frac{\hbar M}{D}\right)^{1/3}, \tag{3.11}$$

$$gq = \frac{1}{2}\left(3\overline{D}^{2/3} + \mu\right). \tag{3.12}$$

By dividing the relation (3.12) by the factor gn, we get the equation of state

$$\frac{\mu}{gn} = 2 - 3\overline{D}^{2/3}. \tag{3.13}$$

The solution of equation (3.10) of the superfluid phase is combined with the equation of state of the Bose-glass phase (3.13) and plotted in Fig 3.2. We find that the chemical potential decreases with the disorder strength in both phases with a discontinuity in the transition region between the superfluid and the Bose glass phase.

3.1.3. Comparison with Huang-Meng Theory

Now we check whether our results are compatible with the Huang-Meng theory [65, 69, 103, 120], where the Bose-glass order parameter of a homogeneous dilute Bose gas at zero temperature in case of weak disorder regime is deduced within the seminal Bogoliubov theory. The Bose-glass order parameter in one dimension via the Huang-Meng theory is proportional to the disorder strength and given by:

$$q_{\mathrm{HM}} = \frac{D}{8\hbar g^{3/2}}\sqrt{\frac{M}{n}} \triangleq \frac{q_{\mathrm{HM}}}{n} = \frac{\overline{D}}{2^{3/2}}. \tag{3.14}$$

To this end we deduce from (3.5) the corresponding formula of the Bose-glass order parameter in case of weak disorder strength:

$$q_w \approx \frac{D}{2^{3/2}\hbar g^{3/2}}\sqrt{\frac{M}{n}} \triangleq \frac{q_w}{n} = \overline{D}. \tag{3.15}$$

Thus, from (3.15) we conclude that our result agrees qualitatively with the Huang-Meng theory, i.e., in the weak disorder regime the Bose-glass order parameter is, indeed, proportional to the disorder strength D. But quantitatively the comparison of (3.14) with (3.15) reveals that a factor of $2^{3/2}$ is missing in our formula (3.15). This is due to the fact that the Hartree-Fock theory does not contain the Bogoliubov channel, which is included in the Huang-Meng theory.

3.2. Thomas-Fermi Approximation

After having treated the homogeneous case, we deal now with the trapped one. To this end we rewrite the self-consistency equations at zero temperature (2.161)–(2.163) already obtained in Section 2.11:

$$q(x) = \frac{D}{\hbar M} Q_0^3(x) \, \frac{n_0(x)}{1 - \frac{D}{\hbar M} Q_0^3(x)}, \tag{3.16}$$

$$\left[-\mu + 2gn(x) + V(x) - gn_0(x) - \frac{D}{\hbar} Q_0(x) - \frac{\hbar^2}{2M} \frac{\partial^2}{\partial x^2} \right] \sqrt{n_0(x)} = 0, \tag{3.17}$$

and

$$n(x) = q(x) + n_0(x)\,, \tag{3.18}$$

where the auxiliary function $Q_0(x)$ is the solution of the following cubic equation:

$$Q_0(x) = \sqrt{\frac{M}{2}} \frac{1}{\sqrt{-\mu + 2gn(x) + V(x) - \frac{D}{\hbar} Q_0(x)}}. \tag{3.19}$$

So we have four coupled self-consistency equations for the densities $n(x)$, $n_0(x)$, $q(x)$, and $Q_0(x)$: three algebraic ones (3.16), (3.18), and (3.19) as well as one nonlinear, differential equation (3.17). Furthermore, we have to take into account the normalization condition:

$$\int_{-\infty}^{\infty} n(x) dx = N, \tag{3.20}$$

where the total number of particles N is the integral of the total density $n(x)$ over the whole space.

The exact analytical solution of the differential equation (3.17) is impossible to obtain even in the absence of disorder. Therefore, we approximate its solution via an approximation method, which is based on the following consideration. If either the number of particles in a gas or the interatomic interaction becomes large, then the kinetic energy term in equation (3.17) can be neglected. This leads to the so-called Thomas-Fermi (TF) approximation.

It turns out that we have to distinguish between two different spatial regions: the superfluid region, where the bosons are distributed in the condensate as well as in the minima of the disorder potential, and the Bose-glass region, where there are no bosons in the condensate so that all bosons contribute to the local Bose-Einstein condensates. The radius of the superfluid region R_{TF1} is called the condensate radius, while the radius of the whole bosonic cloud R_{TF2} is called the cloud radius, and both radii represent Thoma-Fermi radii.

Within the so-called TF approximation the algebraic equations (3.16) and (3.18) remain the same, but the differential equation (3.17) reduces to an algebraic relation in the superfluid region:

$$-\mu + 2gn(x) + V(x) - gn_0(x) - \frac{D}{\hbar} Q_0(x) = 0. \tag{3.21}$$

Outside the superfluid region, i.e., in the Bose-glass region, equation (3.17) reduces simply to $n_0(x) = 0$. The advantage of the TF approximation is that now we have only three coupled algebraic equations.

In order to be able to continue the calculation, we have to specify the trap potential. We choose it to be a harmonic one, i.e., $V(x) = M\Omega^2 x^2/2$, where Ω denotes the trap frequency. We specify also the interaction coupling strength to be $g = 2a\hbar\omega_r$ with the s-wave scattering length a, which has to be positive in order to obtain a stable BEC, and ω_r denotes the transversal trap frequency, which has to be large enough in order to ensure a quasi one-dimensional setup [121, 122].

Since at zero temperature we have two different regions, we treat them separately. We focus first on the superfluid region, then we deal with the Bose-glass one.

3.2.1. Superfluid Region

Comparing Eq. (3.19) with Eq. (3.21), yields $Q_0(x) = \sqrt{\frac{M}{2gn_0(x)}}$. Inserting this result into the self-consistency equations (3.16), (3.18), and (3.21) eliminates their dependence on the auxiliary function $Q_0(x)$, and reduces them in the superfluid region to:

$$-\tilde{\mu} + 2\tilde{n}(\tilde{x}) + \tilde{x}^2 - \tilde{n}_0(\tilde{x}) - 2\frac{\tilde{D}}{\sqrt{\tilde{n}_0(\tilde{x})}} = 0, \tag{3.22}$$

$$\tilde{q}(\tilde{x}) = \tilde{D}\,\frac{\tilde{n}_0(\tilde{x})}{\tilde{n}_0^{3/2}(\tilde{x}) - \tilde{D}}, \tag{3.23}$$

$$\tilde{n}(\tilde{x}) = \tilde{q}(\tilde{x}) + \tilde{n}_0(\tilde{x})\ , \tag{3.24}$$

where $\tilde{n}(\tilde{x}) = n(x)/\overline{n}$ denotes the dimensionless total density, $\tilde{n}_0(\tilde{x}) = n_0(x)/\overline{n}$ the dimensionless condensate density, $\tilde{q}(\tilde{x}) = q(x)/\overline{n}$ the dimensionless Bose-glass order parameter, $\tilde{x} = x/R_{\mathrm{TF}}$ the dimensionless coordinate, $\tilde{\mu} = \mu/\bar{\mu}$ the dimensionless chemical potential, $\tilde{D} = \frac{\xi^3}{\mathcal{L}^3}$ the dimensionless disorder strength, $l = \sqrt{\frac{\hbar}{M\Omega}}$ the oscillator length, $\overline{n} = \bar{\mu}/g$ the maximal total density in the clean case, $\xi = \frac{l^2}{R_{\mathrm{TF}}}$ the coherence length in the center of the trap, and $R_{\mathrm{TF}} = l\sqrt{\frac{2\bar{\mu}}{\hbar\Omega}}$ the TF cloud radius. The chemical potential in the absence of the disorder $\bar{\mu} = \hbar\omega_r\left(\frac{3}{2\sqrt{2}}N\frac{a}{l}\sqrt{\frac{\Omega}{\omega_r}}\right)^{2/3}$ is deduced from the normalization condition (3.20) in the clean case, i.e., $D = 0$, by evaluating:

$$N = \frac{1}{g}\int_{-R_{\mathrm{TF}}}^{R_{\mathrm{TF}}}\left[\bar{\mu} - \frac{1}{2}M\Omega^2x^2\right]dx. \tag{3.25}$$

Now we have three algebraic self-consistency coupled equations (3.22)–(3.24) for the dimensionless condensate density $\tilde{n}_0(\tilde{x})$, the dimensionless Bose-glass order parameter $\tilde{q}(\tilde{x})$ and the sum of them, i.e., the dimensionless total density $\tilde{n}(\tilde{x})$. Inserting equations (3.23) and (3.24) into equation (3.21) gives us one self-consistency equation for the condensate density in the superfluid region:

$$\tilde{n}_0^3(\tilde{x}) + \left(-\tilde{\mu} + \tilde{x}^2\right)\tilde{n}_0^2(\tilde{x}) - \tilde{D}\tilde{n}_0^{3/2}(\tilde{x}) - \tilde{D}\left(-\tilde{\mu} + \tilde{x}^2\right)\sqrt{\tilde{n}_0(\tilde{x})} + 2\tilde{D}^2 = 0. \tag{3.26}$$

This equation is of the sixth order with respect to $\sqrt{\tilde{n}_0(\tilde{x})}$, which makes it impossible to solve analytically. Therefore, we solve it numerically and insert the result into equations (3.23) and (3.24) in order to determine the Bose-glass order parameter $\tilde{q}(\tilde{x})$ and the total density $\tilde{n}(\tilde{x})$, respectively.

3.2.2. Bose-Glass Region

In the Bose-glass region the condensate density vanishes, i.e., $\tilde{n}_0(\tilde{x}) = 0$, and we conclude $\tilde{n}(\tilde{x}) = \tilde{q}(\tilde{x})$. Inserting this into equation (3.16) we get $Q_0(x) = \left(\frac{\hbar M}{D}\right)^{1/3}$, which reduces equation (3.19) to:

$$\tilde{q}(\tilde{x}) = \frac{1}{2}\left(3\tilde{D}^{2/3} + \tilde{\mu} - \tilde{x}^2\right). \tag{3.27}$$

We also need to write down the dimensionless equivalent of the normalization condition (3.20), which reads:

$$\int_{-\tilde{R}_{\mathrm{TF2}}}^{\tilde{R}_{\mathrm{TF2}}}\tilde{n}(\tilde{x})d\tilde{x} = \frac{N}{\overline{n}R_{\mathrm{TF}}} = \frac{4}{3}, \tag{3.28}$$

where $\tilde{R}_{\mathrm{TF2}} = R_{\mathrm{TF2}}/R_{\mathrm{TF}}$ denotes the dimensionless cloud radius, and the total density $\tilde{n}(\tilde{x})$ in equation (3.28) is the combination of the total densities from both the superfluid region and the Bose-glass region.

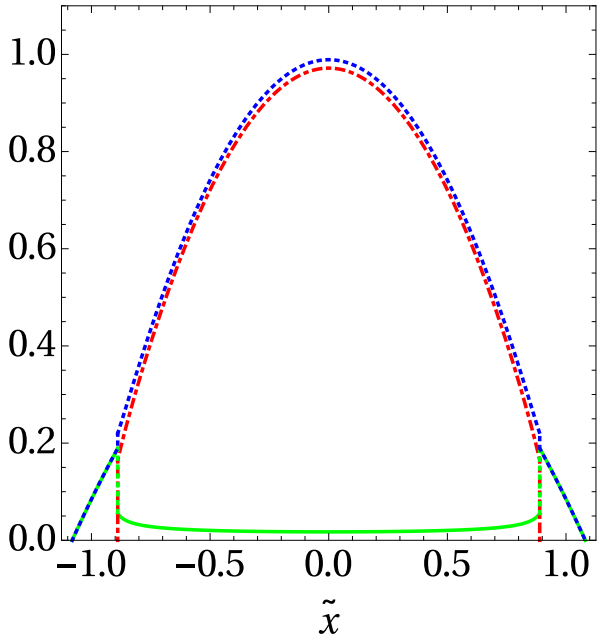

Figure 3.3.: Total density $\tilde{n}(\tilde{x})$ (dotted, blue), condensate density $\tilde{n}_0(\tilde{x})$ (dotted-dashed, red), and Bose-glass order parameter $\tilde{q}(\tilde{x})$ (solid, green) for the dimensionless disorder strength $\tilde{D} = 0.016$.

3.2.3. Thomas-Fermi Results

Before choosing any parameter for our BEC system, we have first to justify using the TF approximation and determine the range of validity of this approximation. To this end we rewrite equation (3.17) in the clean case, i.e., $D = 0$, and we divide it with $\bar{\mu}\sqrt{\tilde{n}}$. This yields:

$$\left[-1 + \tilde{n}(\tilde{x}) + \tilde{x}^2 - \left(\frac{\xi}{R_{\mathrm{TF}}}\right)^2 \frac{\partial^2}{\partial \tilde{x}^2}\right] \sqrt{\tilde{n}(\tilde{x})} = 0. \tag{3.29}$$

Note that in the clean case, the total density coincides with the condensate one. The TF approximation is only justified when the prefactor of the kinetic term $\left(\frac{\xi}{R_{\mathrm{TF}}}\right)^2$ is small enough that the kinetic term can be neglected, i.e.,

$$\xi \ll R_{\mathrm{TF}}. \tag{3.30}$$

In this chapter we perform our study for Rubidium ^{87}Rb and for the following experimentally realistic parameters: $N = 10^6$, $\Omega = 2\pi \times 50\,\mathrm{Hz}$, $\omega_r = 2\pi \times 179\,\mathrm{Hz}$, and $a = 5.29\,\mathrm{nm}$. For those parameters the oscillator length is given by $l = 1.52\,\mu\mathrm{m}$, the coherence length turns out to be $\xi = 45.6\,\mathrm{nm}$, and the Thomas-Fermi radius reads $R_{\mathrm{TF}} = 50.9\,\mu\mathrm{m}$, so the assumption (3.30) for the TF approximation is, indeed, fulfilled. Furthermore, the transverse oscillator length $l_r = \sqrt{\frac{\hbar}{M\omega_r}} = 806.04\,\mathrm{nm}$ is much larger than the scattering length, i.e., $a \ll l_r$, so we are in quasi one-dimensional regime [123].

Using those parameter values we solve equation (3.26) numerically. This equation has six solutions, two complex ones and four real ones, among them only two real solutions yield a positive $\tilde{n}_0(\tilde{x})$ and are, thus, physical. We insert each of the two physical solutions into equations (3.23) and (3.24), then we combine those superfluid region solutions with equation (3.27) describing the Bose-glass region, after that we fix the chemical potential $\tilde{\mu}$ using the normalization condition (3.28). In the end, we select the physical solution with the smallest free energy (2.169) and we insert it into Eq. (3.26) in order to check whether the selected solution does satisfy (3.26). The resulting densities are combined and plotted in Fig. 3.3, where in the superfluid region the densities are plotted with solid lines, and in the Bose-glass region they are plotted with dotted lines.

Figure. 3.3 shows the total density $\tilde{n}(\tilde{x})$ being maximal in the center of the trap and decreases when we move away from the center of the cloud until being zero at the cloud radius, with a tiny jump at the

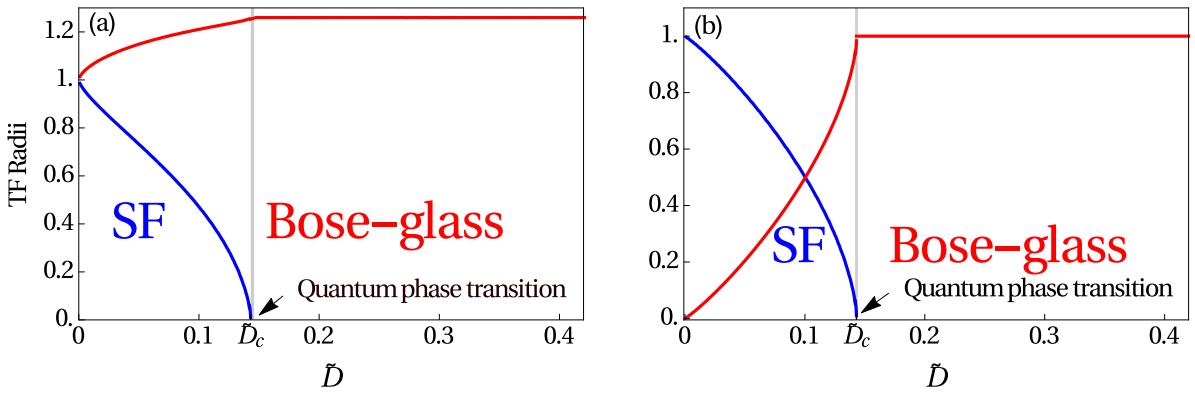

Figure 3.4.: (a) Cloud radius $\tilde{R}_{\mathrm{TF2}}$ (red) and condensate radius $\tilde{R}_{\mathrm{TF1}}$ (blue) and (b) fractional number of condensed particles N_0/N (blue) and in the disconnected local minicondensates Q/N (red) as functions of the dimensionless disorder strength $\tilde{D}$.

condensate radius. The condensate density $\tilde{n}_0(\tilde{x})$ is also maximal in the center of the bosonic cloud and decreases when we move away from the center, then it jumps to zero at the condensate radius which separates the superfluid from the Bose-glass region. The Bose-glass order parameter $\tilde{q}(\tilde{x})$ has a different behavior, it is minimal in the center of the trap, then it keeps increasing when we move away from the center until the condensate radius, where its maximum equals to the total density, then Bose-glass order parameter and total density are on top of each other and decrease until vanishing at the cloud radius. So the three densities turn out to be not continuous at the condensate radius, which is an artifact of the applied Thomas-Fermi approximation.

To study the influence of the disorder on the BEC, we plot the resulting TF radii in Fig. 3.4a as a function of the dimensionless disorder strength. The dimensionless condensate radius $\tilde{R}_{\mathrm{TF1}} = R_{\mathrm{TF1}}/R_{\mathrm{TF}}$ is defined where the condensate density, which is the solution of equation (3.26), stops, which corresponds to solve the equation $\frac{\partial\tilde{x}}{\partial\tilde{n}_0(\tilde{x})}|_{\tilde{x}=R_{\mathrm{TF1}}} = 0$, while the dimensionless cloud radius $\tilde{R}_{\mathrm{TF2}}$ is defined by the condition that the solution of equation (3.27) equals to zero, i.e., $3\tilde{D}^{2/3}+\tilde{\mu}-\tilde{R}^2_{\mathrm{TF2}} = 0$. We see that both cloud and condensate radius coincide in the clean case. The condensate radius decreases, when we increase the disorder strength, until it vanishes at the critical dimensionless disorder value $\tilde{D}_{\mathrm{c}} = 0.143$, which marks a quantum phase transition from the superfluid to the Bose-glass phase. On the other side the cloud radius increases with the disorder in the superfluid phase, but it remains constant in the Bose-glass phase at the value $\tilde{R}_{\mathrm{TF2}} = 1.256$. This means that beyond the critical disorder strength $\tilde{D}_{\mathrm{c}}$ the bosonic cloud is not extending anymore and has a maximal size. The same conclusion can be deduced from Fig. 3.4b, where we remark that the fractional number of the condensate is defined via $N_0/N = \frac{3}{4}\int_{-\tilde{R}_{\mathrm{TF1}}}^{\tilde{R}_{\mathrm{TF1}}} \tilde{n}_0(\tilde{x})\, d\tilde{x}$. Here N_0/N equals to one in the clean case, i.e., all particles are in the condensate, then it decreases with the disorder strength until it vanishes at $\tilde{D}_{\mathrm{c}}$ marking the end of the superfluid phase and the beginning of the Bose-glass phase. Conversely the fraction in the disconnected minicondensates $Q/N = \frac{3}{4}\int_{-R_{\mathrm{TF2}}}^{R_{\mathrm{TF2}}} \tilde{q}(\tilde{x})\, d\tilde{x}$, where Q is the number of particles in the disconnected minicondensates, increases with the disorder until being maximal at $\tilde{D}_{\mathrm{c}}$, then it remains constant and equals to one in the Bose-glass phase, since all particles are in the minima of the disorder potential.

The influence of the disorder on the chemical potential, is shown in Fig. 3.5a. In the superfluid region the chemical potential can be obtained only numerically, while in the Bose-glass region it is deduced from equation (3.27) as follows $\tilde{\mu} = 2^{2/3} - 3\tilde{D}^{2/3}$. The chemical potential decreases starting from one with the disorder strength and is continuous but not differentiable at the quantum phase transition point $\tilde{D}_{\mathrm{c}}$. As already discussed at the end of Section 2.3, the disorder leads to an effective attractive interaction, this causes the chemical potential to decrease with increasing disorder strength.

Since the trap is quite wide, the Bose-glass order parameter in the center of the BEC $\tilde{q}(0)$ is comparable to the one in the homogeneous case. Thus, the dimensionless Huang-Meng result of the Bose-glass order parameter $\tilde{q}_{\mathrm{HM}} = q_{\mathrm{HM}}/\overline{n} = \frac{\tilde{D}}{2^{3/2}\sqrt{\tilde{n}(0)}}$, the dimensionless perturbative result of the

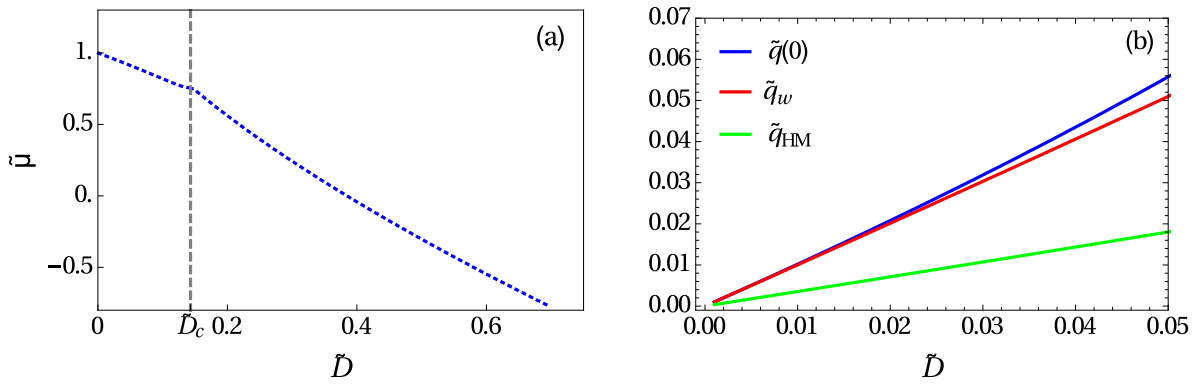

Figure 3.5.: (a) Dimensionless chemical potential $\tilde{\mu}$ and (b) Thomas-Fermi approximated (blue), perturbative (red), and Huang-Meng (green) Bose-glass order parameter in the center of the BEC as functions of the dimensionless disorder strength $\tilde{D}$.

Bose-glass order parameter in the weak disorder $\tilde{q}_w = \frac{\tilde{D}}{\sqrt{\tilde{n}(0)}}$ deduced from (3.23), and the dimensionless exact Bose-glass order parameter in the center of the cloud $\tilde{q}\,(0) = \tilde{D}\,\frac{\tilde{n}_0(0)}{\tilde{n}_0^{3/2}(0)-\tilde{D}}$, are all plotted for the weak disorder regime in Fig. 3.5b to illustrate the qualitative convergence of the three results.

3.3. Numerical Treatment

Now we perform a numerical study for the Bose-condensed gas in one dimension and at zero temperature in a harmonic trapping potential $V(x) = \frac{1}{2}\, M\, \Omega^2\, x^2$. Furthermore, we assume a Gaussian disorder potential $U(x)$ which satisfies the following conditions:

$$\overline{U(x)} = 0 \tag{3.31}$$

and

$$\overline{U(x)U(x')} = D(x - x'), \tag{3.32}$$

where $D(x - x')$ denotes the correlation function.

A one-dimensional BEC in the mean-field Hartree approximation is given by a generalized time-independent Gross-Pitaevskii equation for the condensate wave function $\psi\,(x)$:

$$\left[-\frac{\hbar^2}{2M}\frac{\partial^2}{\partial x^2} - \mu + U(x) + V(x) + g\psi^*(x)\psi(x)\right]\psi(x) = 0. \tag{3.33}$$

Equation (3.33) represents a stochastic nonlinear differential equation which is difficult to solve exactly, therefore we solve it numerically. To this end we have first to generate the random potential $U\,(x)$ before inserting it into equation (3.33).

3.3.1. Generating Random Potential

Motivated by Fourier series, a simple ansatz for generating a random function is performed. The potential is written as a finite superposition of $\sin(kx)$ and $\cos(kx)$ terms with properly picked amplitudes A_n, B_n, and wave numbers k_n [124]:

$$U(x) = \frac{1}{\sqrt{\mathtt{N}}}\sum_{n=0}^{\mathtt{N}-1}\left[A_n\,\cos(k_n\,x) + B_n\,\sin(k_n\,x)\right], \tag{3.34}$$

where $\mathtt{N}$ denotes the number of terms which should be large enough in order to obtain a good approximation for the random potential. Furthermore, we assume A_n and B_n to be mutually independent Gaussian random variables with zero mean and variance $D(0)$:

$$\overline{A_n B_n} = 0, \qquad \overline{A_n A_m} = \overline{B_n B_m} = D(0)\delta_{nm}, \tag{3.35}$$

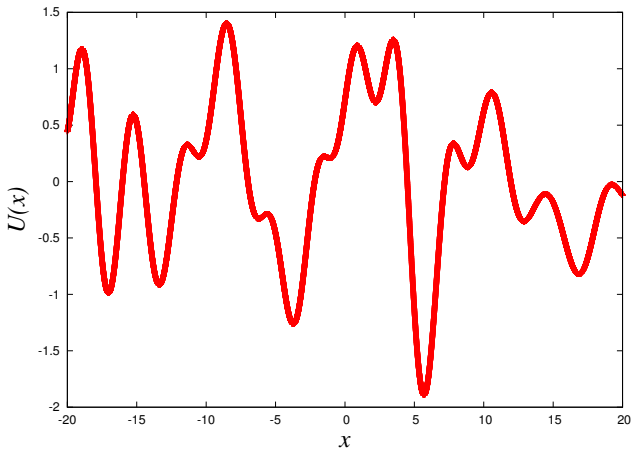

Figure 3.6.: Random potential (3.34) for Gaussian correlation (3.32) in one dimension with $\mathtt{N} = 100$, $D = 1$, and $\lambda = 1$.

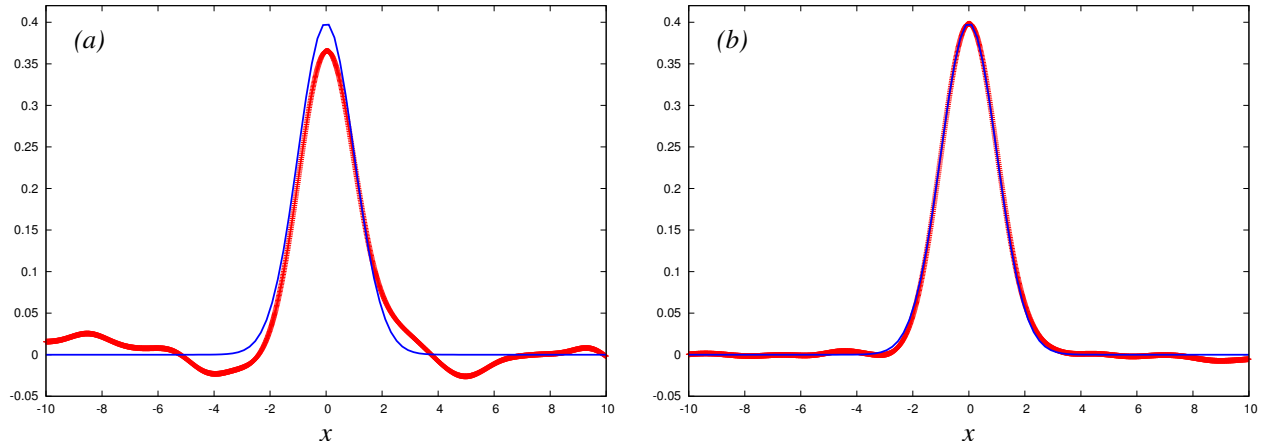

Figure 3.7.: Correlation $\overline{U(x)U(0)}$ (red) with $\mathtt{N} = 100$ averaged over (a) $\mathtt{M} = 1000$ and (b) $\mathtt{M} = 10000$ sample potentials compared to $D(x)$ in equation (3.32) with $D = 1$ and $\lambda = 1$ (blue).

The wave numbers k_n are independent random variables as well, which are picked from the probability distribution:

$$p(k_n) = \frac{S(k_n)}{\int_{-\infty}^{\infty} S(k')dk'}, \tag{3.36}$$

where $S(k)$ defines the spectral density as the Fourier transform of the correlation function:

$$S(k) = \int_{-\infty}^{\infty} dx e^{-ikx} D\left(x\right). \tag{3.37}$$

In the special case of the Gaussian correlated disorder we have

$$D(x - x') = \frac{D}{\sqrt{2\pi}\lambda} e^{-\frac{(x-x')^2}{2\lambda^2}}, \tag{3.38}$$

where λ denotes the correlation length, and D the disorder strength. The probability distribution (3.36) reads in this case:

$$p(k_n) = \frac{\lambda}{\sqrt{2\pi}} e^{-\frac{\lambda^2 k_n^2}{2}}. \tag{3.39}$$

The analytical study in Section 3.2 is done for δ-correlated disorder, but since it is impossible to treat the δ-correlated disorder numerically, we use now the Gaussian correlated disorder (3.38), which specializes to a δ-distributed one by taking the limit $\lambda \to 0$, i.e., $\lim_{\lambda\to 0} D\left(x\right) = D\delta\left(x\right)$.

In order to justify the correct correlation and distribution function of the random process, we show in Fig. 3.6 a typical example of a random potential generated by (3.34) for $D = 1$ and $\lambda = 1$ with

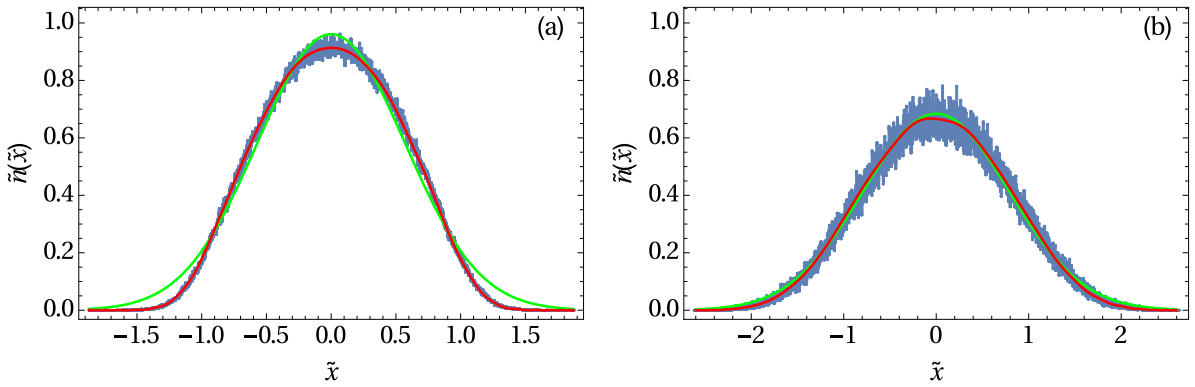

Figure 3.8.: Particle density $\tilde{n}(\tilde{x})$: original data (blue), fitted curve (red), and fitted Gaussian (Green) for (a) $\tilde{D} = 0.067$, (b) $\tilde{D} = 0.603$.

$\mathtt{N} = 100$. The same values of D and λ are used to plot in Fig. 3.7 the correlation function $\overline{U(x)U(0)}$ (red) sampled for $\mathtt{N} = 100$ and averaged over $\mathtt{M} = 1000$ and $\mathtt{M} = 10000$ pseudorandomly generated functions, respectively. The results are compared to the expected correlator $D(x)$ plotted as a blue line, it gives a good approximation. In order to numerically reproduce the correlation function (3.32) to a desired accuracy two numbers have to be appropriately large enough. The first one is the number $\mathtt{N}$ of terms in (3.34), the second one is the number $\mathtt{M}$ of realization of the disorder potential, which are used to evaluate the disorder ensemble average (3.32). It can be shown analytically that the error in reproducing (3.32) in the case $\mathtt{M} \to \infty$ is of the order of $\mathtt{1/N}$ (see Appendix B).

3.3.2. Numerical Results

We insert the generated disorder potential (3.34) into the Gross-Pitaevskii equation (3.33), then we use a C computer program [125–127] that solves the time-independent Gross-Pitaevskii equation in one space dimension in a harmonic trap using the imaginary time propagation. In this way we obtain the numerical solution of the ground-state wave function $\psi(x)$ of equation (3.33) for $\mathtt{M} = 1000$ realizations of the disorder potential and $\mathtt{N} = 10000$. We used different values of the disorder strength D in order to cover the range of weak and intermediate disorder regime. We have chosen the disorder correlation length $\lambda = 0.01\, l$, which is small enough in order to approach the case of δ-correlated disorder.

Performing disorder ensemble averages, we have access to the particle density $n(x) = \overline{\psi(x)^2}$, to the condensate density $n_0(x) = \overline{\psi(x)}^2$ and to the Bose-glass order parameter $q(x) = n(x) - n_0(x)$, which thus corresponds to the variance of the condensate wave function $\psi\,(x)$. In order to be able to compare the numerical results with the analytical ones obtained in Section 3.2, we use the same rescaling parameters for all densities, coordinates, chemical potential, and disorder strength, which were already explained below Eq. (3.24) in order to obtain the respective dimensionless quantities. Before discussing the various numerical results, we show first one typical example in Fig. 3.8, where the total density $\tilde{n}(\tilde{x})$ is plotted for two different values of the disorder strength (blue) showing the original data without any adjustment. We remark that the resulting density is fluctuating around a Gaussian-like curve. Comparing Fig. 3.8a with Fig. 3.8b we conclude that the fluctuations are increasing with the disorder strength. The origin of those fluctuations is that the $\mathtt{M} = 1000$ realizations of the disorder potential (3.34) are not sufficient to produce a smooth curve after having performed the disorder ensemble average. One solution of this problem would be to increase the number $\mathtt{M}$ of the realizations of the disorder potential, which would need longer time specially for the intermediate disorder regime, where the numerics has to be run for a larger spatial range and needs months to be realized. Another solution, which is the one that we adopted, is to extract a continuous smooth curve which fits to our data as it is done in Fig. 3.8 (red). This method is applied to all numerical resulting densities in this chapter. Furthermore, from the Gaussian fit in Fig. 3.8 (green), we remark that the original data of the total density approach a Gaussian form in the intermediate disorder regime much better than in the weak disorder. This can be explained with the fact that increasing the disorder reduces effectively the repulsive interaction between the particles and approaches the case of non-interaction bosons, where

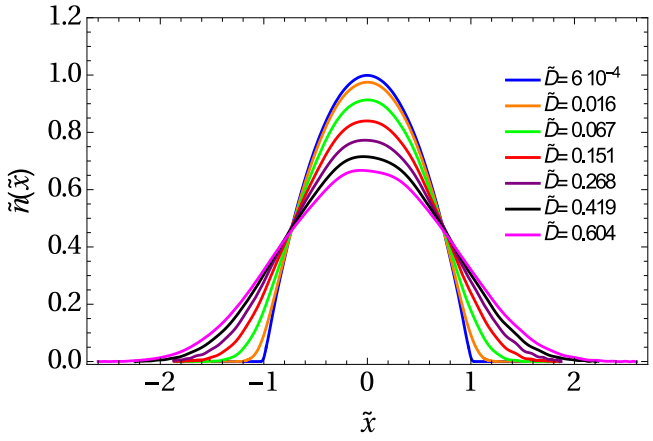

Figure 3.9.: Particle density $\tilde{n}(\tilde{x})$ for increasing disorder strengths $\tilde{D}$ from top to bottom.

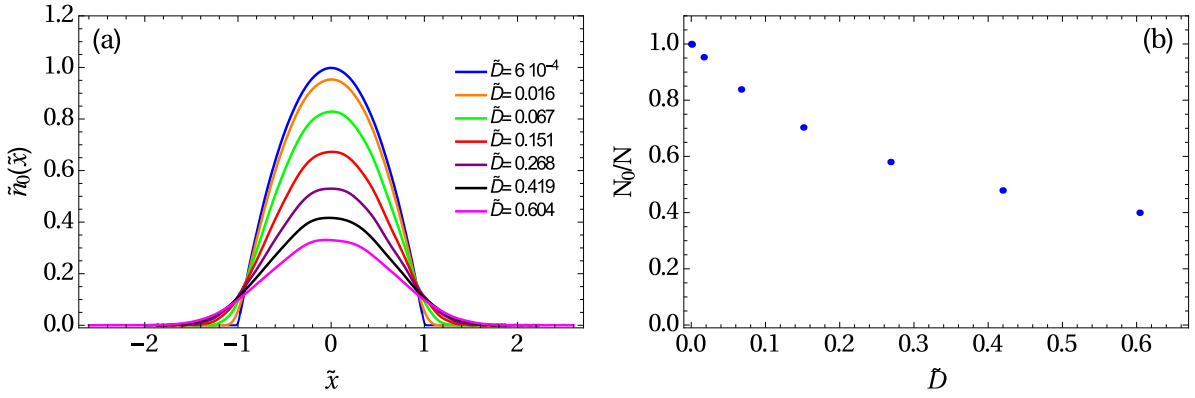

Figure 3.10.: (a) Condensate density $\tilde{n}_0(\tilde{x})$ and (b) fractional number of condensed particles N_0/N for increasing disorder strengths $\tilde{D}$ from top to bottom.

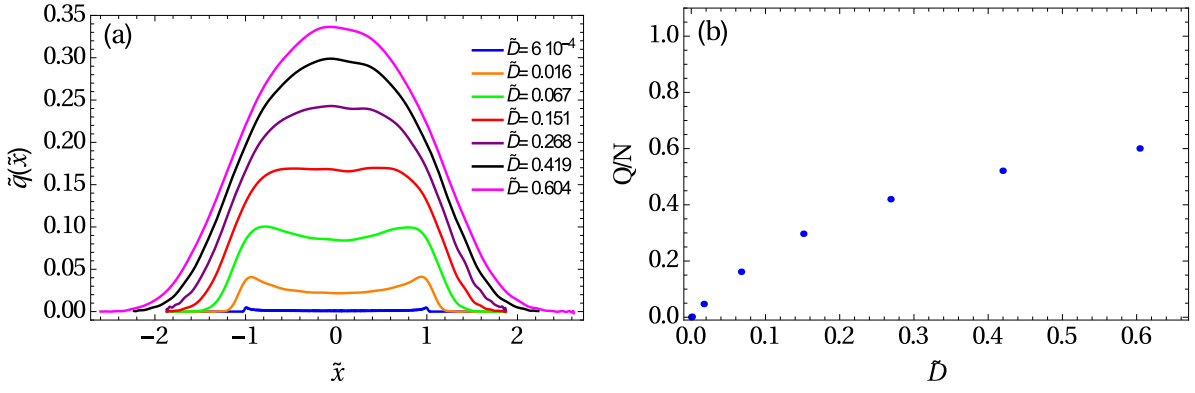

Figure 3.11.: (a) Bose-glass order parameter $\tilde{q}(\tilde{x})$ and (b) fractional number of particles Q/N in the disconnected local minicondensates for increasing disorder strengths $\tilde{D}$ from bottom to top.

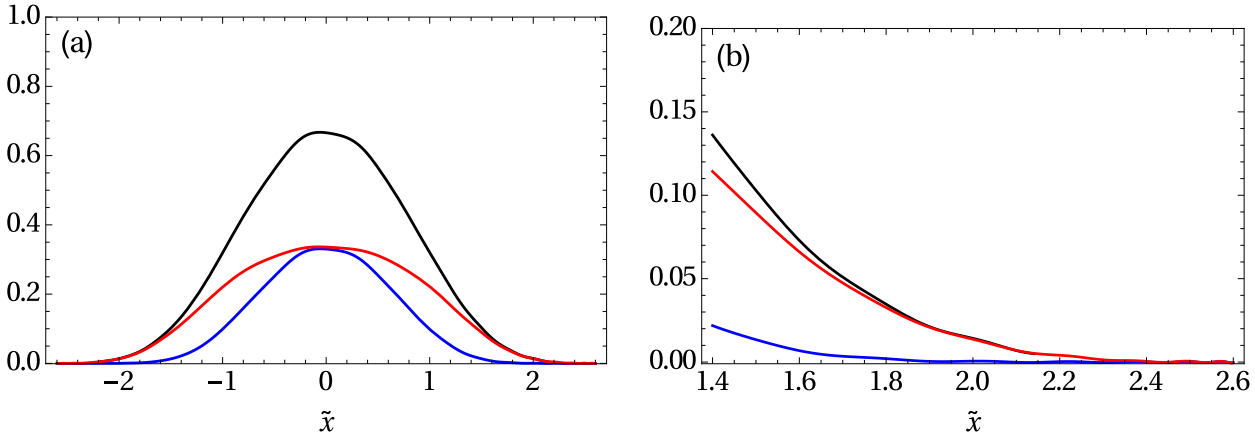

Figure 3.12.: (a) Particle density $\tilde{n}(\tilde{x})$ (black), condensate density $\tilde{n}_0(\tilde{x})$ (blue), Bose-glass order parameter $\tilde{q}(\tilde{x})$ (red) and (b) blow-up of border region for $\tilde{D} = 0.604$.

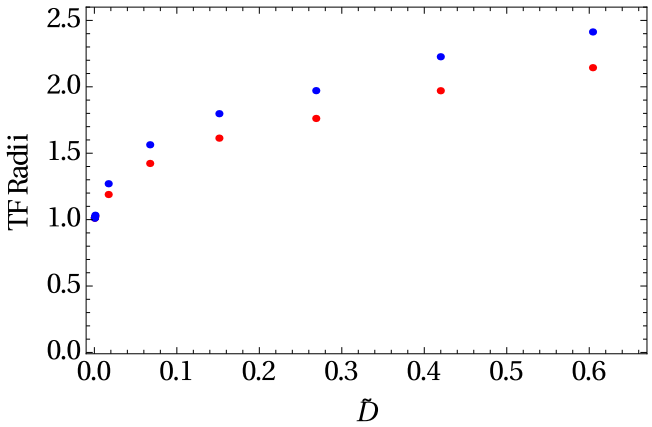

Figure 3.13.: Cloud radius $\tilde{R}_{\mathrm{TF2}}$ (blue) and condensate radius $\tilde{R}_{\mathrm{TF1}}$ (red) as functions of the disorder strength $\tilde{D}$.

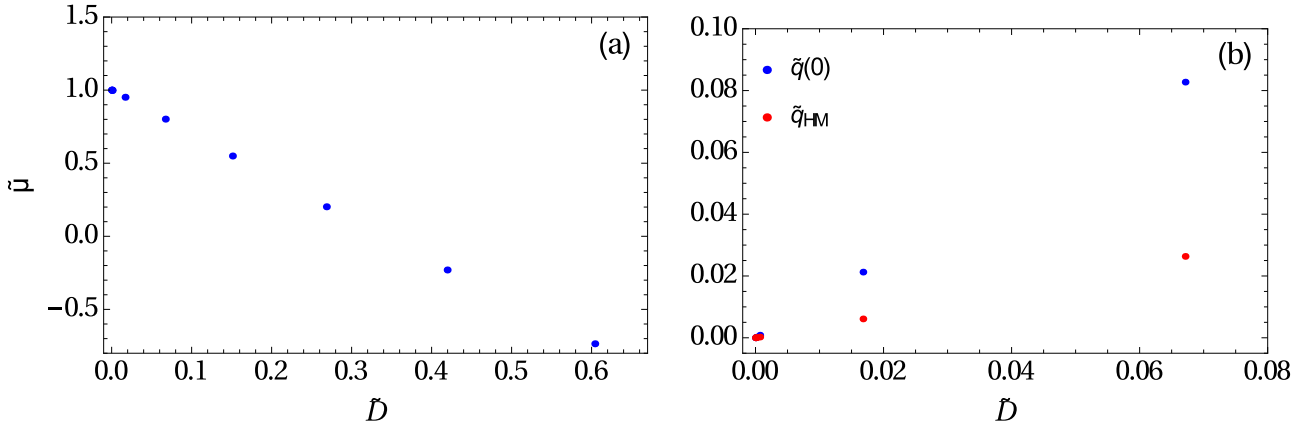

Figure 3.14.: (a) Chemical potential $\tilde{\mu}$ and (b) the numerical (blue) and the Huang-Meng (red) Bose-glass order parameter in the center of the BEC as functions of the disorder strength $\tilde{D}$.

the total density is given by a Gaussian.

In Fig. 3.9 the total density is plotted for different values of the disorder strength. We remark that $\tilde{n}(\tilde{x})$ is always maximal in the trap center and decreases, when we move away from the center, until it finally vanishes. The width of the total density, which is the spatial range, where the total density is not vanishing, is increasing with the disorder strength and the bosonic cloud is becoming larger, while the maximal total density is decreasing with the disorder strength. Figure 3.10a presents the condensate density $\tilde{n}_0(\tilde{x})$ for different disorder strengths and shows that $\tilde{n}_0(\tilde{x})$ has qualitatively the same behavior as the total density in Fig. 3.9. In order to make the picture clearer, we plot in Fig. 3.10b the fractional number of the condensate $N_0/N = \frac{3}{4}\int \tilde{n}_0(\tilde{x})\, d\tilde{x}$ as a function of the disorder strength. This fraction decreases with the disorder strength, which means that more and more particles are leaving the condensate while increasing $\tilde{D}$. Unfortunately, the employed numerical algorithm breaks down for larger values of the disorder strength, and one would have to use other approaches in this case. Therefore we focus on the regimes of weak to moderate disorder. The Bose-glass order parameter is also plotted for different values of $\tilde{D}$ in Fig. 3.11a but it has a complete different behavior from the two previous densities $\tilde{n}(\tilde{x})$ and $\tilde{n}_0(\tilde{x})$. In the weak disorder regime, $\tilde{q}(\tilde{x})$ has a double bump structure and it is maximal at the border of the condensate, while in the strong disorder regime it has a Gaussian-like form. This redistribution is happening, according to Fig. 3.11a, at a disorder strength value between $\tilde{D} = 0.151$ and $\tilde{D} = 0.268$, where it seems that the double bump structure disappears and the Gaussian-like one appears. So, for small disorder local condensates are mainly at the border of the global condensate, but for large disorder the local condensates sit more in the trap center, and this seems to be the main difference between the weak and the intermediate disorder regimes. But in both weak and intermediate disorder regime the width as well as the maximum of the Bose-glass order parameter increase with the disorder. Furthermore, the fraction in the disconnected minicondensates $Q/N = \frac{3}{4}\int \tilde{q}(\tilde{x})\, d\tilde{x}$ plotted in Fig. 3.11b increases with the disorder strength, i.e., with increasing the disorder strength more and more bosons are captured in the minicondensates of the disorder potential. Although the fraction Q/N increases with the disorder, again we have no further information whether in the strong disorder regime all particles will be localized in the minima of the disorder or not.

In order to know if, due to the disorder, the Bose-glass region exists or not, we plot the three densities $n(x)$, $n_0(x)$ and $q(x)$ together in Fig. 3.12 for the relatively strong disorder value $\tilde{D} = 0.604$. Indeed, the blow-up of the intermediate region shows clearly that at the border of the bosonic cloud the condensate vanishes, while the Bose-glass order parameter still persists, so the superfluid and the Bose-glass region coexist in the trap.

Figure 3.13 shows both the condensate radius and the cloud radius, which we define by the length where the condensate density and the total density are equal to 10^{-4}, respectively. Both are almost identical in the weak disorder regime, then they both increase with the disorder strength. This means that the Bose-glass region exists only for intermediate disorder and both the condensate cloud and the bosonic cloud are expanding with $\tilde{D}$. On the other hand, the chemical potential decreases linearly with the disorder strength in Fig. 3.14a, it becomes even negative in the intermediate disorder regime.

In Fig. 3.14b both the Bose-glass order parameter in the center of the BEC $\tilde{q}(0)$ as well as the Huang-Meng Bose-glass order parameter $\tilde{q}_{\mathrm{HM}}$ in weak disorder regime are plotted together in order to check whether the numerical results agree with the Huang-Meng theory or not. We observe the correct qualitative behavior of the Bose-glass order parameter in the trap center $\tilde{q}(0)$, which is proportional to the disorder strength $\tilde{D}$. However, the two order parameters have two different slopes and the linear behavior of the numerical Bose-glass order parameter $\tilde{q}(0)$ does not agree quantitatively with the predictions of the Huang-Meng theory in equation (3.14).

3.4. Comparison Between Thomas-Fermi Approximation and Numerics

Now we compare all results obtained via the TF approximation in Section 3.2 with the numerical ones from Section 3.3 in order to know how far this approximation is applicable. We start first of all by comparing the analytical and numerical densities $\tilde{n}(\tilde{x})$, $\tilde{n}_0(\tilde{x})$, and $\tilde{q}(\tilde{x})$ for two different values of the disorder strength. In Fig. 3.15a and for a relative small value of the disorder strength $\tilde{D} = 0.016$,

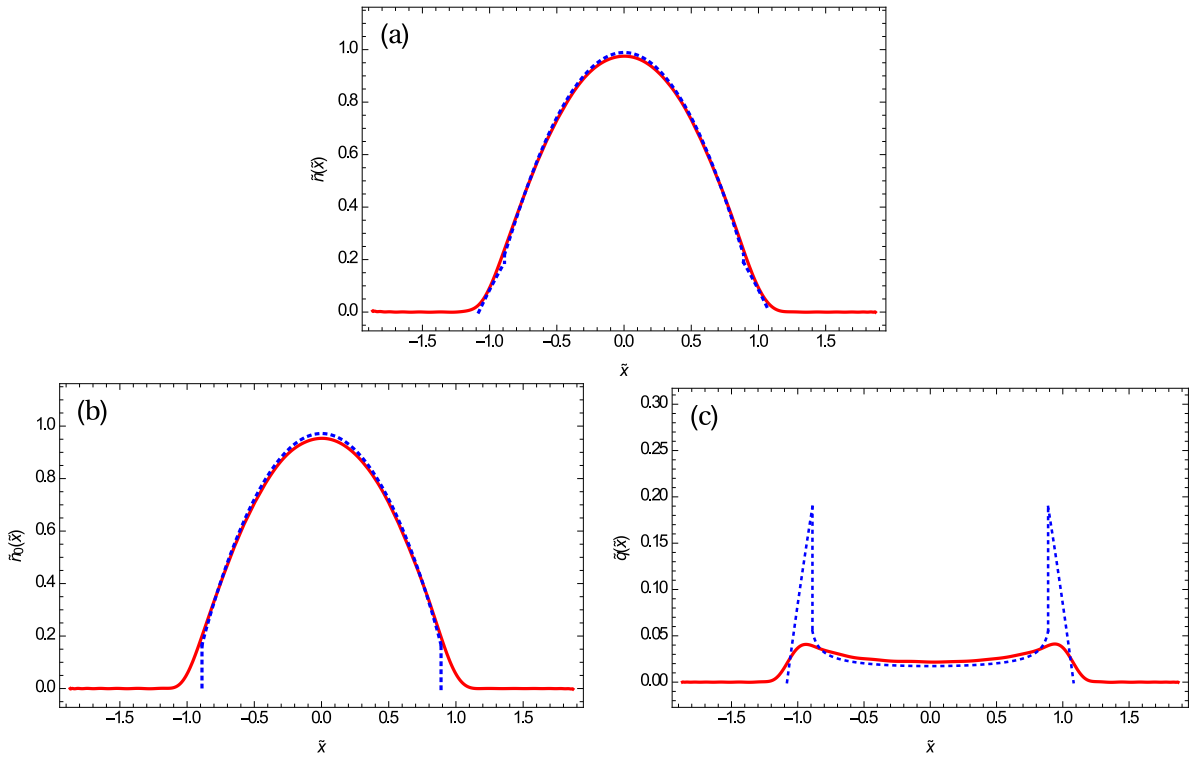

Figure 3.15.: Numerical (solid, red) and analytical (dotted, blue) (a) total density $\tilde{n}(\tilde{x})$, (b) condensate density $\tilde{n}_0(\tilde{x})$, and (c) Bose-glass order parameter $\tilde{q}(\tilde{x})$ for $\tilde{D} = 0.016$.

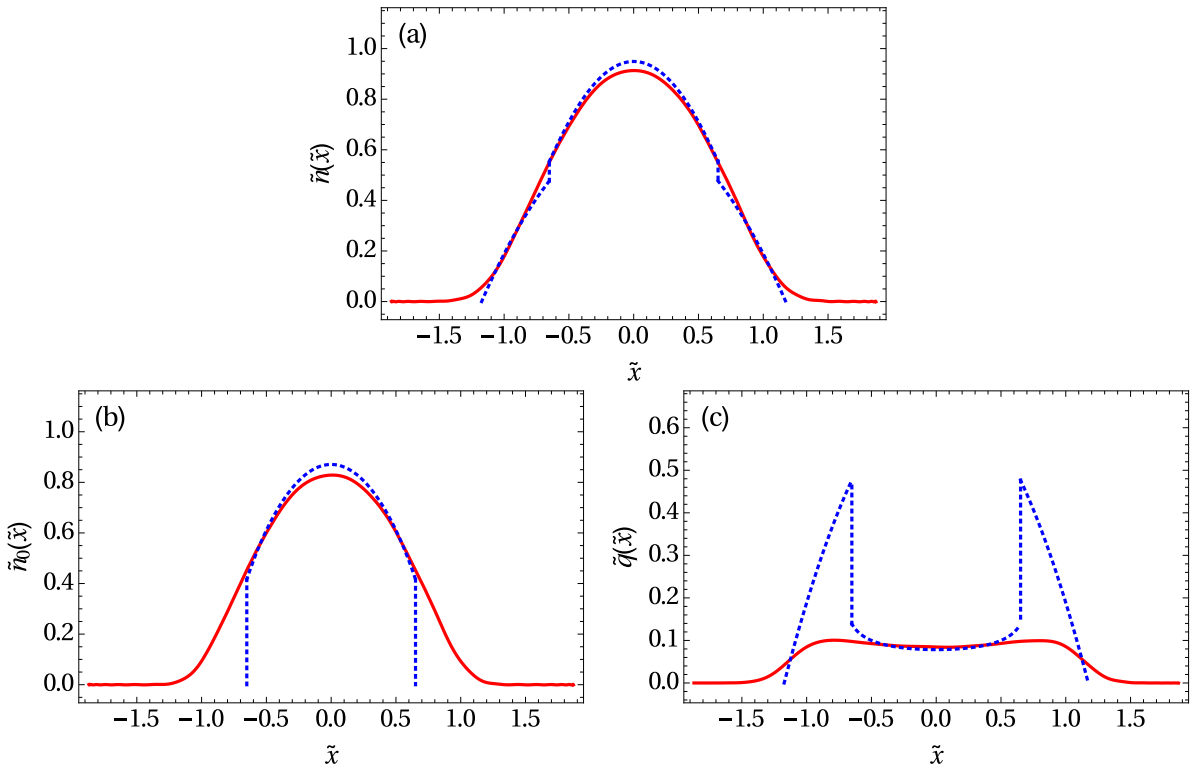

Figure 3.16.: Numerical (solid, red) and analytical (dotted, blue) (a) total density $\tilde{n}(\tilde{x})$, (b) condensate density $\tilde{n}_0(\tilde{x})$, and (c) Bose-glass order parameter $\tilde{q}(\tilde{x})$ for $\tilde{D} = 0.067$.

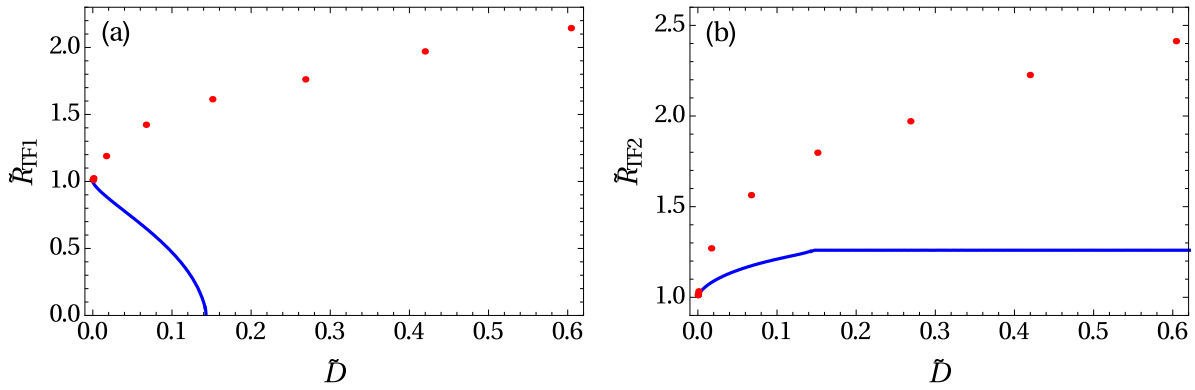

Figure 3.17.: Analytical (solid, blue) and numerical (dotted, red) (a) condensate radius $\tilde{R}_{\mathrm{TF1}}$ and (b) cloud radius $\tilde{R}_{\mathrm{TF2}}$, as functions of the disorder strength $\tilde{D}$.

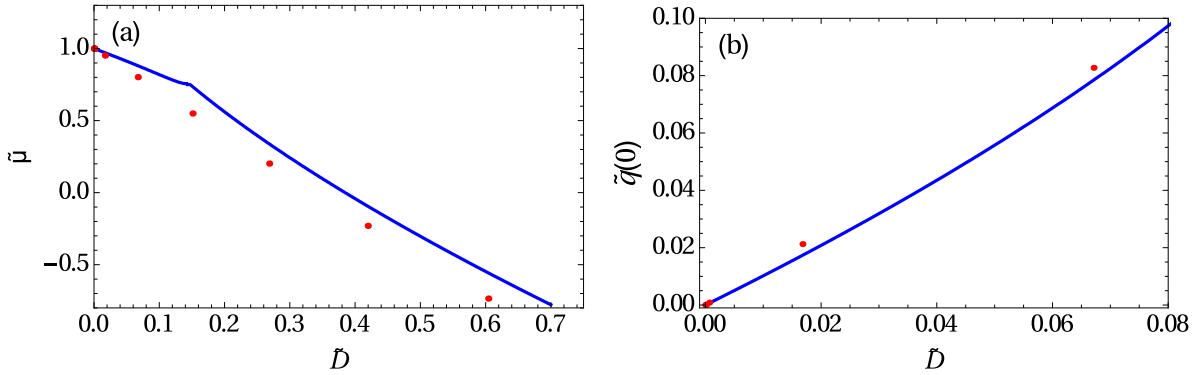

Figure 3.18.: Analytical (solid, blue) and numerical (dotted, red) (a) chemical potential $\tilde{\mu}$ and (b) Bose-glass order parameter in the center of the BEC $\tilde{q}(0)$, as functions of the disorder strength $\tilde{D}$.

the analytical and the numerical total densities agree well, except for the kink of the first one. In Fig. 3.15b the analytical and the numerical condensate density are compatible in the center of the BEC with a tiny discrepancy at the borders of the trap due to the sudden jump of the analytical condensate density. The double bump structure exists in both numerical and analytical Bose-glass order parameter in Fig. 3.15c, also the density is quite similar in the center of the bosonic cloud, the only discrepancy is the maximal value, as the analytical one turns out to be quite high due to the discontinuity caused by the TF approximation. Since the Bose-glass order parameter is quite small in comparison with the condensate and the total density, this discrepancy is not that important. For a higher value of the disorder strength $\tilde{D} = 0.067$, the analytical and the numerical total density plotted in Fig. 3.16a still agree with each other, but for the condensate this is no longer the case. Figure 3.16b shows that there is a tiny deviation between the analytical and the numerical $\tilde{n}_0(\tilde{x})$ in the trap center, but there is a significant difference when we move away from the center due to the analytical jump, which increases with the disorder strength. In Fig. 3.16c the same problem still exists for the Bose-glass order parameter: the analytical bumps are much higher than the numerical ones. With increasing the disorder, the Bose-glass order parameter is becoming more important and of the order of the two other densities $\tilde{n}(\tilde{x})$ and $\tilde{n}_0(\tilde{x})$, and such a discrepancy can no longer be ignored.

In Fig. 3.17a the analytical and the numerical condensate radius agree only in the small disorder regime, but elsewhere they contradict each other. The TF approximation predicts the existence of the Bose-glass phase, where the numerics does not. The same can be remarked for Fig. 3.17b, i.e., the numerical and the analytical cloud radius agree only for vanishing disorder, while in the small disorder regime they agree only qualitatively since both of them are increasing with the disorder strength. In the intermediate disorder regime, the analytics even shows that the size of the bosonic cloud becomes constant, while for the numerics the cloud keeps expanding. Both the analytical and the numerical

chemical potential in Fig. 3.18a are decreasing with the disorder and are compatible, with a total match occurring only in the weak disorder regime. The same can be said about the Huang-Meng Bose-glass order parameter in Fig. 3.18b.

Thus, from the above comparison we conclude that the TF approximation is valid only in the weak disorder regime specially in the center of the trap, where the kinetic energy can be neglected, but it does not represent a good approximation for intermediate disorder. The origin of this invalidity is the fact that ξ becomes a function of the disorder strength and of the order of the Thomas-Fermi radius specially at the border of the bosonic clouds. Furthermore, the quantum fluctuations are more dominating in lower dimensions, this also makes the TF approximation in one dimension not that good. In order to have a global picture of the behavior of the dirty BEC, not only in the presence of weak disorder but also in the presence of intermediate and strong one, we use in the following section another approximation method to treat our problem: the variational method.

3.5. Variational Method

As already explained in the end of Section 2.11, we can apply the variational method to our problem. But since the free energy (2.169) involves the solutions (2.166) of the function $Q_0(x)$ any variational ansatz yields analytically insolvable integrals, we choose to make use of the form (2.126) of the free energy, which is simpler and fits better to the variational treatment at hand. First of all we rewrite the free energy (2.126) for the one-dimensional case at zero temperature and for the harmonic trap potential:

$$\begin{aligned}\mathcal{F} &= \int dx \Bigg\{ -g\left[q(x)+n_0(x)\right]^2 - \frac{g}{2}n_0^2(x) - \sqrt{n_0(x)}\Bigg\{\mu + \frac{\hbar^2}{2M}\frac{\partial^2}{\partial x^2} - 2g\left[q(x)+n_0(x)\right] - \frac{1}{2}M\Omega x^2 \\ &\quad + \frac{D}{\hbar}Q_0(x)\Bigg\}\sqrt{n_0(x)} + \frac{D}{\hbar}Q_0(x)\left[q(x)+n_0(x)\right] \\ &\quad - \frac{D}{\hbar}\sqrt{\frac{M}{2}}\frac{\left[q(x)+n_0(x)\right]}{\sqrt{-\mu+2g\left[q(x)+n_0(x)\right]+\frac{1}{2}M\Omega x^2-\frac{D}{\hbar}Q_0(x)}}\Bigg\}. \end{aligned} \tag{3.40}$$

Now and in order to be able to compare the variational results with the analytical and the numerical ones obtained in Section 3.2 and Section 3.3, respectively, we use the same rescaling parameters already explained below equation (3.24) for all densities, coordinates, chemical potential and disorder strength. To this end, we have to multiply (3.40) with the factor $1/\left(\bar{\mu}\bar{n}R_{\mathrm{TF}}\right)$ to obtain:

$$\begin{aligned}\tilde{\mathcal{F}} &= \int d\tilde{x} \Bigg\{ -\left[\tilde{q}\left(\tilde{x}\right)+\tilde{n}_0\left(\tilde{x}\right)\right]^2 - \frac{1}{2}\tilde{n}_0^2\left(\tilde{x}\right) - \sqrt{\tilde{n}_0\left(\tilde{x}\right)}\Bigg\{\tilde{\mu} + \left(\frac{\xi}{R_{\mathrm{TF}}}\right)^2\frac{\partial^2}{\partial\tilde{x}^2} - 2\left[\tilde{q}\left(\tilde{x}\right)+\tilde{n}_0\left(\tilde{x}\right)\right] - \tilde{x}^2 \\ &\quad + 2\tilde{D}\tilde{Q}_0(\tilde{x})\Bigg\}\sqrt{\tilde{n}_0\left(\tilde{x}\right)} + 2\tilde{D}\tilde{Q}_0(\tilde{x})\left[\tilde{q}\left(\tilde{x}\right)+\tilde{n}_0\left(\tilde{x}\right)\right] \\ &\quad - 2\tilde{D}\frac{\tilde{q}\left(\tilde{x}\right)+\tilde{n}_0\left(\tilde{x}\right)}{\sqrt{-\tilde{\mu}+2\left[\tilde{q}\left(\tilde{x}\right)+\tilde{n}_0\left(\tilde{x}\right)\right]+\tilde{x}^2-2\tilde{D}\tilde{Q}_0(\tilde{x})}}\Bigg\}, \end{aligned} \tag{3.41}$$

where $\tilde{\mathcal{F}} = \mathcal{F}/\left(\bar{\mu}\bar{n}R_{\mathrm{TF}}\right)$ denotes the dimensionless free energy and $\tilde{Q}_0(\tilde{x}) = \sqrt{\frac{2\bar{\mu}}{M}}Q_0(x)$.

Motivated by the analytical and the numerical results presented in Sections 3.2 and 3.3, respectively, we suggest the three following ansatz for the condensate density $\tilde{n}_0\left(\tilde{x}\right)$, the Bose-glass order parameter $\tilde{q}\left(\tilde{x}\right)$, and the auxiliary function $\tilde{Q}_0(\tilde{x})$:

$$\tilde{n}_0\left(\tilde{x}\right) = \alpha e^{-\sigma\tilde{x}^2}, \tag{3.42}$$

$$\tilde{q}\left(\tilde{x}\right) + \tilde{n}_0\left(\tilde{x}\right) = \gamma e^{-\theta\tilde{x}^2}, \tag{3.43}$$

$$\tilde{Q}_0(\tilde{x}) = \frac{\tilde{q}\,(\tilde{x}) + \tilde{n}_0\,(\tilde{x})}{\tilde{D}} - \left(\zeta + \eta\tilde{x}^2\right), \tag{3.44}$$

where α, σ, γ, θ, ζ, and η denote the respective variational parameters. The parameters α and γ are proportional to the number of particles in the condensate and the total number of particles, respectively, while the parameters σ and θ represent the width of the condensate density and the total density, respectively.

Inserting the ansatz (3.42)–(3.44) into the free energy (3.41) and performing the integral over the space yields:

$$\begin{aligned}\tilde{\mathcal{F}} &= \sqrt{\pi}\left\{\frac{\gamma^2}{\sqrt{2\theta}} + \frac{\alpha}{2\sigma^{3/2}} - \frac{\alpha}{4\sqrt{\sigma}}\left(4\tilde{\mu} + \sqrt{2}\alpha\right) + \left(\frac{\xi}{R_{\mathrm{TF}}}\right)^2 \frac{\alpha\sqrt{\sigma}}{2}\right. \\ &\left. + \tilde{D}\left(\frac{2\alpha\zeta}{\sqrt{\sigma}} + \frac{\alpha\eta}{\sigma^{3/2}} - \frac{\gamma\,(\eta + 2\zeta\theta)}{\theta^{3/2}}\right) - \frac{2\tilde{D}\gamma}{\sqrt{1 + 2\tilde{D}\eta}} e^{\frac{2\tilde{D}\zeta - \tilde{\mu}}{2 + 4\tilde{D}\eta}\theta} K_0\left(\frac{2\tilde{D}\zeta - \tilde{\mu}}{2 + 4\tilde{D}\eta}\theta\right)\right\}, \end{aligned} \tag{3.45}$$

where $K_0\,(s)$ represents the modified Bessel function of the second kind. The free energy (3.45) has now to be extremised with respect to the variational parameters α, σ, γ, θ, ζ, and η. This yields the following six algebraic equations:

$$\frac{\sqrt{\pi}}{2\sigma^{3/2}}\left[1 - 2\tilde{\mu}\sigma - \sqrt{2}\alpha\sigma + \left(\frac{\xi}{R_{\mathrm{TF}}}\right)^2 \sigma^2 + 4\tilde{D}\sigma\zeta + 2\tilde{D}\eta\right] = 0, \tag{3.46}$$

$$\frac{\sqrt{\pi}\alpha}{8\sigma^{5/2}}\left[-6 + 4\tilde{\mu}\sigma + \sqrt{2}\alpha\sigma + 2\left(\frac{\xi}{R_{\mathrm{TF}}}\right)^2 \sigma^2 - 8\tilde{D}\sigma\zeta - 12\tilde{D}\eta\right] = 0, \tag{3.47}$$

$$\frac{\sqrt{\pi}}{\theta^{3/2}}\left[\sqrt{2}\gamma\theta - \tilde{D}\,(\eta + 2\zeta\theta)\right] - \frac{2\tilde{D}}{\sqrt{1 + 2\tilde{D}\eta}} e^{\frac{2\tilde{D}\zeta - \tilde{\mu}}{2 + 4\tilde{D}\eta}\theta} K_0\left(\frac{2\tilde{D}\zeta - \tilde{\mu}}{2 + 4\tilde{D}\eta}\theta\right) = 0, \tag{3.48}$$

$$\frac{\sqrt{\pi}\gamma}{4\theta^{5/2}}\left(6\tilde{D}\eta - \sqrt{2}\gamma\theta + 4\tilde{D}\zeta\theta\right) - \tilde{D}\gamma\frac{\sqrt{2\tilde{D}\zeta - \tilde{\mu}}}{\left(1 + 2\tilde{D}\eta\right)^{3/2}} e^{\frac{2\tilde{D}\zeta - \tilde{\mu}}{2 + 4\tilde{D}\eta}\theta}\left[K_0\left(\frac{2\tilde{D}\zeta - \tilde{\mu}}{2 + 4\tilde{D}\eta}\theta\right) - K_1\left(\frac{2\tilde{D}\zeta - \tilde{\mu}}{2 + 4\tilde{D}\eta}\theta\right)\right] = 0, \tag{3.49}$$

$$2\tilde{D}\left\{\sqrt{\pi}\left(\frac{\alpha}{\sqrt{\sigma}} - \frac{\gamma}{\sqrt{\theta}}\right) - \tilde{D}\frac{\gamma\theta}{\left(1 + 2\tilde{D}\eta\right)^{3/2}} e^{\frac{2\tilde{D}\zeta - \tilde{\mu}}{2 + 4\tilde{D}\eta}\theta}\left[K_0\left(\frac{2\tilde{D}\zeta - \tilde{\mu}}{2 + 4\tilde{D}\eta}\theta\right) - K_1\left(\frac{2\tilde{D}\zeta - \tilde{\mu}}{2 + 4\tilde{D}\eta}\theta\right)\right]\right\} = 0, \tag{3.50}$$

$$\begin{aligned}&\tilde{D}\left\{\sqrt{\pi}\left(\frac{\alpha}{\sigma^{3/2}} - \frac{\gamma}{\theta^{3/2}}\right) + 2\tilde{D}\gamma\theta\frac{2\tilde{D}\zeta - \tilde{\mu}}{\left(1 + 2\tilde{D}\eta\right)^{5/2}} e^{\frac{2\tilde{D}\zeta - \tilde{\mu}}{2 + 4\tilde{D}\eta}\theta}\left[K_0\left(\frac{2\tilde{D}\zeta - \tilde{\mu}}{2 + 4\tilde{D}\eta}\theta\right) - K_1\left(\frac{2\tilde{D}\zeta - \tilde{\mu}}{2 + 4\tilde{D}\eta}\theta\right)\right]\right\} \\ &+ 2\tilde{D}^2\frac{\gamma}{\left(1 + 2\tilde{D}\eta\right)^{3/2}} e^{\frac{2\tilde{D}\zeta - \tilde{\mu}}{2 + 4\tilde{D}\eta}\theta} K_0\left(\frac{2\tilde{D}\zeta - \tilde{\mu}}{2 + 4\tilde{D}\eta}\theta\right) = 0. \end{aligned} \tag{3.51}$$

Note that the additional dimensionless particle number equation, which follows from the thermodynamic condition $-\frac{\partial\tilde{\mathcal{F}}}{\partial\tilde{\mu}} = \frac{4}{3}$, gives us a seventh equation:

$$\sqrt{\pi}\frac{\alpha}{\sqrt{\sigma}} - \tilde{D}\frac{\gamma\theta}{\left(1 + 2\tilde{D}\eta\right)^{3/2}} e^{\frac{2\tilde{D}\zeta - \tilde{\mu}}{2 + 4\tilde{D}\eta}\theta}\left[K_0\left(\frac{2\tilde{D}\zeta - \tilde{\mu}}{2 + 4\tilde{D}\eta}\theta\right) - K_1\left(\frac{2\tilde{D}\zeta - \tilde{\mu}}{2 + 4\tilde{D}\eta}\theta\right)\right] = \frac{4}{3}. \tag{3.52}$$

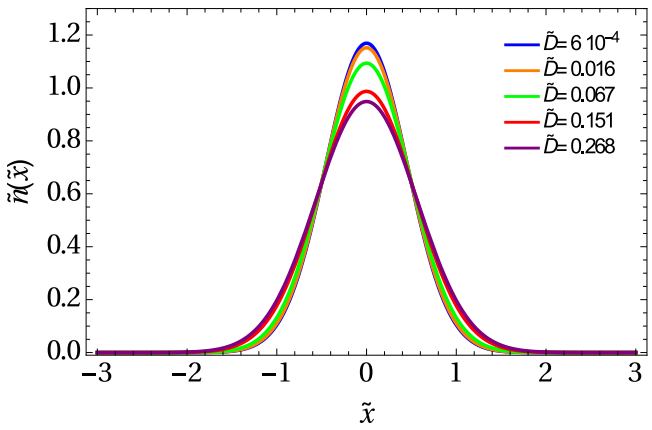

Figure 3.19.: Particle density $\tilde{n}(\tilde{x})$ for increasing disorder strengths $\tilde{D}$ from the top to the bottom.

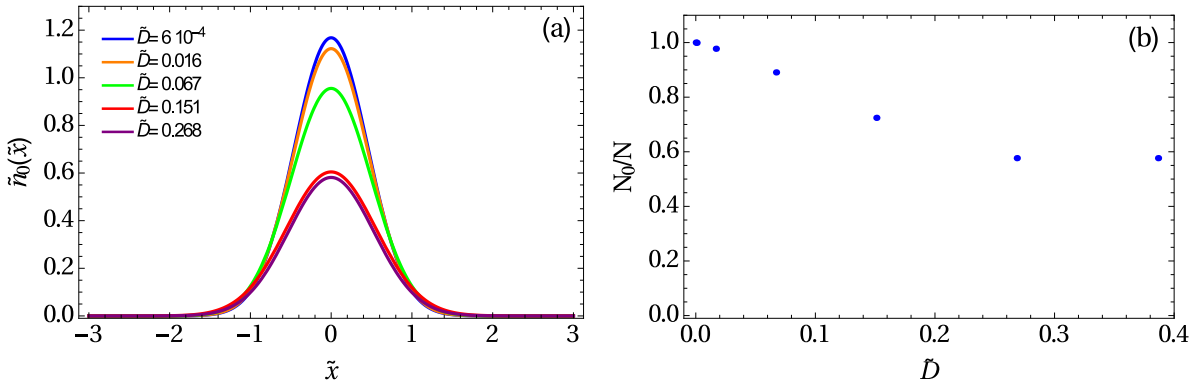

Figure 3.20.: (a) Condensate density $\tilde{n}_0(\tilde{x})$ and (b) fractional number of condensed particles N_0/N for increasing disorder strengths $\tilde{D}$ from the top to the bottom.

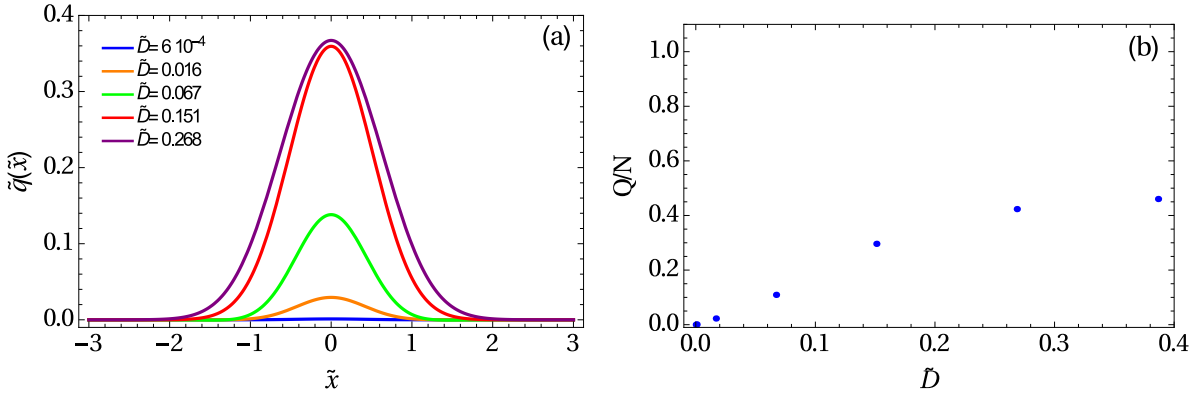

Figure 3.21.: (a) Bose-glass order parameter $\tilde{q}(\tilde{x})$ and (b) fractional number of particles Q/N in the disconnected local minicondensates for increasing disorder strengths $\tilde{D}$ from the bottom to the top.

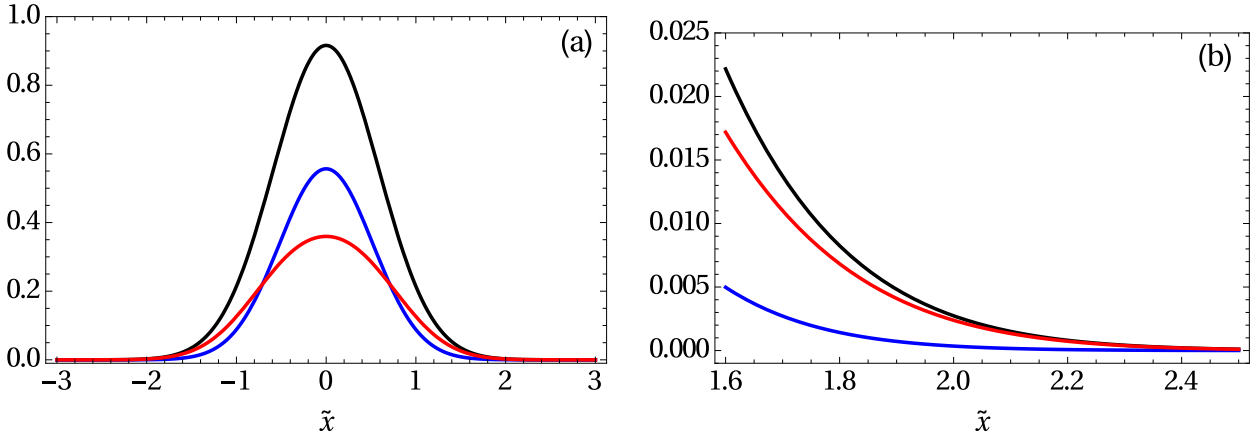

Figure 3.22.: (a) Particle density $\tilde{n}(\tilde{x})$ (black), condensate density $\tilde{n}_0(\tilde{x})$ (blue), Bose-glass order parameter $\tilde{q}(\tilde{x})$ (red) and (b) blow-up of border region for $\tilde{D} = 0.386$.

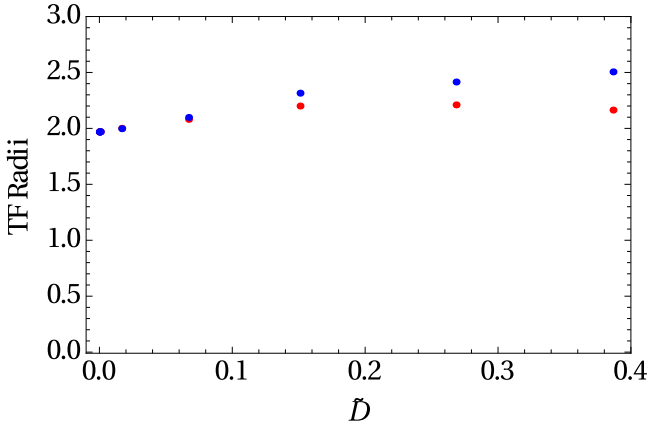

Figure 3.23.: Cloud radius $\tilde{R}_{\mathrm{TF2}}$ (blue) and condensate radius $\tilde{R}_{\mathrm{TF1}}$ (red) as functions of the disorder strength $\tilde{D}$.

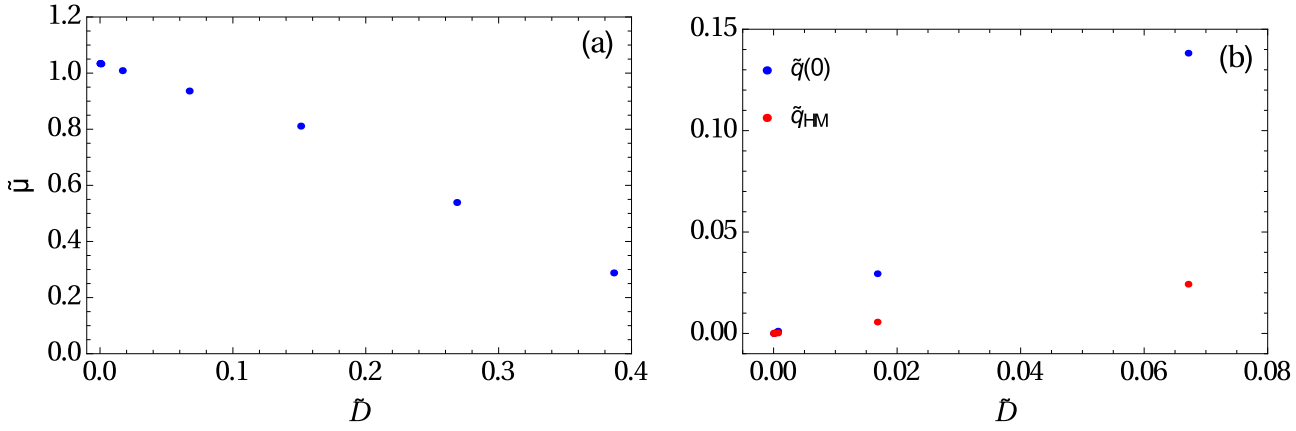

Figure 3.24.: (a) Chemical potential $\tilde{\mu}$ and (b) the variational (blue) and the Huang-Meng (red) Bose-glass order parameter in the center of the BEC, as a function of the disorder strength $\tilde{D}$.

Thus, we have now seven coupled equations (3.46)–(3.52) for seven variables α, σ, γ, θ, ζ, η, and $\tilde{\mu}$. Those equations can not be solved analytically, so we solve them numerically. Furthermore, they have more than one solution, which necessitates to select only the physical one. In order to be able to compare later on the variational results with the numerical ones, we use the same values of the disorder strength used previously in Section 3.3. For each value of the disorder strength, we solve the coupled Eqs. (3.46)–(3.52) numerically, then we insert the resulting variational parameters α, σ, γ, and θ into the variational ansatz (3.42) and (3.43) in order to get the variational total density $\tilde{n}(\tilde{x})$, the variational condensate density $\tilde{n}_0(\tilde{x})$, and the variational Bose-glass order parameter $\tilde{q}(\tilde{x})$.

In Fig. 3.19 the total density $\tilde{n}(\tilde{x})$ is plotted for different disorder strengths, where we see that the density of bosons is always maximal in the center of the cloud, then it decreases when we move away from the center until vanishing at the cloud radius $\tilde{R}_{\mathrm{TF2}}$. The maximal value of the total density decreases with the disorder strength, while its width increases. The condensate density $\tilde{n}_0(\tilde{x})$ in Fig. 3.20a has a similar qualitative behavior as the total density in Fig. 3.19 and vanishes at the condensate radius $\tilde{R}_{\mathrm{TF1}}$. The response of the condensate density to disorder can also be seen in Fig. 3.20b, where the fractional number of condensed particles N_0/N is plotted as a function of the disorder strength. In the clean case all particles are in the condensate, but when we increase the disorder strength more and more particles leave the condensate. Starting from the disorder strength value $\tilde{D} = 0.393$, Eqs. (3.46)–(3.52) turn out to have only complex solutions, the variational approach does not provide any information about our system for higher disorder strengths. So we can not predict if, at a certain critical disorder strength, the condensate density vanishes or remains constant. The Bose-glass order parameter $\tilde{q}(\tilde{x})$ in Fig. 3.21a has a similar shape as the two previous densities $\tilde{n}(\tilde{x})$ and $\tilde{n}_0(\tilde{x})$, it is maximal in the center of the BEC and decreases when we move away from the center. When we increase the disorder strength, the maximal value of the Bose-glass order parameter density as well as its width increase. A better understanding of the influence of the disorder on the local minicondensates can be deduced from Fig. 3.21b, where the fractional number of particles Q/N in the disconnected local minicondensates is zero in the clean case, then increases with the disorder strength. This means that more bosons are going into the local minima of the disorder potential when we increase the disorder strength. Here again and due to the fact, that physical solutions exist only in a limited range of the disorder strength, we are not able to predict if there exists a critical disorder strength value, where either all particles leave the condensate and fill the local minicondensates, or the number of the localized particles remains constant.

In order to know whether the bosonic cloud contains beside the superfluid region also a Bose-glass region, we plot the total density $\tilde{n}(\tilde{x})$, the condensate density $\tilde{n}_0(\tilde{x})$, and the Bose-glass order parameter $\tilde{q}(\tilde{x})$ together in Fig. 3.22 for the disorder strength value $\tilde{D} = 0.386$. The blow-up of the border region in Fig. 3.22b shows clearly that the condensate density vanishes, while the Bose-glass order parameter still persists, which is the definition of the Bose-glass region. The cloud radius $\tilde{R}_{\mathrm{TF2}}$ and the condensate radius $\tilde{R}_{\mathrm{TF1}}$ are defined by the length, where the total density and the condensate density are equal to 10^{-4}, respectively. Both radii are identical in the weak-disorder regime in Fig. 3.23, and both are increasing with the disorder strength. But we have no idea, if for higher disorder strengths they will keep increasing, remain constant, or the condensate radius $\tilde{R}_{\mathrm{TF1}}$ vanishes, i.e., we can not say if a quantum phase transition exists or not. The chemical potential $\tilde{\mu}$ decreases with the disorder strength in Fig. 3.24a. In the end we plot the Bose-glass order parameter in the center of the BEC $\tilde{q}\,(0)$ together with the Huang-Meng result $\tilde{q}_{\mathrm{HM}} = \frac{\tilde{D}}{2^{3/2}\sqrt{\tilde{n}_0}}$ in Fig. 3.24b in order to know if the variational results are compatible with the Huang-Meng theory for weak disorder. In the weak disorder regime, $\tilde{q}\,(0)$ is linearly proportional to the disorder strength, which agrees qualitatively with the Huang-Meng theory but not quantitatively, since there is a significant discrepancy between both results.

3.6. Comparison of Analytical, Numerical and Variational Results

Now we compare the physical quantities obtained via the three different methods, the TF approximation, the numerical method, and the variational method. We start first of all with the densities: the total density $\tilde{n}(\tilde{x})$, the condensate density $\tilde{n}_0(\tilde{x})$, and the Bose-glass order parameter $\tilde{q}(\tilde{x})$ are plotted

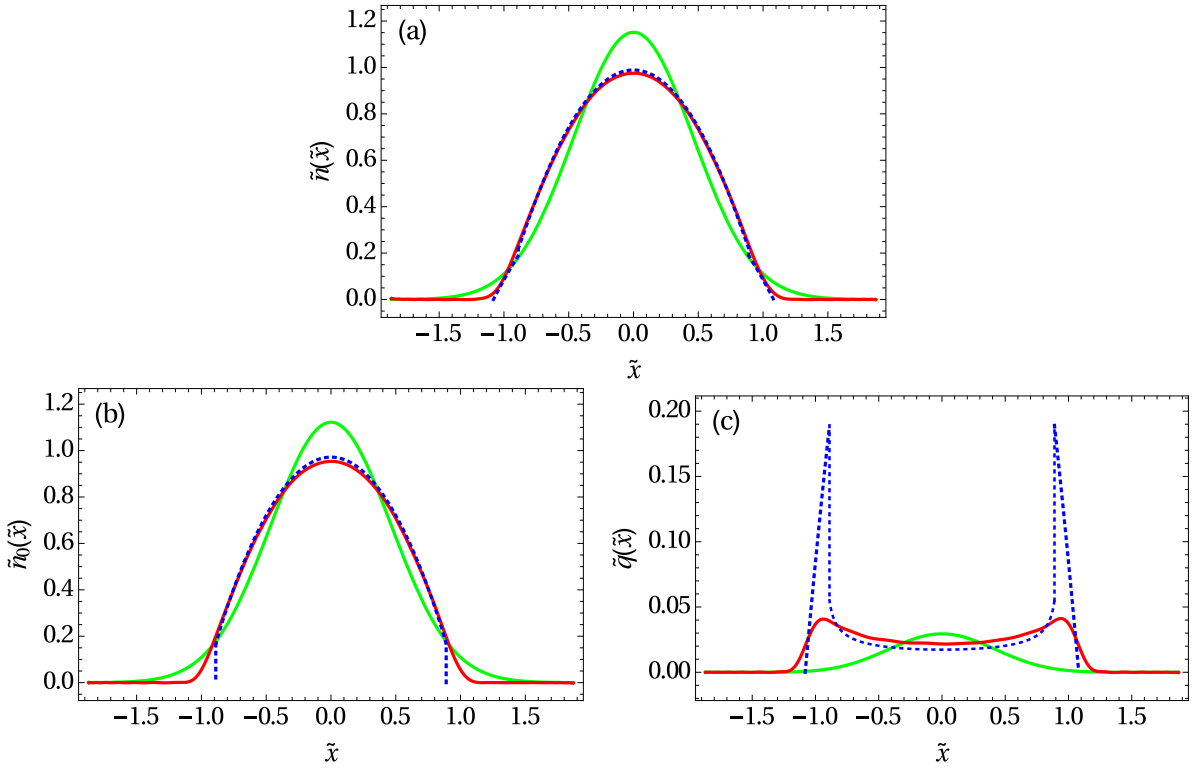

Figure 3.25.: (a) Total density $\tilde{n}(\tilde{x})$, (b) condensate density $\tilde{n}_0(\tilde{x})$, (c) Bose-glass order parameter $\tilde{q}(\tilde{x})$: variational (solid, green), numerical (solid, red), analytical (dotted, blue) for $\tilde{D} = 0.016$.

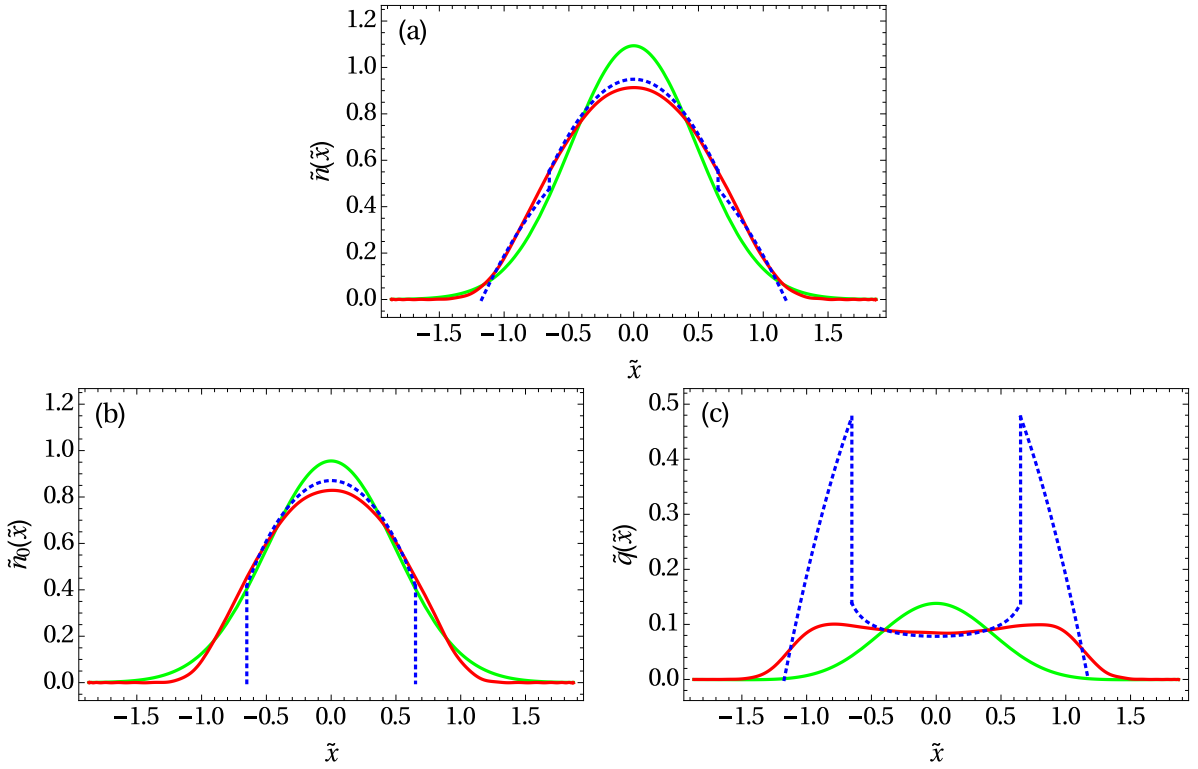

Figure 3.26.: (a) Total density $\tilde{n}(\tilde{x})$, (b) condensate density $\tilde{n}_0(\tilde{x})$, (c) Bose-glass order parameter $\tilde{q}(\tilde{x})$: variational (solid, green), numerical (solid, red), analytical (dotted, blue) for $\tilde{D} = 0.067$.

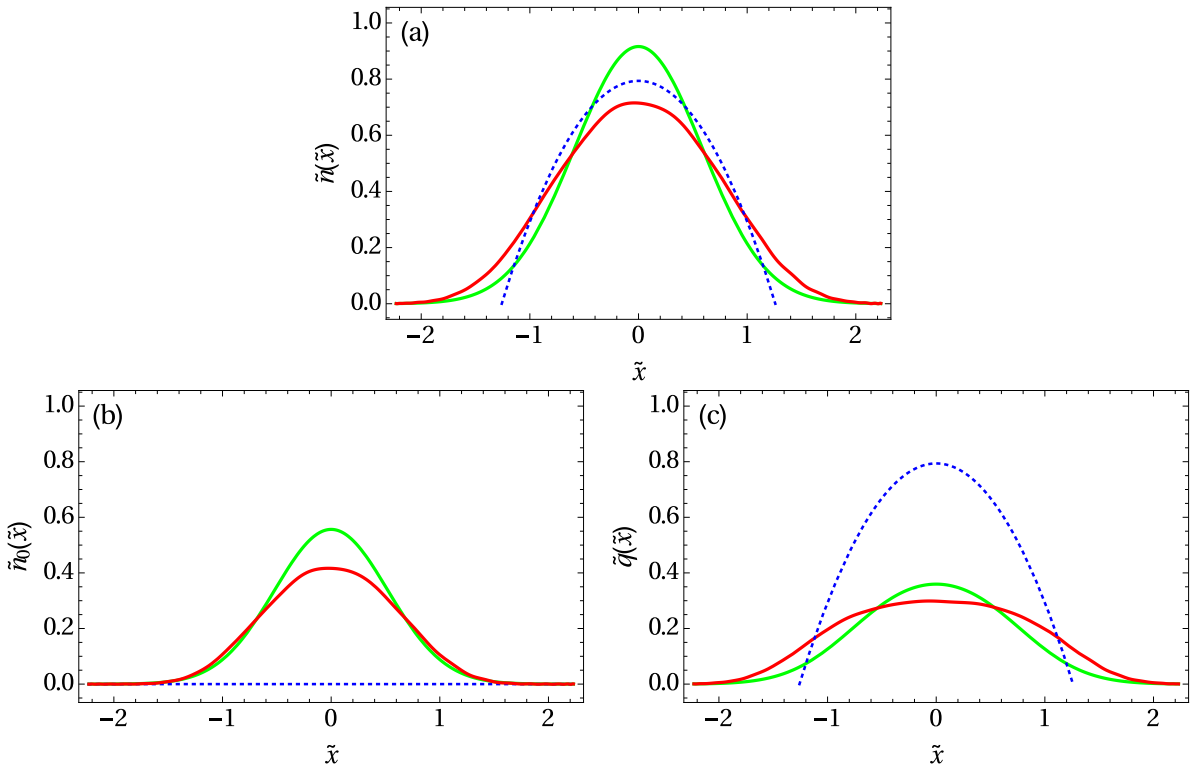

Figure 3.27.: (a) Total density $\tilde{n}(\tilde{x})$, (b) condensate density $\tilde{n}_0(\tilde{x})$, (c) Bose-glass order parameter $\tilde{q}(\tilde{x})$: variational (solid, green), numerical (solid, red), analytical (dotted, blue) for $\tilde{D} = 0.386$.

for three disorder strength values $\tilde{D} = 0.016$, $\tilde{D} = 0.067$, and $\tilde{D} = 0.386$ in Figs. 3.25–3.27, respectively, in order to cover the range of the weak disorder regime as well as the intermediate disorder regime. For $\tilde{D} = 0.016$ the three total densities $\tilde{n}(\tilde{x})$ in Fig. 3.25a agree qualitatively well, but quantitatively the TF approximated total density $\tilde{n}(\tilde{x})$ represents still the best approximation for the numerical total density, especially in the center of the bosonic cloud, where the variational result has some discrepancy. The same can be remarked for the condensate density $\tilde{n}_0(\tilde{x})$ in Fig. 3.25b. For the Bose-glass order parameter $\tilde{q}(\tilde{x})$ in Fig. 3.25c the double bump structure, which exists in both numerical and TF approximated results, is missing in the variational result, which has just a bell form. This makes again the TF approximated Bose-glass order parameter $\tilde{q}(\tilde{x})$ the best approach to the numerical one. For a higher value of the disorder strength $\tilde{D} = 0.067$, Fig. 3.26a shows that the variational, numerical, and TF approximated total densities $\tilde{n}(\tilde{x})$ agree well, except from the deviation of the first one in the center of the BEC. In Fig. 3.26b, and due to the considerable jump of the TF approximated condensate density $\tilde{n}_0(\tilde{x})$, the TF approximation breaks down as we know already from the discussion in Section 3.4. So we focus our comparison only between the numerical condensate density and the variational one, which turn out to fit well despite the tiny shift in the center of the trap. The TF approximated Bose-glass order parameter $\tilde{q}(\tilde{x})$ in Fig. 3.26c has the advantage to have qualitatively the same double bump structure as the numerical one, while the variational Bose-glass order parameter has just a bell form. Physically this means that, according to both the TF approximation and the numerics, the density of the bosons in the local minima of the disorder potential is maximal at the border of the trap, but according to the variational result this density is maximal in the center of the trap.

For the intermediate disorder strength $\tilde{D} = 0.386$, the resulting densities are plotted in Fig. 3.27. The TF approximated total density $\tilde{n}(\tilde{x})$ in Fig. 3.27a is still the best approximation to the numerical one in the center of the bosonic cloud, while at the border of the trap the variational and the numerical total density agree well. According to Fig. 3.4 at the disorder strength value $\tilde{D} = 0.386$, we are in the Bose-glass phase, thus, the TF approximated condensate density $\tilde{n}_0(\tilde{x})$ in Fig. 3.27b is zero, which is not the case for both the numerical and the variational condensate densities, which are compatible and match at the borders of the trap. The variational Bose-glass order parameter $\tilde{q}(\tilde{x})$ also agrees well with the numerical one and both have the same bell shape, while the TF approximated Bose-glass order

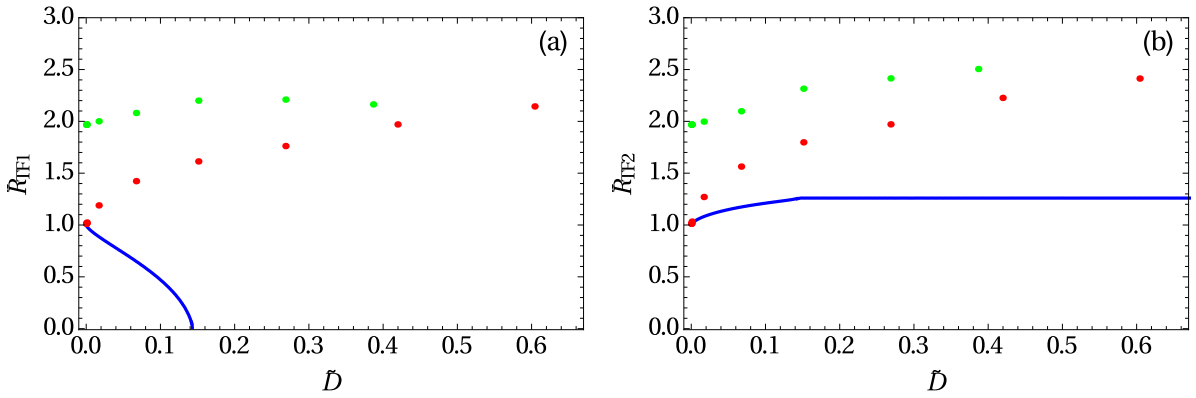

Figure 3.28.: Analytical (solid, blue), numerical (dotted, red), and variational (dotted, green) (a) condensate radius $\tilde{R}_{\mathrm{TF1}}$ and (b) cloud radius $\tilde{R}_{\mathrm{TF2}}$, as functions of the disorder strength $\tilde{D}$.

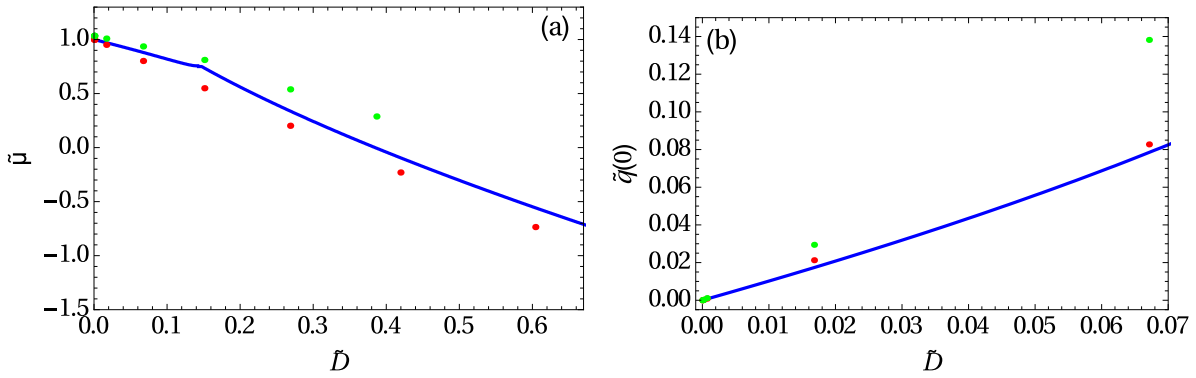

Figure 3.29.: Analytical (solid, blue), numerical (dotted, red), and variational (dotted, green) (a) chemical potential $\tilde{\mu}$ and (b) Bose-glass order parameter in the center of the BEC $\tilde{q}(0)$, as functions of the disorder strength $\tilde{D}$.

parameter has a significant deviation, which is expected since the TF approximation breaks down in the intermediate disorder regime. The TF approximated, the numerical, and the variational Thomas-Fermi radii are plotted together in Fig. 3.28 for comparison. In Fig. 3.28a the variational and the numerical condensate radius $\tilde{R}_{\mathrm{TF1}}$ have the same qualitative behavior, both increase with the disorder strength contrarily to the analytical condensate radius, which decreases with $\tilde{D}$. Furthermore, the analytical $\tilde{R}_{\mathrm{TF1}}$ indicates the existence of a quantum phase transition, while the variational and the numerical treatments break down at a certain critical value of the disorder strength before it could be deduced whether the quantum phase transition exists at larger disorder strength, or does not exist at all. In the weak disorder regime, the analytical and the numerical condensate radii converge, while in the intermediate disorder regime the variational and the numerical condensate radii are the ones which converge. Fig. 3.28b shows that in the weak disorder regime, the variational, the numerical, and the analytical cloud radii agree qualitatively, since the three of them increase with the disorder strength, with a convergence between the variational and the numerical radii. In the intermediate disorder regime the analytical cloud radius remains constant, but both the variational and the numerical cloud radii keep increasing with the disorder strength then converge and, due to the lack of information for higher $\tilde{D}$, we do not know if they will keep increasing or they will become constant.

Concerning the chemical potential, the variational, the numerical, and the analytical chemical potentials agree well in Fig. 3.29a specially for weak disorder where they match. The three of them decrease with the disorder strength. Finally, we plot the variational, numerical, and analytical Bose-glass order parameter in the center of the trap $\tilde{q}(0)$ as functions of the disorder strength in Fig. 3.29b for comparison. The three of them are linearly proportional to the disorder strength and agree qualitatively with the Huang-Meng theory for weak disorder, with a total match between the numerical and the

analytical order parameters, while the variational one has a greater slope which causes a discrepancy with the two other numerical and the analytical Bose-glass order parameters.

From the discussion above, we conclude that the TF approximation is producing satisfying results in the weak disorder regime, which agree well with the numerical ones, especially in the center of the bosonic cloud, where the kinetic energy can be neglected, however it breaks down in the intermediate disorder regime being unable to describe the BEC system properly. On the other side the variational method within the ansatz (3.42)–(3.44) turns out to be a good approximation to describe the BEC system in the intermediate disorder regime and works there better than in the weak one, specially at the border of the cloud where the Bose-glass region is located. This is due to the fact that a stronger disorder reduces the repulsive interaction between the particles and approaches the case of non-interacting bosons, where the densities are Gaussian as in our ansatz. Although the variational method does not provide us physical results for higher disorder strengths, it still treats an important range of the disorder strength. The combined application of the TF approximation for the weak disorder regime together with the application of the variational method for the intermediate disorder regime covers a significant range of disorder strengths. The main difference between the weak and the intermediate disorder regime is where the Bose-glass region appears within the harmonic trap. The detailed numerical simulations show that the Bose-glass region emerges at the edge of the atomic cloud for small disorder strengths, while in the intermediate disorder regime it is located in the trap center. The main question, which still has to be answered, concerns the possible existence of the quantum phase transition from the superfluid to the Bose-glass phase. In view of Ref. [83] the disorder has to overcome energetically the interaction in order to yield such a quantum phase transition. But, according to the numerical and variational results displayed in Fig. 3.28, this turns out to be not the case neither in the weak nor in intermediate disorder regime. Thus it remains to investigate the strong disorder regime in order to be able to detect a possible quantum phase transition, which is beyond the scope of this thesis.

4. 3D at Zero Temperature

In this chapter we consider the dirty three-dimensional BEC system to be at zero temperature, so the thermal density vanishes, i.e., $n_{\rm th}(\mathbf{x}) = 0$. This allows us, as a first step, to study the impact of the disorder on only the distribution of the condensate density and the Bose-glass order parameter as well as the corresponding Thomas-Fermi radii. In particular, two harmonic potential traps are treated in detail, the first one is isotropic and the second one is anisotropic. The latter allows us to study the geometric effect of the trap aspect ratios on the different properties of the dirty BEC system. Furthermore, we qualitatively compare the one- and three-dimensional results.

4.1. Homogeneous Case

We start, again, with the homogeneous case since it is the simplest one, where in the absence of the trap we have $V(\mathbf{x}) = 0$. We distinguish between two different phases, namely, the superfluid phase, where the condensate density contributes to the total density, and the Bose-glass phase, where the condensate vanishes, which we treat separately.

4.1.1. Superfluid Phase

At zero temperature, where $n_{\rm th}(\mathbf{x}) = 0$, we only need Eqs. (2.152)–(2.154), which reduce in the superfluid phase to:

$$n = n_0 + q, \tag{4.1}$$

$$gn_0 = \left(\sqrt{-\mu + d^2 + 2gn} + d\right)^2, \tag{4.2}$$

$$q = \frac{dn_0}{\sqrt{-\mu + d^2 + 2gn}}. \tag{4.3}$$

In this section we drop the spatial dependency of all densities due to the homogeneity. Inserting equations (4.2) and (4.3) into equation (4.1), then dividing by $\sqrt{g}n^{3/2}$ gives us the following algebraic third order equation for the condensate fraction n_0/n:

$$\left(\frac{n_0}{n}\right)^{3/2} - \sqrt{\frac{n_0}{n}} + \overline{d} = 0. \tag{4.4}$$

Here $\overline{d} = \frac{\xi}{\mathcal{L}}$ denotes the dimensionless disorder strength, where $\xi = \frac{\hbar}{\sqrt{2Mgn}}$ stands for the coherence length, and $\mathcal{L} = \frac{2\pi\hbar^4}{M^2 D}$ represents the Larkin length [82, 119]. Figure 4.1 shows that the condensate fraction decreases with increasing disorder strength $\overline{d}$. As more and more particles are localized in the minima of the random potential, our mean-field theory predicts that the condensate density stops to exist at the critical value $\overline{d}_{\rm c} = \sqrt{\frac{1}{3}} - \left(\frac{1}{3}\right)^{3/2} \simeq 0.384$. We interpret this as a sign that a first-order quantum phase transition occurs in the homogeneous BEC from the superfluid phase, where the particles are either condensed or in the local minima of the disorder, to the Bose-glass phase, where there is no condensate at all and all bosons are localized in the minima of the disorder potential. This suggests that a corresponding quantum phase transition will also appear in the trapped case, which is studied in the next section.

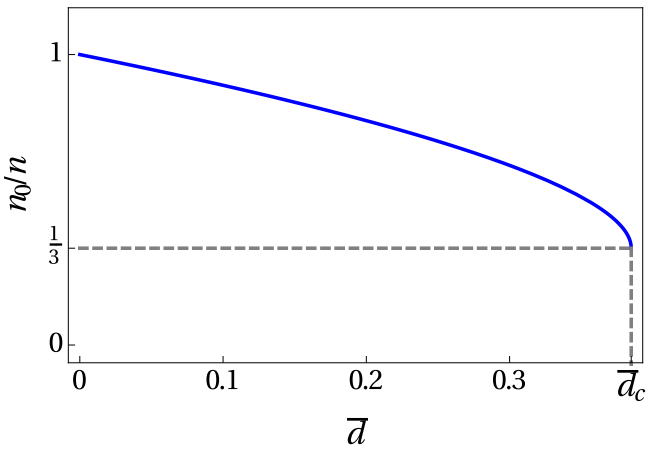

Figure 4.1.: Condensate fraction n_0/n as function of dimensionless disorder strength $\overline{d}$.

Now we look for the equation of state in the superfluid phase. To this end we divide equation (4.2) by the factor gn, which yields:

$$\frac{n_0}{n} = \left(\sqrt{-\frac{\mu}{gn} + \overline{d}^2 + 2} + \overline{d}\right)^2. \tag{4.5}$$

Inserting this result into the condensate fraction equation (4.4) yields the following algebraic cubic equation of state:

$$\left(\sqrt{-\frac{\mu}{gn} + \overline{d}^2 + 2} + \overline{d}\right)^3 - \sqrt{-\frac{\mu}{gn} + \overline{d}^2 + 2} = 0, \tag{4.6}$$

Equation (4.6) is solved using the Cardan method (see Appendix A) and turns out to have three real solutions. Among them we choose the one which satisfies the physical conditions that $\mu = gn$ for $\overline{d} = 0$ and $n_0/n = 1/3$ for $\overline{d} = \overline{d}_c$.

4.1.2. Bose-Glass Phase

In the Bose-glass phase we have $n_0 = 0$ and $n = q$, so we need only equation (2.154), which reduces to:

$$gn = \frac{\mu - d^2}{2}. \tag{4.7}$$

Dividing relation (4.7) by the factor gn, we get the equation of state

$$\frac{\mu}{gn} = 2 + \overline{d}^2. \tag{4.8}$$

Finally, the equation of state of the superfluid phase (4.6) is combined with the equation of state of the Bose-glass phase (4.8) and plotted in Fig. 4.2. It shows that the chemical potential increases with the disorder strength $\overline{d}$ in both phases with a discontinuity in the transition region between the superfluid and the Bose-glass phase:

$$\lim_{\overline{d}\uparrow\overline{d}_c} \frac{\mu}{gn} - \lim_{\overline{d}\downarrow\overline{d}_c} \frac{\mu}{gn} = \frac{1}{3}\left(1 - \sqrt{3}\,\overline{d}_c\right)^2 = \frac{1}{27} \simeq 0.037. \tag{4.9}$$

4.1.3. Comparison with Literature

First we check whether our results are compatible with the Huang-Meng theory [65,69,103,120], where the Bose-glass order parameter of a homogeneous dilute Bose gas at zero temperature in case of weak disorder regime is deduced within the seminal Bogoliubov theory. The Bose-glass order parameter in three dimensions via the Huang-Meng theory is proportional to the disorder strength:

$$q_{\mathrm{HM}} = \frac{d}{\sqrt{2}}\sqrt{\frac{n}{g}} \triangleq \frac{q_{\mathrm{HM}}}{\sqrt{n/g}} = \frac{\overline{d}}{\sqrt{2}}. \tag{4.10}$$

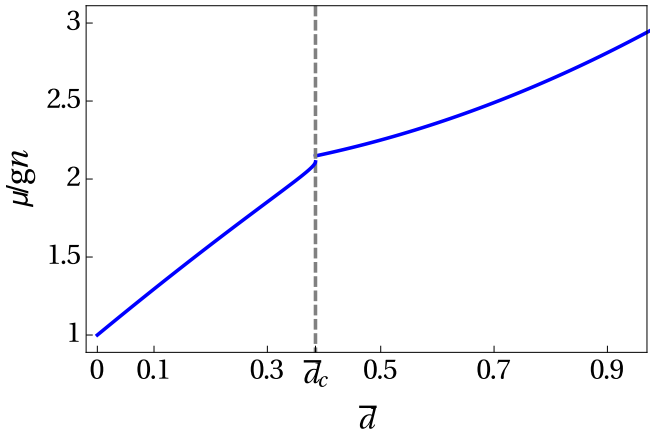

Figure 4.2.: Chemical potential μ in units of gn as function of dimensionless disorder strength $\overline{d}$.

In order to compare with (4.10) we deduce from (4.3) the formula of the Bose-glass order parameter in case of weak disorder strength:

$$q_w \approx d\sqrt{\frac{n}{g}} \triangleq \frac{q_w}{\sqrt{n/g}} = \overline{d}. \tag{4.11}$$

Thus, from (4.11) we conclude that our result agrees qualitatively with the Huang-Meng theory, i.e., in the weak disorder regime the Bose-glass order parameter is, indeed, proportional to the disorder strength d. But quantitatively the comparison of (4.10) with (4.11) reveals that a factor of $\sqrt{2}$ is missing in our formula (4.11). This is due to the fact that the Hartree-Fock theory does not contain the Bogoliubov channel, which is included in the Huang-Meng theory. Note that in the one-dimensional case, as discussed in Subsection 3.1.3, a factor $2^{3/2}$ was missing, while in the three-dimensional case only a factor of $\sqrt{2}$ is missing. This means that our Hartree-Fock theory is more compatible with the literature in higher dimensions than in lower ones.

In Ref. [79] a non-perturbative approach for dirty bosons using the random phase approximation is developed and also a first-order phase transition is found. According to Ref. [79] the disorder strength value corresponding to the quantum phase transition is $\overline{d}_{c_{\mathrm{NPG}}} = 0.53$. Thus, our quantum phase transition disorder value $\overline{d}_c = 0.384$ is of the same order as the one in Ref. [79], but again we miss a factor of $\sqrt{2}$ in our result.

Furthermore, we compare the disorder strength critical value $\overline{d}_c$ with the one obtained in Refs. [82,83]. There a non-perturbative approach is worked out in order to to study the trapped dirty BEC, which starts from the Bose-glass phase and goes towards the superfluid phase for decreasing disorder strength, whereas our approach starts from the superfluid phase and ends up in the Bose-glass phase for increasing disorder strength. In those references the quantum phase transition from the superfluid to the Bose-glass is predicted at the disorder strength value $\overline{d}_{c_{\mathrm{FNP}}} = \sqrt{\frac{3}{8\pi}} \simeq 0.345$, which is of the same order as our $\overline{d}_c = 0.384$.

4.2. Thomas-Fermi Approximation

After having treated the homogeneous case, we deal now with the trapped one. In the three-dimensional case we have also, as it has been done for one dimension, to distinguish between two different regions: the superfluid and the Bose-glass region.

In the superfluid region we rewrite at zero temperature the self-consistency equations (2.152)–(2.155) already obtained in Subsection 2.10.3:

$$n(\mathbf{x}) = n_0(\mathbf{x}) + q(\mathbf{x}), \tag{4.12}$$

$$\left\{-gn_0(\mathbf{x}) + \left[\sqrt{-\mu + d^2 + 2gn(\mathbf{x}) + V(\mathbf{x})} + d\right]^2 - \frac{\hbar^2}{2M}\mathbf{\Delta}\right\}\sqrt{n_0(\mathbf{x})} = 0, \tag{4.13}$$

$$q(\mathbf{x}) = \frac{dn_0(\mathbf{x})}{\sqrt{-\mu + d^2 + 2gn(\mathbf{x}) + V(\mathbf{x})}}. \tag{4.14}$$

So we have three coupled self-consistency equations for the densities: two algebraic ones (4.12) for the total density $n(\mathbf{x})$ and (4.14) for the Bose-glass order parameter $q(\mathbf{x})$ as well as one nonlinear, partial differential equation (4.13) for the condensate density $n_0(\mathbf{x})$. Furthermore, we have to take into account the normalization condition:

$$\int_{-\infty}^{\infty} n(\mathbf{x})d\mathbf{x} = N. \tag{4.15}$$

Since (4.13) represents a nonlinear, partial differential equation, the exact solution is hard to obtain even in the absence of the disorder. In the following we approximate its solution via the Thomas-Fermi approximation already introduced and explained in Section 3.2. Within the Thomas-Fermi approximation the algebraic equations (4.12) and (4.14) remain the same, but the kinetic energy term in the differential equation (4.13) is neglected and the equation reduces to an algebraic relation in the superfluid region:

$$gn_0(\mathbf{x}) = \left[\sqrt{-\mu + d^2 + 2gn(\mathbf{x}) + V(\mathbf{x})} + d\right]^2. \tag{4.16}$$

Inserting this result into Eqs. (4.12) and (4.14) yields:

$$gq(\mathbf{x}) = \frac{d}{\sqrt{-\mu + d^2 + 2gn(\mathbf{x}) + V(\mathbf{x})}}\left[\sqrt{-\mu + d^2 + 2gn(\mathbf{x}) + V(\mathbf{x})} + d\right]^2, \tag{4.17}$$

$$gn(\mathbf{x}) = \frac{1}{\sqrt{-\mu + d^2 + 2gn(\mathbf{x}) + V(\mathbf{x})}}\left[\sqrt{-\mu + d^2 + 2gn(\mathbf{x}) + V(\mathbf{x})} + d\right]^3. \tag{4.18}$$

Note that (4.18) is a self-consistency equation just for the total density $n(\mathbf{x})$, and inserting its solution into (4.16) and (4.17) gives us directly the condensate density $n_0(\mathbf{x})$ and the Bose-glass order parameter $q(\mathbf{x})$, respectively. The advantage of the Thomas-Fermi approximation is that in the superfluid region we have only three coupled algebraic equations, which can be solved.

Outside the superfluid region, i.e., in the Bose-glass region, equation (4.13) is solved by $n_0(\mathbf{x}) = 0$ and equations (4.12) and (4.14) reduce to $n(\mathbf{x}) = q(\mathbf{x})$ and $q(\mathbf{x}) = \left[\mu - d^2 - V(\mathbf{x})\right]/2g$, respectively. Now, and in order to be able to go further in the calculation, we have to specify the trap potential $V(\mathbf{x})$. We first treat the case of a harmonic isotropic trap potential in Section 4.3, then we study the case of a general anisotropic trap in Section 4.4.

4.3. Isotropic Trap

In this section we consider the bosons to be in an isotropic harmonic trap $V(\mathbf{x}) \equiv V(r) = M\Omega^2 r^2/2$, where Ω denotes the trap frequency and $r = |\mathbf{x}|$ the radial coordinate. In this case the dirty BEC model is spherically symmetric. We specify also the two-particle interaction coupling strength in three dimensions to be $g = 4\pi\hbar^2 a/M$ with the s-wave scattering length a, which has to be positive in order to obtain a stable BEC. Since at zero temperature we have two different regions, we treat them separately. We focus first on the superfluid region, then we deal with the Bose-glass region.

4.3.1. Superfluid Region

For an isotropic harmonic trap, Eqs. (4.16)–(4.18) can be written dimensionless as:

$$\tilde{n}_0\left(\tilde{r}\right) = \left[\sqrt{-\tilde{\mu} + 2\tilde{n}(\tilde{r}) + \tilde{r}^2} + \tilde{d}\right]^2, \tag{4.19}$$

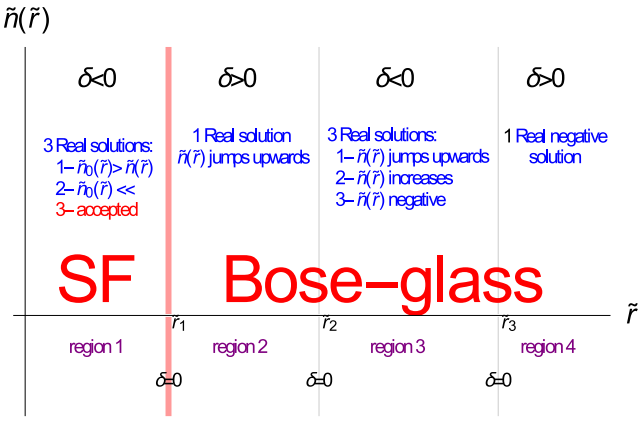

Figure 4.3.: Sign of discriminant δ from Eq. (4.23), where $\tilde{r}_1$, $\tilde{r}_2$, and $\tilde{r}_3$ are respective roots of equation $\delta = 0$.

$$\tilde{q}\left(\tilde{r}\right) = \frac{\tilde{d}}{\sqrt{-\tilde{\mu} + 2\tilde{n}(\tilde{r}) + \tilde{r}^2}} \left[\sqrt{-\tilde{\mu} + 2\tilde{n}(\tilde{r}) + \tilde{r}^2} + \tilde{d}\right]^2, \tag{4.20}$$

$$\tilde{n}\left(\tilde{r}\right) = \frac{1}{\sqrt{-\tilde{\mu} + 2\tilde{n}(\tilde{r}) + \tilde{r}^2}} \left[\sqrt{-\tilde{\mu} + 2\tilde{n}(\tilde{r}) + \tilde{r}^2} + \tilde{d}\right]^3, \tag{4.21}$$

where $\tilde{n}(\tilde{r}) = n(r)/\overline{n}$ denotes the dimensionless total density, $\tilde{n}_0(\tilde{r}) = n_0(r)/\overline{n}$ the dimensionless condensate density, $\tilde{q}(\tilde{r}) = q(r)/\overline{n}$ the dimensionless Bose-glass order parameter, $\tilde{r} = r/R_{\mathrm{TF}}$ the dimensionless radial coordinate, $\tilde{\mu} = (\mu - d^2)/\bar{\mu}$ the dimensionless chemical potential, $\tilde{d} = \frac{\xi}{\mathcal{L}}$ the dimensionless disorder strength, $\xi = \frac{l^2}{R_{\mathrm{TF}}}$ the coherence length in the center of the trap, $l = \sqrt{\frac{\hbar}{M\Omega}}$ the oscillator length, $\overline{n} = \bar{\mu}/g$ the maximal total density in the clean case, and $R_{\mathrm{TF}} = l\sqrt{2\bar{\mu}/\hbar\Omega}$ the clean TF cloud radius. The chemical potential in the absence of the disorder $\bar{\mu} = \frac{15^{2/5}}{2}\left(\frac{aN}{l}\right)^{2/5}\hbar\Omega$, which serves here as the underlying energy scale, is deduced from the normalization condition (4.15) in the clean case, i.e., $d = 0$, by evaluating:

$$\frac{4\pi}{g}\int_0^{R_{\mathrm{TF}}} \left(\bar{\mu} - \frac{1}{2}M\Omega^2 r^2\right) r^2 dr = N. \tag{4.22}$$

Now we have three algebraic self-consistency coupled equations (4.19)–(4.21) for the dimensionless condensate density $\tilde{n}_0\left(\tilde{r}\right)$, the dimensionless Bose-glass order parameter $\tilde{q}\left(\tilde{r}\right)$ and the sum of them, i.e., the dimensionless total density $\tilde{n}(\tilde{r})$. Equation (4.21) is of the third order with respect to the expression $\sqrt{-\tilde{\mu} + 2\tilde{n}(\tilde{r}) + \tilde{r}^2}$, therefore, we use the Cardan method to solve it analytically. The discriminant δ for equation (4.21) has according to Appendix A the following form:

$$\delta = -\frac{4\tilde{\mu}^3}{27} + \frac{4\tilde{\mu}^2\tilde{d}^2}{3} + 8\tilde{\mu}\tilde{d}^4 + 4\tilde{d}^6 + \left(\frac{4\tilde{\mu}^2}{9} - \frac{8\tilde{\mu}\tilde{d}^2}{3} - 8\tilde{d}^4\right)\tilde{r}^2 + \left(-\frac{4\tilde{\mu}}{9} + \frac{4\tilde{d}^2}{3}\right)\tilde{r}^4 + \frac{4}{27}\tilde{r}^6. \tag{4.23}$$

The sign of the discriminant δ determines the number and the kind of the solutions, i.e., whether they are real or complex. Figure 4.3 shows that there are four different spatial regions, where we have to look for the solutions of equation (4.21). Note that this figure is general and independent from the specific parameter values of the BEC system. Those four regions are characterized by the sign of the discriminant δ being positive or negative and are separated with borders, where the discriminant δ vanishes. Regions with $\delta < 0$ have three real solutions, while the regions with $\delta > 0$ have two complex solutions and only one real solution. In the first region only one solution is physically accepted, the two others have to be rejected: one because its corresponding condensate density $\tilde{n}_0(\tilde{r})$ is larger than

the total density $\tilde{n}(\tilde{r})$, which can not be true due to $\tilde{n}(\tilde{r}) = \tilde{n}_0(\tilde{r}) + \tilde{q}(\tilde{r})$, and the other because its corresponding condensate density $\tilde{n}_0(\tilde{r})$ is too small even for an extremely weak disorder strength. In the second region the unique real solution can not be accepted since the total density has an unphysical upward jump after having decreased in the first region. In the third region we have three real solutions for $\tilde{n}(\tilde{r})$ but again none of them is physical: the total density is either jumping upwards, increasing, or negative. The solution of the fourth and last region can also not be retained because it yields a negative density. So, as a conclusion only one solution from the first region can be physically accepted as a solution for equation (4.21). This means that the first region coincides with the superfluid region and outside we have the Bose-glass region. To determine the condensate radius $\tilde{R}_{\mathrm{TF}_1}$, where the solution of (4.21) vanishes, we have to solve the cubic equation $\delta = 0$ with respect to $\tilde{r}^2$ using again the Cardan method and then select the smallest solution, which yields $\tilde{R}_{\mathrm{TF}_1} = \sqrt{\tilde{\mu} - 3\tilde{d}^2 - 6\sqrt{3}\tilde{d}^2 \cos\left(\frac{\pi}{18}\right)}$. Now we have just to insert the obtained particle density $\tilde{n}(\tilde{r})$ into the two other equations (4.19) and (4.20) in order to get both the condensate density $\tilde{n}_0(\tilde{r})$ and the Bose-glass order parameter $\tilde{q}(\tilde{r})$, respectively.

4.3.2. Bose-Glass Region

In the Bose-glass region the condensate vanishes, i.e., $\tilde{n}_0(\tilde{r}) = 0$ and $\tilde{n}(\tilde{r}) = \tilde{q}(\tilde{r})$, and the self-consistency equation (4.14) reduces to:

$$\tilde{q}(\tilde{r}) = \frac{\tilde{\mu} - \tilde{r}^2}{2}. \tag{4.24}$$

This Bose-glass region vanishes at the cloud radius $\tilde{R}_{\mathrm{TF}_2} = \sqrt{\tilde{\mu}}$. We also need to write down the dimensionless equivalent of the normalization condition (4.15), which reads:

$$\int_0^{\tilde{R}_{\mathrm{TF}2}} \tilde{n}(\tilde{r})\tilde{r}^2 d\tilde{r} = \frac{2}{15}, \tag{4.25}$$

where the total density $\tilde{n}(\tilde{r})$ in equation (4.25) is the combination of the total densities from both the superfluid region and the Bose-glass region. The purpose of Eq. (4.25) is to determine the chemical potential from the respective system parameters.

4.3.3. Thomas-Fermi Results

Before choosing any parameters for the BEC system, we have first to justify using the TF approximation and determine the range of validity of this approximation. To this end we rewrite equation (4.13) in the clean case, i.e., $d = 0$ and we divide it by the factor $\bar{\mu}\sqrt{\tilde{n}}$. This yields:

$$\left[-1 + \tilde{n}(\tilde{r}) + \tilde{r}^2 - \left(\frac{\xi}{R_{\mathrm{TF}}}\right)^2 \frac{1}{\tilde{r}^2}\frac{\partial}{\partial\tilde{r}}\left(\tilde{r}^2\frac{\partial}{\partial\tilde{r}}\right)\right] \sqrt{\tilde{n}\,(\tilde{r})} = 0. \tag{4.26}$$

Note that in the clean case, the total density coincides with the condensate one. We read off from Eq. (4.26) that the TF approximation in three dimensions is only justified when $\xi \ll R_{\mathrm{TF}}$.

In this Section we perform our study for ^{87}Rb atoms and for the following experimentally realistic parameters: $N = 10^6$, $\Omega = 2\pi \times 100\,\mathrm{Hz}$, and $a = 5.29\,\mathrm{nm}$. For those parameters the oscillator length reads $l = 1.08\,\mu\mathrm{m}$, the coherence length turns out to be $\xi = 115\,\mathrm{nm}$, and the Thomas-Fermi radius is given by $R_{\mathrm{TF}} = 10.21\,\mu\mathrm{m}$. Thus, the assumption $\xi \ll R_{\mathrm{TF}}$ for the TF approximation is, indeed, fulfilled.

Using those parameter values we solve for the superfluid region equation (4.21) for the total density and insert the result into equations (4.19) and (4.20) to get the condensate density and the Bose-glass order parameter, respectively. This has to be combined with equation (4.24) for the Bose-glass region. After that we fix the chemical potential $\tilde{\mu}$ using the normalization condition (4.25). The resulting densities are combined and plotted in Fig. 4.4, where the densities in the superfluid region are plotted with solid lines, and in the Bose-glass region they are depicted with dotted lines.

In Fig. 4.4 the three densities are maximal in the center of the trap and decrease when we move away from the center until the condensate radius $\tilde{R}_{\mathrm{TF}1}$, where a downward jump of the dimensionless

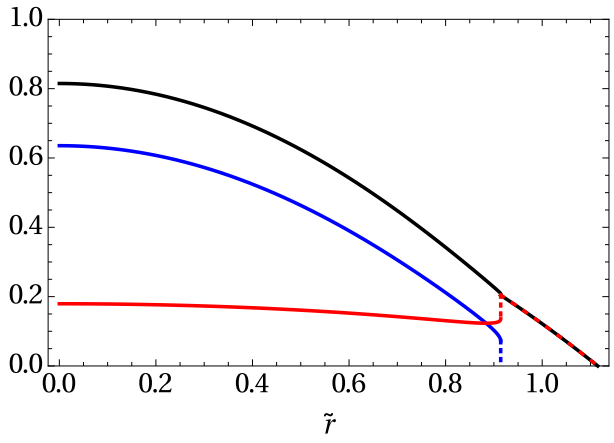

Figure 4.4.: Total density $\tilde{n}(\tilde{r})$ (black), condensate density $\tilde{n}_0(\tilde{r})$ (blue), Bose-glass order parameter $\tilde{q}(\tilde{r})$ (red) as function of radial coordinate $\tilde{r}$ for dimensionless disorder strength $\tilde{d} = 0.175$ both for superfluid region (solid) and Bose-glass region (dashed).

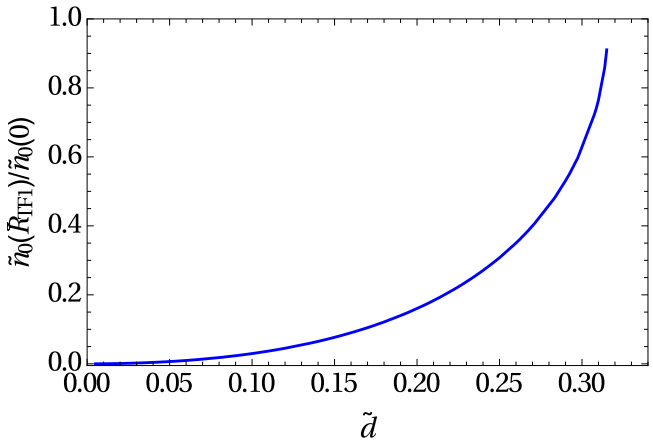

Figure 4.5.: Ratio of $\tilde{n}_0(\tilde{R}_{\mathrm{TF1}})$ and $\tilde{n}_0(0)$ as function of dimensionless disorder strength $\tilde{d}$.

condensate density $\tilde{n}_0(\tilde{r})$, and an upward jump of the Bose-glass order parameter $\tilde{q}(\tilde{r})$ occur in such a way that the total density $\tilde{n}(\tilde{r})$ remains continuous but reveals a discontinuity of the first derivative. In the Bose-glass region both the total density and the Bose-glass parameter coincide and decrease until vanishing at the cloud radius $\tilde{R}_{\mathrm{TF2}}$. The Thomas-Fermi approximation captures the properties of the system in both the superfluid and the Bose-glass region but not in the transition region. This is an artifact of the applied Thomas-Fermi approximation. In order to know for which range of the disorder strength the TF approximation is valid, we plot the ratio of the jump of the condensate density at the condensate radius $\tilde{n}_0(\tilde{R}_{\mathrm{TF1}})$ with respect to the condensate density at the center of the BEC $\tilde{n}_0(0)$ as a function of the dimensionless disorder strength in Fig. 4.5. As only a moderate density jump of about 50% should be reasonable, our approach is restricted to a disorder strength of about $\tilde{d} \simeq 0.3$. For larger disorder strength $\tilde{d}$ one would have to go beyond the Thomas-Fermi approximation and take the influence of the kinetic energy in equation (4.13) into account.

The resulting Thomas-Fermi radii are plotted in Fig. 4.6a. When the disorder strength increases, the condensate radius increases barely, then decreases until being zero, which corresponds to a quantum phase transition occurring at $\tilde{d}_{\mathrm{c}} = \frac{2^{1/5}}{\sqrt{3+6\sqrt{3}\cos\left(\frac{\pi}{18}\right)}} \backsimeq 0.315$. This critical value of the disorder strength is obtained by setting the cloud radius $\tilde{R}_{\mathrm{TF1}}$ to be zero. Thus, superfluidity is destroyed in our model at a critical disorder strength $\tilde{d}_{\mathrm{c}}$, where approximately our Thomas-Fermi approximation breaks down. Let us now compare this critical value of the disorder strength with the one obtained in Refs. [82, 83], where a non-perturbative approach is used, which investigates energetically shape and size of the local minicondensates in the disorder landscape. With this, it is determined for a decreasing disorder

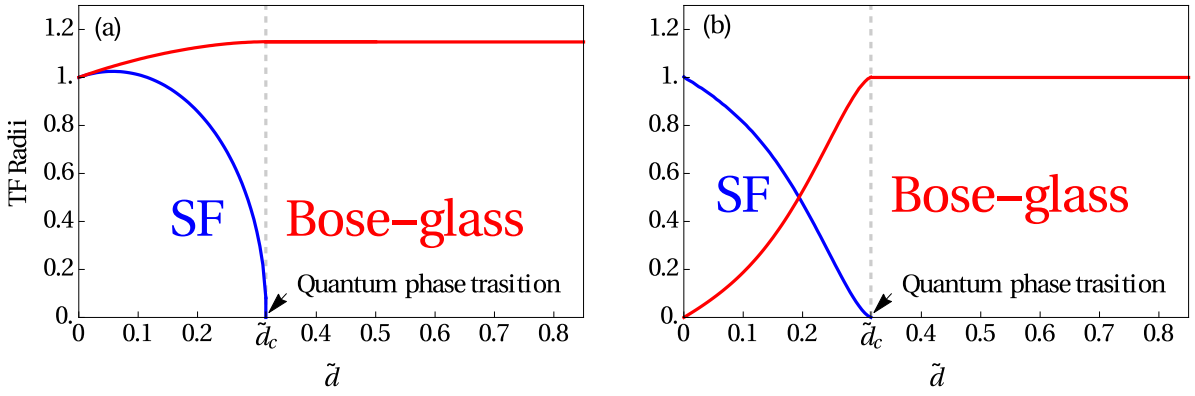

Figure 4.6.: (a) Condensate radius (blue) and cloud radius (red) as well as (b) fractional number of condensed particles N_0/N (blue) and in disconnected local minicondensates Q/N (red), as function of dimensionless disorder strength $\tilde{d}$.

strength, when the Bose-glass phase becomes unstable and goes over into the superfluid phase. In this reference the quantum phase transition is predicted for the dimensionless disorder strength value $\tilde{d} = 0.115$, which is of the same order as our $\tilde{d}_c$.

Contrary to the condensate radius, the cloud radius increases with the disorder strength until it becomes constant, so that in the strong disorder regime the bosonic cloud reaches its maximal radius of $\lim_{\tilde{d}\to\infty} \tilde{R}_{\mathrm{TF2}} = 2^{1/5} \backsimeq 1.148$. This limiting value is obtained by inserting the Bose-glass region density (4.24) into the normalization condition (4.25).

The same physical conclusion can be deduced from Fig. 4.6b, where the fractional number of the condensate is defined via $N_0/N = \frac{15}{2}\int_0^{\tilde{R}_{\mathrm{TF1}}} \tilde{r}^2 \tilde{n}_0(\tilde{r})\, d\tilde{r}$ and plotted as a function of the disorder strength. We remark that N_0/N equals to one in the clean case, i.e., all particles are in the condensate, then it decreases with the disorder strength until it vanishes at $\tilde{d}_c$, marking the end of the superfluid phase and the beginning of the Bose-glass phase. Conversely, the fraction in the disconnected minicondensates $Q/N = \frac{15}{2}\int_0^{\tilde{R}_{\mathrm{TF2}}} \tilde{r}^2 \tilde{q}(\tilde{r})\, d\tilde{r}$, where Q is the number of particles in the disconnected minicondensates, increases with the disorder strength until being maximal at $\tilde{d}_c$. Then it remains constant and equals to one in the Bose-glass phase, since all particles are distributed in the respective minima of the disorder potential.

The influence of the disorder on the chemical potential is shown in Fig. 4.7a. In the superfluid phase the chemical potential can only be obtained numerically, while in the Bose-glass phase it is deduced from inserting equation (4.24) into equation (4.25) yielding $\tilde{\mu}' = \mu/\bar{\mu} = 2^{2/5} + \tilde{d}^2$. The dimensionless chemical potential increases starting from one with increasing the disorder strength and is not differentiable at the quantum phase transition point $\tilde{d}_c$.

Since the trap is quite wide, the Bose-glass order parameter in the center of the BEC $\tilde{q}(0)$ is comparable to the one in the homogeneous case. Therefore, the dimensionless Huang-Meng result of the Bose-glass order parameter obtained in equation (4.10) $\tilde{q}_{\mathrm{HM}} = q_{\mathrm{HM}}/\overline{n} = \frac{\tilde{d}\sqrt{\tilde{n}(0)}}{\sqrt{2}}$, the dimensionless perturbative result of the Bose-glass order parameter in the weak disorder $\tilde{q}_w = \tilde{d}\sqrt{\tilde{n}(0)}$ deduced from (4.20), and the dimensionless exact Bose-glass order parameter in the center of the cloud $\tilde{q}(0) = \frac{\tilde{d}}{\sqrt{-\tilde{\mu}+2\tilde{n}(0)}}\left[\sqrt{-\tilde{\mu}+2\tilde{n}(0)}+\tilde{d}\right]^2$ are all plotted for the weak disorder regime in Fig. 4.7b to illustrate the qualitative convergence of the three results.

From Fig. 4.4 we conclude that the TF approximation is valid only in the center of the trap, where the kinetic energy can be neglected. This is due to the fact that the coherence length ξ is proportional to $1/\sqrt{n(r)}$, thus, it becomes larger at the border of the bosonic cloud and the TF approximation condition is not fulfilled anymore. But still we can conclude that the TF approximation is giving better results in three dimensions in Chapter 4 than in one dimension in Chapter 3 due to the fact that the fluctuations are more virulent in lower dimensions. Furthermore, we conclude from Fig. 4.5 that the TF approximation turns out to be valid only in the weak disorder regime. In order to have a

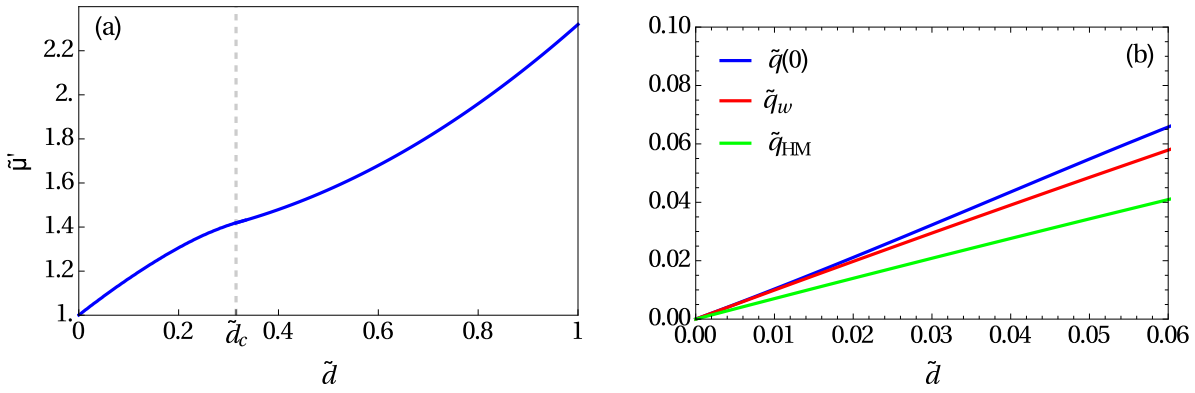

Figure 4.7.: (a) Dimensionless chemical potential $\tilde{\mu}'$ and (b) Thomas-Fermi approximated (blue), perturbative (red), and Huang-Meng (green) Bose-glass order parameter in center of the BEC, as function of dimensionless disorder strength $\tilde{d}$.

global picture of the behavior of the dirty BEC, not only in the presence of weak disorder but also in the presence of intermediate and strong one, we use in the following subsection another approximation method to treat our problem: the variational method.

4.3.4. Variational Method

As already explained in the end of Subsection 2.10.3, we can apply the variational method to our three-dimensional problem. But since the free energy (2.158) involves a root, any variational ansatz yields analytically insolvable integrals. Therefore, we use instead the form (2.126) of the free energy, which is simpler and fits better to the variational treatment at hand. First of all we rewrite the free energy (2.126) for the three-dimensional case at zero temperature and for the isotropic harmonic trap potential:

$$\begin{aligned}\mathcal{F} = 4\pi \int_0^\infty dr r^2 \Bigg\{ & -g\left[q(r)+n_0(r)\right]^2 - \frac{g}{2}n_0^2(r) - \sqrt{n_0(r)}\Bigg\{\mu + \frac{\hbar^2}{2M}\frac{1}{r^2}\frac{\partial}{\partial r}\left(r^2\frac{\partial}{\partial r}\right) - 2g\left[q(r)+n_0(r)\right] \\ & - \frac{1}{2}M\Omega^2 r^2 + \frac{D}{\hbar}Q_0(r)\Bigg\}\sqrt{n_0(r)} + \frac{D}{\hbar}Q_0(r)\left[q(r)+n_0(r)\right] \\ & -2D\sqrt{\pi}\left(\frac{M}{2\pi\hbar^2}\right)^{3/2}\left[q(r)+n_0(r)\right]\sqrt{-\mu+2g\left[q(r)+n_0(r)\right]+\frac{1}{2}M\Omega^2 r^2 - \frac{D}{\hbar}Q_0(r)}\Bigg\}. \end{aligned} \tag{4.27}$$

In order to be able to compare the variational results with the analytical ones obtained in the previous Subsection, we use the same rescaling parameters already introduced above equation (4.22) for all densities, radial coordinate, and disorder strength. To this end, we have to multiply (4.27) with the factor $1/\left(\bar{\mu}\bar{n}R_{\mathrm{TF}}^3\right)$ to obtain:

$$\begin{aligned}\tilde{\mathcal{F}} = 4\pi \int_0^\infty d\tilde{r}\tilde{r}^2 \Bigg\{ & -\left[\tilde{q}\left(\tilde{r}\right)+\tilde{n}_0\left(\tilde{r}\right)\right]^2 - \frac{1}{2}\tilde{n}_0^2\left(\tilde{r}\right) - \sqrt{\tilde{n}_0\left(\tilde{r}\right)}\Bigg\{\tilde{\tilde{\mu}} + \left(\frac{\xi}{R_{\mathrm{TF}}}\right)^2\frac{1}{\tilde{r}^2}\frac{\partial}{\partial\tilde{r}}\left(\tilde{r}^2\frac{\partial}{\partial\tilde{r}}\right) \\ & -2\left[\tilde{q}\left(\tilde{r}\right)+\tilde{n}_0\left(\tilde{r}\right)\right] - \tilde{r}^2 + \tilde{d}\tilde{Q}_0(\tilde{r})\Bigg\}\sqrt{\tilde{n}_0\left(\tilde{r}\right)} + \tilde{d}\tilde{Q}_0(\tilde{r})\left[\tilde{q}\left(\tilde{r}\right)+\tilde{n}_0\left(\tilde{r}\right)\right] \\ & -2\tilde{d}\left[\tilde{q}\left(\tilde{r}\right)+\tilde{n}_0\left(\tilde{r}\right)\right]\sqrt{-\tilde{\mu}'+2\left[\tilde{q}\left(\tilde{r}\right)+\tilde{n}_0\left(\tilde{r}\right)\right]+\tilde{r}^2 - 2\tilde{d}\tilde{Q}_0(\tilde{r})}\Bigg\}, \end{aligned} \tag{4.28}$$

where $\tilde{\mathcal{F}} = \mathcal{F}/\left(\bar{\mu}\bar{n}R_{\mathrm{TF}}^3\right)$ denotes the dimensionless free energy, $\tilde{\mu}' = \mu/\bar{\mu}$ the dimensionless chemical potential, and $\tilde{Q}_0(\tilde{r}) = \frac{1}{\hbar\sqrt{\pi\bar{\mu}}}\left(\frac{2\pi\hbar^2}{M}\right)^{3/2}Q_0(r)$.

Motivated by the analytical results presented in Subsection 4.3.3, we suggest the three following expressions for the condensate density $\tilde{n}_0(\tilde{r})$, the Bose-glass order parameter $\tilde{q}(\tilde{r})$, and the auxiliary function $\tilde{Q}_0(\tilde{r})$:

$$\tilde{n}_0(\tilde{r}) = \alpha e^{-\sigma \tilde{r}^2}, \tag{4.29}$$

$$\tilde{q}(\tilde{r}) + \tilde{n}_0(\tilde{r}) = \gamma e^{-\theta \tilde{r}^2}, \tag{4.30}$$

$$\tilde{Q}_0(\tilde{r}) = 2\frac{\tilde{q}(\tilde{r}) + \tilde{n}_0(\tilde{r})}{\tilde{d}} - \left(\zeta + \eta \tilde{r}^2\right), \tag{4.31}$$

where α, σ, γ, θ, ζ, and η denote the respective variational parameters. The parameters α and γ are proportional to the number of particles in the condensate and the total number of particles, while the parameters σ and θ represent the width of the condensate density and the total density, respectively.

Inserting the ansatz (4.29)–(4.31) into the free energy (4.28) and performing the integral yields:

$$\begin{aligned}\tilde{\mathcal{F}} &= \pi^{3/2}\left\{\frac{\sqrt{2}\gamma^2}{4\theta^{3/2}} + 3\frac{\alpha}{2\sigma^{5/2}} - \frac{\alpha}{8\sigma^{3/2}}\left(8\tilde{\mu}' + \sqrt{2}\alpha\right) + \left(\frac{\xi}{R_{\mathrm{TF}}}\right)^2 \frac{3\alpha}{2\sqrt{\sigma}}\right. \\ &\left. + \tilde{d}\left(\frac{\alpha\zeta}{\sigma^{3/2}} + \frac{3\alpha\eta}{2\sigma^{5/2}} - \frac{\gamma(3\eta + 2\zeta\theta)}{2\theta^{5/2}}\right)\right\} + \frac{2\pi\tilde{d}\gamma\left(\tilde{d}\zeta - \tilde{\mu}'\right)}{\theta\sqrt{1+\tilde{d}\eta}} e^{\frac{\tilde{d}\zeta - \tilde{\mu}'}{2+2\tilde{d}\eta}\theta} K_1\left(\frac{\tilde{d}\zeta - \tilde{\mu}'}{2+2\tilde{d}\eta}\theta\right),\end{aligned} \tag{4.32}$$

where $K_1(s)$ represents the modified Bessel function of second kind. The free energy (4.32) has now to be extremised with respect to the variational parameters α, σ, γ, θ, ζ, and η. This yields the following six algebraic equations:

$$\frac{\pi^{3/2}}{4\sigma^{5/2}}\left[6 - 4\tilde{\mu}'\sigma - \sqrt{2}\alpha\sigma + 6\left(\frac{\xi}{R_{\mathrm{TF}}}\right)^2 \sigma^2 + 4\tilde{d}\sigma\zeta + 6\tilde{d}\eta\right] = 0, \tag{4.33}$$

$$\frac{3\pi^{3/2}\alpha}{16\sigma^{7/2}}\left[-20 + 8\tilde{\mu}'\sigma + \sqrt{2}\alpha\sigma - 4\left(\frac{\xi}{R_{\mathrm{TF}}}\right)^2 \sigma^2 - 8\tilde{d}\sigma\zeta - 20\tilde{d}\eta\right] = 0, \tag{4.34}$$

$$\frac{\pi^{3/2}}{2\theta^{5/2}}\left[\sqrt{2}\gamma\theta - \tilde{d}(3\eta + 2\zeta\theta)\right] + \frac{2\pi\tilde{d}\left(\tilde{d}\zeta - \tilde{\mu}'\right)}{\theta\sqrt{1+\tilde{d}\eta}} e^{\frac{\tilde{d}\zeta - \tilde{\mu}'}{2+2\tilde{d}\eta}\theta} K_1\left(\frac{\tilde{d}\zeta - \tilde{\mu}'}{2+2\tilde{d}\eta}\theta\right) = 0, \tag{4.35}$$

$$\begin{aligned}&\frac{\pi\gamma}{\theta^{7/2}}\left\{\frac{3}{8}\sqrt{\pi}\left(10\tilde{d}\eta - \sqrt{2}\gamma\theta + 4\tilde{d}\zeta\theta\right) - \tilde{d}\theta^{3/2}\frac{\tilde{d}\zeta - \tilde{\mu}'}{\left(1+\tilde{d}\eta\right)^{3/2}} e^{\frac{\tilde{d}\zeta - \tilde{\mu}'}{2+2\tilde{d}\eta}\theta}\right. \\ &\left.\left[\left(-\tilde{d}\zeta + \tilde{\mu}'\right) K_0\left(\frac{\tilde{d}\zeta - \tilde{\mu}'}{2+2\tilde{d}\eta}\theta\right) - \left(4 + 4\tilde{d}\eta + \tilde{\mu}'\theta - \tilde{d}\zeta\theta\right) K_1\left(\frac{\tilde{d}\zeta - \tilde{\mu}'}{2+2\tilde{d}\eta}\theta\right)\right]\right\} = 0,\end{aligned} \tag{4.36}$$

$$\tilde{d}\pi\left\{\sqrt{\pi}\left(\frac{\alpha}{\sigma^{3/2}} - \frac{\gamma}{\theta^{3/2}}\right) - \tilde{d}\frac{\gamma\left(\tilde{d}\zeta - \tilde{\mu}'\right)}{\left(1+\tilde{d}\eta\right)^{3/2}} e^{\frac{\tilde{d}\zeta - \tilde{\mu}'}{2+2\tilde{d}\eta}\theta}\left[K_0\left(\frac{\tilde{d}\zeta - \tilde{\mu}'}{2+2\tilde{d}\eta}\theta\right) - K_1\left(\frac{\tilde{d}\zeta - \tilde{\mu}'}{2+2\tilde{d}\eta}\theta\right)\right]\right\} = 0, \tag{4.37}$$

$$\begin{aligned}&\tilde{d}\frac{\pi}{2}\left\{3\sqrt{\pi}\left(\frac{\alpha}{\sigma^{5/2}} - \frac{\gamma}{\theta^{5/2}}\right) - 2\tilde{d}\gamma\frac{\tilde{d}\zeta - \tilde{\mu}'}{\left(1+\tilde{d}\eta\right)^{5/2}} e^{\frac{\tilde{d}\zeta - \tilde{\mu}'}{2+2\tilde{d}\eta}\theta}\right. \\ &\left.\left[\left(-\tilde{d}\zeta + \tilde{\mu}'\right) K_0\left(\frac{\tilde{d}\zeta - \tilde{\mu}'}{2+2\tilde{d}\eta}\theta\right) - \frac{1}{\theta}\left(1 + \tilde{\mu}'\theta + \tilde{d}(\eta - \zeta\theta)\right) K_1\left(\frac{\tilde{d}\zeta - \tilde{\mu}'}{2+2\tilde{d}\eta}\theta\right)\right]\right\} = 0.\end{aligned} \tag{4.38}$$

Note that the additional dimensionless particle number equation, which follows from the thermodynamic condition $-\frac{\partial \tilde{\mathcal{F}}}{\partial \tilde{\mu}'} = \frac{4}{3}$, yields a seventh equation:

$$\pi^{3/2}\frac{\alpha}{\sigma^{3/2}} - \tilde{d}\frac{\pi\gamma\left(-\tilde{d}\zeta+\tilde{\mu}'\right)}{\left(1+\tilde{d}\eta\right)^{3/2}} e^{\frac{\tilde{d}\zeta-\tilde{\mu}'}{2+2\tilde{d}\eta}\theta}\left[K_0\left(\frac{\tilde{d}\zeta-\tilde{\mu}'}{2+2\tilde{d}\eta}\theta\right) - K_1\left(\frac{\tilde{d}\zeta-\tilde{\mu}'}{2+2\tilde{d}\eta}\theta\right)\right] = \frac{2}{15}. \tag{4.39}$$

Thus, we have now seven coupled equations (4.33)–(4.39) for seven variables α, σ, γ, θ, ζ, η, and $\tilde{\mu}'$. Those equations can not be solved analytically, so we solve them numerically for different values of the dimensionless disorder strength $\tilde{d}$. Furthermore, they turn out to have more than one solution, which necessitates to select only the physical one. For each value of the dimensionless disorder strength $\tilde{d}$, we solve the coupled Eqs. (4.33)–(4.39) numerically, then we insert the resulting variational parameters α, σ, γ, and θ into the variational ansatz (4.29)–(4.31) in order to get the variational total density $\tilde{n}(\tilde{r})$, the variational condensate density $\tilde{n}_0(\tilde{r})$, and the variational Bose-glass order parameter $\tilde{q}(\tilde{r})$, respectively.

In Fig. 4.8 the total density $\tilde{n}(\tilde{r})$ is plotted for different disorder strengths, where we see that the density of bosons is always maximal in the center of the cloud, then it decreases when we move away from the center until it vanishes at the cloud radius $\tilde{R}_{\mathrm{TF2}}$. The maximal value of the total density decreases with the disorder strength. The condensate density $\tilde{n}_0(\tilde{r})$ in Fig. 4.9a has a similar qualitative behavior as the total density, i.e., it is also maximal in the center of the trap and decreases when we move away from the center until it vanishes at the condensate radius $\tilde{R}_{\mathrm{TF1}}$. The maximal value of the condensate density decreases also with the disorder strength. The response of the condensate to disorder can be clearly seen in Fig. 4.9b, where the fractional number of condensed particles N_0/N is plotted as a function of the dimensionless disorder strength $\tilde{d}$. In the clean case all particles are in the condensate, but, when we increase the disorder strength, more and more particles leave the condensate until the condensate vanishes at the critical dimensionless disorder strength $\tilde{d}_{\mathrm{c}} = 0.5183$. The Bose-glass order parameter $\tilde{q}(\tilde{r})$ in Fig. 4.10a has a similar shape as the two previous densities $\tilde{n}(\tilde{r})$ and $\tilde{n}_0(\tilde{r})$, it is maximal in the center of the BEC and decreases when we move away from the center. When we increase the disorder strength, the maximal value of the Bose-glass order parameter also increases. Better understanding of the influence of the disorder on the local minicondensates can be deduced from Fig. 4.10b, where the fractional number of particles Q/N in the disconnected local minicondensates is zero in the clean case then increases with the disorder strength until being one. This means that more and more bosons go into the local minima of the disorder potential when we increase the disorder strength. At the critical disorder strength value $\tilde{d}_{\mathrm{c}} = 0.5183$ all particles are in the minicondensates. In order to know whether the bosonic cloud contains besides the superfluid region also a Bose-glass region, we plot the total density $\tilde{n}(\tilde{r})$, the condensate density $\tilde{n}_0(\tilde{r})$, and the Bose-glass order parameter $\tilde{q}(\tilde{r})$ in the same Fig. 4.11a for the disorder strength value $\tilde{d} = 0.35$. The blow-up of the border region in Fig. 4.11b shows clearly that the condensate density vanishes, while the Bose-glass order parameter still persists, which is the definition of the Bose-glass region. The cloud radius $\tilde{R}_{\mathrm{TF2}}$ and the condensate radius $\tilde{R}_{\mathrm{TF1}}$ are defined by the length, where the total density and the condensate density are equal to 10^{-4}, respectively. Both radii are increasing with the disorder strength in the weak disorder regime in Fig. 4.12. In the intermediate disorder regime, the cloud radius keeps increasing with the disorder strength, while the condensate radius vanishes at the critical disorder value $\tilde{d}_{\mathrm{c}} = 0.5183$, which marks the location of a quantum phase transition. For larger disorder strengths $\tilde{d} > \tilde{d}_{\mathrm{c}}$ Eqs. (4.33)–(4.39) turn out to have negative solutions for the condensate density. So we do not know if for stronger disorder the cloud radius keeps increasing or remains constant, i.e., whether the bosonic cloud continues to extend or whether it has a maximal size. Note that the chemical potential $\tilde{\mu}'$ increases with the disorder strength in Fig. 4.13a. In the end we plot the Bose-glass order parameter in the center of the BEC $\tilde{q}\,(0) = \gamma - \alpha$ together with the dimensionless Huang-Meng result obtained in (4.10) $\tilde{q}_{\mathrm{HM}} = \frac{\tilde{d}\sqrt{\tilde{n}(0)}}{\sqrt{2}}$ in Fig. 4.13b in order to know if the variational results are compatible with the Huang-Meng theory for weak disorder. In the weak disorder regime, $\tilde{q}\,(0)$ is linearly proportional to the disorder strength, which agrees qualitatively with the Huang-Meng theory but not quantitatively, since there is a significant discrepancy of $\sqrt{2}$ of the respective slopes.

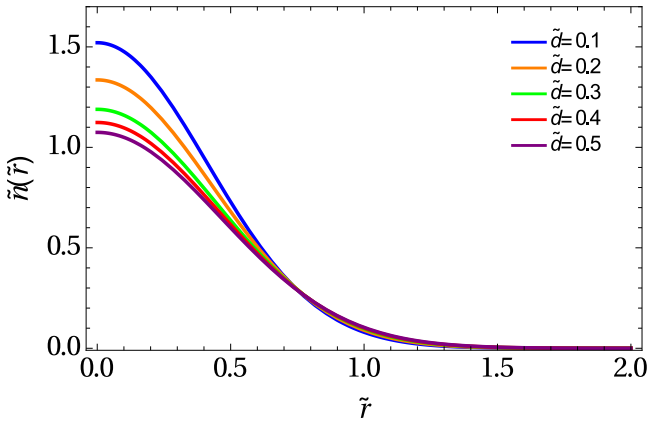

Figure 4.8.: Particle density $\tilde{n}(\tilde{r})$ for increasing dimensionless disorder strengths $\tilde{d}$ from top to bottom.

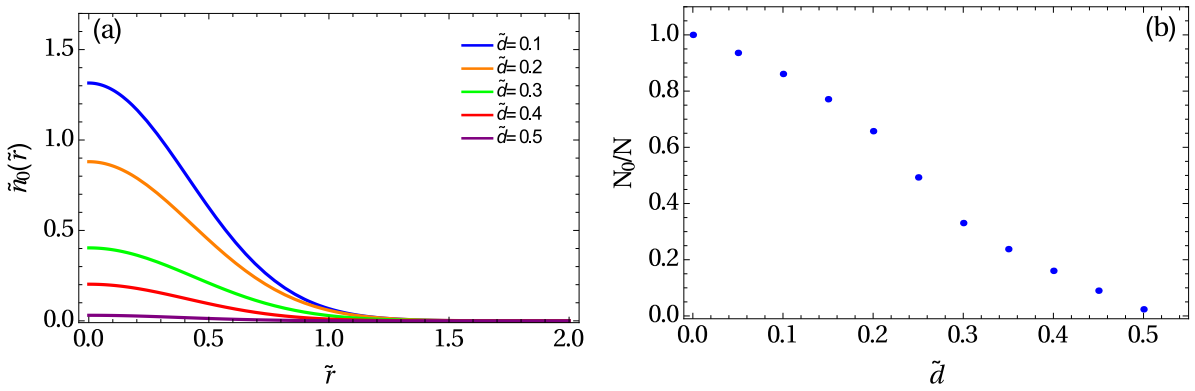

Figure 4.9.: (a) Condensate density $\tilde{n}_0(\tilde{r})$ and (b) fractional number of condensed particles N_0/N for increasing dimensionless disorder strengths $\tilde{d}$ from top to bottom.

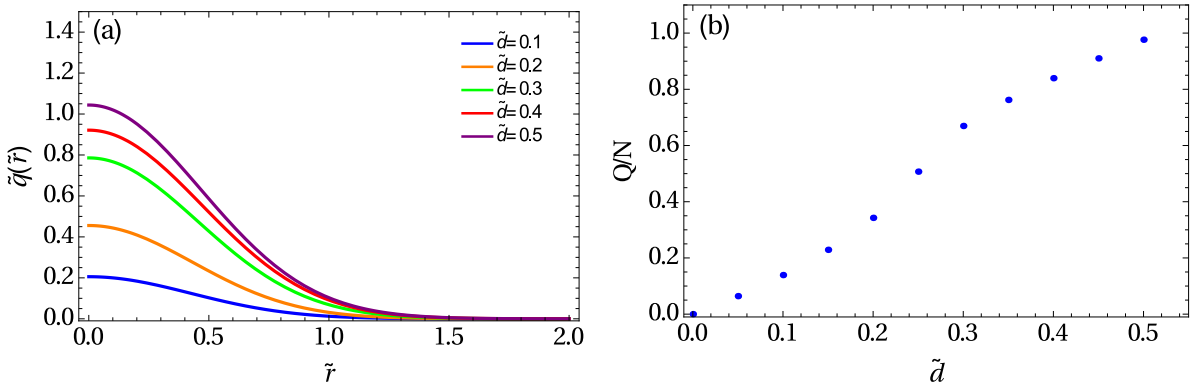

Figure 4.10.: (a) Bose-glass order parameter $\tilde{q}(\tilde{r})$ and (b) fractional number of particles Q/N in disconnected local minicondensates for increasing dimensionless disorder strengths $\tilde{d}$ from bottom to top.

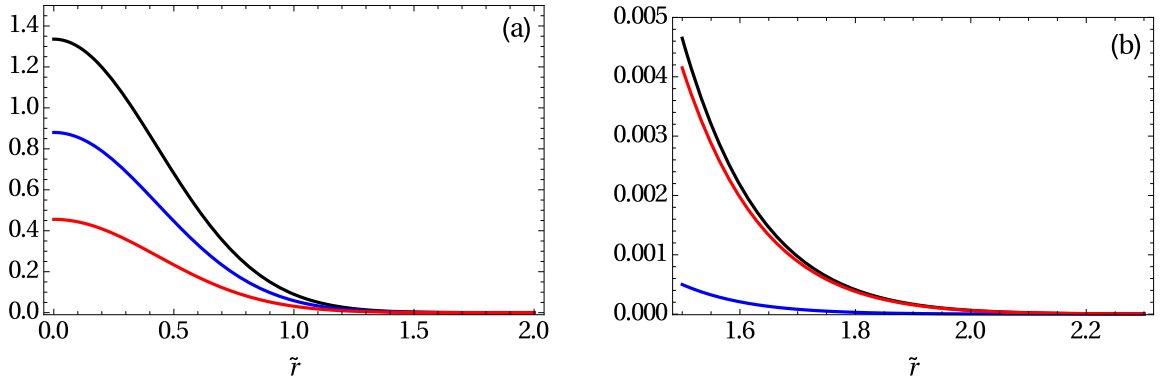

Figure 4.11.: (a) Particle density $\tilde{n}(\tilde{r})$ (black), condensate density $\tilde{n}_0(\tilde{r})$ (blue), Bose-glass order parameter $\tilde{q}(\tilde{r})$ (red) and (b) blow-up of border region for $\tilde{d} = 0.35$.

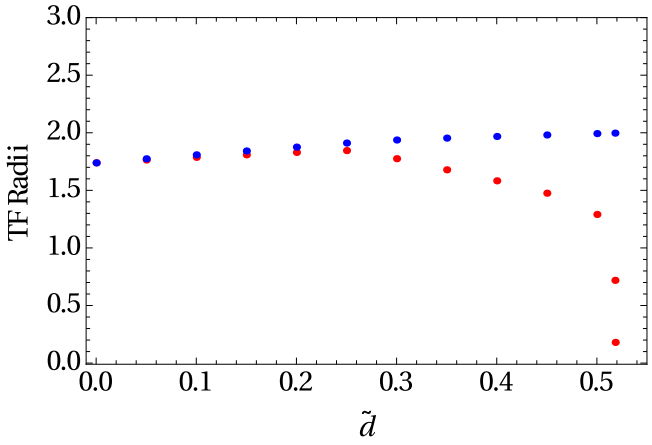

Figure 4.12.: Cloud radius $\tilde{R}_{\mathrm{TF2}}$ (blue) and condensate radius $\tilde{R}_{\mathrm{TF1}}$ (red) as functions of dimensionless disorder strength $\tilde{d}$.

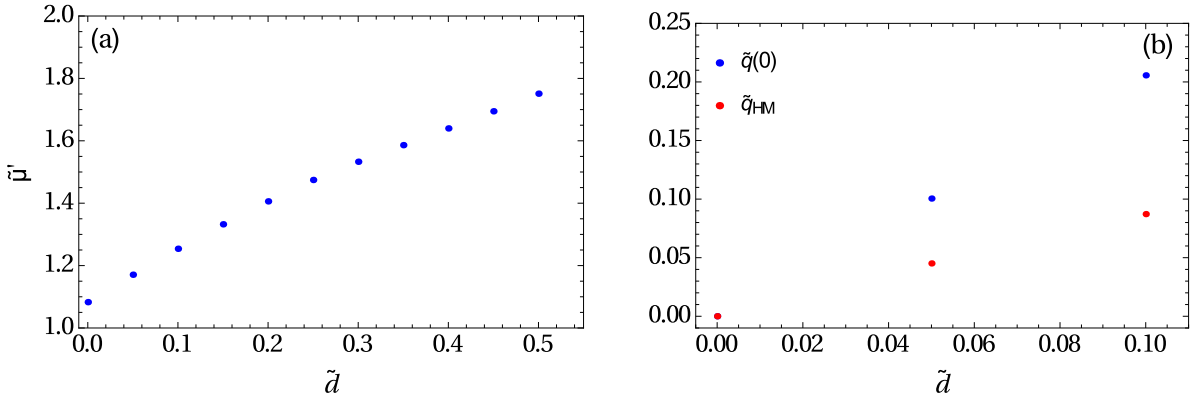

Figure 4.13.: (a) Chemical potential $\tilde{\mu}'$ and (b) variational (blue) and Huang-Meng (red) Bose-glass order parameter in the center of the BEC, as function of dimensionless disorder strength $\tilde{d}$.

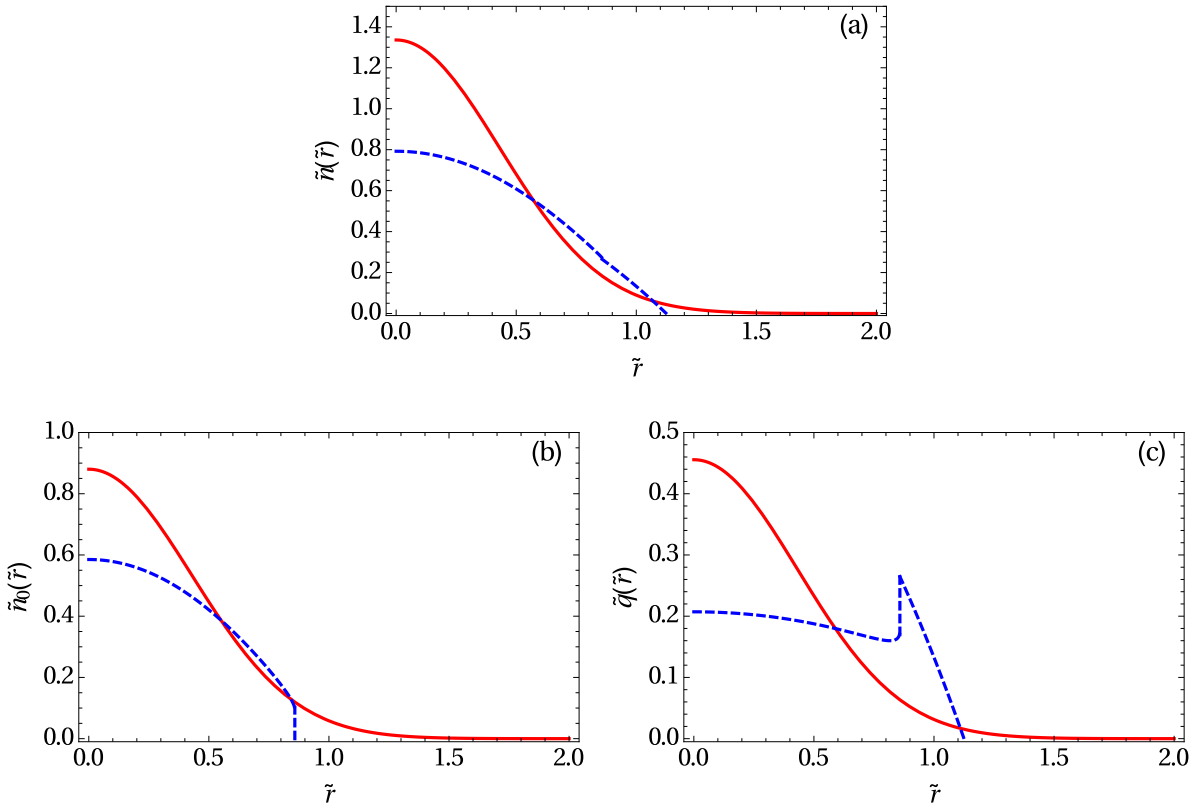

Figure 4.14.: (a) Total density $\tilde{n}(\tilde{r})$, (b) condensate density $\tilde{n}_0(\tilde{r})$, (c) Bose-glass order parameter $\tilde{q}(\tilde{r})$: variational (solid, red), analytical (dashed, blue) for $\tilde{d} = 0.2$.

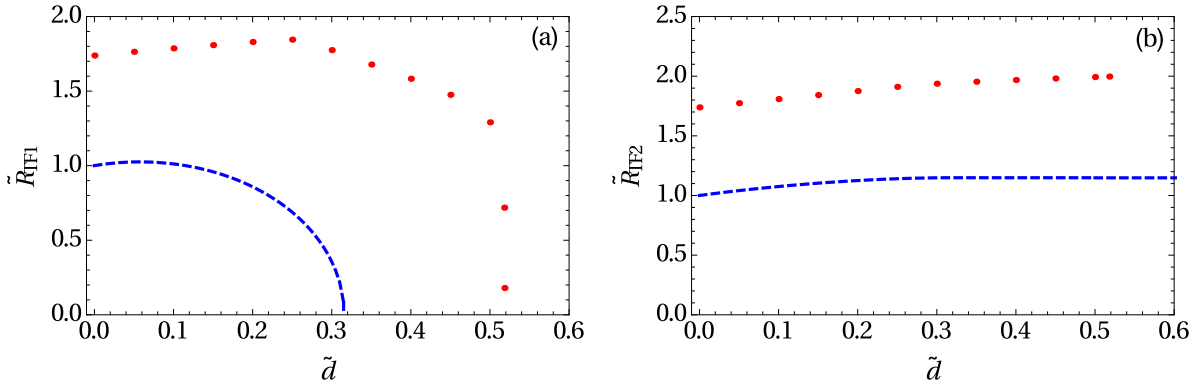

Figure 4.15.: (a) Condensate radius $\tilde{R}_{\mathrm{TF1}}$ and (b) cloud radius $\tilde{R}_{\mathrm{TF2}}$: analytical (dashed, blue) and variational (dotted, red), as functions of the dimensionless disorder strength $\tilde{d}$.

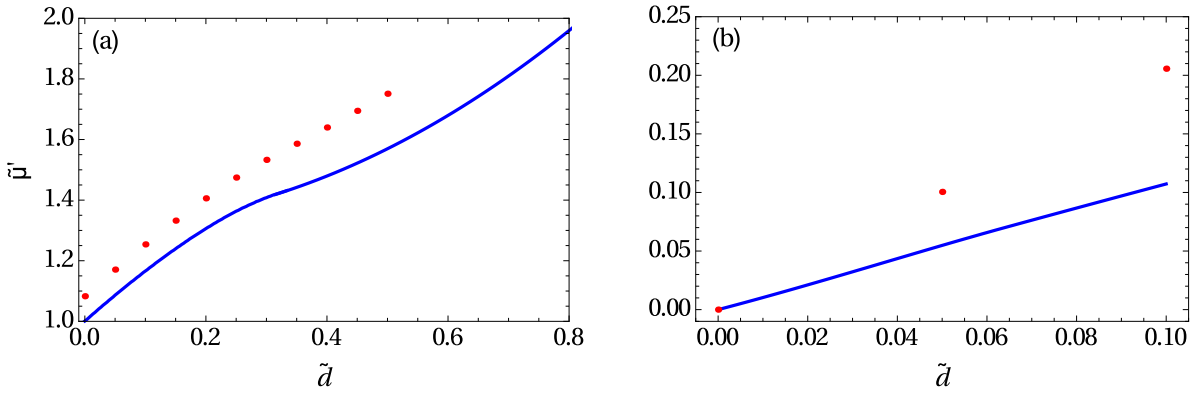

Figure 4.16.: Analytical (solid, blue) and variational (dotted, red) (a) chemical potential $\tilde{\mu}'$ as well as (b) Bose-glass order parameter in center of the BEC $\tilde{q}(0)$ as functions of dimensionless disorder strength $\tilde{d}$.

4.3.5. Comparison Between TF Approximation and Variational results

Now we compare the physical quantities obtained via the two different methods, i.e., the TF approximation and the variational method. We start first of all with the densities: the total density $\tilde{n}(\tilde{r})$, the condensate density $\tilde{n}_0(\tilde{r})$, and the Bose-glass order parameter $\tilde{q}(\tilde{r})$ are plotted for the disorder strength value $\tilde{d} = 0.2$ in Fig. 4.14. We know already from the conclusion at the end of Chapter 3 that the TF approximation describes well the weak disorder regime, while the variational method is suitable to describe the intermediate disorder regime. Based on this conclusion our comparison is more a qualitative than a quantitative one. The total densities $\tilde{n}(\tilde{r})$ in Fig. 4.14a agree qualitatively well, they are both maximal in the center of the bosonic cloud and decrease when we move away from the center. The same can be remarked for the condensate density $\tilde{n}_0(\tilde{r})$ in Fig. 4.14b, except from the jump in the TF approximated condensate density. For the Bose-glass order parameter $\tilde{q}(\tilde{r})$ in Fig. 4.14c we observe that, according to the TF approximation, the density of the bosons in the local minima of the disorder potential is maximal at the border of the trap, but according to the variational result this density is maximal in the center of the trap. The TF approximated and the variational Thomas-Fermi radii are compared with each other in Fig. 4.15. In Fig. 4.15a the variational and the TF approximated condensate radius $\tilde{R}_{\mathrm{TF1}}$ have the same behavior, both increase first barely with the disorder strength $\tilde{d}$ in the weak disorder regime, then decrease with it in the intermediate disorder regime until they vanish at the quantum phase transition. Thus, both analytical and variational condensate radii $\tilde{R}_{\mathrm{TF1}}$ indicate the existence of a quantum phase transition, but at two different values of the disorder strength, namely $\tilde{d}_{\mathrm{c}} = 0.315$ and $\tilde{d}_{\mathrm{c}} = 0.5183$, respectively. Thus, the variational quantum phase transition happens at a larger disorder strength than the TF approximated one. Figure 4.15b shows that, in the weak disorder regime, the variational and the analytical cloud radii $\tilde{R}_{\mathrm{TF2}}$ increase with the disorder strength. In the intermediate disorder regime the analytical cloud radius remains constant, while the variational one keeps increasing with the disorder strength, and due to the lack of information for higher disorder strengths $\tilde{d}$, we do not know if the variational cloud radius keeps increasing or remains constant.

Concerning the chemical potential, the variational and the analytical chemical potentials agree qualitatively well in Fig. 4.16a. Both of them increase with the dimensionless disorder strength $\tilde{d}$. Finally, we compare the variational and analytical Bose-glass order parameter in the center of the trap as functions of the dimensionless disorder strength $\tilde{d}$ in Fig. 4.16b. Both of them are linearly proportional to the disorder strength and agree qualitatively with the Huang-Meng theory for weak disorder, but the variational one has a larger slope, which causes a discrepancy with the analytical Bose-glass order parameter.

From the discussion above, we conclude that the TF approximation and the variational method are producing similar qualitative results in contrast to the one-dimensional case of Chapter 3, where the TF approximated results and the variational ones disagree totally. In particular, a first-order quantum phase transition from the superfluid phase to the Bose-glass phase is detected at a critical disorder strength, whose value is of the same order as the one determined in Refs. [82, 83]. Quantitatively, and

motivated by the conclusion in the end of Chapter 3 for the one-dimensional case, we can say that the TF approximation produces satisfying results in the weak disorder regime, while the variational method is a good approximation to describe the BEC system in the intermediate disorder regime. Furthermore, it has the advantage to be able to describe the border of the cloud where the Bose-glass region is situated, and where the TF approximation fails. Although the variational method does not provide us physical results for higher disorder strengths, its combination together with the TF approximation for the weak disorder regime covers a significant range of the disorder strength.

4.3.6. Qualitative Comparison Between 1D and 3D Results

In this subsection we compare the one-dimensional results obtained in Chapter 3 with the three-dimensional ones obtained in this chapter and discuss the points, where they qualitatively agree or disagree.

We start first with the homogeneous case where, according to Figs. 3.1 and 4.1, a quantum phase transition from the superfluid to the Bose-glass phase exists in one dimension as well as in three dimensions, respectively. Perturbative Bose-glass order parameters in both one and three dimensions given by equations (3.15) and (4.11) agree qualitatively with the Huang-Meng theory. But quantitatively there is a discrepancy of $2\sqrt{2}$ in one dimension and only $\sqrt{2}$ in three dimensions, which indicates that the mean-field theory works better in higher dimensions. The chemical potential decreases with the disorder strength in one dimension in Fig. 3.2 but increases with the disorder strength in three dimensions in Fig. 4.2. This can probably be traced back to the third line of the free energy expression (2.126), which changes its sign.

In the presence of the trap we applied first the TF approximation to the corresponding self-consistency equations. It turned out that the TF approximation breaks down at the critical disorder strength $\tilde{D}_{\mathrm{c}} = 0.143$ in one dimension and $\tilde{d}_{\mathrm{c}} = 0.315$ in three dimensions. We conclude that the disorder validity range is larger in three dimensions than in one dimension. In addition to the TF approximation we also applied a variational ansatz to the free energy. However the TF-approximated and the variational results disagreed totally in one dimension, as shown in Section 3.6, while they agreed qualitatively well in three dimensions according to Subsection 4.3.5. Furthermore, we showed the existence of the Bose-glass region in both dimensions, but in three dimensions it is always localized in the center of the trap, while in one dimension it moves from the border to the center of the trap with increasing the disorder strength. Finally the existence of a quantum phase transition from the superfluid to the Bose-glass phase was confirmed in three dimensions in the intermediate disorder regime in Fig. 4.15a, but could not be detected in one dimension in Fig. 3.28a neither in the weak nor in the intermediate disorder regime. In order to be able to find this quantum phase transition in one dimension, we would have to investigate the strong disorder regime, which is beyond the scope of the present thesis.

4.4. Anisotropic Trap

In this section we consider the general case, where the harmonic trap is a general anisotropic one:

$$V(\mathbf{r}) \equiv V(x,y,z) = M\left(\omega_x^2 x^2 + \omega_y^2 y^2 + \omega_z^2 z^2\right)/2, \tag{4.40}$$

with the trap frequency ω_i along the $i = x, y, z$ axis. In this case Eqs (4.16)–(4.18) of the superfluid region are written as follows:

$$gn_0(x,y,z) = \left[\sqrt{-\mu + d^2 + 2gn(x,y,z) + \frac{M}{2}\left(\omega_x^2 x^2 + \omega_y^2 y^2 + \omega_z^2 z^2\right)} + d\right]^2, \tag{4.41}$$

$$gq(x,y,z) = \frac{d\left[\sqrt{-\mu + d^2 + 2gn(x,y,z) + \frac{M}{2}\left(\omega_x^2 x^2 + \omega_y^2 y^2 + \omega_z^2 z^2\right)} + d\right]^2}{\sqrt{-\mu + d^2 + 2gn(x,y,z) + \frac{M}{2}\left(\omega_x^2 x^2 + \omega_y^2 y^2 + \omega_z^2 z^2\right)}}, \tag{4.42}$$

$$gn(x,y,z) = \frac{\left[\sqrt{-\mu + d^2 + 2gn(x,y,z) + \frac{M}{2}\left(\omega_x^2 x^2 + \omega_y^2 y^2 + \omega_z^2 z^2\right)} + d\right]^3}{\sqrt{-\mu + d^2 + 2gn(x,y,z) + \frac{M}{2}\left(\omega_x^2 x^2 + \omega_y^2 y^2 + \omega_z^2 z^2\right)}}. \tag{4.43}$$

Thus, Eq. (4.43) serves for determining the total density $n(x,y,z)$. Inserting the solution of this equation into (4.41) and (4.42) gives us directly the condensate density $n_0(x,y,z)$ and the Bose-glass order parameter $q(x,y,z)$, respectively. In the Bose-glass region we have instead $n_0(x,y,z) = 0$. In the following we distinguish again between two different regions: the superfluid and the Bose-glass region.

4.4.1. Superfluid region

We transform first our equations into dimensionless ones. To this end we divide equations (4.41)–(4.43) by the value of the chemical potential in the absence of the disorder, which is given by $\bar{\mu} = \frac{15^{2/5}}{2}\left(\frac{aN}{(l_x l_y l_z)^{1/3}}\right)^{2/5}\hbar\left(\omega_x\omega_y\omega_z\right)^{1/3}$. This value is straightforwardly deduced from the normalization condition (4.15) in the clean case, i.e., $d = 0$, by evaluating:

$$\frac{1}{g}\int_{-x_{\mathrm{TF}}}^{x_{\mathrm{TF}}}\int_{-y_{\mathrm{TF}}}^{y_{\mathrm{TF}}}\int_{-z_{\mathrm{TF}}}^{z_{\mathrm{TF}}}\left[\bar{\mu} - \frac{1}{2}M\Omega^2\left(\omega_x^2 x^2 + \omega_y^2 y^2 + \omega_z^2 z^2\right)\right]dxdydz = N, \tag{4.44}$$

where $l_i = \sqrt{\hbar/M\omega_i}$ represents the oscillator length and $i_{\mathrm{TF}} = \sqrt{\frac{2\bar{\mu}}{M\omega_i^2}}$ the TF cloud radius, along the $i = x, y, z$ axis, respectively.

With this Eqs. (4.41)–(4.43) lead the following dimensionless self-consistency equations:

$$\tilde{n}_0(\tilde{x},\tilde{y},\tilde{z}) = \left[\sqrt{-\tilde{\mu} + 2\tilde{n}(\tilde{x},\tilde{y},\tilde{z}) + \tilde{x}^2 + k^2\tilde{y}^2 + \lambda^2\tilde{z}^2} + \tilde{d}\right]^2, \tag{4.45}$$

$$\tilde{q}(\tilde{x},\tilde{y},\tilde{z}) = \frac{\tilde{d}\left[\sqrt{-\tilde{\mu} + 2\tilde{n}(\tilde{x},\tilde{y},\tilde{z}) + \tilde{x}^2 + k^2\tilde{y}^2 + \lambda^2\tilde{z}^2} + \tilde{d}\right]^2}{\sqrt{-\tilde{\mu} + 2\tilde{n}(\tilde{x},\tilde{y},\tilde{z}) + \tilde{x}^2 + k^2\tilde{y}^2 + \lambda^2\tilde{z}^2}}, \tag{4.46}$$

$$\tilde{n}(\tilde{x},\tilde{y},\tilde{z}) = \frac{\left[\sqrt{-\tilde{\mu} + 2\tilde{n}(\tilde{x},\tilde{y},\tilde{z}) + \tilde{x}^2 + k^2\tilde{y}^2 + \lambda^2\tilde{z}^2} + \tilde{d}\right]^3}{\sqrt{-\tilde{\mu} + 2\tilde{n}(\tilde{x},\tilde{y},\tilde{z}) + \tilde{x}^2 + k^2\tilde{y}^2 + \lambda^2\tilde{z}^2}}, \tag{4.47}$$

where $\tilde{n}(\tilde{x},\tilde{y},\tilde{z}) = n(x,y,z)/\bar{n}$ denotes the dimensionless total density, $\tilde{n}_0(\tilde{x},\tilde{y},\tilde{z}) = n_0(x,y,z)/\bar{n}$ the dimensionless condensate density, $\tilde{q}(\tilde{x},\tilde{y},\tilde{z}) = q(x,y,z)/\bar{n}$ the dimensionless Bose-glass order parameter, $\bar{n} = \frac{\bar{\mu}}{g}$ the density in the homogeneous clean case, $k = \omega_y/\omega_x$ and $\lambda = \omega_z/\omega_x$ the trap aspect ratios, $\tilde{\mu} = (\mu - d^2)/\bar{\mu}$ the dimensionless chemical potential, and $\tilde{d} = d/\sqrt{\bar{\mu}}$ the dimensionless disorder strength. Furthermore, $\tilde{x} = \sqrt{M\omega_x^2/2\bar{\mu}}\,x$, $\tilde{y} = \sqrt{M\omega_x^2/2\bar{\mu}}\,y$, and $\tilde{z} = \sqrt{M\omega_x^2/2\bar{\mu}}\,z$ denote the dimensionless coordinates along the x, y, and z axis, respectively.

In order to solve the coupled self-consistency equations (4.45)–(4.47) one should first solve the cubic equation (4.47) with respect to the expression $\sqrt{-\tilde{\mu} + 2\tilde{n}(\tilde{x},\tilde{y},\tilde{z}) + \tilde{x}^2 + k^2\tilde{y}^2 + \lambda^2\tilde{z}^2}$ using the Cardan method of Appendix A and substitute the result into equations (4.45) and (4.46). To this end we calculate the discriminant δ of the cubic equation (4.47), which has the following form:

$$\begin{aligned}\delta = &-\frac{4\tilde{\mu}^3}{27} + \frac{4\tilde{\mu}^2\tilde{d}^2}{3} + 8\tilde{\mu}\tilde{d}^4 + 4\tilde{d}^6 + \left(\frac{4\tilde{\mu}^2}{9} - \frac{8\tilde{\mu}\tilde{d}^2}{3} - 8\tilde{d}^4\right)\left(\tilde{x}^2 + k^2\tilde{y}^2 + \lambda^2\tilde{z}^2\right)\\ &+ \left(-\frac{4\tilde{\mu}}{9} + \frac{4\tilde{d}^2}{3}\right)\left(\tilde{x}^2 + k^2\tilde{y}^2 + \lambda^2\tilde{z}^2\right)^2 + \frac{4}{27}\left(\tilde{x}^2 + k^2\tilde{y}^2 + \lambda^2\tilde{z}^2\right)^3.\end{aligned} \tag{4.48}$$

Figure 4.17 shows that there are four different spatial regions where we have to look for the solutions of equation (4.47). Those regions are characterized by the sign of the discriminant δ in (4.48)

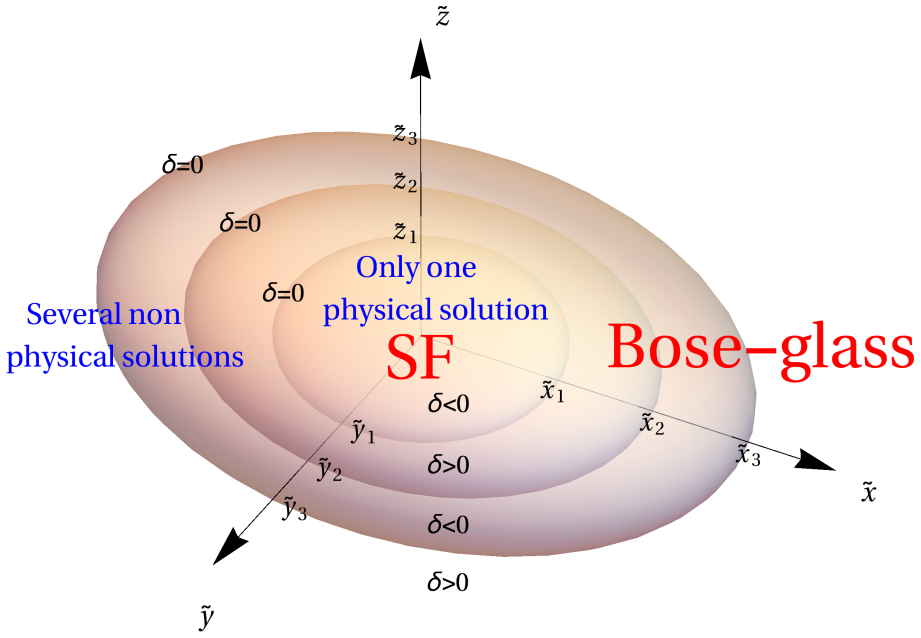

Figure 4.17.: Sign of the discriminant δ from equation (4.48), where $\tilde{x}_1, \tilde{y}_1, \tilde{z}_1$, $\tilde{x}_2, \tilde{y}_2, \tilde{z}_2$ and $\tilde{x}_3, \tilde{y}_3, \tilde{z}_3$ are the respective semiaxes of the ellipsoid solving the equation $\delta = 0$.

being positive or negative and are separated by the border, where the discriminant δ vanishes. After performing an analysis similar to the one in Fig. 4.3, we conclude that equation (4.47) has only one physical solution in the first region, where the discriminant δ is negative. This means that the first region coincides with the superfluid region and coincides outside with the Bose-glass region.

Now we have just to insert the resulting particle density $\tilde{n}(\tilde{x}, \tilde{y}, \tilde{z})$ into the two other equations (4.45) and (4.46) in order to get both the condensate density $\tilde{n}_0(\tilde{x}, \tilde{y}, \tilde{z})$ and the Bose-glass order parameter $\tilde{q}(\tilde{x}, \tilde{y}, \tilde{z})$, respectively.

To determine the border of the superfluid region, i.e., the condensate radii $\tilde{x}_{\mathrm{TF1}}$, $\tilde{y}_{\mathrm{TF1}}$, and $\tilde{z}_{\mathrm{TF1}}$, where the solution of equation (4.47) vanishes, we have to solve the cubic equation $\delta = 0$ with respect to $\tilde{x}^2 + k^2\tilde{y}^2 + \lambda^2\tilde{z}^2$ using again the Cardan method, then select the smallest solution, which corresponds to $\tilde{x}^2 + k^2\tilde{y}^2 + \lambda^2\tilde{z}^2 = \tilde{\mu} - 3\tilde{d}^2 - 6\sqrt{3}\tilde{d}^2 \cos\left(\frac{\pi}{18}\right)$. This solution has a form of an ellipsoid, whose semiaxes are the condensate radii $\tilde{x}_{\mathrm{TF1}} = \sqrt{\tilde{\mu} - 3\tilde{d}^2 - 6\sqrt{3}\tilde{d}^2 \cos\left(\frac{\pi}{18}\right)}$, $\tilde{y}_{\mathrm{TF1}} = \tilde{x}_{\mathrm{TF1}}/k$, and $\tilde{z}_{\mathrm{TF1}} = \tilde{x}_{\mathrm{TF1}}/\lambda$ along the $\tilde{x}$-, $\tilde{y}$-, and $\tilde{z}$-axis, respectively.

4.4.2. Bose-glass region

In this region the condensate vanishes, i.e., $\tilde{n}_0(\tilde{x}, \tilde{y}, \tilde{z}) = 0$, and we have $\tilde{q}(\tilde{x}, \tilde{y}, \tilde{z}) = \tilde{n}(\tilde{x}, \tilde{y}, \tilde{z})$. The self-consistency equation (4.46) is then substituted by

$$-\tilde{\mu} + 2\tilde{n}(\tilde{x}, \tilde{y}, \tilde{z}) + \tilde{x}^2 + k^2\tilde{y}^2 + \lambda^2\tilde{z}^2 = 0. \tag{4.49}$$

The bosonic cloud has the form of an ellipsoid which satisfies the relation $\tilde{x}^2 + k^2\tilde{y}^2 + \lambda^2\tilde{z}^2 = \tilde{\mu}$ and whose semiaxes are the cloud radii $\tilde{x}_{\mathrm{TF2}} = \sqrt{\tilde{\mu}}$, $\tilde{y}_{\mathrm{TF2}} = \tilde{x}_{\mathrm{TF2}}/k$, and $\tilde{z}_{\mathrm{TF2}} = \tilde{x}_{\mathrm{TF2}}/\lambda$ along the $\tilde{x}$-, $\tilde{y}$-, and $\tilde{z}$-axis, respectively. From this we conclude that the BEC has a pancake shape in the case when $\lambda < k$ and $\lambda < 1$, otherwise it has a cigar shape.

We also need to write down the dimensionless equivalent of the normalization condition (4.15), which reads:

$$\int_{-\tilde{x}_{\mathrm{TF2}}}^{\tilde{x}_{\mathrm{TF2}}}\int_{-\tilde{y}_{\mathrm{TF2}}}^{\tilde{y}_{\mathrm{TF2}}}\int_{-\tilde{z}_{\mathrm{TF2}}}^{\tilde{z}_{\mathrm{TF2}}}\tilde{n}(\tilde{x},\tilde{y},\tilde{z})d\tilde{x}d\tilde{y}d\tilde{z}=\frac{8\pi}{15}, \tag{4.50}$$

where the total density $\tilde{n}(\tilde{x},\tilde{y},\tilde{z})$ in equation (4.50) is the combination of the total densities from both the superfluid and the Bose-glass region.

4.4.3. Thomas-Fermi Results

Before choosing any parameters for our BEC system, we have first to justify using the TF approximation in the anisotropic trapped case and determine the range of validity of this approximation. To this end we rewrite equation (4.13) in the clean case, i.e., $d = 0$, and we divide it by the factor $\bar{\mu}\sqrt{\bar{n}}$. This yields:

$$\left[-1+\tilde{n}(\tilde{x},\tilde{y},\tilde{z})+\tilde{x}^2+k^2\tilde{y}^2+\lambda^2\tilde{z}^2-\left(\frac{\xi_x}{x_{\mathrm{TF}}}\right)^2\left(\frac{\partial^2}{\partial\tilde{x}^2}+\frac{\partial^2}{\partial\tilde{y}^2}+\frac{\partial^2}{\partial\tilde{z}^2}\right)\right]\sqrt{\tilde{n}\left(\tilde{x},\tilde{y},\tilde{z}\right)}=0, \tag{4.51}$$

where $\xi_x=\frac{l_x^2}{x_{\mathrm{TF}}}$ denotes the coherence length along the x-axis and $x_{\mathrm{TF}}=\sqrt{2\bar{\mu}/M\omega_x^2}$ the TF radius along the x-axis. The TF approximation in the anisotropic trapped case is only justified when $\xi_x \ll x_{\mathrm{TF}}$.

In this Section we perform our study for Rubidium ^{87}Rb and for the following experimentally realistic parameters: $N = 10^6$, $\omega_x = 2\pi \times 160$ Hz, $k = \sqrt{2}$, $\lambda = 2$, and $a = 5.29$ nm. For those parameters the oscillator lengths read $l_x = 0.85\,\mu$m, $l_y = 0.72\,\mu$m, and $l_z = 0.60\,\mu$m, the coherence length along the x-axis turns out to be $\xi_x = 70.95$ nm, and the TF radius along the x-axis is given by $x_{\mathrm{TF}} = 10.41\,\mu$m. So the assumption $\xi_x \ll x_{\mathrm{TF}}$ for the TF approximation is, indeed, fulfilled. Furthermore, we have a cigar shaped BEC.

Using those parameter values we solve in the superfluid region equation (4.47) for the total density and insert the result into equations (4.45) and (4.46) to get the condensate density and the Bose-glass parameters, respectively. This has to be combined with equation (4.49) in the Bose-glass region. After that we fix the chemical potential $\tilde{\mu}$ by using the normalization condition (4.50). The resulting densities are plotted in Fig. 4.18, where in the superfluid region the densities are plotted with solid lines, and in the Bose-glass region they are plotted with dashed lines.

In Fig. 4.18a the three cuts along the respective axis of the total density coincide in the center of the trap. Furthermore, we remark the proportionality between them. This proportionality depends on the choice of the trap aspect ratios k and λ. Since in our example we have chose $\lambda > k > 1$, the x-cut of the total density is the largest one, then comes the y-cut, and the smallest one is the z-cut. As a consequence, the z-cut of the total density vanishes first, then the y-cut, and in the end the x-cut. The same can be remarked for the condensate density in Fig. 4.18b and for the Bose-glass order parameter in Fig. 4.18c.

The corresponding Thomas-Fermi radii are plotted in Fig. 4.19 as functions of the disorder strength $\tilde{d}$. Here again we remark the proportionality between the three components of each radius, namely the condensate radius and the cloud radius. Since we have used in our plot $\lambda > k > 1$, the condensate radius along x-axis is the largest one, followed by the one along y-axis, and the smallest one is the one along z-axis. The same can be said about the three components of the cloud radius.

Furthermore, we observe that the three components of the condensate radius turn out to vanish at the same critical disorder strength value $\tilde{d}_{\mathrm{c}}=\frac{2^{1/5}}{\sqrt{3+6\sqrt{3}\cos\left(\frac{\pi}{18}\right)}}\backsimeq 0.315$, which corresponds to the location of a quantum phase transition. This critical value of the disorder strength is obtained by setting one of the components of the cloud radius to zero: $\tilde{x}_{\mathrm{TF1}} = 0$, $\tilde{y}_{\mathrm{TF1}} = 0$, or $\tilde{z}_{\mathrm{TF1}} = 0$. Contrary the three components of the cloud radius increase with the disorder strength $\tilde{d}$ in the superfluid phase until they become constant in the Bose-glass phase, where the bosonic cloud has maximal radii of $\lim\limits_{\tilde{d}\to\infty}\tilde{x}_{\mathrm{TF2}} = 2^{1/5}\backsimeq 1.148$, $\lim\limits_{\tilde{d}\to\infty}\tilde{y}_{\mathrm{TF2}} = \tilde{x}_{\mathrm{TF2}}/k\backsimeq 0.811$, and $\lim\limits_{\tilde{d}\to\infty}\tilde{z}_{\mathrm{TF2}} = \tilde{x}_{\mathrm{TF2}}/\lambda\backsimeq 0.574$, which are obtained by inserting the Bose-glass region density (4.49) into the normalization condition (4.50).

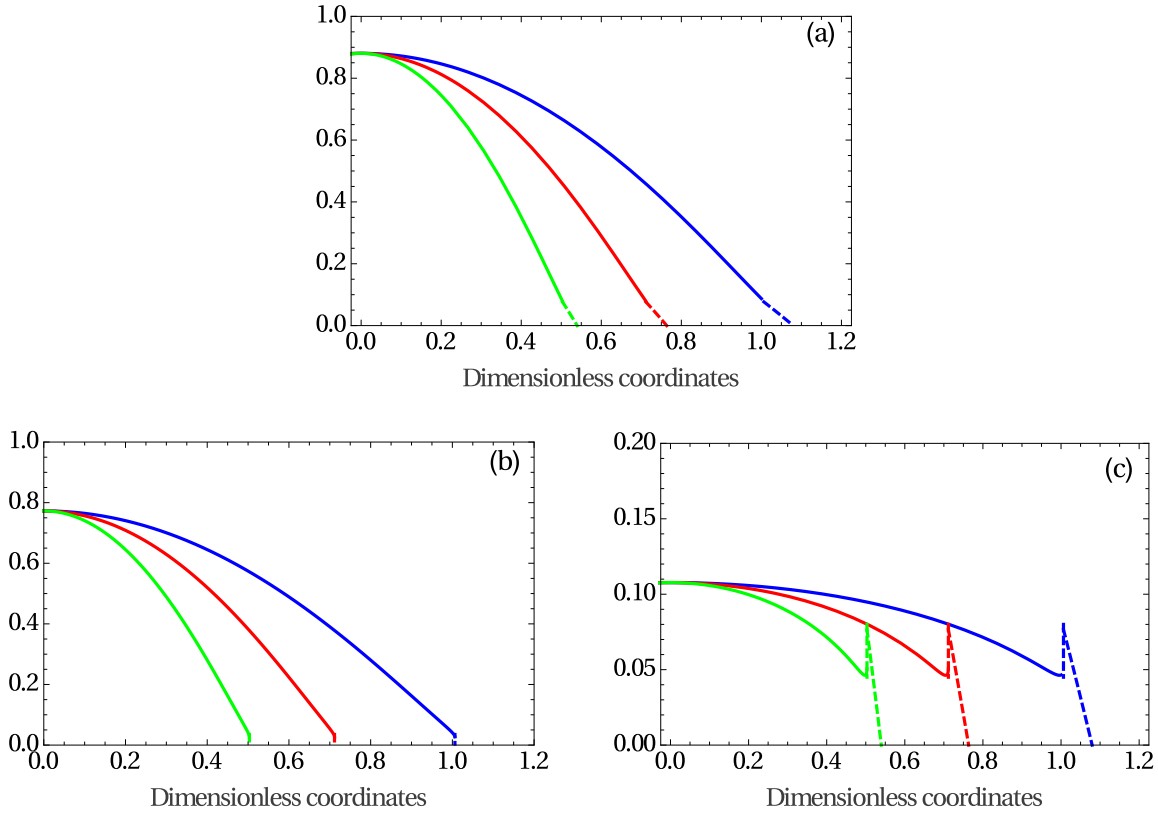

Figure 4.18.: (a) Total density along x-axis $\tilde{n}(\tilde{x},0,0)$ (blue), y-axis $\tilde{n}(0,\tilde{y},0)$ (red), and z-axis $\tilde{n}(0,0,\tilde{z})$ (green), (b) condensate density along x-axis $\tilde{n}_0(\tilde{x},0,0)$ (blue), y-axis $\tilde{n}_0(0,\tilde{y},0)$ (red), and z-axis $\tilde{n}_0(0,0,\tilde{z})$ (green), and (c) Bose-glass order parameter along x-axis $\tilde{q}(\tilde{x},0,0)$ (blue), y-axis $\tilde{q}(0,\tilde{y},0)$ (red), and z-axis $\tilde{n}(0,0,\tilde{z})$ (green), for $\tilde{d}=0.107$ both for superfluid region (solid) and Bose-glass region (dashed).

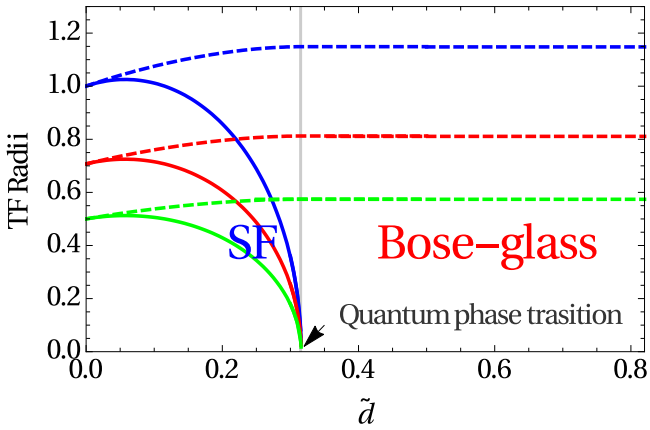

Figure 4.19.: Condensate radii (solid) and cloud radii (dashed) along the $\tilde{x}$- (blue), $\tilde{y}$- (red), and $\tilde{z}$- (green) axis as functions of dimensionless disorder strength $\tilde{d}$.

5. Dirty Bosons in 3D at Finite Temperature

In this chapter we consider a three-dimensional BEC system at finite temperature, so that also the thermal density $n_{\rm th}(\mathbf{x})$ has to be taken into account. After having discussed the homogeneous case, we deal with an isotropic harmonic trap $V(r) = \frac{1}{2}M\Omega^2 r^2$ in TF approximation. At first we restrict ourselves to the clean case, then we treat the disordered one, where we work out the different densities as well as the respective Thomas-Fermi radii. This allows us to study the impact of both temperature and disorder on the distribution of the densities as well as the respective Thomas-Fermi radii.

First of all we rewrite the four self-consistency equations (2.152)–(2.155) obtained in Subsection 2.10.3 for the considered three-dimensional case at finite temperature:

$$n(r) = n_0(r) + q(r) + n_{\rm th}(r)\,, \tag{5.1}$$

$$\left\{-gn_0(r) + \left[\sqrt{-\mu + d^2 + 2gn(r) + V(r)} + d\right]^2 - \frac{\hbar^2}{2M}\frac{1}{r^2}\frac{\partial}{\partial r}\left(r^2\frac{\partial}{\partial r}\right)\right\}\sqrt{n_0(r)} = 0, \tag{5.2}$$

$$q(r) = \frac{dn_0(r)}{\sqrt{-\mu + d^2 + 2gn(r) + V(r)}}, \tag{5.3}$$

$$n_{\rm th}(r) = \left(\frac{M}{2\pi\beta\hbar^2}\right)^{3/2} \varsigma_{3/2}\left(e^{\beta\,[\mu - d^2 - 2gn(r) - V(r)]}\right), \tag{5.4}$$

as well as the corresponding normalization condition

$$N = 4\pi\int_0^\infty r^2 n(r)dr. \tag{5.5}$$

5.1. Homogeneous Case

We start with briefly reviewing the homogeneous case, since it is the simplest one, where we have $V(\mathbf{x}) = 0$, which was already treated in Ref. [84]. We distinguish between three different phases, namely, the superfluid phase, where the condensate density contributes to the total density, the Bose-glass phase, where the condensate vanishes, and the thermal phase, where all bosons are in the excited states. We treat each phase separately.

5.1.1. Superfluid Phase

Equations (5.1)–(5.4) reduce in the superfluid phase to:

$$n = n_0 + q + n_{\rm th}, \tag{5.6}$$

$$gn_0 = \left[\sqrt{-\mu + d^2 + 2gn} + d\right]^2, \tag{5.7}$$

$$q = \frac{dn_0}{\sqrt{-\mu + d^2 + 2gn}}, \tag{5.8}$$

$$n_{\rm th} = \left(\frac{M}{2\pi\beta\hbar^2}\right)^{3/2} \varsigma_{3/2}\left(e^{\beta\,(\mu - d^2 - 2gn)}\right). \tag{5.9}$$

Note that we drop in this section the spatial dependence of all densities due to the homogeneity. Inserting equations (5.7)–(5.9) into equation (5.6), then dividing by $gn^{3/2}$ gives us the following algebraic equation for the condensate fraction n_0/n:

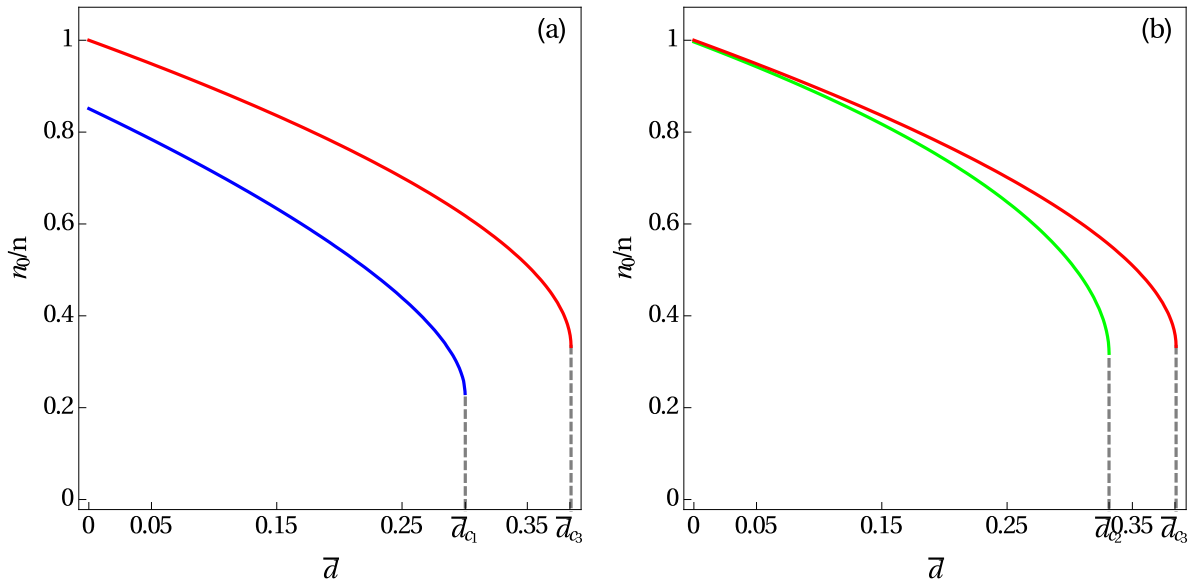

Figure 5.1.: Condensate fraction n_0/n as function of dimensionless disorder strength $\overline{d}$ for (a) $\gamma = 0.0007$, $T/T_c^0 = 0.6$ (blue) and (b) $\gamma = 0.2366$, $T/T_c^0 = 0.6$ (green), as well as $T = 0$ (red).

$$\left(\frac{n_0}{n}\right)^{3/2} - \sqrt{\frac{n_0}{n}} + \overline{d} + \left(\frac{T}{\varsigma\left(\frac{3}{2}\right)^{2/3} T_c^0}\right)^{3/2} \left(\sqrt{\frac{n_0}{n}} - \overline{d}\right) \varsigma_{3/2}\left(e^{-2\frac{T_c^0}{T}\varsigma\left(\frac{3}{2}\right)^{2/3}\gamma^{1/3}\left[\sqrt{\frac{n_0}{n}}-\overline{d}\right]^2}\right) = 0. \quad (5.10)$$

Here $\overline{d} = \frac{\xi}{\mathcal{L}}$ denotes the dimensionless disorder strength, $\gamma = na^3$ is the gas parameter, and $T_c^0 = \frac{2\pi\hbar^2}{Mk_B}\left(\frac{n}{\varsigma\left(\frac{3}{2}\right)}\right)^{2/3}$ abbreviates the critical temperature of the ideal Bose gas, where $\xi = \frac{\hbar}{\sqrt{2Mgn}}$ stands for the coherence length, and $\mathcal{L} = \frac{2\pi\hbar^4}{M^2 D}$ represents the Larkin length [82, 119]. Note that at zero temperature equation (5.10) reduces to (4.4). Figure 5.1 shows that the condensate fraction generically decreases with increasing disorder strength $\overline{d}$. Furthermore, our mean-field theory predicts that the condensate density stops to exist at a critical value $\overline{d}_c$. We interpret this as a sign that a phase transition occurs in the homogeneous BEC from the superfluid to the Bose-glass phase. If we compare in Fig. 5.1a between the blue line, which corresponds to a finite temperature, and the red line, which corresponds to the zero-temperature case of Section 4.1, we observe that $\overline{d}_{c_1} \simeq 0.30 < \overline{d}_{c_3} \simeq 0.384$ and conclude that the critical disorder strength $\overline{d}_c$ decreases with increasing temperature T. Comparing at fixed temperature the blue line from Fig. 5.1a for weakly interacting ^{87}Rb gas, which corresponds to the gas parameter being about $\gamma = 0.0007$ according to Ref. [128], with the green line from Fig. 5.1b for a strongly interacting ^{4}He, which corresponds to the gas parameter being about $\gamma = 0.2366$ according to Ref. [129], yields that $\overline{d}_{c_1} \simeq 0.30 < \overline{d}_{c_2} \simeq 0.331$. But in order to make a quantitative statement about the impact of the interaction strength, one has to take into account that the gas parameter γ is included in the definition of the dimensionless disorder strength $\overline{d} = \frac{d}{\sqrt{gn}}$. With this it turns out that $d_{c_1} > d_{c_2}$, i.e, the critical disorder strength d_c decreases with increasing the gas parameter γ. All these findings suggest that a corresponding phase transition will also appear in the trapped case, which is studied later on in Section 5.4.

Now we determine the equation of state in the superfluid phase. To this end we divide equation (5.7) by the factor gn, which yields:

$$\frac{n_0}{n} = \left(\sqrt{-\frac{\mu}{gn} + \overline{d}^2 + 2} + \overline{d}\right)^2. \quad (5.11)$$

Inserting this result into the condensate fraction equation (5.10) we obtain the following algebraic equation of state:

$$\left(\sqrt{-\frac{\mu}{gn}+\overline{d}^2+2}+\overline{d}\right)^3-\sqrt{-\frac{\mu}{gn}+\overline{d}^2+2}+\left(\frac{T}{\varsigma\left(\frac{3}{2}\right)^{2/3}T_{\mathrm{c}}^0}\right)^{3/2}$$
$$\times\sqrt{-\frac{\mu}{gn}+\overline{d}^2+2}\,\varsigma_{\,3/2}\left(e^{-2\frac{T_{\mathrm{c}}^0}{T}\varsigma\left(\frac{3}{2}\right)^{2/3}\gamma^{1/3}\,\left[-\frac{\mu}{gn}+\overline{d}^2+2\right]}\right)=0 \tag{5.12}$$

5.1.2. Bose-Glass Phase

In the Bose-glass phase we have $n_0=0$, so we only need equations (5.1), (5.3), and (5.4), which reduce to:

$$n=q+n_{\mathrm{th}}, \tag{5.13}$$

$$gn=\frac{\mu-d^2}{2}, \tag{5.14}$$

$$n_{\mathrm{th}}=\left(\frac{M}{2\pi\beta\hbar^2}\right)^{3/2}\varsigma\left(\frac{3}{2}\right). \tag{5.15}$$

Dividing relation (5.14) by the factor gn, we get the corresponding equation of state in the Bose-glass phase

$$\frac{\mu}{gn}=2+\overline{d}^2. \tag{5.16}$$

5.1.3. Thermal phase

In the thermal phase we have $n_0=q=0$ and $n=n_{\mathrm{th}}$, so we need only equation (5.4), which reduces to:

$$1=\left(\frac{T}{\varsigma\left(\frac{3}{2}\right)^{2/3}T_{\mathrm{c}}^0}\right)^{3/2}\varsigma_{\,3/2}\left(e^{2\frac{T_{\mathrm{c}}^0}{T}\varsigma\left(\frac{3}{2}\right)^{2/3}\gamma^{1/3}\,\left(\frac{\mu}{gn}-\overline{d}^2-2\right)}\right). \tag{5.17}$$

Equation (5.17) represents an implicit relation for the equation of the state in the thermal phase.

5.1.4. Phase Diagram

To illustrate our results further, we plot the phase diagram, which is spanned by both the temperature and the disorder strength in Fig. 5.2. The first-order phase transition line between the superfluid and the non-superfluid phase is obtained by solving (5.10) and by evaluating $\frac{\partial\overline{d}}{\partial\, n_0/n}=0$ from (5.10), i.e,

$$\frac{3}{2}\sqrt{\frac{n_0}{n}}-\frac{1}{2\sqrt{n_0/n}}+\frac{1}{2\sqrt{n_0/n}}\left(\frac{T}{\varsigma\left(\frac{3}{2}\right)^{2/3}T_{\mathrm{c}}^0}\right)^{3/2}\varsigma_{\,3/2}\left(e^{-2\frac{T_{\mathrm{c}}^0}{T}\varsigma\left(\frac{3}{2}\right)^{2/3}\gamma^{1/3}\,\left[\sqrt{\frac{n_0}{n}}-\overline{d}\right]^2}\right)$$
$$-\frac{2\gamma^{1/3}}{\sqrt{n_0/n}}\sqrt{\frac{T}{\varsigma\left(\frac{3}{2}\right)^{2/3}T_{\mathrm{c}}^0}}\left(\sqrt{\frac{n_0}{n}}-\overline{d}\right)^2\varsigma_{\,1/2}\left(e^{-2\frac{T_{\mathrm{c}}^0}{T}\varsigma\left(\frac{3}{2}\right)^{2/3}\gamma^{1/3}\,\left[\sqrt{\frac{n_0}{n}}-\overline{d}\right]^2}\right)=0. \tag{5.18}$$

The phase diagram in Fig. 5.2a corresponds to a weakly interacting ^{87}Rb gas, while the phase diagram in Fig. 5.2b corresponds to strongly interacting ^{4}He. The critical disorder strength $\overline{d}_{\mathrm{c}}$ decreases with increasing the temperature T. In the clean case $\overline{d}=0$ there is a critical temperature T_{c} at which the superfluid, which is stable for $T<T_{\mathrm{c}}$, and the thermal Bose-gas, which is stable for $T>T_{\mathrm{c}}$, coexist. Note that, due to the weak repulsive interaction, this critical temperature T_{c} turns out to be larger than the critical temperature of the ideal Bose gas T_{c}^0 by about

$$\Delta T_{\mathrm{c}}=T_{\mathrm{c}}-T_{\mathrm{c}}^0\simeq 1.3\,\gamma^{1/3}T_{\mathrm{c}}^0. \tag{5.19}$$

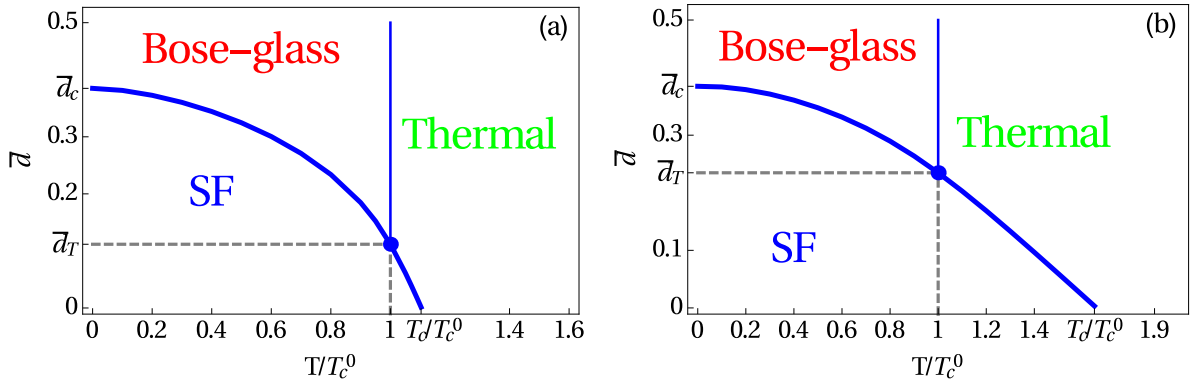

Figure 5.2.: Phase diagram in disorder strength-temperature plane for (a) weakly interacting ^{87}Rb gas with $\gamma = 0.0007$ and (b) strongly interacting ^{4}He with $\gamma = 0.2366$. Thick and thin lines represent first-order and continuous phase transitions, respectively.

Note that the result (5.19) is non-trivial as it involves a resummation of an infrared divergent perturbation series, which has been worked out on the basis of variational perturbation theory in Refs. [130, 131]. Furthermore, (5.19) was confirmed by high-precision Monte Carlo simulations in Ref. [132]. For the weakly interacting Bose gas in Fig. 5.2a we read off $T_c/T_c^0 = 1.103$, which agrees well with the result obtained using formula (5.19) yielding $T_c/T_c^0 \simeq 1.115$. The same can be remarked for the strongly interacting Bose gas in Fig. 5.2b, where we have $T_c/T_c^0 = 1.65$, which agrees well with the result obtained using formula (5.19) $T_c/T_c^0 \simeq 1.796$. Furthermore, there is a triple point $\overline{d}_T$, where all three phases coexist and which is characterized by $T = T_c^0$ and $\mu_c = 2gn = 2g\left(\frac{Mk_BT_c^0}{2\pi\hbar^2}\right)^{3/2}\varsigma\left(\frac{3}{2}\right)$. Thus, within the Hartree-Fock theory of dirty bosons T_c^0 turns out to be the critical temperature for the appearance of the Bose-glass phase. For $\gamma = 0.0007$ we have $\overline{d}_T = 0.111$, while for $\gamma = 0.2366$ we obtain $\overline{d}_T = 0.234$. Below the triple point temperature we have a first-order phase transition from the superfluid to the Bose-glass phase, while above the triple point temperature a first-order phase transition from the superfluid to the thermal phase occurs. Below the triple point disorder we have a first-order phase transition from the superfluid to the thermal phase, while above the triple point disorder we observe a first-order phase transition from the superfluid to the Bose-glass phase, which is followed by a second-order phase transition from the Bose-glass to the thermal phase. At $T = 0$ we are in the zero temperature case, which was already treated in Section 4.1.

5.1.5. Chemical Potential

In Fig. 5.3 we plot the equation of state of the dirty Bose system for the gas parameter $\gamma = 0.0007$. In Fig. 5.3a for increasing disorder strength we fix the temperature at $T = 0.6\,T_c^0$, which corresponds in Fig. 5.2a to the region below the triple point temperature, i.e, we have only two phases, namely, the superfluid and the Bose-glass phase. Therefore, the equation of state of the superfluid phase (5.12) is combined with the equation of state of the Bose-glass phase (5.16) and plotted together in Fig. 5.3a. We read off that the chemical potential increases with the disorder strength $\overline{d}$ with a discontinuity in the transition region between the superfluid and the Bose-glass phase, which occurs at the critical disorder strength $\overline{d}_c$:

$$\lim_{\overline{d}\uparrow\overline{d}_c}\frac{\mu}{gn} - \lim_{\overline{d}\downarrow\overline{d}_c}\frac{\mu}{gn} \simeq 0.037. \tag{5.20}$$

Thus, the transition between the superfluid and the Bose-glass phase is, indeed, of first order as indicated in Fig. 5.2a.

In Fig. 5.3b for increasing temperature we fix the disorder strength at $\overline{d} = 0.3$, which corresponds in Fig. 5.2a to the region above the triple point disorder, i.e, we have three phases, namely, the superfluid, the Bose-glass, and the thermal phase. Thus, the three corresponding equations of state, namely, equations (5.12), (5.16), and (5.17), are combined and plotted together in Fig. 5.3b. In the

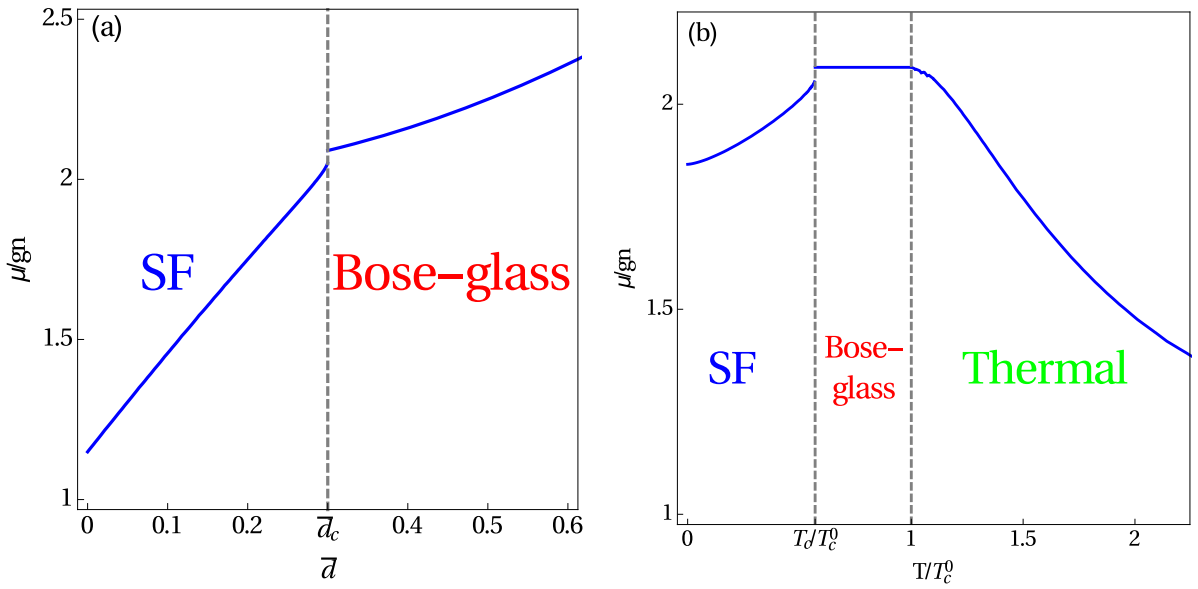

Figure 5.3.: Chemical potential fraction μ in units of gn for $\gamma = 0.0007$ as function of (a) dimensionless disorder strength $\overline{d}$ for $T/T_c^0 = 0.6$ and (b) dimensionless temperature T/T_c^0 for $\overline{d} = 0.3$.

superfluid phase the chemical potential increases with the temperature with a discontinuity at the critical temperature T_c, where the transition region between the superfluid and the Bose-glass phase is located:

$$\lim_{T\uparrow T_c} \frac{\mu}{gn} - \lim_{T\downarrow T_c} \frac{\mu}{gn} \simeq 0.032. \tag{5.21}$$

In the Bose-glass phase the chemical potential stays constant, then decreases with the temperature in the thermal phase. This phase transition occurs continuously at the critical temperature T_c^0. So, we have a first-order phase transition from the superfluid to the Bose-glass phase, which is followed by a second-order phase transition from the Bose-glass to the thermal phase in agreement with Fig. 5.2a.

5.2. Thomas-Fermi Approximation

After having treated the homogeneous case we investigate now the trapped one. First of all we transform equations (5.1)–(5.4) into dimensionless ones by dividing equations (5.1), (5.3), and (5.4) by the maximal value of the density in the clean case at zero temperature $\bar{n} = \bar{\mu}/g$ and dividing equation (5.2) by the factor $\bar{\mu}\sqrt{\bar{n}}$. This yields:

$$\tilde{n}\left(\tilde{r}\right) = \tilde{n}_0\left(\tilde{r}\right) + \tilde{q}\left(\tilde{r}\right) + \tilde{n}_{\mathrm{th}}\left(\tilde{r}\right), \tag{5.22}$$

$$\tilde{q}\left(\tilde{r}\right) = \frac{\tilde{d}\tilde{n}_0\left(\tilde{r}\right)}{\sqrt{-\tilde{\mu} + 2\tilde{n}(\tilde{r}) + \tilde{r}^2}}, \tag{5.23}$$

$$\left\{-\tilde{n}_0\left(\tilde{r}\right) + \left[\sqrt{-\tilde{\mu} + 2\tilde{n}(\tilde{r}) + \tilde{r}^2} + \tilde{d}\right]^2 - \left(\frac{\xi}{R_{\mathrm{TF}}}\right)^2 \frac{1}{\tilde{r}^2}\frac{\partial}{\partial\tilde{r}}\left(\tilde{r}^2\frac{\partial}{\partial\tilde{r}}\right)\right\}\sqrt{\tilde{n}_0\left(\tilde{r}\right)} = 0, \tag{5.24}$$

$$\tilde{n}_{\mathrm{th}}\left(\tilde{r}\right) = \frac{1}{\bar{n}}\left(\frac{M}{2\pi\beta\hbar^2}\right)^{3/2} \varsigma_{3/2}\left(e^{\beta\bar{\mu}\,[\tilde{\mu}-2\tilde{n}(\tilde{r})-\tilde{r}^2]}\right). \tag{5.25}$$

Here $\tilde{n}_0(\tilde{r}) = n_0(r)/\bar{n}$ denotes the dimensionless condensate density, $\tilde{q}(\tilde{r}) = q(r)/\bar{n}$ the dimensionless Bose-glass order parameter, $\tilde{n}_{\mathrm{th}}(\tilde{r}) = n_{\mathrm{th}}(r)/\bar{n}$ the dimensionless thermal density, $\tilde{n}(\tilde{r}) = n(r)/\bar{n}$ the dimensionless total density, $\tilde{r} = r/R_{\mathrm{TF}}$ the dimensionless radial coordinate, $\tilde{\mu} = (\mu - d^2)/\bar{\mu}$ the dimensionless chemical potential, $\tilde{d} = \frac{\xi}{\mathcal{L}}$ the dimensionless disorder strength, $l = \sqrt{\frac{\hbar}{M\Omega}}$ the oscillator

length, $R_{\mathrm{TF}} = \sqrt{2\bar{\mu}/M\Omega^2}$ the TF cloud radius at zero temperature, and $\xi = \frac{l^2}{R_{\mathrm{TF}}}$ the coherence length in the center of the trap at zero temperature. The chemical potential in the absence of the disorder at zero temperature $\bar{\mu} = \frac{15^{2/5}}{2}\left(\frac{aN}{l}\right)^{2/5}\hbar\Omega$ is deduced from the normalization condition (5.5) in the clean case by evaluating:

$$\frac{4\pi}{g}\int_0^{R_{\mathrm{TF}}}\left(\bar{\mu} - \frac{1}{2}M\Omega^2 r^2\right) r^2 dr = N. \tag{5.26}$$

We also need to write down the dimensionless equivalent of the normalization condition (5.5), which reads:

$$\int_0^{\infty} \tilde{n}(\tilde{r})\tilde{r}^2 d\tilde{r} = \frac{2}{15}. \tag{5.27}$$

For the total density $\tilde{n}(\tilde{r})$, the condensate density $\tilde{n}_0(\tilde{r})$, the Bose-glass parameter $\tilde{q}(\tilde{r})$, and the thermal density $\tilde{n}_{\mathrm{th}}(\tilde{r})$ we have three algebraic equations: (5.22), (5.23), and (5.25) and one nonlinear partial differential equation (5.24), which is impossible to solve analytically. Thus, we use here again the TF approximation, so we neglect the kinetic term in the self-consistency equation (5.24), which reduces in the superfluid region to

$$\tilde{n}_0\left(\tilde{r}\right) = \left[\sqrt{-\tilde{\mu} + 2\tilde{n}(\tilde{r}) + \tilde{r}^2} + \tilde{d}\right]^2, \tag{5.28}$$

whereas equations (5.22), (5.23), and (5.25) remain the same. Outside the superfluid region equation (5.24) is solved by $\tilde{n}_0\left(\tilde{r}\right) = 0$.

In the following, we treat first in Section 5.3 the simple clean case, where we have no disorder, in order to study, as a first step, only the impact of thermal fluctuations on the BEC system. Afterwards in Section 5.4 then we treat the general case, where disorder and temperature occur simultaneously.

5.3. Clean Case

Even the simpler clean case represents a challenge and has to be treated in the literature either perturbatively [133] or numerically [134]. In the clean case we have no Bose-glass contribution, as we can reduce $\tilde{q}\left(\tilde{r}\right) = 0$ from (5.23), but a thermal contribution $\tilde{n}_{\mathrm{th}}\left(\tilde{r}\right)$ to the total density $\tilde{n}\left(\tilde{r}\right)$. Therefore, in this section two different cases can be distinguished: in the first one the bosons can be in the condensate or in the excited states, which corresponds to the superfluid region, in the second one all bosons are in the excited states and there is no condensate any more, so this is the thermal region. In the following, we treat those two regions separately.

5.3.1. Superfluid region

In the superfluid region the TF approximated equations (5.22), (5.25), and (5.28) reduce to:

$$\tilde{n}(\tilde{r}) = \tilde{n}_0\left(\tilde{r}\right) + \tilde{n}_{\mathrm{th}}\left(\tilde{r}\right), \tag{5.29}$$

$$\tilde{n}_{\mathrm{th}}\left(\tilde{r}\right) = \frac{g}{\bar{\mu}}\left(\frac{M}{2\pi\beta\hbar^2}\right)^{3/2} \varsigma_{3/2}\left(e^{\beta\bar{\mu}\ [\tilde{\mu} - 2\tilde{n}(\tilde{r}) - \tilde{r}^2]}\right), \tag{5.30}$$

$$\tilde{n}_0\left(\tilde{r}\right) = \tilde{\mu} - 2\tilde{n}_{\mathrm{th}}\left(\tilde{r}\right) - \tilde{r}^2. \tag{5.31}$$

We have now three coupled algebraic self-consistency equations for the condensate density $\tilde{n}_0\left(\tilde{r}\right)$, the thermal density $\tilde{n}_{\mathrm{th}}\left(\tilde{r}\right)$, and the sum of them, i.e., the total density $\tilde{n}\left(\tilde{r}\right)$. Those equations can be straightforwardly decoupled by first inserting equations (5.29) and (5.31) into equation (5.30) in order to get one self-consistency equation for the thermal density:

$$\tilde{n}_{\mathrm{th}}\left(\tilde{r}\right) = \frac{g}{\bar{\mu}}\left(\frac{M}{2\pi\beta\hbar^2}\right)^{3/2} \varsigma_{3/2}\left(e^{\beta\bar{\mu}\ [-\tilde{\mu} + 2\tilde{n}_{\mathrm{th}}(\tilde{r}) + \tilde{r}^2]}\right). \tag{5.32}$$

Inserting again equation (5.31) into equation (5.32), we get one self-consistency equation for the condensate density:

$$\tilde{n}_0\left(\tilde{r}\right) = \tilde{\mu} - \tilde{r}^2 - \frac{2g}{\bar{\mu}}\left(\frac{M}{2\pi\beta\hbar^2}\right)^{3/2} \varsigma_{\,3/2}\left(e^{-\beta\bar{\mu}\tilde{n}_0(\tilde{r})}\right). \tag{5.33}$$

Inserting equation (5.31) into equation (5.29) yields $\tilde{n}_{\mathrm{th}}\left(\tilde{r}\right) = \tilde{\mu} - \tilde{n}\left(\tilde{r}\right) - \tilde{r}^2$. By implementing the latter result into equation (5.32), we obtain one self-consistency equation for the total density

$$\tilde{n}(\tilde{r}) = -\tilde{\mu} + 2\tilde{n}(\tilde{r}) + \tilde{r}^2 + \frac{g}{\bar{\mu}}\left(\frac{M}{2\pi\beta\hbar^2}\right)^{3/2} \varsigma_{\,3/2}\left(e^{\beta\bar{\mu}\ \left[\tilde{\mu}-2\tilde{n}(\tilde{r})-\tilde{r}^2\right]}\right), \tag{5.34}$$

Equations (5.32)–(5.34) contain the polylogarithmic function $\varsigma_{\,3/2}$, which makes them impossible to solve analytically. Therefore, we solve those equations numerically, but due to the polylogarithmic function $\varsigma_{\,3/2}$, the numerically obtained densities turn out to be fluctuating in the transition region, which separates the superfluid region from the thermal one [135]. The physical origin of those fluctuations is the Poisson sum formula (2.144), where a series is transformed into another one. It represent a duality transformation, where the right-hand side of (2.144) is valid for high temperatures, while its left-hand side is valid for low temperatures [136]. Thus, in view of an analytic treatment, we apply the Robinson formula [115, 137]:

$$\varsigma_{\,\nu}\left(e^{x}\right) = \Gamma\left(1-\nu\right)\left(-x\right)^{\nu-1} + \sum_{k=0}^{\infty}\frac{x^k}{k!}\varsigma\left(\nu-k\right), \qquad x<0. \tag{5.35}$$

Close to the transition boundary the condensate density vanishes, so according to equation (5.31) the expression $\tilde{\mu}-2\tilde{n}\left(\tilde{r}\right)-\tilde{r}^2$ goes to zero, which motivates to truncate the Robinson expansion at the first order:

$$\begin{aligned}\varsigma_{\,3/2}\left(e^{\beta\bar{\mu}\ \left[\tilde{\mu}-2\tilde{n}(\tilde{r})-\tilde{r}^2\right]}\right) \approx & \Gamma\left(-\frac{1}{2}\right)\sqrt{-\beta\bar{\mu}\ \left[\tilde{\mu}-2\tilde{n}\left(\tilde{r}\right)-\tilde{r}^2\right]} + \varsigma\left(\frac{3}{2}\right) \\ & + \beta\bar{\mu}\ \left[\tilde{\mu}-2\tilde{n}\left(\tilde{r}\right)-\tilde{r}^2\right]\varsigma\left(\frac{1}{2}\right).\end{aligned} \tag{5.36}$$

Using this approximation, equations (5.29)–(5.31) can be written as follows:

$$\tilde{n}(\tilde{r}) = \tilde{n}_0\left(\tilde{r}\right) + \tilde{n}_{\mathrm{th}}\left(\tilde{r}\right), \tag{5.37}$$

$$\tilde{n}_{\mathrm{th}}\left(\tilde{r}\right) = \frac{\tilde{\mu}-\tilde{n}_0\left(\tilde{r}\right)-\tilde{r}^2}{2}, \tag{5.38}$$

$$\tilde{n}_0\left(\tilde{r}\right) \approx \tilde{\mu} - \tilde{r}^2 - \frac{2g}{\bar{\mu}}\left(\frac{M}{2\pi\beta\hbar^2}\right)^{3/2}\left[\Gamma\left(-\frac{1}{2}\right)\sqrt{\beta\bar{\mu}\ \tilde{n}_0\left(\tilde{r}\right)} + \varsigma\left(\frac{3}{2}\right) - \beta\bar{\mu}\ \tilde{n}_0\left(\tilde{r}\right)\varsigma\left(\frac{1}{2}\right)\right]. \tag{5.39}$$

Equation (5.39) represents a quadratic equation with respect to $\sqrt{\tilde{n}_0\left(\tilde{r}\right)}$ and has, thus, two solutions:

$$\begin{aligned}\tilde{n}_0\left(\tilde{r}\right) = & \left[-1+2g\beta\left(\frac{M}{2\pi\beta\hbar^2}\right)^{3/2}\varsigma\left(\frac{1}{2}\right)\right]^{-2}\left\{-\frac{2g}{\bar{\mu}}\left(\frac{M}{2\pi\beta\hbar^2}\right)^{3/2}\sqrt{\pi\beta\bar{\mu}}\right. \\ & \left.\pm\sqrt{\frac{4\pi\beta g^2}{\bar{\mu}}\left(\frac{M}{2\pi\beta\hbar^2}\right)^{3} - 4\left[\frac{1}{2}-\beta g\left(\frac{M}{2\pi\beta\hbar^2}\right)^{3/2}\varsigma\left(\frac{1}{2}\right)\right]\left[\frac{-\tilde{\mu}+\tilde{r}^2}{2}+\frac{g}{\bar{\mu}}\left(\frac{M}{2\pi\beta\hbar^2}\right)^{3/2}\varsigma\left(\frac{3}{2}\right)\right]}\right\}^2.\end{aligned} \tag{5.40}$$

We choose the one with the positive sign, which corresponds to the numerical solution of equation (5.33), i.e., to the one without Robinson approximation. We insert the chosen solution of condensate density $\tilde{n}_0\left(\tilde{r}\right)$ into equation (5.38) in order to get the thermal density $\tilde{n}_{\mathrm{th}}\left(\tilde{r}\right)$, and the sum of them then represents the particle density $\tilde{n}(\tilde{r})$. The condensate radius $\tilde{R}_{\mathrm{TF1}}$, which separates the superfluid

region from the thermal region, is obtained by differentiating equation (5.39) with respect to $\tilde{n}_0(\tilde{r})$, then setting $\frac{\partial \tilde{r}}{\partial \tilde{n}_0(\tilde{r})}\Big|_{\tilde{r}=\tilde{R}_{\mathrm{TF}_1}} = 0$. The resulting condensate density $\tilde{n}_0\left(\tilde{R}_{\mathrm{TF1}}\right)$ should be inserted again into equation (5.39) in order to get the analytical expression of the condensate radius

$$\tilde{R}_{\mathrm{TF1}} = \sqrt{\tilde{\mu} - \frac{2g}{\bar{\mu}}\left(\frac{M}{2\pi\beta\hbar^2}\right)^{3/2} \varsigma\left(\frac{3}{2}\right) + \frac{1}{\bar{\mu}}\left(\frac{M}{2\pi\beta\hbar^2}\right)^{3} \frac{4\pi\beta g^2}{1 - 2g\beta\left(\frac{M}{2\pi\beta\hbar^2}\right)^{3/2}\varsigma\left(\frac{1}{2}\right)}}. \tag{5.41}$$

5.3.2. Thermal region

In the thermal region the condensate vanishes, i.e., $\tilde{n}_0(\tilde{r}) = 0$ and $\tilde{n}_{\mathrm{th}}(\tilde{r}) = \tilde{n}(\tilde{r})$. In that case the self-consistency equation (5.25) reduces to:

$$\tilde{n}(\tilde{r}) = \frac{g}{\bar{\mu}}\left(\frac{M}{2\pi\beta\hbar^2}\right)^{3/2} \varsigma_{\,3/2}\left(e^{\beta\bar{\mu}\ [\tilde{\mu} - 2\tilde{n}(\tilde{r}) - \tilde{r}^2]}\right). \tag{5.42}$$

Equation (5.42) contains the polylogarithmic function $\varsigma_{\,3/2}$ and, thus, can not be solved analytically. Furthermore, the Robinson formula (5.36) can not be applied in the thermal region, since it gives a diverging density, which can not be accepted as a physical solution. Thus, the density of the thermal region (5.42) can only be treated numerically. The cloud radius $\tilde{R}_{\mathrm{TF2}}$, where the thermal density and, as a consequence, the total density vanish is defined here by the length, where the dimensionless thermal density $\tilde{n}(\tilde{r})$ is equal to 10^{-5}.

5.3.3. Thomas-Fermi Results

In this Section we perform our study for ^{87}Rb atoms and for the following experimentally realistic parameters: $N = 10^6$, $\Omega = 100\,\mathrm{Hz}$, and $a = 5.29\,\mathrm{nm}$. For those parameters the oscillator length reads $l = 2.72\,\mu\mathrm{m}$, the coherence length in the center of the trap turns out to be $\xi = 348.89\,\mathrm{nm}$ and the Thomas-Fermi radius is given by $R_{\mathrm{TF}} = 21.29\,\mu\mathrm{m}$, so the assumption $\xi \ll R_{\mathrm{TF}}$ for the TF approximation is, indeed, fulfilled.

Using those parameter values, we solve the superfluid region equation (5.39) for the condensate density $\tilde{n}_0(\tilde{r})$ and insert the result into equations (5.38) and (5.37) to get the thermal density $\tilde{n}_{\mathrm{th}}(\tilde{r})$ and the total density $\tilde{n}(\tilde{r})$, respectively. This has to be combined with equation (5.42) for the thermal region. After that the chemical potential $\tilde{\mu}$ has to be fixed using the normalization condition (5.27), where the total density $\tilde{n}(\tilde{r})$ is the combination of the total densities from both the superfluid region and the thermal region. The integral over the superfluid region in equation (5.27) is done analytically, while the integral over the thermal region is done using a method for numerical integration called Simpson's rule [138], which is a numerical approximation of definite integrals. The principle of this method is to decompose the interval of the integral of a function $f(x)$ into mini intervals $[\mathfrak{a}, \mathfrak{b}]$ where:

$$\int_{\mathfrak{a}}^{\mathfrak{b}} f(x)\,dx \approx \frac{\mathfrak{b} - \mathfrak{a}}{6}\left[f(\mathfrak{a}) + 4f\left(\frac{\mathfrak{a} + \mathfrak{b}}{2}\right) + f(\mathfrak{b})\right]. \tag{5.43}$$

The resulting densities are combined and plotted in Fig. 5.4 for the temperature $T = 60$ nK, where in the superfluid region the densities are plotted with solid lines, and in the thermal region with dotted lines.

Figure 5.4 shows that the condensate density $\tilde{n}_0(\tilde{r})$ is maximal at the center of the cloud and decreases when we move away from the center until the condensate radius $\tilde{R}_{\mathrm{TF1}}$, where it jumps to zero. For the chosen parameters the jump is too small to be visible but it exists as shown in the blow-up. The thermal density $\tilde{n}_{\mathrm{th}}(\tilde{r})$ is behaving oppositely: it is increasing with increasing $\tilde{r}$ until attending its maximum at the condensate radius $\tilde{R}_{\mathrm{TF1}}$, then for $\tilde{r} > \tilde{R}_{\mathrm{TF1}}$ it decreases exponentially to zero. The total density $\tilde{n}(\tilde{r})$ is maximal in the center of the trap and decreases when we move away from it until vanishing. Note that in the thermal region the total density $\tilde{n}(\tilde{r})$ and the thermal density $\tilde{n}_{\mathrm{th}}(\tilde{r})$ coincide. Although both the condensate density $\tilde{n}_0(\tilde{r})$ and the thermal density $\tilde{n}_{\mathrm{th}}(\tilde{r})$

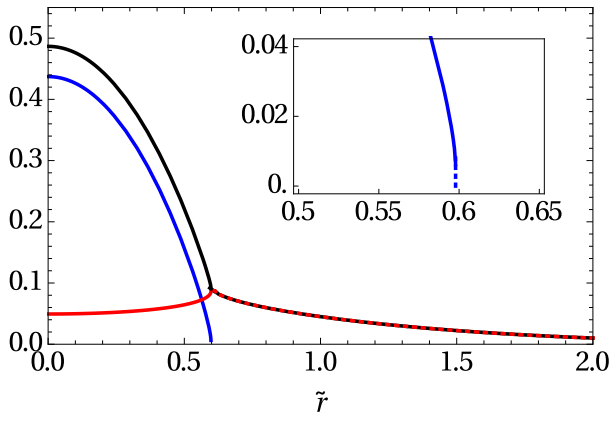

Figure 5.4.: Total density $\tilde{n}(\tilde{r})$ (black), condensate density $\tilde{n}_0(\tilde{r})$ (blue), and thermal density $\tilde{n}_{\mathrm{th}}(\tilde{r})$ (red) with blow-up of transition region as a function of radial coordinate $\tilde{r}$ for $T = 60$ nK in superfluid region (solid lines) and in thermal region (dotted lines), where chemical potential results in $\tilde{\mu} = 0.566$.

are discontinuous at the condensate radius $\tilde{R}_{\mathrm{TF1}}$, the total density $\tilde{n}(\tilde{r})$ remains continuous but reveals a discontinuity of the first derivative. We conclude from Fig. 5.4 that the condensate is situated in the center of the trap, while the bosons in the excited states are located at the border of the trap.

In order to know how the temperature changes the Thomas-Fermi radii, we plot them in Fig. 5.5a as functions of the temperature T. This figure reveals the existence of two phases, a superfluid phase, where the bosons are either in the condensate or in the excited states, and a thermal phase, where all particles are in the excited states. The condensate radius $\tilde{R}_{\mathrm{TF1}}$ decreases with the temperature until it vanishes at the critical temperature T_{c} marking a phase transition. The critical temperature T_{c} is the solution of the equality $\tilde{R}_{\mathrm{TF1}} = 0$, i.e.,

$$\left[\tilde{\mu}_c - \frac{2g}{\bar{\mu}}\left(\frac{Mk_BT_{\mathrm{c}}}{2\pi\hbar^2}\right)^{3/2}\varsigma\left(\frac{3}{2}\right)\right]\left[1 - \frac{2g\sqrt{T_{\mathrm{c}}}}{k_B}\left(\frac{Mk_B}{2\pi\hbar^2}\right)^{3/2}\varsigma\left(\frac{1}{2}\right)\right] + \frac{4\pi g^2 T_{\mathrm{c}}^2}{\bar{\mu}k_B}\left(\frac{Mk_B}{2\pi\hbar^2}\right)^3 = 0, \quad (5.44)$$

where $\tilde{\mu}_c$ is the critical chemical potential at the phase transition, whose first-order correction follows from (5.42)

$$\tilde{\mu}_c = 2\tilde{n}(0) = \frac{2g}{\bar{\mu}}\left(\frac{Mk_BT_{\mathrm{c}}}{2\pi\hbar^2}\right)^{3/2}\varsigma\left(\frac{3}{2}\right). \quad (5.45)$$

For our chosen parameters we obtain from solving (5.44) and (5.45) $T_{\mathrm{c}} = 65.71$ nK and $\tilde{\mu}_c = 0.08$, the former agreeing with Fig. 5.5a. The critical temperature can be compared with the first-order correction with respect to g

$$\frac{T_{\mathrm{c}} - T_{\mathrm{c}}^0}{T_{\mathrm{c}}^0} = -1.33\frac{a}{l}N^{1/6}, \quad (5.46)$$

where $T_{\mathrm{c}}^0 = \frac{\hbar\Omega}{k_B}\left(\frac{N}{\varsigma(3)}\right)^{1/3}$ denotes the critical temperature for the non-interacting BEC. Equation (5.46) is obtained by inserting (5.42) and (5.45) into the normalization condition (5.27) and by expanding the result up to the first order with respect to the contact interaction strength g [133,139]. We read off from (5.46) that the repulsive interaction reduces the critical temperature. For our chosen parameters we get $T_{\mathrm{c}}^0 = 71.87$ nK. According to the formula (5.46) the critical temperature for the interacting case has the value $T_{\mathrm{c}} = 70.01$ nK, which is nearly the one obtained above and in Fig. 5.5a. On the other hand the cloud radius $\tilde{R}_{\mathrm{TF2}}$ turns out to increase with the temperature.

In Fig. 5.5b the fractional number of the condensate is defined via $N_0/N = \frac{15}{2}\int_0^{\tilde{R}_{\mathrm{TF1}}}\tilde{r}^2\tilde{n}_0(\tilde{r})\,d\tilde{r}$ and is plotted as a function of the temperature T. We remark that N_0/N equals to one at zero temperature, i.e., all particles are in the condensate, then it decreases with the temperature until it vanishes at T_{c}, marking the end of the superfluid phase and the beginning of the thermal phase. Conversely, the

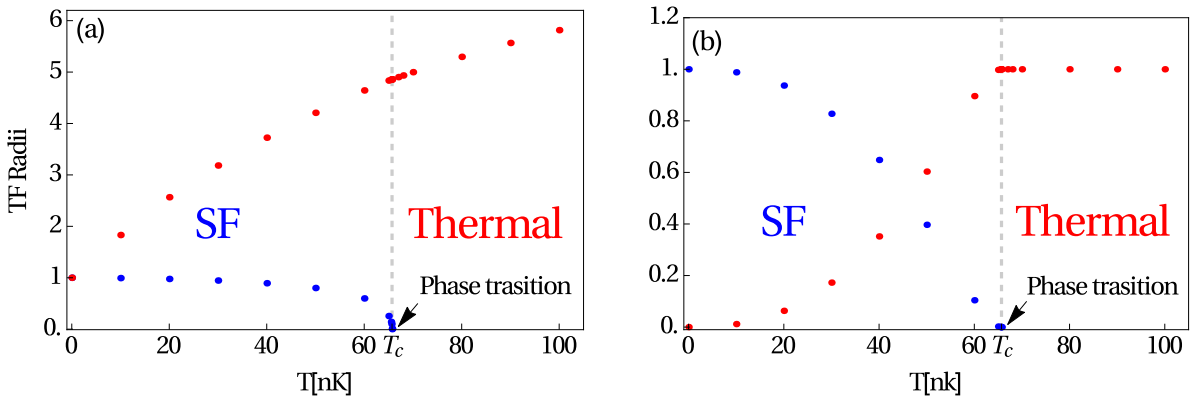

Figure 5.5.: (a) Condensate radius $\tilde{R}_{\mathrm{TF1}}$ (blue) and cloud radius $\tilde{R}_{\mathrm{TF2}}$ (red) and (b) fractional number of condensed particles N_0/N (blue) and in excited states N_{th}/N (red) as function of temperature T.

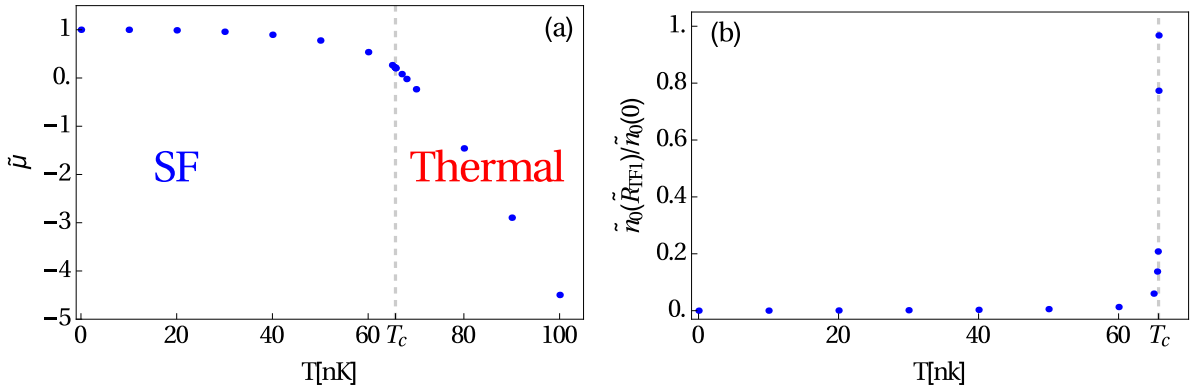

Figure 5.6.: (a) Dimensionless chemical potential $\tilde{\mu}$ and (b) Ratio of $\tilde{n}_0(\tilde{R}_{\mathrm{TF1}})$ and $\tilde{n}_0(0)$ as function of temperature T.

fractional number of the particles in the thermal states $N_{\mathrm{th}}/N = \frac{15}{2}\int_0^{\tilde{R}_{\mathrm{TF2}}} \tilde{r}^2 \tilde{n}_{\mathrm{th}}(\tilde{r})\, d\tilde{r}$, where N_{th} is the number of particles in the excited states, increases with the temperature until being maximal at T_{c}, then it remains constant and equals to one in the thermal phase since all particles are in the excited states.

The influence of the temperature on the chemical potential is shown in Fig. 5.6a. In both the superfluid phase and the thermal phase the chemical potential can only be obtained numerically. The chemical potential decreases with the temperature slowly in the superfluid phase and faster in the thermal phase. In order to know for which temperature range the TF approximation is valid, we plot the ratio of the jump of the condensate density at the condensate radius $\tilde{n}_0(\tilde{R}_{\mathrm{TF1}})$ with respect to the condensate density at the center of the BEC $\tilde{n}_0(0)$ as a function of the temperature in Fig. 5.6b. We remark that this ratio is negligible for $T < T_{\mathrm{c}}$ and has a sudden jump for $T \approx T_{\mathrm{c}}$. This means that the TF approximation is valid in the superfluid phase but not at the transition region, where one would have to go beyond the Thomas-Fermi approximation and take the influence of the kinetic energy in equation (5.24) into account.

5.4. Disordered Case

In this section we consider the BEC system to be in a disordered landscape and at finite temperature. We investigate the effect of both temperature and disorder on the properties of the system, in particular on the respective densities and Thomas-Fermi radii. Thus, we have to solve the dimensionless algebraic equations (5.22), (5.23), (5.25), (5.28) and the normalization condition (5.27).

In the following we distinguish between three different regions: the superfluid region, where the

bosons are distributed in the condensate as well as in the minima of the disorder potential and in the excited states, the Bose-glass region, where there are no bosons in the condensate so that all bosons contribute to the local Bose-Einstein condensates or to the excited states, and the thermal region, where all bosons are in the excited states, see Fig. 1.6. To this end, we treat each region separately. We start first with the thermal region and the Bose-glass region, since they are easier to treat, then we focus on the superfluid region, which is more complicated.

5.4.1. Thermal Region

In the thermal region only the thermal component contributes to the total density, so we have $\tilde{n}_0(\tilde{r}) = \tilde{q}\,(\tilde{r}) = 0$ and $\tilde{n}_{\rm th}\,(\tilde{r}) = \tilde{n}(\tilde{r})$. In this case we need just equation (5.25), which reduces to

$$\tilde{n}_{\rm th}\,(\tilde{r}) = \frac{g}{\bar{\mu}}\left(\frac{M}{2\pi\beta\hbar^2}\right)^{3/2} \varsigma_{\,3/2}\left(e^{\beta\bar{\mu}\ [\tilde{\mu}-2\tilde{n}_{\rm th}(\tilde{r})-\tilde{r}^2]}\right), \tag{5.47}$$

and can be solved only numerically. The cloud radius $\tilde{R}_{\rm TF3}$, which characterizes the end of the thermal region, is determined here by setting $\tilde{n}_{\rm th}\left(\tilde{R}_{\rm TF3}\right) = 10^{-5}$ in equation (5.47).

5.4.2. Bose-Glass Region

In the Bose-glass region the condensate vanishes, i.e., $\tilde{n}_0(\tilde{r}) = 0$, and we need only the self-consistency equations (5.22), (5.23), and (5.25), which reduce to:

$$\tilde{n}(\tilde{r}) = \frac{\tilde{\mu}-\tilde{r}^2}{2}, \tag{5.48}$$

$$\tilde{q}\,(\tilde{r}) = \frac{\tilde{\mu}-\tilde{r}^2}{2} - \frac{g}{\bar{\mu}}\left(\frac{M}{2\pi\beta\hbar^2}\right)^{3/2} \varsigma\left(\frac{3}{2}\right), \tag{5.49}$$

$$\tilde{n}_{\rm th}\,(\tilde{r}) = \frac{g}{\bar{\mu}}\left(\frac{M}{2\pi\beta\hbar^2}\right)^{3/2} \varsigma\left(\frac{3}{2}\right). \tag{5.50}$$

Note that the self-consistency equation (5.50) reveals that the thermal density in the Bose-glass region remains spatially constant, which we consider to be an artifact of the TF approximation. The Bose-glass radius $\tilde{R}_{\rm TF2} = \sqrt{\tilde{\mu} - 2\frac{g}{\bar{\mu}}\left(\frac{M}{2\pi\beta\hbar^2}\right)^{3/2}\varsigma\left(\frac{3}{2}\right)}$, which characterizes the end of the Bose-glass region and the beginning of the thermal region, is determined by setting $\tilde{q}\left(\tilde{R}_{\rm TF_2}\right) = 0$ in equation (5.49).

5.4.3. Superfluid Region

In the superfluid region all densities contribute to the total density and the four algebraic coupled equations (5.22), (5.23), (5.25), and (5.28) have to be taken into account. As a first step, we decouple them in order to get for each density its own self-consistency equation. Inserting equations (5.23), (5.25), and (5.28) into equation (5.22) yields the following self-consistency equation for the total density $\tilde{n}(\tilde{r})$:

$$\tilde{n}\,(\tilde{r}) = \frac{\left[\sqrt{-\tilde{\mu}+2\tilde{n}(\tilde{r})+\tilde{r}^2}+\tilde{d}\right]^3}{\sqrt{-\tilde{\mu}+2\tilde{n}(\tilde{r})+\tilde{r}^2}} + \frac{g}{\bar{\mu}}\left(\frac{M}{2\pi\beta\hbar^2}\right)^{3/2} \varsigma_{\,3/2}\left(e^{\beta\bar{\mu}\ [\tilde{\mu}-2\tilde{n}(\tilde{r})-\tilde{r}^2]}\right). \tag{5.51}$$

From equation (5.28) we deduce the expression of the total density $\tilde{n}(\tilde{r})$ as a function of the condensate density $\tilde{n}_0(\tilde{r})$ as follows:

$$\tilde{n}(\tilde{r}) = \frac{\left[\sqrt{\tilde{n}_0(\tilde{r})}-\tilde{d}\right]^2 + \tilde{\mu} - \tilde{r}^2}{2}. \tag{5.52}$$

This result can be inserted in equation (5.51) in order to get the self-consistency equation for the condensate density $\tilde{n}_0(\tilde{r})$:

$$\left[\sqrt{\tilde{n}_0(\tilde{r})}-\tilde{d}\right]^2+\tilde{\mu}-\tilde{r}^2-\frac{2\tilde{n}_0^{3/2}(\tilde{r})}{\sqrt{\tilde{n}_0(\tilde{r})}-\tilde{d}}-\frac{2g}{\bar{\mu}}\left(\frac{M}{2\pi\beta\hbar^2}\right)^{3/2}\varsigma_{3/2}\left(e^{-\beta\bar{\mu}\left[\sqrt{\tilde{n}_0(\tilde{r})}-\tilde{d}\right]^2}\right)=0. \tag{5.53}$$

Inserting equation (5.52) into equation (5.23) yields a quadratic equation with respect to $\sqrt{\tilde{n}_0(\tilde{r})}$:

$$\tilde{n}_0(\tilde{r})-\frac{\tilde{q}\,(\tilde{r})}{\tilde{d}}\sqrt{\tilde{n}_0(\tilde{r})}+\tilde{q}\,(\tilde{r})=0. \tag{5.54}$$

Since $\sqrt{\tilde{n}_0(\tilde{r})}$ should always be positive, equation (5.54) has just one physical solution:

$$\sqrt{\tilde{n}_0(\tilde{r})}=\frac{\tilde{q}\,(\tilde{r})}{2\tilde{d}}+\frac{1}{2}\sqrt{\frac{\tilde{q}^2\,(\tilde{r})}{\tilde{d}^2}-4\tilde{q}\,(\tilde{r})}. \tag{5.55}$$

Inserting expression (5.55) into equation (5.53) yields the self-consistency equation for the Bose-glass order parameter $\tilde{q}\,(\tilde{r})$:

$$\begin{aligned}&\frac{\tilde{d}^2}{2\tilde{q}^2\,(\tilde{r})}\left[\frac{\tilde{q}\,(\tilde{r})}{2\tilde{d}}+\frac{1}{2}\sqrt{\frac{\tilde{q}^2\,(\tilde{r})}{\tilde{d}^2}-4\tilde{q}\,(\tilde{r})}\right]^4-\frac{\tilde{q}\,(\tilde{r})}{\tilde{d}}\left[\frac{\tilde{q}\,(\tilde{r})}{2\tilde{d}}+\frac{1}{2}\sqrt{\frac{\tilde{q}^2\,(\tilde{r})}{\tilde{d}^2}-4\tilde{q}\,(\tilde{r})}\right]\\&+\frac{\tilde{\mu}-\tilde{r}^2}{2}-\frac{g}{\bar{\mu}}\left(\frac{M}{2\pi\beta\hbar^2}\right)^{3/2}\varsigma_{3/2}\left(e^{-\beta\bar{\mu}\,\frac{\tilde{d}^2}{\tilde{q}^2(\tilde{r})}\left[\frac{\tilde{q}(\tilde{r})}{2\tilde{d}}+\frac{1}{2}\sqrt{\frac{\tilde{q}^2(\tilde{r})}{\tilde{d}^2}-4\tilde{q}(\tilde{r})}\right]^4}\right)=0.\end{aligned} \tag{5.56}$$

Implementing equation (5.25) into equation (5.51) yields the following equation:

$$\begin{aligned}&\left[-\tilde{\mu}+2\tilde{n}(\tilde{r})+\tilde{r}^2\right]^{3/2}+6\tilde{d}\left[-\tilde{\mu}+2\tilde{n}(\tilde{r})+\tilde{r}^2\right]\\&+\left[2\tilde{n}_{\mathrm{th}}\,(\tilde{r})-\tilde{\mu}+\tilde{r}^2+6\tilde{d}^2\right]\sqrt{-\tilde{\mu}+2\tilde{n}(\tilde{r})+\tilde{r}^2}+2\tilde{d}^3=0,\end{aligned} \tag{5.57}$$

which is a cubic equation with respect to the expression $\sqrt{-\tilde{\mu}+2\tilde{n}(\tilde{r})+\tilde{r}^2}$ and can be solved exactly using the Cardan method (see Appendix A). The discriminant $\delta\,(\tilde{r})$ of the cubic equation (5.57) has the form:

$$\begin{aligned}\delta\,(\tilde{r})=&\frac{4}{27}\left\{27\tilde{d}^6+54\tilde{d}^4\left[\tilde{\mu}-2\tilde{n}_{\mathrm{th}}\,(\tilde{r})-\tilde{r}^2\right]+9\tilde{d}^2\left[-\tilde{\mu}+2\tilde{n}_{\mathrm{th}}\,(\tilde{r})+\tilde{r}^2\right]^2\right.\\&\left.-\left[\tilde{\mu}-2\tilde{n}_{\mathrm{th}}\,(\tilde{r})-\tilde{r}^2\right]^3\right\}.\end{aligned} \tag{5.58}$$

For the parameters used later on it turns out to be negative, so equation (5.57) has three real solutions. However, we choose the only that solution which satisfies the condition $\sqrt{-\tilde{\mu}+2\tilde{n}(\tilde{r})+\tilde{r}^2}>0$, which is:

$$\begin{aligned}\sqrt{-\tilde{\mu}+2\tilde{n}(\tilde{r})+\tilde{r}^2}=&\sqrt[3]{\frac{6\tilde{d}^2+\tilde{\mu}-2\tilde{n}_{\mathrm{th}}\,(\tilde{r})-\tilde{r}^2+i\sqrt{-\delta\,(\tilde{r})}}{2}}\\&+\sqrt[3]{\frac{6\tilde{d}^2+\tilde{\mu}-2\tilde{n}_{\mathrm{th}}\,(\tilde{r})-\tilde{r}^2-i\sqrt{-\delta\,(\tilde{r})}}{2}}-2\tilde{d}.\end{aligned} \tag{5.59}$$

Inserting the solution (5.59) into equation (5.25) gives us the self-consistency equation for the thermal density $\tilde{n}_{\mathrm{th}}\,(\tilde{r})$:

$$\tilde{n}_{\mathrm{th}}\,(\tilde{r})=\frac{g}{\bar{\mu}}\left(\frac{M}{2\pi\beta\hbar^2}\right)^{3/2}\varsigma_{3/2}\left(e^{-\beta\bar{\mu}\left[\sqrt[3]{\frac{6\tilde{d}^2+\tilde{\mu}-2\tilde{n}_{\mathrm{th}}(\tilde{r})-\tilde{r}^2+i\sqrt{-\delta(\tilde{r})}}{2}}+\sqrt[3]{\frac{6\tilde{d}^2+\tilde{\mu}-2\tilde{n}_{\mathrm{th}}(\tilde{r})-\tilde{r}^2-i\sqrt{-\delta(\tilde{r})}}{2}}-2\tilde{d}\right]^2}\right). \tag{5.60}$$

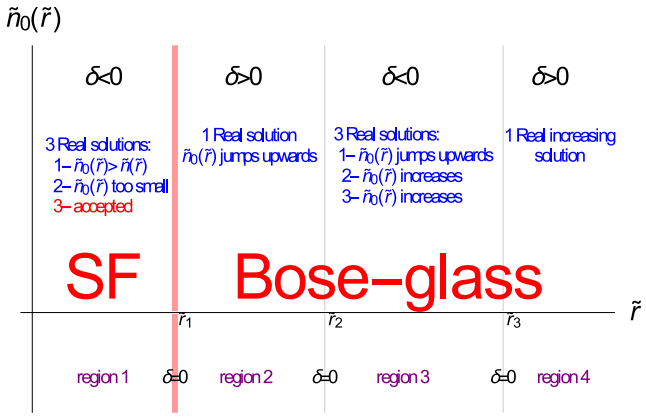

Figure 5.7.: Sign of discriminant δ in equation (5.62), where $\tilde{r}_1$, $\tilde{r}_2$ and $\tilde{r}_3$ are respective roots of equation $\delta = 0$.

Finally we obtained four algebraic decoupled self-consistency equations (5.51), (5.53), (5.56), and (5.60) for the total density $\tilde{n}(\tilde{r})$, the condensate density $\tilde{n}_0(\tilde{r})$, the Bose-glass order parameter $\tilde{q}(\tilde{r})$, and the thermal density $\tilde{n}_{\mathrm{th}}(\tilde{r})$, respectively. We should now solve those equations in order to get the explicit expression of each density as a function of the spatial coordinate. All those self-consistency equations (5.51), (5.53), (5.56) and (5.60) contain the polylogarithmic function $\varsigma_{3/2}$ which makes them impossible to solve analytically. Therefore, we solve them numerically, but we obtain non-physical oscillating densities around the first transition region, which separates the superfluid region from the Bose-glass region due to the Poisson sum formula (2.144) as already explained above equation (5.35). Thus, in view of an analytic treatment, we apply again the Robinson formula (5.35). Note that it is not necessary to solve all the self-consistency equations (5.51), (5.53), (5.56) and (5.60), it is enough to solve one of them and to insert the result into other algebraic equations. In the following we choose to solve for the condensate density $\tilde{n}_0(\tilde{r})$.

At the transition boundary the condensate density $\tilde{n}_0(\tilde{r})$ reaches its minimal value, so from equation (5.28) we deduce that the quantity $\tilde{\mu} - 2\tilde{n}(\tilde{r}) - \tilde{r}^2$ goes to zero. Thus, we can approximate the polylogarithmic function with the help of the Robinson formula (5.35) as follows:

$$\varsigma_{3/2}\left(e^{-\beta\bar{\mu}\left[\sqrt{\tilde{n}_0(\tilde{r})}-\tilde{d}\right]^2}\right) \approx \Gamma\left(-\frac{1}{2}\right)\sqrt{\beta\bar{\mu}}\left[\sqrt{\tilde{n}_0(\tilde{r})}-\tilde{d}\right]+\varsigma\left(\frac{3}{2}\right)-\beta\bar{\mu}\left[\sqrt{\tilde{n}_0(\tilde{r})}-\tilde{d}\right]^2\varsigma\left(\frac{1}{2}\right). \quad (5.61)$$

Using approximation (5.61), equation (5.53), which determines the condensate density, can be rewritten approximatively as follows:

$$\begin{aligned} 0 = &\left[\sqrt{\tilde{n}_0(\tilde{r})}-\tilde{d}\right]^3\left[1-2g\beta\left(\frac{M}{2\pi\beta\hbar^2}\right)^{3/2}\varsigma\left(\frac{1}{2}\right)\right]+2\left[g\left(\frac{M}{2\pi\beta\hbar^2}\right)^{3/2}\Gamma\left(-\frac{1}{2}\right)\sqrt{\beta/\bar{\mu}}+3\tilde{d}\right] \\ &\times\left[\sqrt{\tilde{n}_0(\tilde{r})}-\tilde{d}\right]^2+\left[2\frac{g}{\bar{\mu}}\left(\frac{M}{2\pi\beta\hbar^2}\right)^{3/2}\varsigma\left(\frac{3}{2}\right)+6\tilde{d}^2-\tilde{\mu}+\tilde{r}^2\right]\left[\sqrt{\tilde{n}_0(\tilde{r})}-\tilde{d}\right]+2\tilde{d}^3, \end{aligned} \quad (5.62)$$

which is a cubic equation with respect to $\sqrt{\tilde{n}_0(\tilde{r})}$.

Still we have to rewrite the other densities as functions of the condensate density $\tilde{n}_0(\tilde{r})$. To this end we insert equation (5.52) into equation (5.23), which yields:

$$\tilde{q}(\tilde{r}) = \frac{\tilde{d}\tilde{n}_0(\tilde{r})}{\sqrt{\tilde{n}_0(\tilde{r})}-\tilde{d}}. \quad (5.63)$$

Inserting (5.52) into (5.25) and applying the Robinson formula (5.61) yields

$$\tilde{n}_{\mathrm{th}}(\tilde{r}) = \frac{g}{\bar{\mu}}\left(\frac{M}{2\pi\beta\hbar^2}\right)^{3/2}\left\{\Gamma\left(-\frac{1}{2}\right)\sqrt{\beta\bar{\mu}}\left[\sqrt{\tilde{n}_0(\tilde{r})}-\tilde{d}\right]+\varsigma\left(\frac{3}{2}\right)-\beta\bar{\mu}\left[\sqrt{\tilde{n}_0(\tilde{r})}-\tilde{d}\right]^2\varsigma\left(\frac{1}{2}\right)\right\}. \quad (5.64)$$

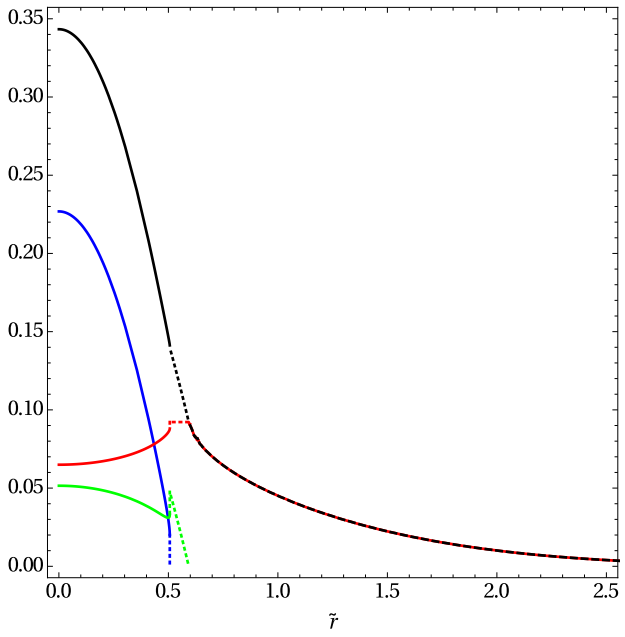

Figure 5.8.: Total density $\tilde{n}(\tilde{r})$ (black), condensate density $\tilde{n}_0(\tilde{r})$ (blue), Bose-glass order parameter $\tilde{q}(\tilde{r})$ (green), and thermal density $\tilde{n}_{\mathrm{th}}(\tilde{r})$ (red) as functions of the radial coordinate $\tilde{r}$, for $\tilde{d} = 0.088$ for superfluid region (solid lines), Bose-glass region (dotted lines), and thermal region (dashed lines). Since N is fixed, $\tilde{\mu}$ can be deduced and results in $\tilde{\mu} = 0.535$.

Now we can solve the cubic self-consistency equation for the condensate density (5.62) via the Cardan method (see Appendix A) and insert the solution into equations (5.52), (5.63), and (5.64) in order to get directly $\tilde{n}(\tilde{r})$, $\tilde{q}(\tilde{r})$, and $\tilde{n}_{\mathrm{th}}(\tilde{r})$, respectively.

The cubic equation (5.62) is characterized by a discriminant δ whose sign determines the number and the kind of the solutions, i.e., whether they are real or complex. This method allows us to get a unique physical solution for the equation (5.62) as it is shown in detail in Fig. 5.7 for the condensate density $\tilde{n}_0(\tilde{r})$. Figure 5.7 shows that there are four different spatial regions, where we have to look for the solutions of equation (5.62). Those regions are characterized by the sign of the discriminant δ being positive or negative and are separated with borders, where the discriminant δ vanishes. After performing an analysis similar to the one in Fig. 4.3, we conclude that equation (5.62) has only one physical solution in the first region, where the discriminant δ is negative. This means that the first region coincides with the superfluid region and outside we have the Bose-glass region as well as the thermal region. In order to determine the border of the superfluid region, i.e., the condensate radius $\tilde{R}_{\mathrm{TF1}}$, where the solution of equation (5.62) vanishes and which characterizes the end of the superfluid region as well as the beginning of the Bose-glass region, we derive equation (5.62) with respect to $\tilde{n}_0(\tilde{r})$, then we set $\left.\frac{\partial \tilde{r}}{\partial \tilde{n}_0(\tilde{r})}\right|_{\tilde{r}=\tilde{R}_{\mathrm{TF}_1}} = 0$, which yields:

$$3\left[\sqrt{\tilde{n}_0\left(\tilde{R}_{\mathrm{TF1}}\right)}-\tilde{d}\right]^2\left[1-2g\beta\left(\frac{M}{2\pi\beta\hbar^2}\right)^{3/2}\varsigma\left(\frac{1}{2}\right)\right]+4\left[g\left(\frac{M}{2\pi\beta\hbar^2}\right)^{3/2}\Gamma\left(-\frac{1}{2}\right)\sqrt{\beta/\bar{\mu}}+3\tilde{d}\right]$$
$$\times\left[\sqrt{\tilde{n}_0\left(\tilde{R}_{\mathrm{TF1}}\right)}-\tilde{d}\right]+\left[2\frac{g}{\bar{\mu}}\left(\frac{M}{2\pi\beta\hbar^2}\right)^{3/2}\varsigma\left(\frac{3}{2}\right)+6\tilde{d}^2-\tilde{\mu}+\tilde{R}_{\mathrm{TF1}}^2\right]=0, \tag{5.65}$$

The result (5.65) is inserted again into equation (5.62) in order to get the analytical expression of the condensate radius $\tilde{R}_{\mathrm{TF1}}$. As the final formula for $\tilde{R}_{\mathrm{TF1}}$ is too involved, it is not displayed here.

5.4.4. Thomas-Fermi Densities

In this Section we perform our study for ^{87}Rb atoms and for the following experimentally realistic parameters: $N = 10^6$, $\Omega = 100\,\mathrm{Hz}$, and $a = 5.29\,\mathrm{nm}$. For those parameters the oscillator length reads $l = 2.72\,\mu\mathrm{m}$, the coherence length turns out to be $\xi = 348.89\,\mathrm{nm}$, and the Thomas-Fermi radius is given by $R_{\mathrm{TF}} = 21.29\,\mu\mathrm{m}$, so the assumption $\xi \ll R_{\mathrm{TF}}$ for the TF approximation is, indeed, fulfilled.

Using those parameter values and choosing the temperature to be $T = 60$ nK as well as the dimensionless disorder strength $\tilde{d} = 0.088$ we solve for the superfluid region equation (5.62) for the condensate density $\tilde{n}_0(\tilde{r})$ and insert the result into equations (5.52), (5.63), and (5.64) in order to get the other densities $\tilde{n}(\tilde{r})$, $\tilde{q}(\tilde{r})$, and $\tilde{n}_{\mathrm{th}}(\tilde{r})$, respectively. This has to be combined with equation (5.47) for the thermal region as well as equations (5.48)–(5.50) for the Bose-glass region. After that we fix the chemical potential $\tilde{\mu}$ using the normalization condition (5.27), where the total density $\tilde{n}(\tilde{r})$ is the combination of the total densities from the superfluid region, the Bose-glass region, and the thermal region according to (5.34). The resulting densities are combined and plotted in Fig. 5.8, where in the superfluid region the densities are plotted with solid lines, in the Bose-glass region with dotted lines, and in the thermal region with dashed lines.

Figure 5.8 shows that the condensate density $\tilde{n}_0(\tilde{r})$ is maximal at the center of the cloud, then it decreases until attending its minimum at the condensate radius $\tilde{R}_{\mathrm{TF1}} = 0.506$. The Bose-glass order parameter $\tilde{q}(\tilde{r})$ is also maximal in the center of the cloud, it decreases until the condensate radius $\tilde{R}_{\mathrm{TF1}}$, where is jumps upward, then it decreases until attending its minimum at the Bose-glass radius $\tilde{R}_{\mathrm{TF2}} = 0.588$. The thermal density $\tilde{n}_{\mathrm{th}}(\tilde{r})$ is behaving differently: it is increasing until attending its maximum at the condensate radius $\tilde{R}_{\mathrm{TF1}}$, it stays constant until the Bose-glass radius $\tilde{R}_{\mathrm{TF2}}$, then it decreases exponentially to zero. Note that in the thermal region the thermal density coincides with the total density. The fact that the thermal density remains constant in the Bose-glass region is an artifact of the TF approximation. The total density $\tilde{n}(\tilde{r})$ is maximal in the center of the trap and decreases when we move away from the center until it vanishes at the cloud radius $\tilde{R}_{\mathrm{TF3}} = 4.642$. We note also that, at the condensate radius $\tilde{R}_{\mathrm{TF1}}$, a downward jump of the condensate density $\tilde{n}_0(\tilde{r})$, an upward jump of the Bose-glass order parameter $\tilde{q}(\tilde{r})$, and an upward jump of the thermal density $\tilde{n}_{\mathrm{th}}(\tilde{r})$ occur in such a way that the total density $\tilde{n}(\tilde{r})$ remains continuous but reveals a discontinuity of the first derivative. The Thomas-Fermi approximation captures the properties of the system within the superfluid region, the Bose-glass region, and the thermal region but not in the transition between two regions, namely, between the superfluid region and the Bose-glass region and between the Bose-glass region and the thermal region. This represents another artifact of the applied TF approximation.

In the following we investigate separately the impact of increasing the temperature T and the disorder strength $\tilde{d}$ on the properties of the dirty boson system, namely, the Thomas-Fermi radii, the chemical potential, and the fractional number of condensed particles N_0/N, in the disconnected local minicondensates Q/N, and in the excited states N_{th}/N.

5.4.5. Temperature Influence

We start first with studying the influence of the temperature on the dirty boson system. To this end, we fix the disorder strength to be $\tilde{d} = 0.088$ and increase the temperature T. The Thomas-Fermi radii, namely, the condensate radius $\tilde{R}_{\mathrm{TF1}}$, the Bose-glass radius $\tilde{R}_{\mathrm{TF2}}$, and the cloud radius $\tilde{R}_{\mathrm{TF3}}$, are plotted as functions of the temperature T in Fig. 5.9. Figure 5.9a shows that both the condensate radius $\tilde{R}_{\mathrm{TF1}}$ and the Bose-glass radius $\tilde{R}_{\mathrm{TF2}}$ decrease with the temperature T until they vanish. The blow-up in Fig. 5.9b reveals that the condensate radius $\tilde{R}_{\mathrm{TF1}}$ vanishes at $T_{\mathrm{c}_1} = 64.625$ nK, which corresponds to a phase transition from the superfluid to the Bose-glass phase. This critical value of the temperature is obtained by setting the condensate radius $\tilde{R}_{\mathrm{TF1}}$ to be zero. The Bose-glass radius $\tilde{R}_{\mathrm{TF2}}$ vanishes at $T_{\mathrm{c}_2} = 65.625$ nK, which corresponds to a phase transition from the Bose-glass phase to the thermal phase. This critical value of the temperature is obtained by setting the Bose-glass radius $\tilde{R}_{\mathrm{TF2}}$ to zero. The existence of two phase transitions means that we are qualitatively above the triple point introduced in Fig. 5.2. Note that the difference of both critical temperatures $\triangle T_{\mathrm{c}} = T_{\mathrm{c}_2} - T_{\mathrm{c}_1}$ is quite small, which is expected, since from (5.47) one can deduce that the shift $\triangle T$ goes quadratic with the disorder strength $\tilde{d}$, which means that the linear temperature shift vanishes in agreement with

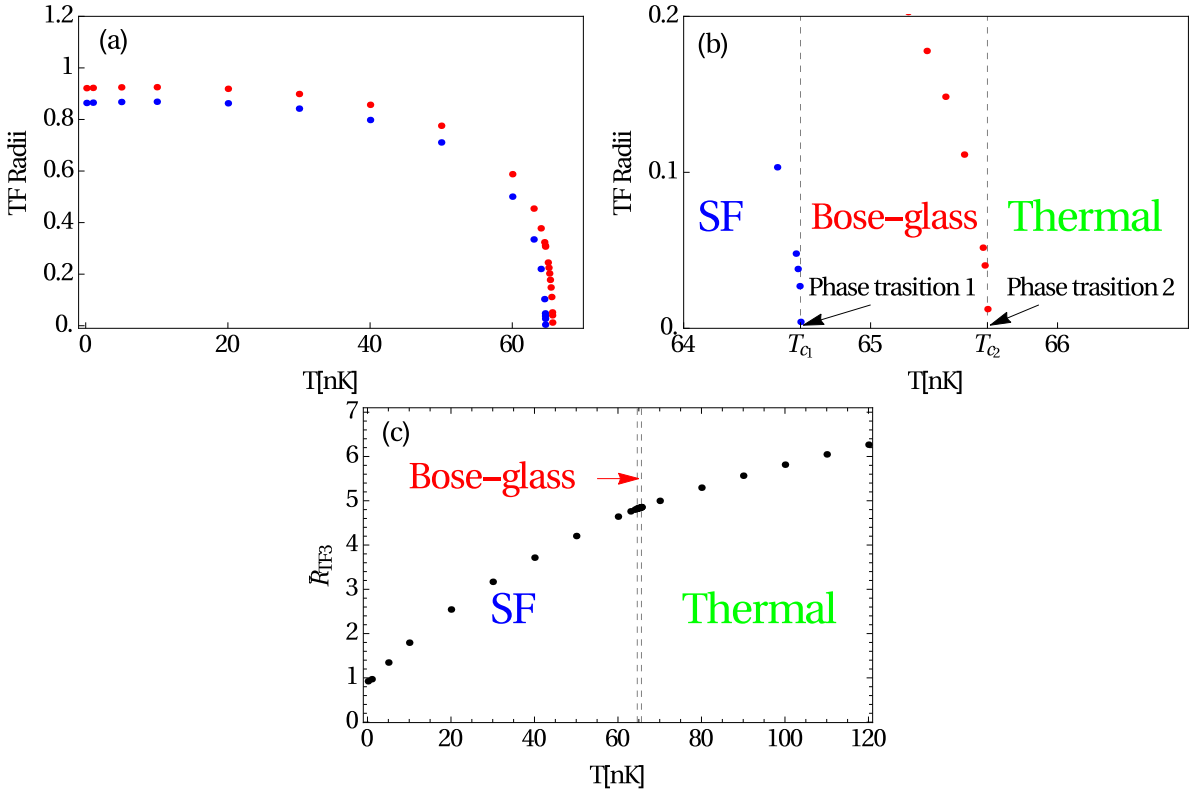

Figure 5.9.: (a) Condensate radius $\tilde{R}_{\mathrm{TF1}}$ (blue) and Bose-glass radius $\tilde{R}_{\mathrm{TF2}}$ (red), (b) blow-up of Bose-glass phase, and (c) cloud radius $\tilde{R}_{\mathrm{TF3}}$ (black) as functions of temperature T.

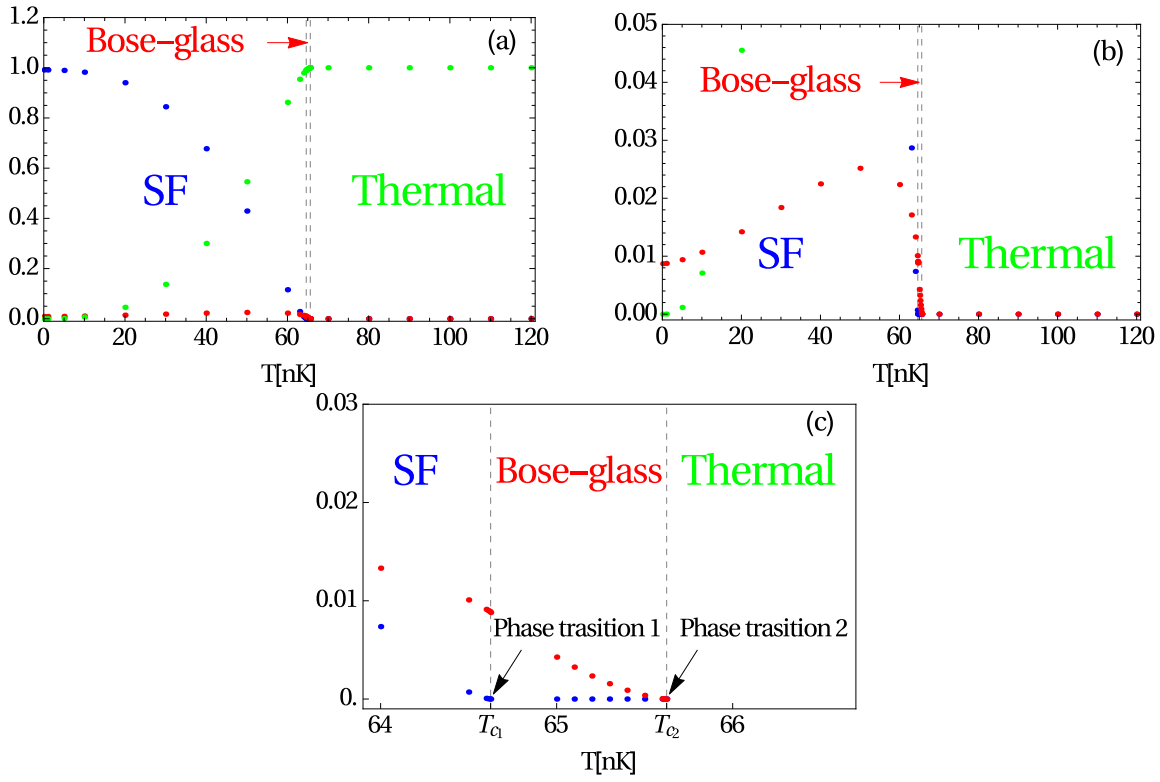

Figure 5.10.: (a) Fractional number of condensed particles N_0/N (blue), in disconnected local mini-condensates Q/N (red), and in excited states N_{th}/N (green), (b) blow-up of fractional number Q/N, and (c) blow-up of Bose-glass phase as functions of temperature T.

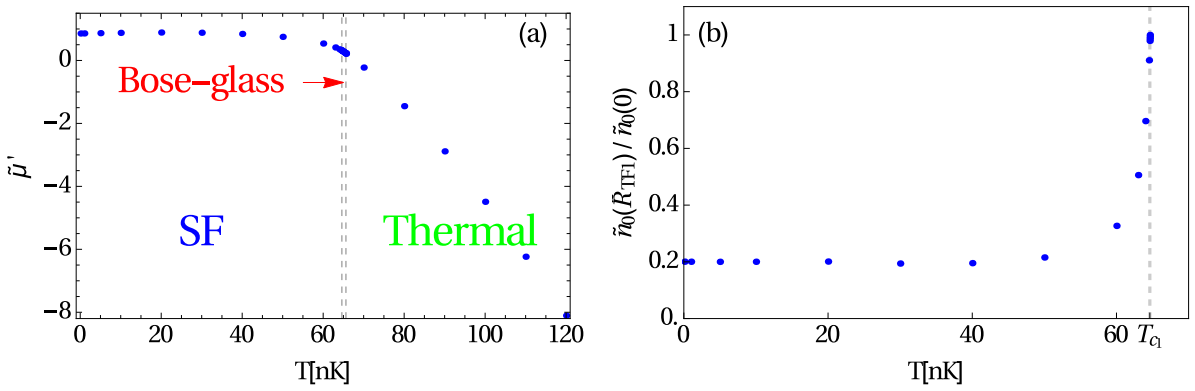

Figure 5.11.: (a) Dimensionless chemical potential $\tilde{\mu}' = \frac{\mu}{\tilde{\mu}}$ and (b) ratio $\tilde{n}_0(\tilde{R}_{\mathrm{TF1}})/\tilde{n}_0(0)$ as functions of temperature T.

Ref. [140]. Contrarily, the cloud radius $\tilde{R}_{\mathrm{TF3}}$ increases with the temperature T in Fig 5.9c.

The fractional number of the condensate $N_0/N = \frac{15}{2}\int_0^{\tilde{R}_{\mathrm{TF1}}} \tilde{r}^2\tilde{n}_0(\tilde{r})\,d\tilde{r}$, in the disconnected minicondensates $Q/N = \frac{15}{2}\int_0^{\tilde{R}_{\mathrm{TF2}}} \tilde{r}^2\tilde{q}(\tilde{r})\,d\tilde{r}$, and in the excited states $N_{\mathrm{th}}/N = \frac{15}{2}\int_0^{\tilde{R}_{\mathrm{TF3}}} \tilde{r}^2\tilde{n}_{\mathrm{th}}(\tilde{r})\,d\tilde{r}$ are plotted in Fig. 5.10a as functions of the temperature T. We remark that in the superfluid phase N_0/N decreases with the temperature T until vanishing at the critical T_{c_1} marking the end of the superfluid phase and the beginning of the Bose-glass phase as is illustrated in the blow-up in Fig 5.10c. Conversely, in Fig 5.10b the fraction Q/N increases with the temperature T until being maximal at about $T = 50$ nK, then decreases until vanishing at the critical temperature T_{c_2} marking the end of the Bose-glass phase and the beginning of the thermal phase as it is shown in the blow-up in Fig 5.10c. In Fig. 5.10a the fraction N_{th}/N increases starting from zero with the temperature T until being equal to one at the critical temperature T_{c_2}, then it remains constantly equal to one. We conclude that with increasing the temperature until about $T = 50$ nK, more and more particles are leaving the condensate towards the local minicondensates or the excited states. For the temperature range $50\ \mathrm{nK} < T < T_{c_1}$ the particles are leaving both the condensate and the local minicondensates towards the excited states. When the condensate vanishes at the critical temperature T_{c_1}, the particles keep leaving the local minicondensates towards the excited states until the critical temperature T_{c_2}, where all particles are in the excited states.

The influence of the temperature on the chemical potential is shown in Fig. 5.11a. In the three phases, namely, the superfluid phase, the Bose-glass phase, and the thermal phase , the chemical potential can be obtained only numerically via the normalization condition (5.27). It decreases with the temperature T slowly in the superfluid phase and faster in the Bose-glass as well as the thermal phase.

In order to know for which range of the temperature T the TF approximation is valid, we plot the ratio of the jump of the condensate density at the Thomas-Fermi condensate radius $\tilde{n}_0(\tilde{R}_{\mathrm{TF}_1})$ with respect to the condensate density at the center of the BEC $\tilde{n}_0(0)$ as a function of the temperature T in Fig. 5.11b. We remark that this ratio is negligible for $T < T_{c_1}$ and has a sudden jump for $T \approx T_c$. This means that the TF approximation is valid in the superfluid phase but not at the transition region from the superfluid to the Bose-glass phase, where one would have to go beyond the TF approximation and take the influence of the kinetic energy in equation (5.24) into account.

5.4.6. Disorder Influence

Now we study the influence of increasing the disorder strength $\tilde{d}$ on the dirty boson system for the fixed temperature $T = 60$ nK. The influence of the disorder on the chemical potential is shown in Fig. 5.12a. In both the superfluid phase and the Bose-glass phase the chemical potential can be obtained only numerically via the normalization condition (5.27). In the weak disorder regime, located in the superfluid phase, the chemical potential decreases with the disorder strength $\tilde{d}$, then in the intermediate and strong disorder regime, located partially in the superfluid phase and in the Bose-

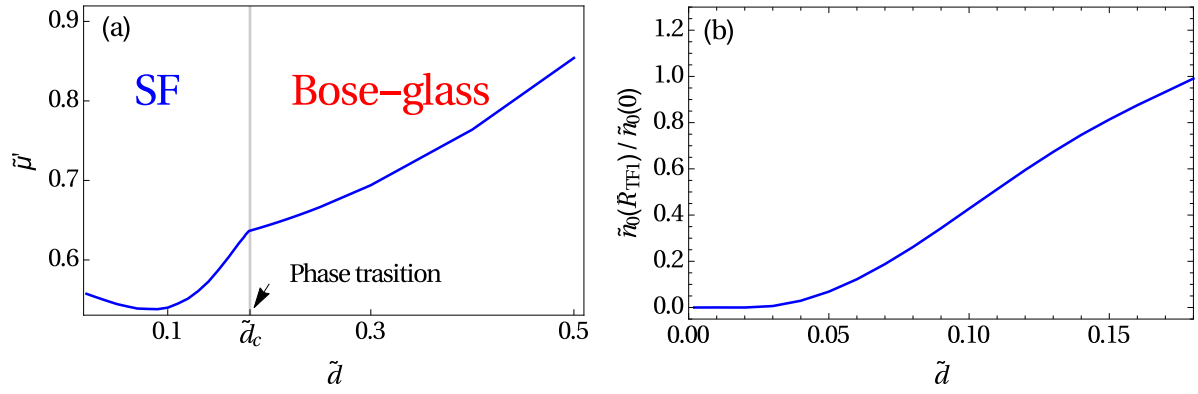

Figure 5.12.: (a) Dimensionless chemical potential $\tilde{\mu}' = \frac{\mu}{\tilde{\mu}}$ and (b) ratio $\tilde{n}_0(\tilde{R}_{\rm TF1})/\tilde{n}_0(0)$ as functions of disorder strength $\tilde{d}$.

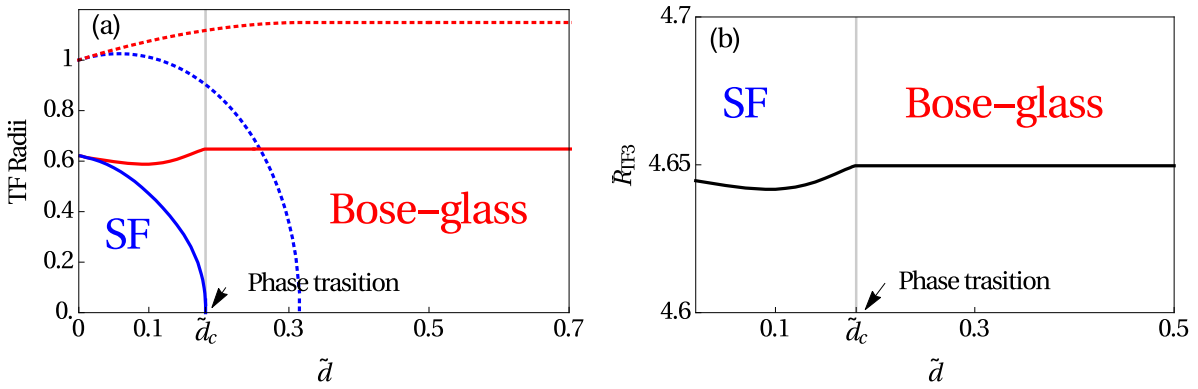

Figure 5.13.: (a) Condensate radius $\tilde{R}_{\rm TF1}$ at $T = 60$ nK (solid, blue) and at $T = 0$ (dotted, blue), Bose-glass radius $\tilde{R}_{\rm TF2}$ at $T = 60$ nK (solid, red) and at $T = 0$ (dotted, red) and (b) cloud radius $\tilde{R}_{\rm TF3}$ at $T = 60$ nK (solid, black) as functions of disorder strength $\tilde{d}$.

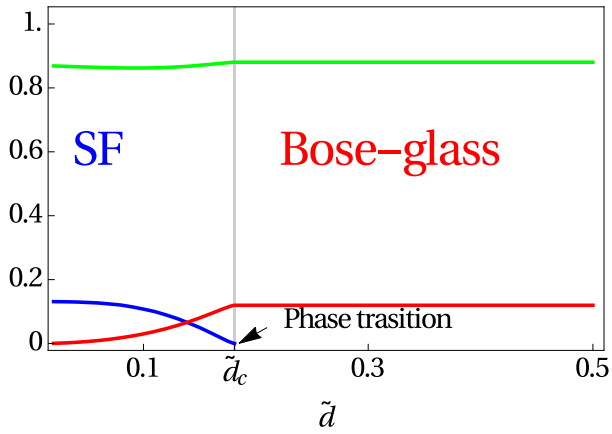

Figure 5.14.: Fractional number of condensed particles N_0/N (blue), in disconnected local miniconden-sates Q/N (red), and in excited states $N_{\rm th}/N$ (green), as functions of disorder strength $\tilde{d}$.

glass phase, it increases with the disorder strength $\tilde{d}$ with a discontinuity of the first derivative at the critical disorder $\tilde{d}_c = 0.181$. This is due to the combined effect of disorder and temperature. According to the zero-temperature result in Fig. 4.7a the chemical potential increases with the disorder strength $\tilde{d}$, while the clean result in Fig. 5.6a reveals that the chemical potential decreases with the temperature T. Thus, in the weak disorder regime the influence of the temperature on the bosonic system is stronger than the influence of the disorder potential, which makes the chemical potential to decrease with the disorder strength. In the intermediate and strong disorder regime the disorder turns out to have a stronger influence on the dirty boson system than the temperature, which makes the chemical potential increase with the disorder strength.

In order to know for which range of the disorder strength $\tilde{d}$ the TF approximation is valid, we plot the ratio of the jump of the condensate density at the Thomas-Fermi condensate radius $\tilde{n}_0(\tilde{R}_{\mathrm{TF}_1})$ with respect to the condensate density at the center of the BEC $\tilde{n}_0(0)$ as a function of the disorder strength $\tilde{d}$ in Fig. 5.12b. As only a moderate density jump of about 50% should be reasonable, our approach is restricted to a dimensionless disorder strength of about $\tilde{d} \simeq 0.11$. For larger disorder strength $\tilde{d}$ one would have to go beyond the TF approximation and take the influence of the kinetic energy in (5.24) into account.

The Thomas-Fermi radii, namely, the condensate radius $\tilde{R}_{\mathrm{TF1}}$, the Bose-glass radius $\tilde{R}_{\mathrm{TF2}}$, and the cloud radius $\tilde{R}_{\mathrm{TF3}}$, are plotted as functions of the disorder strength $\tilde{d}$ in Fig. 5.13. According to the behavior of the Thomas-Fermi radii, we distinguish two different disorder regimes, namely, the weak disorder regime and the intermediate one. The existence of those two different regimes is due to the combined effect of disorder and temperature as already explained above for the chemical potential. Figure 5.13a shows that, when the disorder strength $\tilde{d}$ increases, the condensate radius $\tilde{R}_{\mathrm{TF1}}$ increases barely, then decreases until being zero, which corresponds to a phase transition at about $\tilde{d}_c = 0.181$. This critical value of the disorder strength is obtained by setting the cloud radius $\tilde{R}_{\mathrm{TF1}}$ to zero. Thus, superfluidity is destroyed in our model at a critical disorder strength, where approximately our TF approximation breaks down. Contrarily, the Bose-glass radius $\tilde{R}_{\mathrm{TF2}}$ decreases when the disorder strength $\tilde{d}$ increases in the weak disorder regime, then increases in the intermediate disorder regime until the phase transition, then it becomes constant, so that the bosonic cloud has a maximal Bose-glass radius of $\lim_{\tilde{d}\to\infty} \tilde{R}_{\mathrm{TF2}} = 0.647$. Figure 5.13a shows also that in the weak disorder regime the condensate radius $\tilde{R}_{\mathrm{TF1}}$ and the Bose-glass radius $\tilde{R}_{\mathrm{TF2}}$ coincide, i.e., there is no Bose-glass region, only the superfluid and the thermal regions coexist. Furthermore, the comparison of the condensate radius $\tilde{R}_{\mathrm{TF1}}$ and the Bose-glass radius $\tilde{R}_{\mathrm{TF2}}$ at finite temperature with the ones at zero temperature, respectively, reveals that increasing the temperature decreases the critical disorder strength value $\tilde{d}_c$, where the phase transition is taking place. In Fig 5.13b the cloud radius $\tilde{R}_{\mathrm{TF3}}$ decreases with the disorder strength $\tilde{d}$ in the weak disorder regime, then increases with it in the intermediate disorder regime until becoming constant at the phase transition, so that the bosonic cloud has a maximal size of $\lim_{\tilde{d}\to\infty} \tilde{R}_{\mathrm{TF3}} = 4.649$.

In Fig. 5.14 the fractional number of the condensate N_0/N, in the disconnected minicondensates Q/N, and in the excited states N_{th}/N are plotted as functions of the disorder strength $\tilde{d}$. We remark that in the superfluid phase N_0/N decreases with the disorder strength $\tilde{d}$ until vanishing at $\tilde{d}_c$ marking the end of the superfluid phase and the beginning of the Bose-glass phase. Conversely, Q/N and N_{th}/N increase with the disorder strength $\tilde{d}$, i.e., more and more particles are leaving the condensate towards the local minicondensates or the excited states. In the Bose-glass phase, both fractions Q/N and N_{th}/N remain constant.

6. Summary and Outlook

The dirty boson problem represents a challenging quantum many-body system due to the combined effect of disorder and two-particle interaction, which can lead to localization and superfluidity. A quite recent non-perturbative investigation of the dirty boson problem was worked out in Ref. [84], where the model of a three-dimensional weakly interacting homogeneous Bose gas in a delta-correlated disorder potential at finite temperature was studied within the Hartree-Fock mean-field theory by applying the Parisi replica method. The major result was to qualitatively locate the superfluid, the Bose-glass, and the normal phase in the disorder-temperature phase diagram. To this end a Bose-glass order parameter was introduced in close analogy to the Edwards-Anderson order parameter of spin glasses, which quantifies in the disorder ensemble average the number of bosons being localized in the respective minima of the random landscape. Motivated by this, we extended in our thesis the theory of Ref. [84] to the experimentally relevant trapped confinement and to a general number of spatial dimensions and applied it to the quasi one-dimensional and to the three-dimensional dirty BEC.

6.1. Summary

Our thesis begun with **Chapter 1**, where we briefly discussed the experimental and theoretical history of BEC in general and the physics of dirty bosons in particular. In **Chapter 2** we followed Ref. [97], where we described at first the underlying dirty BEC model, and showed that the disorder ensemble average of the grand-canonical free energy could be calculated by using the Parisi replica method. This led to the replicated action (2.25), where the disorder-induced interaction turns out to be nonlocal in both space and time. After that we made use of the Bogoliubov approximation (2.27), where we split the Bose fields into their background, which stands for the condensate wave function, and the fluctuations describing the non-condensed fraction. Furthermore, we assumed replica symmetry, i.e., we treated all replica fields in the replicated action (2.25) on equal footing and we applied the semiclassical approximation due to the harmonic trapping confinement. In Section 2.6, we specialized the general formalism to a delta-correlated disorder potential and to a contact interaction potential. We physically interpreted the order parameters of our theory as off-diagonal long-range orders of certain correlation functions. In this way we showed that the condensate density as the superfluid order parameter is related to the 2-point correlation (2.114), whereas the Bose-glass order parameter follows from the 4-point correlation (2.115). In this way, and after applying the replica limit, we were able to derive the grand-canonical free energy (2.126) as well as the corresponding self-consistency equations (2.89)–(2.92) of the dirty boson model for a general spatial dimension. Finally, we specialized our formalism to three dimensions in Section 2.10 and to one dimension in Section 2.11. In the latter case we had to restrict ourselves to zero temperature due to the limitation of the Cardan method, which was introduced in Appendix A. Note that the two-dimensional case is not treated here, since the Hartree-Fock mean-field theory turned out to diverge in two dimensions, which warrants both a regularization and a renormalization and, thus, lies out of the scope of the present thesis.

Chapter 3 followed Ref. [98] and investigated analytically and numerically the quasi one-dimensional dirty BEC at zero temperature. The preliminary treatment of the homogeneous case in Section 3.1 revealed a qualitative compatibility with the Huang-Meng theory [64] in the weak disorder regime, where the Bose-glass order parameter is linearly proportional to the disorder strength. After having treated the homogeneous case, we investigated the trapped one via three different approaches. Due to the nonlinearity of the generalized Gross-Pitaevskii (GP) equation (3.17), the first approach in Section 3.2 is based on applying the Thomas-Fermi (TF) approximation to the underlying set of self-consistency equations. We had to distinguish between two different regions, namely, the superfluid and the Bose-glass one, and treated both separately. In addition, it turned out that the range of validity of

the TF approximation is restricted to weak disorder. We corroborated the analytical treatment with a second numerical approach in Section 3.3, where we generated the random potential according to Eq. (3.34) and inserted it into the corresponding time-independent GP equation (3.33) of the dirty boson model. After solving the latter equation using a C program [126], we performed the disorder ensemble averages of the wave function as well as identified its first and second cumulant with the condensate density and the Bose-glass order parameter, respectively. In Section 3.4 we compared the Thomas-Fermi approximated densities and their radii with the numerical ones in Figs. 3.15–3.17. This confirmed the fact that the mini-condensates in the local minima of the random potential occur for weak disorder preferentially at the border of the condensate and that the TF approximation is only valid in the weak disorder regime, especially in the center of the trap. This motivated us to perform in Section 3.5, for the intermediate disorder regime, a third variational approach within the ansatz (3.42)–(3.44), where we optimized width and particle number in the global condensate and the local mini-condensates. The final comparison between the three approaches, namely, the TF approximation, the numerics, and the variational method in Section 3.6 yielded the conclusion that there is no quantum phase transition between the superfluid and the Bose-glass phase in the weak and intermediate disorder regime in one dimension. Furthermore, we concluded that the variational method within the ansatz (3.42)–(3.44) describes well the intermediate disorder regime especially at the border of the trap, and that the mini-condensates in the local minima of the random potential occur for intermediate disorder strength preferentially in the trap center according to the TF approximation. So the combination of those two analytical methods covered a significant range of the disorder strengths and allowed us to understand the numerically observed redistribution of the local mini-condensates in the trap.

Chapter 4 investigated the three-dimensional dirty boson system at zero temperature [99], where the thermal density vanishes. The preliminary treatment of the homogeneous case in Section 4.1 revealed in Fig. 4.1 the existence of a first-order quantum phase transition from the superfluid phase to the Bose-glass phase at a critical disorder strength, which qualitatively agrees with Ref. [83]. The qualitative compatibility with the Huang-Meng theory [64] was proven in the weak disorder regime, where the Bose-glass order parameter is linearly proportional to the disorder strength. On the basis of the homogeneous case we dealt with the harmonically trapped confinement in Section 4.2 by applying the TF approximation to the corresponding self-consistency equations obtained via the Hartree-Fock mean-field theory (4.12)–(4.14). Then we specialized to an isotropic trap in Section 4.2, where we distinguished between two regions in Fig. 4.4, namely, the superfluid and the Bose-glass region, which were treated separately. The TF approximation turned out to give better results in three dimensions than in one dimension due to the fact that the fluctuations are more virulent in lower dimensions. In analogy with the one-dimensional case treated in Chapter 3, we additionally inserted a variational ansatz (4.29)–(4.31) for the three-dimensional dirty BEC into the corresponding free energy (4.28). The respective densities and their radii obtained via the TF approximation and the variational method were compared in Subsection 4.3.5 and turned out to coincide qualitatively contrary to the one-dimensional case. In particular, in both cases a first-order quantum phase transition from the superfluid phase to the Bose-glass phase is detected in Fig. 4.15 at critical disorder strengths, whose values are of the same order as the one given by Ref. [83].

After that we made in Subsection 4.3.6 a detailed qualitative comparison between the one-dimensional results obtained in Chapter 3 and the three-dimensional ones obtained in Chapter 4. In particular, the Bose-glass region in three dimensions is located in the center of the trap, while in one dimension it is situated in the border of the trap in the weak disorder regime and in the center in the intermediate disorder regime. Furthermore, we found a quantum phase transition from superfluid to Bose-glass phase in three dimensions in the intermediate disorder regime. But in one dimension this phase transition could not be detected neither in the weak nor in the intermediate disorder regime. In order to be able to see the phase transition, the disorder has to overcome the interaction, which is possible only in the strong disorder regime and this is beyond the scope of this thesis.

Considering an anisotropic trap potential in Section 4.4 we found out in Fig. 4.18 that the cuts of each density along the respective axis are proportional to each other. We remarked also the same proportionality between the corresponding Thomas-Fermi radii in Fig. 4.19, which turned out to depend on the trap aspect ratios.

In **Chapter 5** we considered the three-dimensional BEC system to be at finite temperature [99]. We restricted ourselves as previously first to the homogeneous case in Section 5.1, where the disorder-temperature phase diagram is plotted in Fig. 5.2 for both weak and strong interacting dirty Bose models. The location of the corresponding first- and second-order phase transitions were discussed in detail. After having treated the homogeneous case, we investigated as a next step the trapped clean one in Section 5.3 using the Thomas-Fermi approximation and the Robinson approximation (5.36). We distinguished between two regions, the superfluid and the thermal one, and we treated them separately. A phase transition from the superfluid phase to the thermal phase was found in Fig. 5.5 at a critical temperature, whose value agrees approximately with the one in Refs. [133, 139]. Finally, we treated the full disorder problem, where both temperature and disorder fluctuations occur. In particular, as already schematically indicated in Fig. 1.6, three regions coexist in Fig. 5.8, namely, the superfluid, the Bose-glass, and the thermal one. In order to investigate the temperature impact only, we fixed in Subsection 5.4.5 the disorder strength to be larger and considered an increasing temperature. Two phase transitions were detected in Fig. 5.9, namely, a first-order transition from the superfluid to the Bose-glass phase and a second-order transition from the Bose-glass to the thermal phase. In contrast to that we studied in Subsection 5.4.6 only the disorder impact, therefore we fixed the temperature to be smaller and considered an increasing disorder strength. This yielded a first-order phase transition from the superfluid phase to the Bose-glass phase as shown in Fig. 5.13.

All these theoretical predictions concerning the dirty boson problem still have to be checked quantitatively in experiments, but in order to make this possible, further refinements and extensions of this work are necessary.

6.2. Outlook

In this thesis we studied the dirty Bose gas in equilibrium, but in view of experiments it is mandatory to study also how the system evolves in time. On the one hand, TOF absorption pictures and their disorder ensemble averages have to be calculated. The findings in the present thesis suggest that, instead of the usual bimodal density distribution, a tri-modal distribution occurs as sketched in Fig. 1.6. A detailed analysis of the three components should make it possible to determine how many bosons are in the disorder ensemble average in the global condensate, in the local minicondensates, and in the thermal states. On the other hand, also the disorder impact on collective excitation frequencies should be investigated, as they are accessible to a high accuracy experimentally. Based on the results of our Hartree-Fock mean-field theory we expect reasonable predictions for the intermediate disorder regime, thus improving the preliminary results within the Huang-Meng theory of weak disorder in Ref. [78]. One can even think about reconciling our Hartree-Fock theory with the Huang-Meng one by finding a way to include the Bogoliubov channel in the Hartree-Fock theory. Furthermore, in this thesis we restricted ourselves in Section 2.6 to the contact interaction and the delta-correlated disorder, but one could, in principle, use the Hartree-Fock mean-field theory also for a general interaction potential and an experimentally relevant disorder potential with finite correlation length like the Gaussian or the Lorentzian correlated disorder.

The Hartree-Fock mean-field theory was applied in this thesis to the one-dimensional and the three-dimensional dirty Bose gas systems within the TF approximation, but one can also go beyond the TF approximation and take the kinetic term in the generalized Gross-Pitaevskii equation (2.91) into account. This should yield smoothened density plots. Furthermore, the one-dimensional case was treated at zero temperature only, but one can look for a mathematical tool to deal with the cubic equation (2.164) and study the one-dimensional finite-temperature case as well. The two-dimensional case, which was not considered here, could also be investigated within the Hartree-Fock mean-field theory by taking care of the divergency within a suitable renormalization procedure. It would also be interesting to calculate some further physical properties of the dirty Bose model like superfluidity and to investigate it for increasing disorder strength or temperature or both. In addition, and in close analogy to the disorder-temperature phase diagram of the homogeneous Bose in Subsection 5.1.4, it remains open how the disorder-temperature phase diagram looks like for the dirty trapped Bose gas.

Finally, and as already explained in Section 1.4, one has to verify the stability of our replica symmetry

solutions, therefore the Hessian would have to be computed. In addition, the replica symmetry can, in principle, also be broken either in discrete steps or even continuously. Practically one would have to compare the free energies associated with the RS and RSB solutions and check whether the free energy of the RSB solution is smaller. If this is the case, this would proof that RS is, indeed, broken. In the case of dirty bosons it is still unknown whether RSB lowers the free energy or not.

A. Cardan Method

One meets often the problem of solving a cubic equation, which is an equation of the form

$$az^3 + bz^2 + cz + d = 0, \tag{A.1}$$

where the coefficients a, b, c and d are nonzero and assumed to be real.

The mathematical tool to deal with such equations is the Cardan method [118]. One has first to reduce the cubic equation by performing the following variable transformation:

$$y = z - \frac{b}{3a} \tag{A.2}$$

in order to get the reduced cubic equation

$$y^3 + py + q = 0, \tag{A.3}$$

where we have introduced the abbreviations

$$\begin{cases} p = -\frac{b^2}{3a^2} + \frac{c}{a} \\ \\ q = \frac{b}{27a}(\frac{2b^2}{a^2} - \frac{9c}{a}) + \frac{d}{a} \end{cases} \tag{A.4}$$

As a solution ansatz, we set:

$$y = u + v. \tag{A.5}$$

Since one can freely dispose of one of the unknown quantities u or v, they can be chosen such that they satisfy:

$$\begin{cases} u^3 + v^3 = -q \\ u^3 v^3 = -\frac{p^3}{27} \end{cases}. \tag{A.6}$$

Thus, we conclude that both u^3 and v^3 solve the quadratic equation:

$$x^2 + qx - \frac{p^3}{27} = 0. \tag{A.7}$$

The discriminant of this quadratic equation is

$$\delta = q^2 + \frac{4}{27}p^3 \tag{A.8}$$

and their solutions are:

$$\begin{cases} u^3 = \frac{-q+\sqrt{\delta}}{2} & \text{and } v^3 = \frac{-q-\sqrt{\delta}}{2} \text{ if } \delta \text{ is positive} \\ u^3 = \frac{-q+i\sqrt{-\delta}}{2} & \text{and } v^3 = \frac{-q-i\sqrt{-\delta}}{2} \text{ if } \delta \text{ is negative} \\ u^3 = v^3 = -\frac{q}{2} & \text{if } \delta \text{ is zero} \end{cases} \tag{A.9}$$

Now we just need to associate the three cubic roots of u^3 and v^3 in order to obtain three couples (u, v) such that $uv = -\frac{p}{3}$ is fulfilled, which follows from (A.6), then we substitute the three couples of u and v in the expression (A.5) and finally we insert the obtained results into the expression (A.2). In this way, we obtain the three following solutions of the cubic equation (A.1) as functions of the discriminant δ:

- If $\delta > 0$ equation (A.1) has one real solution and two complex conjugate solutions:

  $x_1 = \sqrt[3]{\frac{-q+\sqrt{\delta}}{2}} + \sqrt[3]{\frac{-q-\sqrt{\delta}}{2}} - \frac{b}{3a}$

  $x_2 = e^{\frac{2i\pi}{3}} \sqrt[3]{\frac{-q+\sqrt{\delta}}{2}} + e^{-\frac{2i\pi}{3}} \sqrt[3]{\frac{-q-\sqrt{\delta}}{2}} - \frac{b}{3a}$

  $x_3 = e^{-\frac{2i\pi}{3}} \sqrt[3]{\frac{-q+\sqrt{\delta}}{2}} + e^{\frac{2i\pi}{3}} \sqrt[3]{\frac{-q-\sqrt{\delta}}{2}} - \frac{b}{3a}$

- If $\delta < 0$ equation (A.1) has only real solutions:

  $x_1 = \sqrt[3]{\frac{-q+i\sqrt{-\delta}}{2}} + \sqrt[3]{\frac{-q-i\sqrt{-\delta}}{2}} - \frac{b}{3a}$

  $x_2 = e^{\frac{2i\pi}{3}} \sqrt[3]{\frac{-q+i\sqrt{-\delta}}{2}} + e^{-\frac{2i\pi}{3}} \sqrt[3]{\frac{-q-i\sqrt{-\delta}}{2}} - \frac{b}{3a}$

  $x_3 = e^{-\frac{2i\pi}{3}} \sqrt[3]{\frac{-q+i\sqrt{-\delta}}{2}} + e^{\frac{2i\pi}{3}} \sqrt[3]{\frac{-q-i\sqrt{-\delta}}{2}} - \frac{b}{3a}$

- If $\delta = 0$ equation (A.1) all solutions are real, but two are degenerate:

  $x_1 = \frac{3q}{p} - \frac{b}{3a}$ and $x_{2,3} = -\frac{3q}{2p} - \frac{b}{3a}$

Since it is not evident to recognize the real solutions, it is more appropriate to write them in their trigonometric form:

- $\delta > 0$

  $x_1 = 2\sqrt{\frac{p}{3}} \sinh\left[\frac{1}{3}\sinh^{-1}\left(-\frac{3q}{2p}\sqrt{\frac{3}{p}}\right)\right] - \frac{b}{3a}$ if $p > 0$

  $x_1 = 2\sqrt{\frac{p}{3}} \sinh\left[\frac{1}{3}\sinh^{-1}\left(-\frac{3q}{2p}\sqrt{\frac{3}{p}}\right)\right] - \frac{b}{3a}$ if $p < 0$

  $x_2 = e^{\frac{2i\pi}{3}} \sqrt[3]{\frac{-q+\sqrt{\delta}}{2}} + e^{-\frac{2i\pi}{3}} \sqrt[3]{\frac{-q-\sqrt{\delta}}{2}} - \frac{b}{3a}$

  $x_3 = e^{-\frac{2i\pi}{3}} \sqrt[3]{\frac{-q+\sqrt{\delta}}{2}} + e^{\frac{2i\pi}{3}} \sqrt[3]{\frac{-q-\sqrt{\delta}}{2}} - \frac{b}{3a}$

- $\delta < 0$ equation (A.1) has only real solutions:

  $x_1 = 2\sqrt{-\frac{p}{3}} \cos\left[\frac{1}{3}\arccos\left(-\frac{q}{2}\sqrt{-\frac{27}{p^3}}\right)\right] - \frac{b}{3a}$

  $x_2 = 2\sqrt{-\frac{p}{3}} \cos\left[\frac{1}{3}\arccos\left(-\frac{q}{2}\sqrt{-\frac{27}{p^3}}\right) + \frac{2\pi}{3}\right] - \frac{b}{3a}$

  $x_3 = 2\sqrt{-\frac{p}{3}} \cos\left[\frac{1}{3}\arccos\left(-\frac{q}{2}\sqrt{-\frac{27}{p^3}}\right) - \frac{2\pi}{3}\right] - \frac{b}{3a}$

- $\delta = 0$

  $x_1 = \frac{3q}{p} - \frac{b}{3a}$ and $x_{2,3} = -\frac{3q}{2p} - \frac{b}{3a}$

B. Numerical Appendix

In Section 3.3 we reviewed an efficient method to generate a one-dimensional Gaussian random potential $U(x)$ whose first moment vanishes according to (3.31) and whose second moment is given by some correlation function $D(x-x')$ via (3.32). To this end one writes $U(x)$ as a finite superposition of $\sin(kx)$ and $\cos(kx)$ terms with properly randomly picked amplitudes A_n, B_n, and wave numbers k_n [124]:

$$U(x) = \frac{1}{\sqrt{\mathtt{N}}} \sum_{n=0}^{\mathtt{N}-1} \left[A_n \cos(k_n x) + B_n \sin(k_n x) \right]. \tag{B.1}$$

Here $\mathtt{N}$ denotes the number of terms, which should be large enough in order to obtain a good approximation for the random potential. Furthermore, we assume A_n and B_n to be mutually independent Gaussian random variables with zero mean and variance $D(0)$:

$$\overline{A_n B_n} = 0, \qquad \overline{A_n A_m} = \overline{B_n B_m} = D(0)\delta_{nm}. \tag{B.2}$$

The wave numbers k_n are independent random variables as well, which are picked from the probability distribution:

$$p(k_n) = \frac{S(k_n)}{\int_{-\infty}^{\infty} S(k')dk'}, \tag{B.3}$$

where $S(k)$ defines the spectral density as the Fourier transform of the correlation function:

$$S(k) = \int_{-\infty}^{\infty} dx e^{-ikx} D(x). \tag{B.4}$$

This method to generate a random potential $U(x)$ can be used to calculate expectation values approximately as is visualized in Fig. 3.7. In this appendix, we show quantitatively, that the choice of the parameter $\mathtt{N}$ allows to tune the accuracy of this approximation [141]. For the considerations to follow we will introduce the average with respect to the wave number k as a new abbreviation:

$$\langle \bullet \rangle_k = \int_{-\infty}^{\infty} dk\, p(k)\, \bullet \ . \tag{B.5}$$

For instance, we obtain for due to spectral density (B.4) and the probability distribution (B.3)

$$\langle e^{ikx} \rangle_k = \langle e^{-ikx} \rangle_k = D(x)/D(0) \ . \tag{B.6}$$

Here we have assumed that the correlation function $D(x)$ is symmetric, i.e., $D(x) = D(-x)$, which implies that the correlation function (B.4) is even, i.e., $S(k) = S(-k)$.

Calculating the 2-point correlation of the random potential, we get with definition (B.1)

$$\begin{aligned} \overline{U(x)U(x')} =& \frac{1}{\mathtt{N}} \sum_{n=0}^{\mathtt{N}-1} \sum_{m=0}^{\mathtt{N}-1} \big[\langle A_n A_m \cos(k_n x)\cos(k_m x') \rangle_k + \langle B_n B_m \sin(k_n x)\sin(k_m x') \rangle_k \\ &+ \langle A_n B_m \cos(k_n x)\sin(k_m x') \rangle_k + \langle B_n A_m \sin(k_n x)\cos(k_m x') \rangle_k \big]. \end{aligned} \tag{B.7}$$

Using the property (B.2) this simplifies to

$$\overline{U(x)U(x')} = \frac{D(0)}{\mathtt{N}} \sum_{n=0}^{\mathtt{N}-1} \big[\langle \cos(k_n x)\cos(k_n x') \rangle_k + \langle \sin(k_n x)\sin(k_n x') \rangle_k \big]. \tag{B.8}$$

Using (B.6), we finally get the result

$$\overline{U(x)U(x')} = \frac{D(0)}{\mathtt{N}} \sum_{n=0}^{\mathtt{N}-1} \langle \cos[k_n(x-x')] \rangle_k = D(x-x') \ . \tag{B.9}$$

The result (B.9) of the 2-point correlation is valid for any $\mathtt{N}$ and no limit $\mathtt{N} \to \infty$ is needed. So no error occurs for approximating the 2-point correlation. But note that the accuracy of approximating the 2-point correlation still depends on the number $\mathtt{M}$ of sample potentials, as is illustrated in Fig. 3.7.

Let us consider now the 4-point correlation, for which we would expect, if $U(x)$ is a normal distributed function, Wick's theorem to be satisfied:

$$\begin{aligned} \overline{U(x_1)U(x_2)U(x_3)U(x_4)} \ &= \ D(x_1-x_2)D(x_3-x_4) + D(x_1-x_3)D(x_2-x_4) \\ &\quad + D(x_1-x_4)D(x_2-x_3). \end{aligned} \tag{B.10}$$

Inserting (B.1) using (B.2) yields after some calculation

$$\begin{aligned} \overline{U(x_1)U(x_2)U(x_3)U(x_4)} \ &= \tfrac{D(0)^2}{\mathtt{N}^2} \textstyle\sum_{n,m} \langle \cos[k_n(x_1-x_2)] \cos[k_m(x_3-x_4)] + \cos[k_n(x_1-x_3)] \\ &\quad \times \cos[k_m(x_2-x_4)] + \cos[k_n(x_1-x_4)] \cos[k_m(x_2-x_3)] \rangle. \end{aligned} \tag{B.11}$$

In order to calculate the expectation values, one has to carefully distinguish between two cases. For the $\mathtt{N}(\mathtt{N}-1)$ terms in the sum with $n \neq m$, one gets

$$\begin{aligned} \langle \cos(k_n x) \cos(k_m x') \rangle \ &= \langle \cos(k_n x) \rangle_{k_n} \langle \cos(k_m x') \rangle_{k_m} \\ &= \langle e^{ik_n x} \rangle_{k_n} \langle e^{ik_m x'} \rangle_{k_m} \\ &= D(x) D(x') / D(0) \ . \end{aligned} \tag{B.12}$$

For the $\mathtt{N}$ terms with $n = m$, however, the average is slightly different:

$$\begin{aligned} \langle \cos(k_n x) \cos(k_n x') \rangle \ &= \frac{1}{2} \langle \cos\left[k_n(x-x')\right] + \cos\left[k_n(x+x')\right] \rangle_{k_n} \\ &= \frac{1}{2} \langle e^{ik_n(x+x')} + e^{ik_n(x-x')} \rangle_{k_n} \\ &= \Big[D(x-x') + D(x+x') \Big] / 2D(0)^2 \ . \end{aligned} \tag{B.13}$$

Therefore, Eq. (B.11) yields a form that is straightforwardly comparable with (B.10)

$$\begin{aligned} \overline{U(x_1)U(x_2)U(x_3)U(x_4)} \ &= D(x_1-x_2)D(x_3-x_4) + D(x_1-x_3)D(x_2-x_4) \\ &\quad + D(x_1-x_4)D(x_2-x_3) + \tfrac{1}{\mathtt{N}} \Delta(x_1,x_2,x_3,x_3). \end{aligned} \tag{B.14}$$

It is seen that Wick's theorem (B.10) is satisfied in the limit $\mathtt{N} \to \infty$ as the deviation

$$\begin{aligned} &\Delta(x_1,x_2,x_3,x_4) = -D(x_1-x_2)D(x_3-x_4) - D(x_1-x_3)D(x_2-x_4) - D(x_1-x_4)D(x_2-x_3) \\ &+ \frac{D\,(0)}{2} \left\{ D\big[(x_1-x_2)-(x_3-x_4)\big] + D\big[(x_1-x_2)+(x_3-x_4)\big] + D\big[(x_1-x_3)-(x_2-x_4)\big] \right. \\ &\left. + D\big[(x_1-x_3)+(x_2-x_4)\big] + D\big[(x_1-x_4)-(x_2-x_3)\big] + D\big[(x_1-x_4)+(x_2-x_3)\big] \right\} \end{aligned} \tag{B.15}$$

is suppressed by a factor $1/\mathtt{N}$.

In the special case of Gaussian correlated disorder we have

$$D(x-x') = \ D\,(0) \exp\left\{ -\tfrac{(x-x')^2}{2\lambda^2} \right\}, \quad D\,(0) = \frac{D}{\sqrt{2\pi}\lambda}, \tag{B.16}$$

where λ denotes the correlation length and D the disorder strength. The computation of the error (B.15) due to the randomization parameter $\mathtt{N}$ in the Gaussian correlated disorder case yields

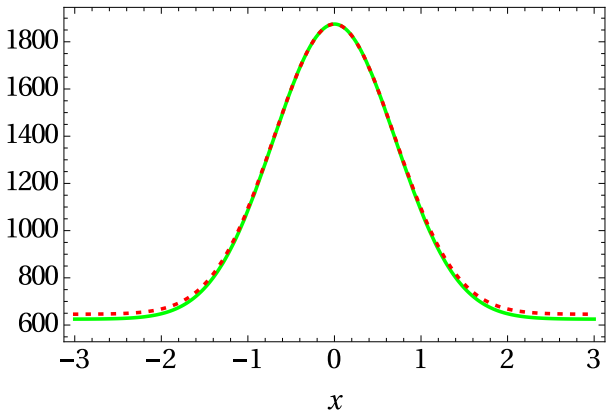

Figure B.1.: Numerical generation of $\overline{U(0)^2 U(x)^2}$ according to (B.1) (dotted, red) compared to Wick's Theorem (B.10) (solid, green) for Gaussian correlated disorder (B.16) with the parameters $D(0) = 25$, $\lambda = 1$, and $\mathtt{N} = 30$.

$$\begin{aligned}\Delta(x_1,x_2,x_3,x_4) = \quad & \Bigg\{ D(x_1-x_2)D(x_3-x_4)\left[\cosh\left(\frac{(x_1-x_2)(x_3-x_4)}{\lambda^2}\right)-1\right] \\ & + D(x_1-x_3)D(x_2-x_4)\left[\cosh\left(\frac{(x_1-x_3)(x_2-x_4)}{\lambda^2}\right)-1\right] \\ & + D(x_1-x_4)D(x_2-x_3)\left[\cosh\left(\frac{(x_1-x_4)(x_2-x_3)}{\lambda^2}\right)-1\right]\Bigg\}. \end{aligned} \tag{B.17}$$

As seen in Fig. B.1, the deviation of the expected 4-point correlation is small, as it scales with $1/\mathtt{N}$.

In this appendix it was shown, that, using the straight-forwards ansatz (B.1), it is possible to generate random functions. The numerically generated expressions resemble the imposed properties of normally distributed random functions with a given correlation function quite well. Thus, we expect simulations of physical quantities due to randomness to be quite accurate.

Bibliography

[1] R. P. Feynman, *Quantum mechanical computers*, Found. Phys. **16**, 507 (1987).

[2] S. Bose, *Planck's Law and Light Quantum Hypothesis*, Z. Phys. **26**, 178 (1924).

[3] A. Einstein, *Quantentheorie des einatomigen idealen Gases*, Sitzungsbericht der Preussischen Akademie der Wissenschaften, Physikalisch-Mathematische Klasse, p. 3 (1925).

[4] H. Perrin, *Ultra cold atoms and Bose-Einstein condensation for quantum metrology*, Eur. Phys. J. Special Topics **172**, 37 (2009).

[5] N. N. Bogoliubov, *On the theory of superfluidity*, J. Phys. USSR **11**, 23 (1947).

[6] K. Huang and C. N. Yang, *Quantum-mechanical many-body problem with hard-sphere interaction*, Phys. Rev. **105**, 767 (1957).

[7] K. Huang, C. N. Yang, and J. M. Luttinger, *Imperfect Bose gas with hard-sphere interaction*, Phys. Rev. **105**, 776 (1957).

[8] E. P. Gross, *Structure of a quantized vortex in boson systems*, Nuovo Cimento **20**, 454 (1961).

[9] L. P. Pitaevskii, *Vortex lines in an imperfect Bose gas*, Sov. Phys.-JETP **13**, 451 (1961).

[10] M. H. Anderson, J. R. Ensher, M. R. Matthews, C. E. Wieman, and E. A. Cornell, *Observation of Bose-Einstein Condensation in a Dilute Atomic Vapor*, Science **269**, 198 (1995).

[11] E. A. Cornell and C. E. Wieman, *The Bose-Einstein Condensate*, Scientific American **278**, 40 (1998).

[12] K. B. Davis, M. O. Mewes, M. R. Andrews, N. J. van Druten, D. S. Durfee, D. M. Kurn, and W. Ketterle, *Bose-Einstein Condensation in a Gas of Sodium Atoms*, Phys. Rev. Lett. **75**, 3969 (1995).

[13] C. C. Bradley, C. A. Sackett, J. J. Tollett, and R. G. Hulet, *Evidence of Bose-Einstein Condensation in an Atomic Gas with Attractive Interactions*, Phys. Rev. Lett. **75**, 1687 (1995).

[14] C. C. Bradley, C. A. Sackett, and R. G. Hulet, *Bose-Einstein Condensation of Lithium: Observation of Limited Condensate Number*, Phys. Rev. Lett. **78**, 985 (1997).

[15] D. G. Fried, T. C. Killian, L. Willmann, D. Landhuis, S. C. Moss, D. Kleppner, and T. J. Greytak, *Bose-Einstein condensation of atomic hydrogen*, Phys. Rev. Lett. **81**, 3811 (1998).

[16] A. Robert, O. Sirjean, A. Browaeys, J. Poupard, S. Nowak, D. Boiron, C. I. Westbrook, and A. Aspect, *A Bose-Einstein Condensate of Metastable Atoms,* Science **292**, 461 (2001).

[17] C. Raman, M. Köhl, R. Onofrio, D. S. Durfee, C. E. Kuklewicz, Z. Hadzibabic, and W. Ketterle, *Evidence for a Critical Velocity in a Bose-Einstein Condensed Gas*, Phys. Rev. Lett. **83**, 2502 (1999).

[18] L. D. Landau, *The theory of superfluidity of helium II*, J. Phys. USSR **5**, 71 (1941).

[19] M. R. Matthews, B. P. Anderson, P. C. Haljan, D. S. Hall, C. E. Wieman, and E. A. Cornell, *Vortices in a Bose-Einstein Condensate*, Phys. Rev. Lett. **83**, 2498 (1999).

[20] K. W. Madison, F. Chevy, W. Wohlleben, and J. Dalibard, *Vortex Formation in a Stirred Bose-Einstein Condensate*, Phys. Rev. Lett. **84**, 806 (2000).

[21] C. Ryu, M. F. Andersen, P. Cladé, V. Natarajan, K. Helmerson, and W. D. Phillips, *Flow of a Bose-Einstein condensate in a toroidal trap*, Phys. Rev. Lett. **99**, 260 (2007).

[22] M. O. Mewes, M. R. Andrews, N. J. van Druten, D. M. Kurn, D. S. Durfee, and W. Ketterle, *Bose-Einstein Condensation in a Tightly Confining dc Magnetic Trap,* Phys. Rev. Lett. **77**, 416 (1996).

[23] W. Ebeling, A. Engel, B. Esser, and R. Feistel, *Diffusion and Reaction in Random Media and Models of Evolution Processes*, J. Stat. Phys. **37,** 369 (1984).

[24] Y. C. Zhang, *Diffusion in a Random Potential: Hopping as a Dynamical Consequence of Localization*, Phys. Rev. Lett. **56,** 2113 (1986).

[25] J. P. Gleeson, *Passive Motion in Dynamical Disorder as a Model for Stock Market Prices*, Physica A **351,** 523 (2005).

[26] J. Shiferaw and Y. Y. Goldschmidt, *Localization of a Polymer in Random Media: Relation to the Localization of a Quantum Particle*, Phys. Rev. E **63,** 051803 (2001).

[27] R. Folman, P. Krüger, J. Schmiedmayer, J. Denschlag, and C. Henkel, *Microscopic atom optics: from wires to an atom chip*, Adv. At. Mol. Opt. Phys. **48**, 263 (2002).

[28] D. W. Wang, M. D. Lukin, and E. Demler, *Disordered Bose-Einstein condensates in quasi-one-dimensional magnetic microtraps*, Phys. Rev. Lett. **92**, 076802 (2004).

[29] T. Schumm, J. Esteve, C. Figl, J. B. Trebbia, C. Aussibal, H. Nguyen, D. Mailly, I. Bouchoule, C. I. Westbrook, and A. Aspect, *Atom chips in the real world: the effects of wire corrugation*, Eur. Phys. J. D **32**, 171 (2005).

[30] J. Fortágh and C. Zimmermann, *Magnetic Microtraps for Ultracold Atoms*, Rev. Mod. Phys. **79**, 235 (2007).

[31] J. C. Dainty (Ed.), *Laser Speckle and Related Phenomena*, Springer, Berlin, 1975.

[32] J. E. Lye, L. Fallani, M. Modugno, D. S. Wiersma, C. Fort, and M. Inguscio, *A Bose-Einstein condensate in a random potential*, Phys. Rev. Lett. **95**, 070401 (2005).

[33] D. Clément, A. F. Varón, M. Hugbart, J. A. Retter, P. Bouyer, L. Sanchez-Palencia, D. M. Gangardt, G. V. Shlyapnikov, and A. Aspect, *Suppression of Transport of an Interacting Elongated Bose-Einstein Condensate in a Random Potential*, Phys. Rev. Lett. **95**, 170409 (2005).

[34] J. W. Goodman, *Speckle Phenomena in Optics: Theory and Applications*, Viva Books Private Limited, 2010.

[35] J. C. Dainty, *An introduction to Gaussian speckle*, Proc. SPIE **243**, 2 (1980).

[36] http://www.2physics.com/2010

[37] http://en.wikipedia.org/wiki/Speckle_pattern

[38] D. Sherrington and S. Kirkpatrick, *Solvable Model of a Spin Glass*, Phys. Rev. Lett. **53**, 1792 (1975).

[39] G. Parisi, *Field Theory, Disorder and Simulations*, World Scientific, Singapore, 1992.

[40] V. Dotsenko, *An Introduction to the Theory of Spin Glasses and Neural Networks*, World Scientific, Singapore, 1994.

[41] M. P. A. Fisher, P. B. Weichman, G. Grinstein, and D. S. Fisher, *Boson Localization and the Superfluid-Insulator Transition*, Phys. Rev. B **40**, 546 (1989).

[42] B. C. Crooker, B. Hebral, E. N. Smith, Y. Takano, and J. D. Reppy, *Superfluidity in a Dilute Bose Gas*, Phys. Rev. Lett. **51**, 666 (1983).

[43] B. Damski, J. Zakrzewski, L. Santos, P. Zoller, and M. Lewenstein, *Atomic Bose and Anderson Glasses in Optical Lattices*, Phys. Rev. Lett. **91**, 080403 (2003).

[44] T. Schulte, S. Drenkelforth, J. Kruse, W. Ertmer, J. Arlt, K. Sacha, J. Zakrzewski, and M. Lewenstein, *Routes Towards Anderson-Like Localization of Bose-Einstein Condensates in Disordered Optical Lattices*, Phys. Rev. Lett. **95**, 170411 (2005).

[45] P. W. Anderson, *Absence of Diffusion in Certain Random Lattices*, Phys. Rev. **109**, 1492 (1958).

[46] J. Billy, V. Josse, Z. Zuo, A. Bernard, B. Hambrecht, P. Lugan, D. Clement, L. Sanchez-Palencia, P. Bouyer, and A. Aspect, *Direct Observation of Anderson Localization of Matter-Waves in a Controlled Disorder*, Nature **453**, 891 (2008).

[47] G. Roati, C. D'Errico, L. Fallani, M. Fattori, C. Fort, M. Zaccanti, G. Modugno, M. Modugno, and M. Inguscio, *Anderson Localization of a Non-Interacting Bose-Einstein Condensate*, Nature **453**, 895 (2008).

[48] C. M. Aegerter and G. Maret, *Coherent Backscattering and Anderson Localization of Light*, Progress in Optics **52**, 1 (2009).

[49] M. Segev, Y. Silberberg, and D. N. Christodoulides, *Anderson localization of light*, Nature Photonics **7**, 197 (2013).

[50] D. S. Wiersma, P. Bartolini, A. Lagendijk, and R. Righini, *Localization of light in a disordered medium*, Nature **390**, 671 (1997).

[51] M. Störzer, P. Gross, C. M. Aegerter, and G. Maret, *Observation of the critical regime near Anderson localization of light*, Phys. Rev. Lett. **96**, 063904 (2006).

[52] T. Schwartz, G. Bartal, S. Fishman, and M. Segev, *Transport and Anderson localization in disordered two-dimensional photonic lattices*, Nature **446**, 52 (2007).

[53] Y. Lahini, A. Avidan, F. Pozzi, M. Sorel, R. Morandotti, D. N. Christodoulides, and Y. Silberberg, *Anderson Localization and Nonlinearity in One-Dimensional Disordered Photonic Lattices*, Phys. Rev. Lett. **100**, 013906 (2008).

[54] P. Krüger, L. M. Andersson, S. Wildermuth, S. Hofferberth, E. Haller, S. Aigner, S. Groth, I. Bar-Joseph, and J. Schmiedmayer, Phys. Rev. A **76**, 063621 (2007).

[55] L. Fallani, J. E. Lye, V. Guarrera, C. Fort, and M. Inguscio, *Ultracold Atoms in a Disordered Crystal of Light: Towards a Bose Glass*, Phys. Rev. Lett. **98**, 130404 (2007).

[56] U. Gavish and Y. Castin, *Matter-Wave Localization in Disordered Cold Atom Lattices*, Phys. Rev. Lett. **95**, 020401 (2005).

[57] B. Gadway, D. Pertot, J. Reeves, M. Vogt, and D. Schneble, *Glassy Behavior in a Binary Atomic Mixture*, Phys. Rev. Lett. **107**, 145306 (2011).

[58] S. Sachdev, *Quantum Phase Transitions*, Second Edition, Cambridge University Press, 2011.

[59] G. G. Batrouni, R. T. Scalettar, and G. T. Zimanyi, *Quantum critical phenomena in one-dimensional Bose systems*, Phys. Rev. Lett. **65**, 1765 (1990).

[60] R. T. Scalettar, G. G. Batrouni, and G. T. Zimanyi, *Localization in interacting, disordered, Bose systems*, Phys. Rev. Lett. **66**, 3144 (1991).

[61] W. Krauth, N. Trivedi, and D. Ceperley, *Superfluid-Insulator Transition in Disordered Boson Systems*, Phys. Rev. Lett. **67**, 2307 (1991).

[62] P. A. Crowell, F. W. Van Keuls, and J. D. Reppy, *Onset of superfluidity in* ^{4}He *films adsorbed on disordered substrates*, Phys. Rev. B **55**, 12620 (1997).

[63] J. W. Lee, M. C. Cha, and D. Kim, *Phase diagram of a disordered boson Hubbard model in two dimensions*, Phys. Rev. Lett. **87**, 247006 (2001).

[64] K. Huang and H. F. Meng, *Hard-Sphere Bose Gas in Random External Potentials*, Phys. Rev. Lett. **69**, 644 (1992).

[65] S. Giorgini, L. Pitaevskii, and S. Stringari, *Effects of disorder in a dilute Bose gas*, Phys. Rev. B **49**, 12938 (1994).

[66] M. Kobayashi and M. Tsubota, *Bose-Einstein condensation and superfluidity of a dilute Bose gas in a random potential*, Phys. Rev. B **66**, 174516 (2002).

[67] B. Abdullaev and A. Pelster, *Bose-Einstein condensate in weak 3d isotropic speckle disorder*, Europ. Phys. J. D **66**, 314 (2012).

[68] A. Boudjemaa, *Dipolar Bose gas in a weak isotropic speckle disorder*, Phys. Rev. A **91**, 053619 (2015).

[69] A. V. Lopatin and V. M. Vinokur, *Thermodynamics of the Superfluid Dilute Bose Gas with Disorder*, Phys. Rev. Lett. **88**, 235503 (2002).

[70] G. M. Falco, A. Pelster, and R. Graham, *Thermodynamics of a Bose-Einstein condensate with weak disorder*, Phys. Rev. A **75**, 063619 (2007).

[71] C. Krumnow and A. Pelster, *Dipolar Bose-Einstein condensates with weak disorder*, Phys. Rev. A **84**, 021608(R) (2011).

[72] B. Nikolić, A. Balaž, and A. Pelster, *Dipolar Bose-Einstein condensates in weak anisotropic disorder*, Phys. Rev. A **88**, 013624 (2013).

[73] M. Ghabour and A. Pelster, *Bogoliubov theory of dipolar Bose gas in a weak random potential*, Phys. Rev. A **90**, 063636 (2014).

[74] A. Boudjemâa, *Two-dimensional dipolar bosons with weak disorder*, Phys. Lett. A, **379**, 2484 (2015).

[75] A. Boudjemâa, *Superfluidity and Bose-Einstein condensation in a dipolar Bose gas with weak disorder*, J. Low Temp. Phys. **180**, 377 (2015).

[76] C. Gaul and C. A. Müller, *Bogoliubov excitations of disordered Bose-Einstein condensates*, Phys. Rev. A **83**, 063629 (2011).

[77] C. A. Müller and C. Gaul, *Condensate deformation and quantum depletion of Bose-Einstein condensates in external potentials*, New J. Phys. **14**, 075025 (2012).

[78] G. M. Falco, A. Pelster, and R. Graham, *Collective oscillations in trapped Bose-Einstein condensed gases in the presence of weak disorder*, Phys. Rev. A **76**, 013624 (2007).

[79] P. Navez, A. Pelster, and R. Graham, *Bose condensed gas in strong disorder potential with arbitrary correlation length*, App. Phys. B **86**, 395 (2007).

[80] V. I. Yukalov and R. Graham, *Bose-Einstein-condensed systems in random potentials*, Phys. Rev. A **75**, 023619 (2007).

[81] V. I. Yukalov, E. P. Yukalova, K. V. Krutitsky, and R. Graham, *Bose-Einstein-condensed gases in arbitrarily strong random potentials*, Phys. Rev. A **76**, 053623 (2007).

[82] T. Nattermann and V. L. Pokrovsky, *Bose-Einstein Condensates in Strongly Disordered Traps*, Phys. Rev. Lett. **100**, 060402 (2008).

[83] G. M. Falco, T. Nattermann, and V.L. Pokrovsky, *Weakly interacting Bose gas in a random environment*, Phys. Rev. B **80**, 104515 (2009).

[84] R. Graham and A. Pelster, *Order via Nonlinearity in Randomly Confined Bose Gases*, Int. J. Bif. Chaos **19**, 2745 (2009).

[85] G. E. Astrakharchik, J. Boronat, J. Casulleras, and S. Giorgini, *Superfluidity versus Bose-Einstein condensation in a Bose gas with disorder*, Phys. Rev. A **66**, 023603 (2002).

[86] H. Meier and M. Wallin, *Quantum Critical Dynamics Simulation of Dirty Boson Systems*, Phys. Rev. Lett. **108**, 055701 (2012).

[87] R. Ng and E. S. Sørensen, *Quantum Critical Scaling of Dirty Bosons in Two Dimensions*, Phys. Rev. Lett. **114**, 255701 (2015).

[88] G. Parisi, *On the replica approach to random directed polymers in two dimensions*, J. Phys. France **51**, 1595 (1990).

[89] M. Mezard and G. Parisi, *Replica Field Theory for Random Manifolds*, J. Phys. I France **1**, 809 (1991).

[90] J. L. de Almeida and D. J. Thouless, *Stability of the Sherrington-Kirkpatrick Solution of a Spin Glass Model*, J. Phys. A. **11**, 983 (1978).

[91] D. J. Thouless, J. R. L. de Almeida, and J. M. Kosterlitz, *Stability and susceptibility in Parisis solution of a spin glass model*, J. Phys. C. **13**, 3271 (1980).

[92] P. D. Gujrati, *Breakdown of Replica Analyticity in the One-Dimensional Axis Model*, Phys. Rev. B **32**, 3319 (1985).

[93] G. Parisi, *The Order Parameter for Spin Glasses: a Function on the Interval 0-1*, J. Phys. A **13,** 1101 (1980).

[94] M. Mezard, G. Parisi, and M. A. Virasoro, *Spin Glass Theory and Beyond*, World Scientific, Singapore, 1986.

[95] A. Engel, *Replica Symmetry Breaking in Zero Dimension*, Nucl. Phys. B **410**, 617 (1993).

[96] M. Mezard and G. Parisi, *Manifolds in random media: two extreme cases*, J. Physique I **2**, 2231 (1992).

[97] T.Khellil and A. Pelster, `arXiv:1510.04985`.

[98] T. Khellil, A. Balaž, and A. Pelster, `arXiv:1511.08882`.

[99] T. Khellil and A. Pelster, `arXiv:1512.04870`.

[100] M. H. W. Chan, K. I. Blum, S. Q. Murphy, G. K. S. Wong, and J. D. Reppy, *Disorder and the Superfluid Transition in Liquid* ^{4}He, Phys. Rev. Lett. **61**, 1950 (1988).

[101] G. K. S. Wong, P. A. Crowell, H. A. Cho, and J. D. Reppy, *Superfluid critical behavior in filled porous media*, Phys. Rev. Lett. **65**, 2410 (1990).

[102] J. D. Reppy, *Superfluid helium in porous media*, J. Low Temp. Phys. **87**, 205 (1992).

[103] M. Koboyashi and M. Tsubota, *Bose-Einstein condensation and superfluidity of a dilute Bose gas in a random potential*, Phys. Rev. B **66**, 174516 (2002).

[104] H. Kleinert, *Gauge Fields in Condensed Matter Vol I: SUPERFLOW AND VORTEX LINES* , World Scientific, Singapore, 1989.

[105] H. Risken, *The Fokker-Planck Equation: Methods Of Solution And Applications,* Second Edition, Springer, 1996.

[106] A. Griffin, *Conserving and gapless approximations for an inhomogeneous Bose gas at finite temperatures*, Phys. Rev. B **53**, 9341 (1996).

[107] J. O. Andersen, *Theory of the weakly interacting Bose gas*, Rev. Mod. Phys. **76**, 599 (2004).

[108] B. De Witt, *Dynamical Theory of Groups and Fields*, Gordon and Breach, New York, 1965.

[109] R. Jackiw, *Functional Evaluation of the Effective Potential*, Phys. Rev. D **9**, 1686 (1974).

[110] H. Kleinert and V. Schulte-Frohlinde, *Critical Properties of Φ^4-Theories*, World Scientific, Singapore, 2001.

[111] I. S. Gradshteyn and I.M. Ryzhik, *Table of Integrals, Series, and Products,* Corrected and Enlarged Edition, Academic Press, New York, 1980.

[112] K. H. Fischer and J. A. Hertz, *Spin Glasses*, Cambridge University Press, Cambridge, 1991.

[113] S. F. Edwards and P. W. Anderson, *Theory of Spin Glasses*, J. Phys. F: Met. Phys. **5**, 965 (1975).

[114] G. M. Falco, *Variational approach for Bose–Einstein condensates in strongly disordered traps*, J. Phys. B: At. Mol. Opt. Phys. **42**, 215303 (2009).

[115] H. Kleinert, *Path Integrals in Quantum Mechanics, Statistics, Polymer Physics, and Financial Markets*, Fifth Edition, World Scientific, Singapore, 2009.

[116] V. M. Pérez-Garcia, H. Michinel, J. I. Cirac, M. Lewenstein, and P. Zoller, *Low Energy Excitations of a Bose-Einstein Condensate: A Time-Dependent Variational Analysis*, Phys. Rev. Lett. **77**, 5320 (1996).

[117] V. M. Pérez-Garcia, H. Michinel, J. I. Cirac, M. Lewenstein, P. Zoller, *Dynamics of Bose-Einstein condensates: Variational solutions of the Gross-Pitaevskii equations*, Phys. Rev. A **56**, 1424 (1997).

[118] W. Greiner, *Classical Mechanics, Systems of Particles and Hamiltonian Dynamics*, Springer, New York, 2003.

[119] A. I. Larkin, *Effect of inhomogeneities on the structure of the mixed state of superconductors*, Zh. Eksp. Theor. Fiz **58**, 1466 (1970).

[120] G. M. Falco, A. Pelster, and R. Graham, *Thermodynamics of a Bose-Einstein condensate with weak disorder*, Phys. Rev. A **75**, 063619 (2007).

[121] H. Perrin, Y. Colombe, B. Mercier, V. Lorent, and C. Henkel, *Diffuse reflection of a Bose-Einstein condensate from a rough evanescent wave mirror*, J. Phys. B: At. Mol. Opt. Phys. **39**, 4649 (2006).

[122] R. Carretero-González, D. J. Frantzeskakis, and P. G. Kevrekidis, *Nonlinear waves in Bose-Einstein condensates: physical relevance and mathematical techniques*, Nonlinearity **21**, R139 (2008).

[123] A. M. Kamchatnov, *Expansion of Bose-Einstein condensates in lower dimensions*, J. Exp. Theor. Phys. **98**, 908 (2004).

[124] J. Majda and P. Kramer, *Simplified Models for Turbulent Diffusion: Theory, Numerical Modelling, and Physical Phenomena*, Phys. Rep. **314**, 237 (1999).

[125] P. Muruganandam and S. K. Adhikari, *Fortran programs for the time-dependent Gross-Pitaevskii equation in a fully anisotropic trap*, Comput. Phys. Commun. **180**, 1888 (2009).

[126] D. Vudragović, I. Vidanović, A. Balaž, P. Muruganandam, and S. K. Adhikari, *C programs for solving the time-dependent Gross-Pitaevskii equation in a fully anisotropic trap*, Comput. Phys. Commun. **183**, 2021 (2012).

[127] R. Kishor Kumar, L. E. Young-S, D. Vudragović, A. Balaž, P. Muruganandamd, and S. K. Adhikari, *Fortran and C programs for the time-dependent dipolar Gross-Pitaevskii equation in an anisotropic trap*, Comput. Phys. Commun. **195**, 117 (2015).

[128] F. Dalfovo, S. Giorgini, L. P. Pitaevskii, and S. Stringari, *Theory of Bose-Einstein condensation in trapped gases*, Rev. Mod. Phys. **71**, 463 (1999).

[129] R. K. Pathria and P. D. Beale, *Statistical Mechanics*, Third Edition, Elsevier, 2011.

[130] H. Kleinert, *Five-Loop Critical Temperature Shift in Weakly Interacting Homogeneous Bose-Einstein Condensate*, Mod. Phys. Lett. B **17**, 1011 (2003).

[131] B. Kastening, *Bose-Einstein condensation temperature of a homogeneous weakly interacting Bose gas in variational perturbation theory through seven loops*, Phys. Rev. A **69**, 043613 (2004).

[132] V. A. Kashurnikov, N. V. Prokof'ev, and B. V. Svistunov, *Critical Temperature Shift in Weakly Interacting Bose Gas*, Phys. Rev. Lett. **87**, 120402 (2001).

[133] S. Giorgini, L. P. Pitaevskii, and S. Stringari, *Condensate fraction and critical temperature of a trapped interacting Bose gas*, Phys. Rev. A **54** 4633 (1996).

[134] P. Ohberg and S. Stenholm, *A Hartree–Fock study of a Bose condensed gas*, J. Phys. B: At. Mol. Opt. Phys. **30** 2749 (1997).

[135] I. Vasić, private communication, 2012.

[136] K. Glaum, H. Kleinert, and A. Pelster, *Condensation of ideal Bose gas confined in a box within a canonical ensemble*, Phys. Rev. A **76**, 063604 (2007).

[137] J.E. Robinson, *Note on the Bose-Einstein Integral Functions*, Phys. Rev. **83**, 678 (1951).

[138] D. M. Young and R. T. Gregory, *A survey of numerical mathematics*, Dover, New York, 1988.

[139] M. Houbiers, H. T. C. Stoof, and E. A. Cornell, *Critical temperature of a trapped Bose gas: Mean-field theory and fluctuations*, Phys. Rev. A **56** 2041 (1996).

[140] M. Timmer, A. Pelster, and R. Graham, *Disorder-induced shift of condensation temperature for dilute trapped Bose gases*, Europhys. Lett. **76**, 760 (2006).

[141] M. Düttmann, *A Variational Methods in Disorder Problems Testing Approximation Techniques with and without Replicas on a Zero-Dimensional Disorder Model*, Diploma Thesis, Freie Universität Berlin, Germany (2009).

List of Publications

1. T.Khellil and A. Pelster, *Hartree-Fock Mean-Field Theory for Trapped Dirty Bosons*, `arXiv:1510.04985`.
2. T. Khellil, A. Balaž, and A. Pelster, *Dirty bosons in a quasi-one-dimensional harmonic trap*, `arXiv:1511.08882`.
3. T. Khellil and A. Pelster, *Dirty bosons in a three-dimensional harmonic trap*, `arXiv:1512.04870`.

Acknowledgements

At the end of my thesis I would like to thank all those people who made this thesis possible and an unforgettable experience for me.

First of all, I would like to express my sincere gratitude to my supervisor Priv.-Doz. Dr. Axel Pelster for the continuous advice of my Ph.D study, for his patience, motivation, and immense knowledge. I thank him for the systematic guidance, great effort he put into training me in the scientific field, and for facilitating all the needed requirements. He integrated me into the work group and introduced me into this subject. Furthermore, from him I learned innumerable mathematical tricks being extremely valuable for solving many physical problems. His diligence, comments and passion for physics have enriched me and the discussions with him have always been very instructive. Also I am deeply indebted to him for his occasional directional corrections and constructive criticism in the preparation of this script.

Special thanks goes to the head of our group, Prof. Dr. Dr. h.c. mult. Hagen Kleinert, for the opportunity to work in his group, which has been both an honor and a privilege.

I would also like to express my sincere gratitude to Prof. Dr. Jürgen Bosse for his insightful comments. In particular, I would like to mention his critical reading of this manuscript, which improved its readability, as well as the support letters for extending the PhD scholarship.

I would like to acknowledge the German Academic Exchange Service (DAAD) who supported my PhD thesis through a fellowship. In particular I am indebted to Ms. Anke Bahrani from DAAD for her administrative help and continuous support. I would also like to thank Prof. Dr. Abdelhafid Bounamis from my home university in Algeria for his kind help throughout the process to get the DAAD-scholarship.

I would also like to express grateful thanks to Dr. Antun Balaž from the Scientific Computer Laboratory (SCL) Institute of Physics, University of Belgrade, Serbia, where numerical simulations of Section 3.3 were run on the PARADOX supercomputing facility under projects ON171017, NAI-DBEC, and IBEC, which were supported within a binational exchange program by both DAAD and the Ministry of Education, Science, and Technological Development of the Republic of Serbia.

I thank my colleagues at the Free University of Berlin with whom I had stimulating discussions and from whom I got support by any technical problem. It was a nice international experience, where I learned a lot in science and life as well.

My sincere thanks go to my family: my mother Messouda, my sister Mounia and my two brothers Safoin and Mohamed for supporting and encouraging me spiritually in my studies right from the beginning, when the idea of doing my PhD in Germany was still a dream.

Finally, I take this opportunity to express the profound gratitude from my deep heart to my husband Jens for his care, love, and continuous support. In addition, my heartfelt thanks go to my husband's parents Birgit and Manfred for their kindness and moral support.